School of Doctoral Studies in Biological Sciences

University of South Bohemia in České Budějovice
Faculty of Science

Biosensors for Environmental Monitoring and Biomedical Applications

Ph.D. Thesis

Mgr. Štofik Marcel

Supervisor: doc. RNDr. Jiří Masojídek, CSc.
The Institute of Microbiology of the Academy of Sciences in Třeboň

České Budějovice 2012

Annotation

Study of biosensors has become an essential part of research in biotechnology. Biosensors as fast, portable, highly sensitive, and low-cost bioanalytical detection devices have been utilized in many fields of human activity.

The first part of the presented work focuses on electrochemical biosensors for rapid environmental screening of herbicides as water pollutants. A sol-gel immobilization method for a photosystem II (PSII) complex is studied in order to enhance the sensitivity and the signal strength and stability of a PSII-based biosensor. Computer simulations of a PSII biosensor are employed with the aim to find out how the immobilization membrane properties influence the biosensor parameters. Newly developed immobilization by a thin-layer membrane based on the results of computer simulations and revised measurement protocols are presented.

The second part of the work is devoted to synthesis and electrochemical detection of newly developed metal labels for electrochemical immunosensors. The synthesis of dendrimer-encapsulated silver nanoparticles and biorecognition properties of biotin-nanocomposite conjugates are discussed. For detection of synthesized labels, a microfluidic detector was manufactured and tested and different approaches to packing of a microfluidic chip employing polydimethylsiloxane (PDMS) were investigated. Newly designed microstructures for a microfluidic separator of magnetic beads (MBs) were studied by computer simulations. The separator was made and trapping of MBs for the further employment in MBs-based immunoassays are presented.

Declaration [in Czech]

Prohlašuji, že svoji disertační práci jsem vypracoval samostatně pouze s použitím pramenů a literatury uvedených v seznamu citované literatury.

Prohlašuji, že v souladu s § 47b zákona č. 111/1998 Sb. v platném znění souhlasím se zveřejněním své disertační práce, a to v nezkrácené podobě elektronickou cestou ve veřejně přístupné části databáze STAG provozované Jihočeskou univerzitou v Českých Budějovicích na jejích internetových stránkách, a to se zachováním mého autorského práva k odevzdanému textu této kvalifikační práce. Souhlasím dále s tím, aby toutéž elektronickou cestou byly v souladu s uvedeným ustanovením zákona č. 111/1998 Sb. zveřejněny posudky školitele a oponentů práce i záznam o průběhu a výsledku obhajoby kvalifikační práce. Rovněž souhlasím s porovnáním textu mé kvalifikační práce s databází kvalifikačních prací Theses.cz provozovanou Národním registrem vysokoškolských kvalifikačních prací a systémem na odhalování plagiátů.

České Budějovice, 22.5.2012   ....
                                                            jméno a příjmení

This thesis originated from a partnership of the Faculty of Science, University of South Bohemia, the Institute of Microbiology of the Academy of Sciences in Třeboň and the Department of Biology, Jan Evangelista Purkyně University in Ústí nad Labem, supporting doctoral studies in the Biophysics study programme.

List of papers and author's contribution (see Annexes)

The thesis is based on the following papers and manuscripts listed in chronological order, and added in full as separate parts in the Annexes:

I. **Štofik, M.**, Šoltová, P., Formanová, M., Masojídek, J., and Malý, J., 2008. Development of novel immobilization strategies for a PSII biosensor based on sol-gel and thin layer methods. *Manuscript in preparation*.
Marcel Štofik was responsible for management of experiments, measurements and writing the manuscript.

II. **Štofik, M.**, Strýhal, Z., and Malý, J., 2009. Dendrimer-encapsulated silver nanoparticles as a novel electrochemical label for sensitive immunosensors. Biosensors and Bioelectronics. Vol. 24, no. 7, pp. 1918-1923 (IF = 5.361).
Marcel Štofik was partially responsible for management of experiments, measurements and preparation the manuscript.

III. Malý, J., Lampová, H., Semerádtová, A., **Štofik, M.** and Kováčik, L., 2009. The synthesis and characterization of biotin-silver-dendrimer nanocomposites as novel bioselective labels. Nanotechnology. Vol. 20, no. 38, pp. 385101 (IF = 3.652).
Marcel Štofik collaborated on experiments, measurements and revision of the manuscript.

IV. **Štofik, M.**, Malý, J., and Frolík, J., 2010. An electrochemical microfluidic detector for ASV detection of metallic labels in immunoanalytical assays. *Manuscript prepared for submission*.
Marcel Štofik was responsible for management of experiments, measurements and writing the manuscript.

V. **Štofik, M.**, and Malý, J., 2011. Držák pro mikrofluidní čip z polymeru polydimethylsiloxanu, Application of utility model PUV 2011-25393, registered 27-12-2011 at the Industrial Property Office.
Marcel Štofik was responsible for designing, managing the fabrication of holder and writing the manuscript.

VI. **Štofik, M.**, and Malý, J., 2012. Magnetic beads trapping in a microfluidic system - computer simulations of magnetic field and fabrication of a magnetic separator. *Manuscript in preparation*.
Marcel Štofik was responsible for management of experiments, measurements and writing the manuscript.

I declare that my role in the publications and manuscripts was as stated above. On behalf of the co-authors, the declaration is confirmed by:

Mgr. Jan Malý, Ph.D.   ....

In Ústí nad Labem, 22 may 2012   ....
                                                                    Marcel Štofik, the author

Abbreviations and symbols

AFM	Atomic force microscopy
Ag-DNCs	Silver-dendrimer nanocomposites
BSA	Bovine serum albumin
DCC	N,N´-dicyclohexylcarbodiimide
DGS	Diglyceryl silane
DMSO	Dimethyl sulfoxide
DPASV	Differential pulse anodic stripping voltammetry
EBL	Electron beam lithography
EI	Electrochemical immunoassays
ELISA	Enzyme-linked immunosorbent assay
EMI	Electrochemical magneto-immunoassays
FTIR	Fourier transform infrared spectroscopy
G5, G6, G7 dendrimer	Fith, sixth, seventh generation dendrimer
GA	Glutaraldehyde
LED	Light-emitting diode
LOC	Lab-on-a-Chips
LOD	Limit of detection
MBs	Magnetic beads
MFS	Microflow cell system
MPs	Magnetic particles
PAMAM-OH dendrimer	Hydroxyl-terminated polyamidoamine dendrimer
PDMS	Polydimethylsiloxane
PEG	Polyethylene glycol
PMMA	Polymethyl methacrylate
PSII	Photosystem II
RSP	Reference standard of phytotoxicity
SAMs	Self-assembled monolayers
SPR	Surface plasmon resonance
TEM	Transmission electron microscopy
XPS	X-ray photoelectron spectroscopy
µTAS	Micro total analysis systems

Contents

1. Introduction

1.1. Sensors and biosensors

A chemical sensor is a device which transforms chemical information into an analytically useful signal. Chemical sensors contain two basic functional units: a receptor part and a transducer part. In the receptor part of a sensor, chemical information is transformed into a form of energy which may be measured by the transducer. The receptor is based on physical, chemical, or biochemical detection principles. The transducer part is a device capable of transforming the energy carrying chemical information about a sample into useful analytical signal (Hulanicki et al. 1991).

Biosensors are chemical sensors which use specific biochemical reactions mediated by isolated enzymes, immunosystems, tissues, organelles or whole cells to detect chemical compounds usually by electrical, thermal or optical signals (Nagel et al. 1992). According to recommendations of the International Union of Pure and Applied Chemistry, biosensors are defined as self-contained integrated devices capable of providing specific quantitative or semi-quantitative analytical information (Thévenot et al. 2001).

The beginning of the era of biosensors is dated by the development of an amperometric glucose oxidase biosensor published in 1962 (Clark & Lyons 1962). This type of biosensor was also the first commercially available biosensor introduced to the market by the Yellow Springs Instrument Company (Ohio, USA) in 1975 (Newman & Turner 2005). General advantages of biosensors are rapid and sensitive detection, portability, low cost production and possible miniaturization. For wider commercial use, the biosensors have to fulfill a number of criteria. They have to be highly specific and stable for long-term storage. The analysis has to proceed without a complicated pre-treatment. The response should be accurate, precise, reproducible, and linear over the whole range of regarded concentrations with low noise-to-signal ratio. Depending on their use, they have to be biocompatible with tiny probes and provide a real-time analysis. Even semi-skilled operators have to be able to use biosensors (Grieshaber et al. 2008). As it is demanding to satisfy all the listed criteria, only a few types of such devices have been commercially produced so far.

On the other hand, biosensors as analytical devices have already found their application in many fields of human activity such as in biological and medical diagnostics (Vo-Dinh & Cullum 2000; Piunno & Krull 2005; Wang & Katz 2010), environmental monitoring (Marco & Barceló 1996; Baeumner 2003; Belkin 2003; Rodriguez-Mozaz et al. 2006; Rogers 2006), safety control or defense interest (Paddle 1996; Shah & Wilkins 2003; Pohanka et al. 2007), or food quality monitoring (Mello & Kubota 2002; Leonard et al. 2003; Amine et al. 2006; Lazcka et al. 2007). Besides, there has been a great interest in research in the domain of biosensors which has increased mainly in the past two decades and thus, the potential for biosensor applications has

extended rapidly. The amount of published articles on the topic "biosensor" has doubled every 5 years (www.webofknowledge.com).

Two features are essential for the functioning of a biosensor: (i) biological recognition and (ii) a transducer element. The general classification of biosensors is based on these two functional features. According to the transducer, the biosensors are usually divided into electrochemical, optical, and piezoelectric (mass transport) classes. Electrochemical biosensors include sensing molecules which translate the sensed information into an electric signal proportional to the concentration of the analyte. In optical biosensors, the recorded information is converted into a signal which is detected on the basis of absorption, luminescence, or light scattering. Piezoelectric biosensors have sensing molecules which are attached to a piezoelectric surface, where the sensed signal is translated into mechanical vibrations as interactions between the analyte and the sensing molecules. These vibrations can be modified into an electrical signal.

1.2. *Electrochemical biosensors and detection techniques*

Electrochemical biosensors are probably the most widely used types of biosensors due to their fast response, their simplicity, and their lower costs in comparison with optical, calorimetric and piezoelectric biosensors (Mehrvar & Abdi 2004).

There are three main types of electrochemical biosensors according to the method of electrochemical detection (Mikkelsen & Cortón 2004):

- Amperometric biosensors where the current produced on a working electrode in response to applied potential is measured. Under mass-transport-controlled conditions, it is directly proportional to analyte concentration. Many biosensors work on this detection principle (Gregg & Heller 1990).

- Potentiometric biosensors monitor the difference in potential established on a permselective membrane in a solution by using two electrodes. The principle is based on using an ion-selective electrode or an ion-sensitive field-effect transistor. During the measurement, no significant current is flowing between the electrodes. The biosensors based on this method rely on a logarithmic relationship between the measured potential and analyte concentration (Mulchandani et al. 1999; Lakard et al. 2004).

- Conductometric biosensors measure the changes in electric current according to applied voltage between two electrodes in bulk solution. The measured current is directly proportional to the conductivity of the solution as a result of chemical or biological processes dictated by ionic strength. An interdigitated array of electrodes is often preferred in a biosensor transducer construction (Cullen et al. 1990; Sheppard et al. 1993).

Amperometric biosensors use an electroanalytical technique which measures current as a function of potential. In chronoamperometry the current is measured as a function of time under the condition of fixed potential. By applying this technique, the oxidation or reduction potential of electroactive species has to be known and its

concentration in an analyzed sample is proportional to the measured current. When the potential varies in time under specific conditions and the current is measured as a function of potential, the technique is called voltammetry or voltamperometry. In voltammetry or voltamperometry, the occurrence of a sharp peak in the presence of electroactive species is registered in a voltammogram (a graph of current vs. applied voltage). Voltammetry techniques can be divided into chronoamperometry, polarography or polarommetry, cyclic voltammetry and different types of pulse voltammetry techniques for determination of electroactive or other analyzed species in the target solution (Wang 2006a).

Stripping analysis represents a highly sensitive electrochemical technique employed mainly for analysis of trace metals (Wang 1985). Its sensitivity is attained by employment of two consequent analytical steps. First, when a small portion of metal ions in solution are preconcentrated on an electrode by electrolytic deposition. Second, the deposited species are dissoluted (stripped) by using various stripping techniques. These techniques are annotated as anodic stripping voltammetry, potentiometric stripping analysis, adsorptive stripping voltammetry and potentiometry, cathodic stripping voltammetry, abrasive stripping voltammetry. Another advantage of stripping analysis is that more than one type of metal can be measured simultaneously at concentration levels as low as 10^{-10} M using relatively inexpensive instrumentation (Wang 2006a).

Transducers for amperometric biosensors can be constructed in two (reference and working) or three (reference, working and counter) electrode configurations. The advantage of a three-electrode configuration is better control of the potential on the working electrode. The reaction takes place on the working electrode and the material of the working electrode can influence the performance of an assay. The most popular are compounds containing mercury, carbon, or noble metals such as platinum and gold. The reference electrode controls stable potential applied on the working electrode and the counter electrode carries the measured current. Reference electrodes are often submerged in an aqueous medium such as silver/silver chloride or the saturated calomel electrode. For counter electrodes, also noble metals such as platinum are suitable. These electroanalytical components are parts of a simple analytical electrochemical cell.

The most common technology for the mass production of transducers for electrochemical biosensors is thin-film technology (Albareda-Sirvent et al. 2000). Due to low costs, portability and versatility of such fabricated transducers, screen-printed sensors have become very popular. They enable *in-vivo* and *in-vitro* assays of real samples and there is a number of commercial sources which offer sensors with various electrode configurations (Tudorache & Bala 2007).

Now, one of the fastest growing platforms for the development of bioanalytical tools including electrochemical sensors is a microfluidic lab-on-chip platform (Mark et al. 2010), where miniaturization of micro- or nano-sized electrochemical transducers can

be performed by microfabrication. Besides, a microfluidic lab-on-chip platform enables automated or semi-automated electrochemical analysis (Cunningham 2001).

1.3. *Biosensor recognition elements and their immobilization*

Sensing elements of biosensors can be divided into two categories which differ in their natural function:

- Biocatalytic recognition elements exploiting enzymes (Albareda-Sirvent et al. 2000), cells (Pancrazio et al. 1999) or cells tissues (Campàs et al. 2008). Biocatalytical biosensors are the best known and they have been most frequently applied. The principle of this category of biosensors is that an immobilized biocatalyst is incorporated into the sensor and transient or steady-state responses are monitored by an integrated detector.

- Affinity recognition elements – the recognition element is a bioreceptor which recognizes and binds particular targets with high affinity. Biosensors of this category are based on the interaction between biomolecules and substances present in the analytes, i.e. mostly antibody-antigen interactions (North 1985), receptor proteins interactions which are of nonimune origine (Panayotou et al. 1993), and nucleic acid binding interactions (Millan & Mikkelsen 1993). At present, an improvement of the binding properties of bioreceptors is enabled by the progress in molecular biology (genetic engineering) (Hock et al. 2002).

Suitable location of biorecognition elements in electrochemical biosensors is in the immediate vicinity of the transducer or directly on its surface, often on the surface of the working electrode. This is performed by suitable immobilization techniques that depend on the bioreceptor. The employed procedures are binding to a solid surface by physical or chemical adsorption, or by a covalent bond, cross-linking between molecules, entrapment within a membrane, within a surfactant matrix, a polymer or a microcapsule (Sheldon 2007; Sassolas et al. 2012). In an immobilization process, it is important that biomolecules retain their stable form with sufficient activity and recognition properties for the effective biosensing after immobilization.

The immobilization of biomolecules by adsorption to a solid support is proceeded mainly by electrostatic or van der Waals forces, hydrophilic/hydrophobic interactions (weaker binding), or by ionic binding (stronger binding). Advantages of these immobilization techniques are that they are relatively simple and inexpensive and do not chemically modify the immobilized molecules. A disadvantage is the tendency of the immobilized molecules to release from the carrier when a fluid media is used. In spite of that, stable biosensors with good characteristics might be constructed by employment of simple adsorption (Bonnet 2003).

To overcome the tendency of the immobilized molecules to leach from the carrier during the adsorption immobilization and to fix the molecules to the support tightly, covalent binding techniques can be applied. Covalent immobilization might be preferred

when working in aqueous solutions and when denaturing factors exist (Hanefeld et al. 2009). A disadvantage of covalent binding is chemical modification of the immobilized molecules that can lead to a loss of their biocatalytical recognition or binding abilities. Although it is difficult to attain uniform orientation of molecules when using the covalent immobilization, there are techniques which solve this problem, such as immobilization of proteins to surfaces through immobilization of glycoproteins through carbohydrate residues, immobilization of biotinylated proteins to surfaces containing avidin, or immobilization of proteins through a polyhistidine tail to immobilized metal affinity chromatography supports (Rao et al. 1998). Biosensors with the covalent type of immobilization have a biorecognition element bound to the surface of a transducer through functional groups which are not essential for the recognition activity of the biosensors. The binding is generally carried out by initial activation of the surface using multifunctional reagents, followed by enzyme coupling to the activated support. Self-assembled monolayers (SAMs) can serve as an interface layer between the immobilization surface and the species present in the solution or in the vapor phase (Chaki & Vijayamohanan 2002). SAMs are created by chemisorption which provides strong covalent binding of organic molecules to different types of substrates and can provide the thin self-assembled monolayers with a tunable thickness (Ulman 1991). Chemisorption can also be used for direct biomolecule immobilization (without any interface) on a gold surface when a direct bond between thiol groups and the gold substrate is created. To facilitate the creation of the bond, cysteine amino acids can be incorporated genetically into the native enzyme for effective immobilization on a gold electrode surface (Gwenin et al. 2007). To facilitate direct covalent immobilization of biomolecules on the solid support of a transducer, immobilization through conducting polymers has been widely studied and employed (Ahuja et al. 2007).

Cross-linking immobilization is performed by a suitable bifunctional crosslinking agent. In this technique, biomolecules are not attached to the surface of the transducer, but cross-linked together, and a functionally inert protein such as albumin is added to the immobilization matrix as a stabilization factor. This method is attractive because of its simplicity; however, the influence of the cross-linking immobilization on the stabilization of the proteins has been discussed (Martinek & Torchilin 1988; Wong & Wong 1992). Although cross-linking can stabilize the biomolecules due to strong chemical binding between the biomolecules, it can decrease their activity as a result of distortion of the conformation of the active biomolecule and chemical alterations of the active site during the cross-linking process. Glutaraldehyde is one of the well-known and one of the frequently used crosslinkers (Walt & Agayn 1994).

In comparison with covalent immobilization immobilization by entrapment can be more suitable for biorecognition molecules. The sensing elements are not chemically modified and are entrapped into the immobilization matrix with preserving their native conformation. Although direct contact with the environment is prevented, mass transfer limitations and low enzyme loading can be an issue (Lalonde and Margolin 2002). One of the widely used entrapment techniques is immobilization in silica sol–gel matrices

which are formed by hydrolytic polymerizations (Pierre 2004). The entrapment into silica gel is based on growing of siloxane polymer chains around the encapsulated biomolecules. Additives such as polyethylene glycol (Soares et al. 2006) or albumin can be added to immobilization matrices.

1.4. *Biosensors for environmental monitoring*

Environmental pollution is the result of the fabrication and the use of existing and newly developed chemicals. Industrial production of chemicals contributes to the improvement of human health, welfare and lifestyle. On the other hand, the air, soil and water pollution has become a serious problem over the past few decades. High levels of chemical residues in the environment and accumulation of chemicals in food chains can have a severe impact on the human health and the ecosystems.

Pollutants are chemical compounds and they are usually classified according to their chemical structure. All of them have a specific mode of action and they are described as cytotoxic, carcinogenic, mutagenic or genotoxic compounds. Biosensors as bioanalytical tools can be used for their detection and monitoring. Environmental pollutants are toxic and they often have an inhibitory effect on enzymes and cells organisms. This effect is widely used in biosensors when considering their construction. Analytical tests including biosensoric analyses provide information about the presence of a single chemical. However, the toxic effect on organisms occurs either at high concentrations of a single substance or at low concentrations of a mixture of substances. Therefore, the overall toxicity is monitored rather by whole organisms than by biosensors, e.g. wastewater, which is often monitored by biotests with various prokaryotic and eukaryotic organisms. (Castillo 2001). For this purpose, bacterial biotests (Bitton & Dutka 1983) or fish bioassays (Sprague 1969; Loose et al. 1993) can be used.

Biosensors for detection of organic type pollutants include biosensors for pesticides (Bauer et al. 1996), polychlorinated biphenyls (Bender & Sadik 1998), phenols (Ruzgas 1995), bisphenol A (Yin et al. 2009), and many others. These biosensors are based on different types of detection including electrochemical analysis and have been reviewed widely in (Andreescu & Sadik 2004; Barceló et al. 2004; Rodriguez-Mozaz et al. 2006).

Inorganic types of pollutants are mainly heavy metals, phosphates and nitrates. Enzyme-based, protein-based, DNA-based, whole-cell based, and genetically modified organism-based biosensors have been tested for the detection of heavy metals such as mercury, iron, copper, cadmium, chromium, lead, zinc, nickel aluminum, and arsen (Corbisier 1999; Verma & Singh 2005). Electrochemical biosensors for heavy metal detection also use the principles of inhibition of enzymes such as inhibition of urease (Krawczyński vel Krawczyk et al. 2000), alkaline phosphatase (Berezhetskyy et al. 2008), glucose oxidase (Ghica & Brett 2008), acetylcholinesterase (Stoytcheva 2002), or

nitrate reductase (Wang et al. 2009). Phosphate (Wollenberger et al. 1992) and nitrate (Larsen et al. 1997) determining electrochemical biosensors have also been developed.

1.4.1. Biosensors for the detection of pesticides

Pesticides are an important group of environmental pollutants. There are several classes of pesticides depending on the target organisms against which they act. They are widely used in agriculture for the regulation of the growth of plants, as defoliants, as agents which prevent the premature fall of fruit, or inhibit the deterioration of crops by pests such as insects, fungi, mollusks, bacteria and others. These chemicals belong mainly to organophosphate and carbamate pesticides. They are preferred to e.g. organochlorine pesticides for their relatively low persistency in the environment (Skládal et al. 1997).

Detection of pesticides which acts on the catalytic activity of enzymes from the cholinesterase group has been the most frequent biosensoric detection method based on an electrochemical principle (Bernabei et al. 1991; Skládal 1996). The principle is based on enzymatic hydrolysis of acetylcholine on choline and acetic acid in the presence of acetylcholinesterase. Because organophosphorus pesticides imitate the molecular shape of the substrate acetylcholine, they can bind irreversibly to the esteratic active sites of the enzyme and inhibit its activity (Trojanowicz & Hitchman 1996). For immunosensing of pesticides, binding proteins have been developed (Miller & Lenz 2001) and there are many electrochemical biosensors integrated into flow-injection analysis (Prieto-Simón et al. 2006). The detection of pesticides can also be performed by stripping analysis without the use of enzymes (Liu & Lin 2005) or by bacterial electrochemical sensors (Stoytcheva 2010).

Besides cholinesterase, other enzymes such as tyrosinase, alkaline phosphatase, aldehyde dehydrogenase, acid phosphatase, acetolactate synthetase or peroxidase have been employed (Solé et al. 2003a; Solé et al. 2003b; Solna et al. 2005).

In general, most of the above mentioned methods use enzyme systems based on substrate conversion or inhibition of the enzyme activity, and bioaffinity assays based mainly on antibody-antigen interactions (Nistor & Emneus 1999).

1.4.2. Biosensors for the detection of herbicides based on photosynthetic proteins

Herbicides are a group of pesticides widely used to improve crop production by weed suppression. There are many strategies for monitoring of herbicides in soil and water according to their inhibition mechanisms on the photosynthetic apparatus. For the detection of herbicides which block electron transport chain, electrochemical biosensors based on photosynthetic proteins have been developed (Giardi & Pace 2005). Besides photosynthetic proteins, also whole cells biosensors (Podola et al. 2004; Shitanda et al. 2005) and immunoaffinity detection techniques (Fránek & Hruška 2005) can be used.

Many biosensors based on blocking the photosynthetic electron transport chain use PSII as a sensing element (Giardi et al. 2001). PSII is a multi-enzymatic chlorophyll-

protein complex embedded in the thylakoid membrane of cyanobacteria, algae and higher plants, which catalyses oxidation of water to molecular oxygen transporting electrons to plastoquinone and protons inside thylakoids. It consists of about 25 polypeptides which make up a reaction center, of a water-splitting system called an oxygen-evolving complex, and of a light-harvesting chlorophyll protein complex for algae and plants, and phycobilisomes for cyanobacteria. The PSII reaction center is composed of D1 and D2 proteins, cytochrome b_{559} and few low molecular mass polypeptides. Both, D1 and D2 proteins have binding sites for 4 chlorophylls, 2 pheophytins, 1 non-heme iron, 1 or 2 carotenoids and 2 quinones, Q_A (bound to D2) and Q_B (bound to D1) (Mattoo et al. 1999). Photosynthetic herbicides block electron flow through the PSII complex by binding to the Q_B binding site of the D1 protein (Moreland 1980; Duke 1990).

Koblížek and co-workers developed an electrochemical biosensor for the detection of residual triazine-, urea- and phenolic-type herbicides (Koblížek et al. 1998). They used isolated PSII complex from the thermophilic cyanobacterium, *Synechococcus elongatus*. The PSII preparation was immobilized between the dialysis membrane and the Teflon membrane of the Clark oxygen electrode mounted in a flow cell with illumination. In further development of the biosensor, the PSII complex was immobilized on a screen-printed sensor composed of a graphite working electrode and a Ag/AgCl reference electrode deposited on a polymeric substrate (Koblížek et al. 2002). Both biosensors achieved high sensitivity with the limit of detection (LOD) 5×10^{-10} M and 1×10^{-9} M for diuron, respectively. Similarly, an amperometric multi-biosensor biosensor with thylakoids isolated from spinach immobilized on the surface of screen-printed sensors composed of a graphite-working electrode was set-up by Tuoloupakis at al. (2005). This biosensor was successfully tested on river samples where the LOD of $\sim 1 \times 10^{-8}$ M for diuron was found. Both types of biosensors used a crosslinking immobilization method by glutaraldehyde (GA). Another amperometric biosensor with immobilized thylakoids extracted from spinach on a screen printed electrode achieved even a nanomolar range of the LOD for diuron (Bettazzi et al 2007).

With the aim to enhance the sensitivity of biosensors, the further development of biosensors focused mainly on searching suitable immobilization techniques such as immobilization of an isolated PSII complex on SAMs of electrodeposited conductive layers with a mediatorless detection principle (Malý et al. 2005), or immobilization of thylakoid membranes on SAMs with a mediated electron transport to a working electrode (Bhalla & Zazubovich 2011). A laser-induced forward transfer immobilization technique for stable and highly efficient junctions between biomaterial and solid-state devices onto screen-printed sensors was performed for spinach thylakoids (Touloupakis et al. 2012). In order to improve these biosensors further, there have been attempts to employ genetically modified proteins because of their better stability (Sugiura & Inoue 1999).

In spite of the fact that these biosensors can detect even nanomolar concentrations of certain classes of herbicides, they are not selective. Another drawback can be the instability of the biosensors when their photosensitive protein complex is illuminated by day light. On the other hand, it is possible to miniaturize them into a compact form, they are rapid, and they outperform the standardized inhibition tests. When compared with the standard algal growth inhibition test as the method of a pollutant assay defined by the European Standard (EN ISO 8692:2004), electrochemical biosensors based on a PSII complex can achieve two-orders higher sensitivity for diuron and the time of the assay can be reduced from 72 hours to 1 hour (Masojídek et al. 2011). Other photosynthesis-based biosensors are reviewed by other authors (Giardi et al. 2001; Giardi & Pace 2005; Campàs et al. 2008).

1.5. *Biosensors for biomedical applications*

Biosensors for biomedical applications are targeted to detect biomedical analytes (Tombelli et al. 2005; Ahmed et al. 2008) such as microbe pathogens (Lazcka et al. 2007), proteins, or typical disease markers in blood or other body fluids (Luppa et al. 2001). Biomedical biosensors can also be used in molecular diagnostics (Piunno & Krull 2005), or drug action analysis (Cui et al. 2006).

A number of successful attempts on development of effective biosensors have been published. Chung et al. (2011) demonstrated a semi-integrated biosensor for the detection of rare circulating tumor cells in blood. The system consisted of a cell enrichment module by a combination of immunomagnetic isolation and size filtration in a syringe set-up and a cell identification module where the cells were further concentrated via magnetic sorting in microfluidic channels and captured by antibodies on a microelectrode array. Single electrodes achieved high sensitivity down to 10 cells and a wider detection range up to hundreds of cells in milliliter-sized blood samples could be detected by impedance spectroscopy. The biosensor enabled to follow the changes of the number of circulating tumor cells (CTCs) in patients, which is highly demanded for therapy monitoring applications. Brahim (2001) constructed a biosensor with amperometric determination of cholesterol. The response time of the biosensor was 30 s and when it was applied to the analysis of cholesterol in serum samples of clinical patients, the value of 0.998 was obtained for the correlation between the biosensor measurements and the results obtained by a standard hospital method using an Abbott V.P. Chemistry Analyzer. A uric acid amperometric biosensor was developed which showed high thermal stability and an electrocatalytic activity to the oxidation of uric acid without the presence of an electron mediator (Zhang 2004). When the results of the biosensor were compared with the results carried out by a local hospital using a spectrophotometric method, the results preciously corresponded.

There also exist commercial biosensors for *ex-vivo* and *in-vivo* clinical monitoring of glucose, lactate, uric acid, cholesterol and other substances in blood samples (Ramsay 1998, Malhotra & Chaubey 2003).

Despite the progress in the development of biosensors for biomedical application, their actual use is often problematic. The reasons, why biosensors, which are successful in academic environment, are not transferred to the market, lay in the functional properties of the biosensors. These are sensitivity and selectivity when using real samples, multiplexing for the possibility of simultaneous determination of several biomarkers where arrays of sensors need to be developed on the same chip, miniaturization, portability, and automated functioning for operation without special training (Song et al. 2006). There are a number of other criteria which need to be taken into account such as the cost of assay, regulatory requirements, control of the quality, instrumentation design and the selection of test parameters.

1.5.1. Electrochemical immunosensing

Immunoassays are widely used for clinical purposes, either because no other type of assay system is feasible, or because they are often the most effective and suitable analytical method (Gosling 1990). They have become a standardized bioanalytical method for quantification of proteins or other small molecules. Immunoassays can be classified as homogeneous or heterogeneous. In a homogeneous immunoassay, antibodies interact with antigens directly in the solution. The difference between bounded and unbounded proteins is determined by physical or chemical changes during the binding reactions. In a heterogeneous immunoassay, antibodies are immobilized on a solid support and interact with other immunoreactants at the boundary layer. A heterogeneous immunoassay is a multistep assay with multiple mixing, incubating and washing steps. A specific format of a heterogeneous immunoassay with enzyme labels is called an Enzyme-Linked Immunosorbent Assay (ELISA). In an ELISA, microtitre plates are often used as solid supports. In a heterogeneous immunoassay, also test tubes, plastic beads or other types of solid supports can be used. Both types of immunoassays can be further classified into competitive or non-competitive assays. In competitive assays, target antigens compete with labeled antigens for a limited number of antibody binding sites. The signal is inversely proportional to the antigen concentration. Competitive assays are mostly used for small antigens with a limited number of binding sites. In non-competitive assays, antigens are binding by an excess of antibodies and subsequently detected after binding of a second set of labeled antibodies. Labeled antibodies bind to the antigen at a different binding site. Non-competitive immunoassays are also called "sandwich" immunoassays and are suitable for larger antigens with more binding sites. Their signal is proportional to the antigen concentration.

In comparison with nearly all other analytical techniques, electrochemical detection assays have the advantage of being inexpensive, robust and relatively simple to operate (Caygill et al. 2010). Due to improvement of immunoassay formats in biosensors (North 1985; Rogers 2000) and their sensitivity and promptness, electrochemical immunoassays have been widely used and a number of different approaches have been developed (Heineman et al. 1979; Warsinke et al. 2000; Díaz-González et al. 2005; Ng et al. 2010).

1.5.2. Labels for electrochemical immunosensors

Immunoassays take part in bioaffinity assays, where bioaffinity elements determine the selectivity, sensitivity, and stability of the assays. In general, affinity-based biosensors can be divided into two main categories: label-free and labeled. Label-free biosensors do not contain labels for signal detection. Their advantage is that they enable a real-time measurement including the evaluation of binding kinetic parameters. Most label-free biosensors are optical such as surface plasmon resonance (SPR), acoustic based on quartz crystal resonators, and calorimetric (Cooper 2003). Electrochemical detection employs capacitive biosensors (Berggren et al. 2001). Apart from that, also (volt)amperometric electrochemical methods have been used for signal detection in label-free biosensors based on the use of oligonucleotides (Souza et al. 2011), DNAs (Wang 1999), or aptamers (Le Floch et al. 2006).

Labeled biosensors utilize specific labels, which are attached (conjugated) to one of the binding recognition elements, either to the ligand or to the receptor, and in immunoassays to antibodies or antigens. Detection or amplification of the biosensor signal is performed by optical, electrochemical, or other suitable method capable of recognizing the label. Radioisotopes (Yalow & Berson 1959), enzymes (Nakane & Pierce 1966), fluorescent dye (Coons 1956) labels have been the first immunoanalytical labels used in immunohistology. They have become standard labels in immunoassays and immunosensors. With the progress in synthesis of nanomaterials, new detection strategies have allowed to use other types of labels such as metals, alloys, semiconductors, magnetic particles (Richardson et al. 2001), and other materials (Liu & Lin 2007).

Unique chemical and physical properties of nanoparticles make them suitable for designing new and improved sensing devices, especially electrochemical sensors and biosensors (Luo et al. 2006). Apart from their use for immobilization of biomolecules, for catalysis of electrochemical reactions, for enhancement of electron transfer, and as reactants, nanoparticles can be also used for labeling biomolecules. The majority of research has been focused on two types of nanolabels, quantum dots and metallic nanoparticles (Penn 2003). A detailed overview of their use is reviewed in (Niemeyer 2001; (Hernández-Santos et al. 2002; Penn 2003).

Quantum dots and metallic nanoparticles as analytical labels of biomolecules in combination with stripping voltammetry represent a very powerful electrochemical analytical method (Wang 2006b). Immunoassays, where immunoreactants are employed with electrochemical detection of metallic labels, are also reported as electrochemical metalloimmunoassays. Generally, the principle of metalloimmunoassays is based on two analytical steps. The first step includes specific immunoaffinity reactions, which are followed by sensitive electrochemical stripping analysis. The sensitivity of metalloimmunoassays is competitive with a colorimetric ELISA (Dequaire et al. 2000) and can be further enhanced. An electrochemical DNA hybridization detection assay

using silver nanoparticles as an oligonucleotide labeling tag, for example, it allows to determine the trace of 0.5 pM of the target oligonucleotides (Cai et al. 2002).

Quantum dots such as cadmium sulfide, zinc sulfide, copper sulfide, and lead sulfide can be used to differentiate the signals of proteins or DNA targets in combination with a sandwich immunoassay and a hybridization assay, respectively. By stripping voltammetry, the corresponding metals are detected by a distinct voltammetric peak. A multi-target detection of proteins (Liu et al. 2004) and DNA (Wang et al. 2003) has been demonstrated with the possibility of multiplexing and carrying out multiple measurements at once.

Widely reported metal nanoparticles are gold (Dequaire et al. 2000) and silver nanoparticles (Cai et al. 2002). Also alloys such as Cu@Au have also been successfully applied in immunosensors (Cai et al. 2003).

Enhancement of immunosensors with metal labels can be performed by application of metal-enhanced gold nanoparticles, where functional gold nanoparticles act as catalysts to reduce gold or silver ions on themselves (Chen et al. 2007). The nanopaticles are enlarged and when they are detected, a higher signal can be measured. Another strategy for enhancement of sensitivity is loading more tags per a labeled biorecognition molecule, thus per a binding event. It can be accomplished by linking the biomolecules to polymeric carriers, which carry the sensing tags on their surface or by hiding the tags in the interior of the polymeric structures (Katz et al. 2004).

For the purpose of carrying metal nanoparticles, dendrimers can be used (Tomalia et al. 1990). Dendrimers are highly branched monodisperse macromolecules. Their physical and chemical properties are dependent on their structure. The main structural parts of dendrimers are a core, a shell and end-groups. They are reported as well-suited carriers of metallic nanoparticles (Crooks et al. 2001). Nanoparticles are stabilized by encapsulation within the dendrimer, and therefore they do not agglomerate. Due to their fairly uniform composition and structure, dendrimers yield well-defined nanoparticle replicas. Another advantage of dendrimers as nanoscaffolds for carrying metal nanoparticles is a variety of functional groups that can be attached to their terminal branches. The branches are exposed on the periphery of the polymer, which can facilitate linking to biorecognition agents by a suitable method.

Dendrimers which carry metal nanoparticles are also referred to as metallodendrimers. According to the four most common configurations with nanoparticles in the dendrimer structure, nanocomposites can be classified into dendrimer-encapsulated metal nanoparticles, dendrimers modified on the periphery with metal ions or complexes, core metallodendrimers, and focal-point metallodendrimers (Niu & Crooks 2003).

The published results show that dendrimer-encapsulated silver nanoparticles used as electrochemical labels have a high potential for development of a sensitive microfluidic metalloimmunosensor with detection limits comparable to ELISA methods (Malý et al. 2009; Štofik et al. 2009; Szymanski et al. 2010; Szymanski et al. 2011).

1.5.3. Magnetic bead-based immunosensors

Magnetic particles (MPs) or magnetic beads have been studied as solid supports in immunoassays (Guesdon & Avrameas 1977) and electrochemical immunoassays (Robinson et al. 1985; Weetall & Hotaling 1987). In electrochemical immunoassays (EI), immunoreactants are mostly immobilized on the surface of the transducer. In magneto-electrochemical sensing or in electrochemical magneto-immunoassays (EMI), MBs are used as an immobilization solid phase. In an EMI, the immunoreaction is performed outside of the transducer and the whole assay usually takes place in test tubes. In each incubation and washing step, immunoreactants are mixed in a shaking mixer and concentrated on the wall of the tube by using a commercially available magnetic separator, or other type of a strong magnet. After the immunoreactions, the MBs complexed with immunoreactants are transferred to an electrochemical detector and electrochemical detection follows. MBs can be magnetically concentrated onto a working electrode or in its immediate vicinity with a magnet (Yu et al. 2006; Eguílaz et al. 2010; Moreno-Guzmán et al. 2011) and the measurement is carried out.

A comparison of both methods, EI and EMI, has been reported by Centi et al. (Centi et al. 2007). Electrochemical detection was performed on screen-printed electrodes. Although both methods were optimized for electrochemical immunosensing, EMI allowed to obtain faster and more sensitive immunochemical detection. Other reported strategies for magneto-electrochemical immunosensing have concentrated for example on MBs as suitable carriers of covalently bonded enzymes for planar biosensors (Varlan et al. 1995), or on development of a flow injection magnetoimmunosensor (Solé et al. 1998). MBs can also serve as label carriers (Mani et al. 2009). They amplify the signal as a result of high load of enzyme in EI. The results obtained by such an assay are comparable to an ELISA platform. Also the results of EMI (Gundersen et al. 1992) are comparable with standard ELISA tests.

MBs are chemically and physically stable substances, biocompatible and they can be easily and quickly accumulated from large volumes of samples by applying magnetic forces on them. The surface of MBs can be chemically modified, which enables to attach biomolecules such as DNA, enzymes or antibodies. These advantages allow an enormous number of immunoassay formats (Zacco et al. 2006; Kuramitz 2009). Moreover, application of functionalized MBs in immunoassays as solid supports for immunoreactants can improve the performance of the immunological reaction due to increased surface. High loading of immunoreactants is allowed. Immunoreactions can profit from faster assay kinetics because MBs can be dispersed easily into the solution with only a gentle shaking. The analytical target does not have to migrate far in the MBs colloidal suspension.

Electrochemical magneto-immunosensors can be miniaturized and the whole immunoassay can be automated. A biosampling and an electromagnetic separation concept for miniaturized and automated EMI systems have been proposed (Choi et al. 2000). An integrated microfluidic biochemical detection system based on MBs as both

immobilization surfaces and bio-molecule carriers was developed for fast and low-volume immunoassays using magnetic beads (Choi et al. 2002). The total time required for an immunoassay was less than 20 min including the sample incubation time, and the volume of sample was less than 50 µL for five repetitive assays. The key components in the presented system were a detector and a magnetic separator.

1.5.4. Microfluidic devices

Microfluidics is known as a technique for precise control and manipulation of fluids in sub-millimeter dimensions. The definition of microfluidics was suggested as the study of flows – simple or complex, mono- or multiphasic- in artificial microsystems, i.e. systems that are fabricated using new technologies (Tabeling 2005). Microfluidics is closely connected to bioanalytical methods because the analyzed targets nearly always deal with fluids, *in-vitro* and *in-vivo* (Berthier & Silberzan 2010). Target molecules are extracted from a liquid environment, reactions on these targets are also performed in a liquid environment and in most cases, the confinement of the targets is easier in a liquid than in a gas environment.

Microfluidics is related to miniaturization and the advances in microfabrication technology enable to fabricate devices with micron or sub-micron sizes. Such devices can perform the treatment, the separation, the analysis of a sample and more. They are designed to circumvent the complexities of a sample and its matrix. Systems containing such small devices with the possibility of automation are called micro total analysis systems (µTAS) or lab-on-a-chips (LOC) (Manz et al. 1990; Harrison et al. 1992).

A complete set of fluidic operations combined with well-established fabrication technology ensuring that partial elements will be connectible, ideally in a monolithically integrated way or at least by a well-defined, ready-to-use interconnection and packaging process, creates a broad multi-segment microfluidic platform (Haeberle & Zengerle 2007). The whole platform can include other capillary, pressure driven, centrifugal, electrokinetic, and acoustic platforms (Mark et al. 2010).

According to the market of biomedical applications, there are several important requirements for microfluidic platforms such as portability and wearability, especially for the self- and point-of-care testing segments (Mark et al. 2010). The aim is therefore to manufacture miniaturized, hand-held devices with low energy consumption. Other criteria are the number of samples or assays per day, the cost of the instrument and the costs of an assay, the number of different parameters to be analyzed per sample, the amount of sample or reagents required per assay, the variety of laboratory operations that can be realized, precision, which means the volume and time resolution and the flexibility to adapt liquid handling protocols without fabricating a new chip.

Due to the possibility of miniaturization of detection devices and the accessibility of microfabrication technology to a wider research community, there has been a great interest in the employment of microfluidics in analytical devices over the past years. First, there is a strong microfluidic platform as a result of developed industrial

technology for the fabrication of microprocessors, and second, there is highly developed sensing technology via bioanalytical methods. By combining both, sophisticated miniaturized diagnostic bioanalytical tools with complex functions could be manufactured and used also out of the developed-world laboratory (Yager et al. 2006). Many µTASs and LOCs systems suitable for *in-vivo*, *in-vitro* uses and for point-of-care, self-diagnostic and laboratory analysis are reviewed in (Manz et al. 1990; Vandaveer et al. 2004; Weibel & Whitesides 2006; Yager et al. 2006; Mark et al. 2010).

2. Objectives

The main aims of the presented thesis were (i) to upgrade and improve the already developed electrochemical PSII biosensor (Koblížek et al. 2002) by a novel immobilization method and by optimization of the current measurement protocols; and (ii) to develop dendrimer-encapsulated metal nanoparticles as electrochemical labels for a microfluidic electrochemical immunosensor.

(i)   For the first series of experiments, the following partial objectives have been set in order to:

- perform and optimize sol-gel encapsulation of a PSII complex with biocompatible diglyceryl silane (DGS) and to determine the basic parameters of a PSII-based biosensor.

- compare the performance of biosensors prepared by sol-gel encapsulation with the performance of biosensors prepared by the currently used covalent crosslinking immobilization method for detection of herbicides.

- employ numerical model of the PSII-based biosensor in order to determine the degree to which the thickness of an immobilization matrix influences the performance of the biosensor.

- optimize herbicide assay of the biosensor based on the results of numerical simulations and on the results of the optimized sol-gel immobilization technique.

(ii)   For the second series of experiments, the following partial objectives have been set in order to:

- synthesize and characterize electrochemical labels with silver nanoparticles encapsulated in a dendrimer scaffold, suitable for development of an electrochemical immunosensor.

- construct a microfluidic electrochemical cell for amperometric and voltammetric electrochemical determination of analytes.

- employ a sensitive anodic stripping voltammetry technique for determination of synthesized electrochemical metal labels in bulk solution and in a microfluidic electrochemical cell.

- manufacture an effective magnetic separator embedded in a microfluidic system for trapping micron-sized magnetic particles for performing immunoassays directly in a microfluidic chip.

- perform model electrochemical immunoassays with synthesized metallic labels in a microfluidic chip with an embedded magnetic separator.

3. Materials and methods

This chapter gives a brief account of the most important methods employed in this thesis. A detailed description of all methods, materials, and chemicals can be found in the articles and manuscripts listed in Annexes.

3.1. *Preparation of PSII-based enzyme electrodes*

Preparation of covalent-crosslinking mixture

The mixture of PSII and bovine serum albumin (BSA) was prepared by mixing of 5 µL of BSA and 5 µl of a PSII complex in an eppendorf tube using a vortex. Then, 2 µL of GA were added and the mixture was mixed again.

Preparation of sol-gel mixture

DGS in deionized water was sonicated in an eppendorf tube for 15 minutes. Six µL of 10% BSA and 6 µL of the PSII complex in suspension (the content of chlorophyll ~ 125 µg/mL) were mixed thoroughly in an eppendorf tube on a vortex. Immediately after the sonication, 4 µL of DGS was added and mixed.

Immobilization of the PSII complex mixture

The surface of amperometric sensors was cleaned with distilled water and dried out with a nitrogen flow before each immobilization. The sensors were placed on a wet filter paper in an opened Petri dish. The suspension of the PSII complex was slowly thawed. 0.4 µL of the mixture was immediately dropped on the surface of the working electrode of each sensor. The opened Petri dishes with the sensors were stored at 4 °C for 20 min and then closed. Two series of biosensors were prepared – one with covalently crosslinked PSII complex and the other with the PSII complex immobilised in sol-gel.

Immobilization of thin enzyme mixture

A thin layer of the immobilization mixture on the surface of the working electrode was prepared by drop imprints. 0.5 µL of the PSII mixture was dropped on the surface of the working electrode and the whole volume was sucked back into the pipette immediately. Only a trace of the PSII complex in the immobilization mixture was left on the surface of the working electrode.

3.2. *Amperometric measurements with PSII-based sensors*

The amperometric measurements were performed using screen-printed 3-electrode sensors with a working, a reference, and an auxiliary electrode (type AC1.W1.R1), and a microflow cell system (MFS) operated by a control box unit connected to a computer with Bioanalyzer software (BVT Technologies, a.s.). Such a compact device enabled semiautomated measurements with data processing.

The principle of measurement with the PSII biosensor is based on recording the current generated by photosynthetic electron flow from water to artificial electron

acceptors (quinone) in isolated PSII complex immobilized on the printed electrode is illuminated by short pulses of red light-emitting diode (LED).

A protocol for detection of herbicides consisted of three main steps. The first step was the negative sample control, i.e. the measured current of the biosensor was left to stabilize and a series of light pulses (light/dark) was initiated. The second step was the sample analysis, i.e. the measured sample was added to the solution and another series of light pulses (light/dark) was initiated. Finally, the reference standard of phytotoxicity (RSP) was added and the last pulses (light/dark) were initiated. The measurement finished after a given series of light/dark pulses.

3.3. *Computer simulations of the PSII-based biosensor*

The computer simulations were performed with Biomodel software (Malý 2006). First, the basic parameters of the biosensor model (the initial concentration of substrate and enzyme, the diffusion coefficient for substrate, product and inhibitor, and kinetic constants) were fixed. Then, thickness of the membrane and concentration of enzyme were altered. The signal of the PSII biosensor was studied in relation with the responses of the biosensor to low (5×10^{-9} M) and high (1×10^{-7} M) inhibitor concentrations. The simulations were performed on a standard personal computer and the data were evaluated by using SigmaPlot software.

3.4. *Synthesis of dendrimer-encapsulated silver nanoparticles*

Prior to silver nanocomposite synthesis, the generation 7 (G7) hydroxyl-terminated polyamidoamine (PAMAM-OH) dendrimer were desiccated by methanol evaporation in a dryer (50 °C, 1 h) and dissolved in distilled water to yield stock solutions. Stable dendrimer nanocomposites were synthesized by mixing dendrimer and silver nitrate water solution in a molar ratio of 1/2000 dendrimer/Ag (I), and subsequent reduction of silver with sodium borohydride in 1:1 volume ratio dropwise at constant speed (10 mL/min). During the synthesis, the solution was stirred slowly. The synthesis of nanoparticles occurred immediately after the dendrimer/Ag (I) and the $NaBH_4$ solutions were mixed. The reaction was observed as color changes and the stability of the prepared nanocomposites was controlled by monitoring of a sharp plasmonic peak at 410 nm by UV-VIS spectrophotometer (Unicam UV 500, Thermo Spectronics, USA).

Nanocomposites were characterized by: (i) UV–VIS spectral analysis, (ii) atomic force microscopy (AFM) with an atomic force microscope Integra Probe Nanolaboratory (NT-MDT, Russia) with the close-loop sample scanning arrangement and the semi-contact resonance mode, (iii) transmission electron microscopy (TEM) with a Tecnai G2 Sphera 20 microscope equipped with a LaB6 cathode and a 2048×2048 Gatan Ultrascan 1000 CCD camera of a pixel size 14 μm, and (iv) X-ray photoelectron spectroscopic (XPS) analysis with a custom made X-ray photoelectron spectroscope (X-ray source: Specs XR 50, input power 200 W, Al/Mg anode, without monochromator;

Electron energy analyzer: Specs PHOIBOS, hemispherical, single channeltron; System's ultimate pressure: $<10^{-8}$ Pa)

3.5. Synthesis of a biotin-dendrimer conjugate

Biotinylated G7 PAMAM–OH dendrimers were prepared by an N,N´-dicyclohexylcarbodiimide (DCC) coupling method based on esterification of primary hydroxyls in the presence of carboxylic acids and DCC in an anhydrous environment of dimethyl sulfoxide (DMSO). First, the stock solution of dendrimer in dry DMSO was prepared by drying the dendrimer solution in an eppendorf tube under a stream of pure nitrogen and dissolving in DMSO. Biotin was added to the eppendorf tube with the dendrimer and mixed. In the same way, DCC was added to the reagent solution and mixed again. The conjugation reaction was performed for 48 h at laboratory temperature under moderate mixing on a rotary shaker. Then, the conjugate was dialyzed with a regular exchange of solvents through dialysis tubes with 8 kDa pores (Dispo-Biodialyzer, regenerated cellulose, Sigma-Aldrich Inc.). The resulting conjugate was stored at 4 ºC. For the synthesis of biotinylated dendrimer nanocomposites, biotin-dendrimer conjugate was mixed with silver nitrate and silver was reduced under similar conditions as described above.

Biotinylated dendrimers and dendrimer nanocomposites were characterized by: (i) spectral analysis, (ii) fourier transform infrared (FTIR) spectral analysis (a Nicolet iS10 FTIR spectrometer, Thermo Scientific, USA), (iii) AFM, and (iv) TEM. Binding analysis was performed by a SPR system (SensiQ, Nomadics ICx, USA), and ELISA assays.

3.6. Fabrication of an electrochemical cell and sensing electrodes

For the fabrication of an electrochemical cell, two methods were employed.

Integration of a carbon microfibre into SU-8 photoresist

The electrodes of the cell were prepared on cut and cleaned silicon wafers. The wafers were coated by SU-8 25 photoresist (MicroChem Corp., USA). The photoresist was heated (softbaked) on a hotplate and a single carbon microfibre (diameter 10 µm), separated from a multi-filament tow (Goodfellow Cambridge Ltd., UK) was put on the photoresist surface and the substrates were transferred again to a hotplate. The photoresist melted during several seconds and allowed the bottom side of the carbon microfibre to stick firmly on its surface. Then, the photoresist was exposed to UV light and heated again. Gold (Au counter electrode) and silver (Ag pseudoreference electrode) layers were deposited on the photoresist with an implemented carbon working electrode through a mask by sputter-coating (Agar, Agar Scientific Ltd., UK). The second photoresist layer was spun on the substrates and microchannel patterns (printed on transparency foil with a laser photoplotter (Pragoboard, s.r.o., Czech Republic) were deposited. The final microfluidic chip with a microchannel in SU-8 photoresist and

integrated electrodes was obtained after the second photoresist layer was processed. The microfluidic electrochemical cell was inserted into a home-made polymethyl methacrylate (PMMA) holder combined with a PDMS spacer.

A lift-off technique combined with silver electroplating

The electrodes of the cell were fabricated on cut and cleaned glass substrates. First, Au counter and working electrodes were prepared. 500 ml of a negative resist (nLOF 2070, MicroChemicals GmbH, Germany) was deposited by a pipette in the center of the glass substrate and spincoated in a one step process at 4000 rpm for 30 s, ramp 500 rpm. Then, the resist was softbaked at 100 °C for 5 min on a hotplate. The substrates were left to cool down and rest for 2 hours. After that, they were exposed to UV light through a suitable mask (counter and working electrodes) for 85 s and left to stand for two hours again. Post exposure baking followed at 120 °C for 90 s with a subsequent 2-hour relaxation. Finally, the substrates were developed in an AZ 826 MIF developer for 60-75 s, rinsed with deionized water, and dried out by a nitrogen flow. Such a substrate was ready for metal sputtering (Q150T Turbo-Pumped Sputter Coater/Carbon Coater, Quorum Technologies, Ltd., UK). Chromium (Cr) was used as an adhesion layer for the Au electrodes and was sputtered for 10 s. Then, the Au sputtering lasted 210 s. After the sputtering, the substrates were treated in DMSO until all resist residues were removed. Second, Ag pseudoreference electrodes were deposited using the same protocol as described above. The only difference was that Ag was sputtered for 180 s. After the substrate was cleaned in DMSO, electroplating was performed at 30 mA for 10 min. The electroplating solution consisted of 3 g of silver chloride, 50 g of sodium thiosulphate, and 19 mL of sodium bisulphite dissolved in 91.5 mL of deionized water.

3.7.   *Electrochemical analysis and fluid sampling in the microfluidic system*

The sampling of fluids was performed by syringe pumps, injection valves, and a microautosampler (FIAlab Instruments, USA) with appropriate software. The FIAlab system enabled precise pump timing and valve actuation by macro algorithms.

The electrochemical amperometric measurements, cyclic voltammetry, and differential pulse anodic stripping voltammetry (DPASV) detection were performed on Autolab PGSTAT 12 potentiostat (EcoChemie, Netherlands). The data were processed with General Purpose Electrochemical system (GPES) Autolab software. This software included a module for the control of the measurement processes developed in time.

The combination of designed macros in FIAlab and of the Autolab software enabled the automatic control of fluid flow according to the selected electrochemical measurement.

3.8. Designing and fabrication of masks for UV lithography

The work flow of designing a mask was set as: (i) mask designing in CorelDRAW, (ii) picture saving in the CorelDRAW native format and subsequent exporting to TIFF or PSD bitmap files, (iii) picture slicing in Photoshop or Gimp and (iv) saving the sliced pictures into TIFF files in a grayscale 8 bits color depth mode.

Glass substrates were cleaned and a chromium (Cr) opaque layer was deposited by sputtering (Q150T Turbo-Pumped Sputter Coater/Carbon Coater, Quorum Technologies, Ltd., UK). Then, negative or positive resist was deposited on the glass substrates and the designed mask patterns were deposited by electron beam lithography (EBL) in an electron microscope (VEGAII, TESCAN, Ltd., Czech Republic) with a DrawBeam software module of the microscope. The resists were developed and the Cr layer was etched. The resist residues were cleaned.

3.9. Fabrication of an SU-8 resist mold and casting of michochannels in PDMS

For the purpose of PDMS casting, a resist mold was prepared. Glass substrates were cleaned and cured. A photoresist (SU-8 2150, MicroChem Corp., USA) was deposited on substrates and softbaked. Microchannels were patterned by UV exposure through a mask and the photoresist was baked and developed. The prepared resist mold was combined with a metal mold manufactured and employed especially for this purpose.

The PDMS polymer was mixed thoroughly with a curing agent in a plastic Petri dish (ratio 10:1, v/v). The Petri dish was put into vacuum and cured until all bubbles disappeared. While the PDMS mixture was cured in the vacuum, the metal mold and the photoresist mold were prepared. The cured PDMS was carefully poured into the metal mold on the photoresist pattern in such a way that it overflowed the edges of the metal mold opening slightly. Then, a glass board was put on the metal mold in order to prevent bubble formation. Finally, the top of the metal mold was covered by a metal desk. The complete mold was immediately put on a hotplate (with 90 °C, where the PDMS was cured. After the PDMS was gently peeled from the substrate, the PDMS cast was cut to the required size and channels for fluid were punched with a suitable needle.

3.10. Computer simulations of magnetic field

Computer simulations of magnetic field were performed by a static physical model in COMSOL Multiphysic software. The model evaluated the current density in the microcoil wires, and then it calculated and plotted magnetic field, magnetic field gradient and magnetic energy gradient. The obtained data were evaluated in SigmaPlot software.

3.11. Fabrication of copper microstructures

First, copper (Cu) was sputtered on the top of the chromium (Cr) adhesion layer on cleaned glass substrates using a sputter coater (Q150T Turbo-Pumped Sputter Coater/Carbon Coater, Quorum Technologies, Ltd., UK). Positive photoresist was deposited on the substrates, heated and exposed to UV light - photoresist patterning with the desired shape of the microstructure. After the photoresist was heated again, the patterns were developed. Then, copper electroplating was performed in an electroplating solution with a laboratory power supply HC-D3030DPD (GM Electronic, Ltd., Czech Republic). Finally, the resist residues were stripped and the Cu (seed) and Cr (adhesion) layers were etched. The fabricated microcoils were isolated by SU-8 25 photoresist. The prepared chip was combined with the PDMS spacer with microchannels and a glass cover with tubings.

4. Results and discussion

4.1. A biosensor based on an isolated photosystem II complex

The development of a PSII biosensor used in this study dates back to 1998 when Koblížek at al. (1998) published an article about immobilization of PSII particles isolated from the thermophilic cyanobacterium *Synechococcus elongatus* between the dialysis membrane and the Teflon membrane of a Clark oxygen electrode mounted in a flow cell. The flow cell was illuminated by a cluster of red light emitting diodes. The evolution of oxygen was measured upon 20 s of illumination. The illumination and the fluid flow were controlled by a custom-made control box and a modified Gilson HPLC system, respectively. The biosensor showed sensitive detection of residual triazine-, urea- and phenolic-type herbicides. A significant improvement of this biosensor was done by covalent crosslinking immobilization of the PSII complex with glutaraldehyde on screen printed sensors (Koblížek et al. 2002). This amperometric biosensor offered a simple and a powerful method for immobilization of a sensing element. The operation was simplified by a flow cell with an integrated LED diode for illumination and since that, it was possible to use any commercially available screen printed sensors in combination with flow cells adopted for this purpose. The main technical improvement made by the company BVT Technologies, a. s. (http://www.bvt.cz) was development of the MFS cell able to operate automatically under software control.

In this thesis, sol-gel immobilization is described as a new method for immobilization of a PSII complex onto a screen printed electrode of the PSII-based biosensor. A newly developed immobilization procedure based on a thin membrane using modified measurement protocols is presented. They improve the biosensor sensitivity in a sense of more accurate measurements and enable to shorten the whole biosensor assay significantly (Paper I in Annexes).

A sol-gel process involves hydrolysis of precursor monomers, such as metal alkoxides, either under acidic or basic conditions followed by polycondensation of the hydroxylated units. The entrapment of enzyme into an immobilization matrix by a sol-gel process is based on growing of siloxane polymer chains around the encapsulated biomolecules. For sol-gel immobilization, a diglyceryl silane sol-gel precursor was selected as it can form glycerol during the sol-gel process. Glycerol is often used as a conservant or a cryoprotectant of biomaterial in storage buffers (Nishizawa et al. 1993). Glycerol (20 %, w/v) was also present in the storage solution of isolated PSII particles (Šetlíková et al. 1999) used during the study. Glycerol which is formed during a sol-gel process is better than methanol or ethanol formed in a siloxane matrix when the common tetramethoxysilane or tetraethoxysilane precursors are used (Brook et al. 2004) because methanol and ethanol can have a damaging effect on thylakoids (Meunier et al. 2009).

The results showed a positive effect of the sol-gel immobilization on the induced signal of the immobilized PSII complex. The measured signal of the biosensors after sol-

gel immobilization was approximately two times higher than the signal of the biosensors with covalent crosslinking by glutaraldehyde. It indicates that for the PSII complex, sol-gel immobilization is more suitable than covalent crosslinking. The advantage of the immobilization of photosynthetic complexes via a sol-gel process for retaining their photostability and activity was also described by other authors (Meunier et al. 2009; Kopnov et al. 2011). In our optimization tests with the sol-gel matrix composition, it was found out that the highest signal of biosensors was obtained with the highest content of PSII in the immobilization matrix. The signal of biosensors increased significantly when the content of the silica precursor decreased. It can be explained by lower density of the silica network and better diffusion of the artificial electron transport mediators (quinones) to the working electrode. Also Meunier et al. (2009) showed that thylakoids immobilized in a sol-gel matrix lose their activity with high contents of a sol-gel precursor. They also found out that during the first few hours of silica polymerization, hybrid gels undergo a rapid shrinkage and that the rate of the shrinkage is increased with an increase in the sol-gel precursor. Thus, the bioactivity of thylakoids within silica materials depends mainly on the silica density and on the chemical environment, both of which are controlled by the precursor concentration and by minimizing the shrinkage.

On the other hand, the apparent Michaelis-Menten constant, long term stability, and inhibition parameters measured in the presence of diuron spoke in favor of the crosslinking method. Since no other methods were tested to study the kinetics of the PSII behavior in the examined immobilization membranes, it is difficult to explain this finding. There are a number of possible reasons why lower degree of inhibition was found in sol-gel biosensors, for example higher activity of the PSII or higher concentration of BSA in the sol-gel membrane in comparison with a membrane prepared by covalent cross-linking by GA. The inhibition parameters could also be influenced by worse adhesion of the sol-gel immobilization membrane to the working electrode. These suggestions are discussed in details in Annexes. Another reason could be the fact that an immobilization membrane affects the conformation of the PSII complex in such a way that an alternative electron transfer pathway from the PSII to the electron mediator is partially enabled. Larom et al. (2010) identified a site *in silico*, poised in the vicinity of a Q_A intermediate quinone acceptor, which could serve as a potential binding site for redox active proteins. They engineered a novel electron transfer pathway from water to a soluble protein electron carrier without harming the normal function of photosystem II in the cyanobacterium *Synechocystis sp*. PCC 6803.

In this study, significant improvements of the PSII biosensor were achieved in the sense of more accurate measurements and in shortening of the bioassay duration by adjustment of the immobilization technique and the measurement protocol. The modifications were based on the results obtained by solving a numerical model of the biosensor. It was found out that the thickness of the immobilization membrane has a strong impact on the biosensor sensitivity and on the course of the measured signal. The modeled conditions showed a good correlation with the experimental data. The PSII-complex mixture was immobilized by drop imprints on the surface of the working

electrode so that a thin PSII-membrane layer on the working electrode of the screen printed sensor was created. The timing of light/dark periods (generated by light pulses when red LED are switched on/off) was adjusted, which led to shortening of the assay time and to an increase in the accuracy of the measurements. The number of the measured peaks increased from 12 to 60 in one bioassay and the time of a bioassay was reduced from 45 min to 15 min.

When using the new immobilization technique and measurement protocol, it was found out that precision of the operator is crucial for successful fabrication of the biosensor. It can be supposed that the properties of the biosensor can be further improved by employment of an automated technique for controlling the thickness of the layer of the PSII mixture, for example by spincoating, nanoliter dropcasting, dipcoating etc.

4.2. Dendrimer-encapsulated silver nanoparticles as sensitive electrochemical labels

Amplification of the signal of metalloimmunoassays can be achieved by loading more detectable tags per a labeled biorecognition molecule, which can be accomplished by a suitable label carrier (Katz et al. 2004). Because dendrimers can act as carriers of metal nanoparticles, it was proposed to develop dendrimer-encapsulated silver nanoparticles to serve as sensitive electrochemical labels for metalloimmunosensor assays. The amount of loaded metal tags depends on the dendrimer size (dendrimer generation). The advantage of dendrimers is not only in their potential to increase the loading volume of metal tags by selection of a suitable generation, but also in the high number of possible types of end-groups which can be possessed by dendrimers. They can be modified easily by suitable chemistry for the purpose of binding dendrimers to molecules with biorecognition properties.

In the presented study, ethylenediamine core type of PAMAM-OH dendrimers of generation 5, 6 and 7 were selected for synthesis of stable dendrimer-encapsulated silver nanoparticles (Paper II in Annexes). Silver-dendrimer nanocomposites (Ag-DNCs) were synthesized with several fixed ratios of silver/dendrimer. After characterization of the Ag-DNCs by UV-VIS spectrophotometry, AFM, TEM and XPS, the G7 Ag-DNCs compounds synthesized from 2000 molar excess of silver were selected as the best candidate for development of an electrochemical label. It was shown by reduction of silver ions conjugated with tertiary amines located inside of a PAMAM dendrimer that the synthesized nanoparticles are embedded in the interior of the dendrimer (Balogh & Tomalia 1998). The molar ratio of silver ions and dendrimers proved to be important for synthesis of stable nanocomposites and it differs depending on the dendrimer generation. Higher dendrimer generations had more amine tertiary groups, so more silver ions can be present in the solution for synthesis purposes. On the other hand, if there is an excess of silver ions for the given generation of a dendrimer, nanoparticles are formed not only inside of the dendritic shell, but also on the periphery of the dendrimer, which can lead

to agglomeration of the synthesized nanocomposites. Therefore, a suitable ratio of silver ions to dendrimers has to be selected. Silver nanoparticles are then formed predominantly in the interior of the dendrimers, where they are well protected from aggregation, which results in stable nanocomposites. Such nanocomposites were successfully detected by sensitive electrochemical stripping analysis in bulk solution and in a microfluidic electrochemical cell. For further details, see Paper II, IV in Annexes.

The biorecognition properties of the synthesized label were further demonstrated by conjugation with biotin, see Paper III in Annexes. Two strategies of conjugation of the G7 PAMAM-OH dendrimers with biotin were tested: (i) direct biotinylation of dendrimer hydroxyl groups, and (ii) biotinylation of dendrimer hydroxyl groups with a polyethylene glycol (PEG) spacer. The biorecognition properties of the conjugates were tested by an ELISA and SPR binding analysis. First, dendrimer conjugation with biotin was performed. Then, silver nanoparticles were synthesized in the prepared conjugates. The conjugates prepared by both procedures showed that the biorecognition properties of biotin, covalently bonded to the G7 PAMAM-OH dendrimer, are not affected by synthesis of the nanoparticles. When a PEG spacer was used for the conjugation of dendrimer and biotin, it was found out that under defined conditions, the biotinylated nanocomposites showed a high level of aggregation. This undesirable property was caused by synthesis of nanoparticles not only in the interior of the dendrimers, but also in their periphery.

Both studies showed that dendrimers can serve as suitable nanoscaffolds for synthesis of stable metal nanoparticles which can be electrochemically sensed after dissolution under acidic conditions. The advantage of such nanocomposites is the possibility of their conjugation with a suitable biorecognition element, which can be used for a sensitive electrochemical immunosensor.

4.3.   An electrochemical microfluidic detector

For electrochemical immunosensing, it was necessary to develop an electrochemical cell suitable for detection of low volumes of the target analyte. This need has arisen from the fact that immunoassays use only low volumes of immunoreactants so the electrochemical detection cannot be performed in a common electrochemical cell with a volume of several milliliters. As small volumes of analytes can be manipulated effectively in microfluidic systems, we decided to construct a microfluidic detector.

Generally, an electrochemical detector requires a build-in working, reference, and auxiliary electrode. The electrodes can be implemented into a microfluidic system by different ways such as through drilled holes, by electroplating, by metal sputtering with an electron-beam evaporation process, or by screen-printing techniques. In our study, a microfluidic electrochemical detector was constructed on a silicon wafer by combination of photolithography, polydimethoxysilane (PDMS) molding and metal sputtering techniques (Paper IV in Annexes). A microchannel in SU-8 resist with an integrated carbon microfiber as the working electrode, the counter (gold) electrode and the

pseudoreference (silver) electrode fabricated by metal sputtering, was enclosed with a PDMS cover. This ensemble was inserted into a PMMA holder providing connection with an automatic liquid dosing system. With this arrangement, successful (volt)amperometric detections were performed. Synthesized dendrimer-encapsulated silver nanoparticles were detected successfully by the constructed detector and the influence of the flow-rate and of the deposition potential of silver were investigated. It was found out that the sensitivity of the detection can be further increased by optimization of these two parameters. Another important factor for detection sensitivity was the concentration of solvent for the dissolution of nanoparticles. The determined LOD of 6.45×10^{-12} M of dissolved silver nanocomposites in a microfluidic electrochemical cell was calculated statistically. In comparison with the calculated LOD of 0.9×10^{-12} M of nanocomposites determined in bulk solution (Paper II in Annexes), no improvement has been achieved. However, assuming that the detection volume in the microfluidic system was 25 µL, and the detection volume in a commercial electrochemical cell was 25 mL, there were approx. 9.71×10^7 dendrimers detected in the microfluidic system in comparison with 1.35×10^{10} dendrimers detected in the commercial electrochemical cell. It means an improvement by 2-3 orders of magnitude expressed in the amount of single detected molecules of dendrimers.

During the use of the microfluidic detector, two main problems appeared. Both of them were technical. One problem was related to the microfluidic interface for the tubings. The other was connected with the electrochemical measurement, where a fluctuation of the adjusted potential of the electrodes appeared in some of the measurements. Such electrochemical behavior can result from an unsuitable shape and arrangement of the electrodes. It can lead, for example, to generation of uncompensated resistance (Myland & Oldham 2000).

It was found out that the manufactured holder from PMMA had several disadvantages. The most important disadvantages were poor adhesion of the PDMS to the PMMA and the fact that it was difficult to find a suitable parallel position of the upper and the bottom part of the holder for their proper tightening. Both holder parts were packed together by four screws and any sign of improper tightening caused disruption of the adhesion of the PDMS to the SU-8 resist layer. Unequal forces induced by the screws exposed the PDMS spacer to high pressures, which led to deformation of the microchannel and caused permeation of the fluid outside of the microchannels or breaking of the fluid flow in the microchannel. As a result, a new holder for a microfluidic chip was designed and constructed (Fig. 1, Paper V in Annexes). Since the holder construction has finished just recently, it could not have been tested properly yet.
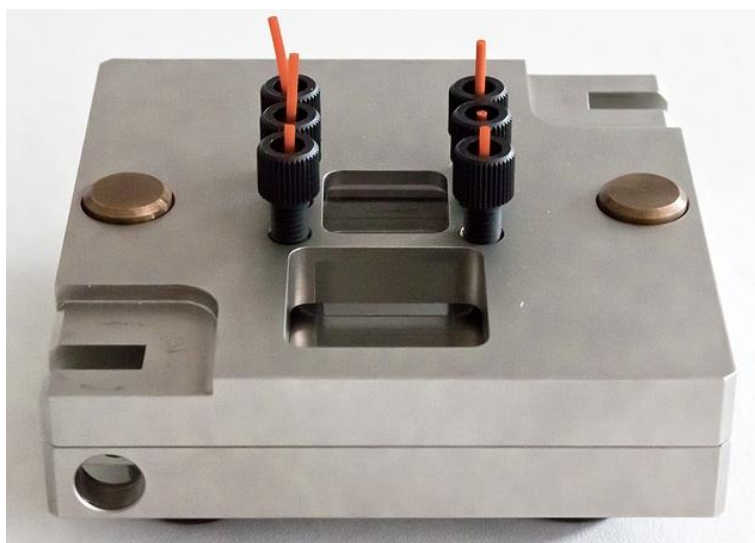
Figure 1. A newly designed holder for a microfluidic chip.

In another packing approach, microchannels were fabricated in PDMS by employment of a new metal casting mold especially designed and manufactured for the PDMS fabrication. The PDMS could be then combined with glass substrates including all necessary tubings for a microfluidic chip. The fabrication of microchannels in PDMS and the glass cover with tubings is discussed in Paper VI in Annexes. For production of all electrodes in an electrochemical detector, a lift-off technique combined with silver electroplating can be applied. A combination of magnetron sputtering of chromium, gold and silver, and a lift-off technique was tested successfully and protocols for manufacturing the electrodes were optimized. The production of silver electrodes was combined with electroplating. A detailed microfabrication protocol is described above in Materials and methods. The advantage of a lift-off technique is better control of the size and shape of the electrodes, and of their position on the microfluidic chip. The stability of the electroplated Ag electrode can be further improved, for example by chemical oxidation treatment with ferric chloride solution for formation of an Ag/AgCl microelectrode (Polk et al. 2006). A fabricated array of gold microelectrodes via a lift-off technique is presented in Figure 2.
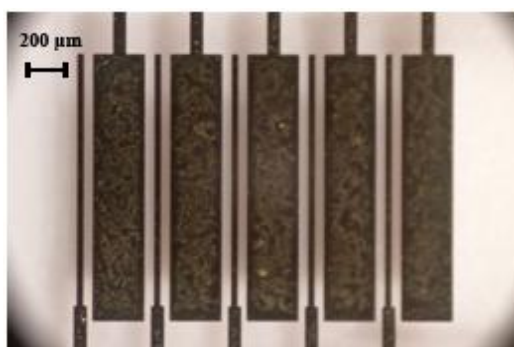

Figure 2. An array of gold electrodes produced by a lift-off technique.

4.4. *Magnetic beads trapping – immobilization in a microfluidic system*

In electrochemical immunosensing, immunoreactions can proceed outside the electrochemical detection cell. When it is desired that the immunoreactions and detection proceed at the same place, immunorectants have to be anchored somewhere in the immediate vicinity of the electrochemical detector or directly on the working electrode (Michaeli et al. 2005). When the immobilization of immunoreactants is performed on the working electrode, the immobilization surface is limited and the active surface of the working electrode can be passivated. When functionalized MBs are used as the immobilization surface for immunoreactants, the immobilization surface can be enlarged by an increase in the concentration of MBs. Another advantage of MBs is their ability to be captured at any desired place by strong magnetic forces.

One of the aims of this study was to fabricate a microfluidic system with an embedded electromagnetic microcoil which could trap MBs effectively at a desired place, in the immediate vicinity of the microfabricated working electrode. A similar system was already proposed, where antibody-coated beads were introduced into a microchannel and separated above an electromagnet integrated in a microfluidic chip (Choi et al. 2000). Then, antigens were injected into the microchannel and only the target antigens were immobilized on antibody-coated beads. Finally, labeled antibodies were injected and at the end of the assay, substrate was injected into the microchannel. In case of metalloimmunosensing, solvent for dissolution of metal labels has to be injected into the microchannel instead of substrate.

Details of the fabrication and testing of the magnetic bead separator embedded in a microfluidic chip are described in Paper VI in Annexes. The electromagnetic microcoil was manufactured on a glass substrate and the microfluidic chip was packed with a tubing interface fabricated on a glass cover. As microcoil fabrication using one metallization layer is less technically demanding and more suitable for rapid prototyping, we focused on this type of production process. Because electromagnetic microcoils fabricated by employment of one metallization layer generate weaker magnetic forces in comparison with electromagnetic microcoils fabricated by employment of more than one metallization layers and because the geometry of microcoils has a strong impact on the trapping profile of magnetic beads (Ramadan et al. 2008; Fulcrand et al. 2009), the design of the separator was considered important for effective MBs trapping.

A planar multiwire meander microcoil was designed and its effectivity of the generation of magnetic field was compared with a simple meander microcoil by computer simulations. Higher performance of the newly proposed multiwire meander microcoil in comparison with a simple meander microcoil was confirmed. The generated magnetic field and the magnetic energy gradient of the multiwire microcoil did not drop as rapidly in larger distances from the microcoil as in case of a simple planar microcoil with one wire. Thus, the newly designed multiwire microcoils will be more effective for

MBs trapping. Some of the results correlated with previously published results (Ramadan 2004).

The most challenging step of this study was the optimization of microfabrication protocols. The protocols consisted of the following steps:

- Fabrication of positive and negative masks by electron beam lithography.

- Fabrication of a PDMS microchannel by soft lithography.

- Copper electroplating and UV lithography for the fabrication and the isolation of a microcoil.

- Packing of a microfluidic chip.

When the MBs trapping was tested, it was found out that although a multiwire microcoil can be more effective in the generation of the gradient of magnetic field in comparison with a simple meander microcoil, the generated magnetic forces were not strong enough to trap the MBs. The use of weak neodymium-iron-boron permanent magnets, which magnetize the MBs and attract them to the immediate vicinity of the electromagnetic microcoil, was necessary. Above the electromagnetic microcoil, the MBs were trapped by magnetic forces generated by the microcoil.

The trapping of MBs was confirmed experimentally and a microfluidic electrochemical system with embedded microcoils for localized magnetic trapping will be further developed and implemented into a MBs-based electrochemical immunoassay.

5. Conclusions

(i) **A novel immobilization procedure for the PSII-based biosensor was developed.**

- Sol-gel immobilization of the PSII complex was studied as a novel immobilization method with biocompatible diglyceryl silane. During the testing of a sol-gel immobilization matrix, the amounts of the PSII complex, diglyceryl silane, and serum albumin were optimized. It was found out that the amount of a sol-gel precursor and of serum albumin in the immobilization membrane has a strong impact on the intensity of the biosensor signal. A disadvantage of a sol-gel immobilization method for biosensors with a thick immobilization membrane was weak adhesion of the silicate matrix to the surface of the working electrode.

- The advantage of the biosensors prepared by immobilization of the PSII complex in silicate gel was significantly higher signal as compared with the biosensors with the PSII complex crosslinked by glutaraldehyde. However, the evaluation of long-term stability, inhibition parameters and limit of detection favorised covalent immobilization by glutaraldehyde crosslinking. It was concluded that sol-gel immobilization might be a more suitable method to monitor PSII activity than that based on crosslinking. However, further studies have to be performed to promote practical use.

- Computer simulations of the functional properties of the PSII-based biosensor in the presence of an inhibitor showed that the signal of the biosensor will be more accurate and the processes better distinguishable in thinner biomembranes with lower contents of the PSII complex. Some of the unusual behavior of the biosensor signal observed under certain experimental conditions was explained by changing variables, mainly the membrane thickness and the amount of enzyme in the immobilization matrix.

- A further improvement of the biosensor was achieved by improvement of the immobilization technique. To obtain a thin biomembrane, immobilization procedure by drop imprints on the working electrode was performed. Modifications of the immobilization protocol resulted in accurate and fast assay.

(ii) **Dendrimer-encapsulated silver nanoparticles as electrochemical labels were developed for a microfluidic electrochemical immunosensor. For the purpose of microfluidic assays, a microfluidic electrochemical detector and a microfluidic magnetic beads separator for immobilization of immunoreactants directly in a microfluidic microchannel were designed, constructed and tested.**

- The synthesis of silver nanoparticles in a dendrimer shell was performed and proved by several analytical techniques. Generation 7 of hydroxyl-terminated

polyamidoamine dendrimer was selected as the most suitable scaffold for synthesized nanoparticles in order to preserve a high amount of silver and long-time stability. The synthesized nanocomposites were successfully biotinylated and the biorecognition properties of the conjugates were confirmed by ELISA and SPR assays.

- A microfluidic electrochemical cell was constructed with an embedded carbon microwire as the working electrode and with sputtered gold as the counter electrode, and sputtered silver as the pseudoreference electrode. Amperometric and voltammetric electrochemical techniques were perfomed with the constructed electrochemical cell. As an alternative technique for an electrode used in an electrochemical cell, a lift-off technique was optimized for fabrication. Due to problems with a home-made PMMA holder for a microfluidic electrochemical cell, a novel, robust metal holder was designed and manufactured. Also a glass cover with tubing connectors combined with microchannels in polydimethylsiloxane was manufactured and successfully tested.

- Sensitive electrochemical detection of the nanocomposites was compared in the standard and manufactured microfluidic electrochemical cells using anodic stripping voltammetry.

- For immobilization of biorecognition elements in a microfluidic chip, a magnetic separator with an embedded multiwire planar microcoil was designed, constructed and tested. The separator showed effective separation of magnetic beads when combined with small permanent magnets. It might be implemented into a microfluidic chip with an electrochemical cell.

- Metalloimmunoassay with the synthesized electrochemical labels has not been carried out yet due to complicated fabrication of the microfluidic chip. However, it will be further developed using novel electrochemical metal labels and the microfluidic chip. The chip with the electrochemical detector and the embedded magnetic separator will be constructed according to the developed microfabrication protocols.

6. References

AHMED, M. U., HOSSAIN, M. M. and TAMIYA, E., 2008. Electrochemical biosensors for medical and food applications. Electroanalysis. Vol. 20, no. 6, pp. 616–626.

AHUJA, T., MIR, I., KUMAR, D. and RAJESH, 2007. Biomolecular immobilization on conducting polymers for biosensing applications. Biomaterials. Vol. 28, no. 5, pp. 791–805.

ALBAREDA-SIRVENT, M., MERKOÇI, A. and ALEGRET, S., 2000. Configurations used in the design of screen-printed enzymatic biosensors. A review. Sensors and Actuators B: Chemical. Vol. 69, no. 1-2, pp. 153–163.

AMINE, A., MOHAMMADI, H., BOURAIS, I. and PALLESCHI, G., 2006. Enzyme inhibition-based biosensors for food safety and environmental monitoring. Biosensors and Bioelectronics. Vol. 21, no. 8, pp. 1405–1423.

ANDREESCU, A. and SADIK, O. A., 2004. Trends and challenges in biochemical sensors for clinical and environmental monitoring. Pure and applied chemistry. Vol. 76, no. 4, pp. 861–878.

BAEUMNER, A. J., 2003. Biosensors for environmental pollutants and food contaminants. Analytical and Bioanalytical Chemistry. Vol. 377, no. 3, pp. 434–445.

BALOGH, L. and TOMALIA, D. A., 1998. Poly(amidoamine) dendrimer-templated nanocomposites. 1. Synthesis of zerovalent copper nanoclusters. Journal of the American Chemical Society. Vol. 120, no. 29, pp. 7355–7356.

BARCELÓ, D., RODRIGUEZ-MOZAZ, S., MARCO, M.-P. and LOPEZ DE ALDA, M. J., 2004. Biosensors for environmental monitoring of endocrine disruptors: a review article. Analytical and Bioanalytical Chemistry. Vol. 378, no. 3, pp. 588–598.

BAUER, Ch. G., EREMENKO, A. V., EHRENTREICH-FÖRSTER, E., BIER, F. F., MAKOWER, A., HALSALL, H. B., HEINEMAN, W. R. and SCHELLER, F. W., 1996. Zeptomole-detecting biosensor for alkaline phosphatase in an electrochemical immunoassay for 2,4-dichlorophenoxyacetic acid. Analytical Chemistry. Vol. 68, no. 15, pp. 2453–2458.

BELKIN, S., 2003. Microbial whole-cell sensing systems of environmental pollutants. Current Opinion in Microbiology. Vol. 6, no. 3, pp. 206–212.

BENDER, S. and SADIK, O. A., 1998. Direct electrochemical immunosensor for polychlorinated biphenyls. Environmental Science & Technology. Vol. 32, no. 6, pp. 788–797.

BEREZHETSKYY, A. L., SOSOVSKA, O. F., DURRIEU, C., CHOVELON, J.-M., DZYADEVYCH, S. V. and TRAN-MINH, C., 2008. Alkaline phosphatase

conductometric biosensor for heavy-metal ions determination. IRBM. Vol. 29, no. 2-3, pp. 136–140.

BERGGREN, Ch., BJARNASON, B. and JOHANSSON, G., 2001. Capacitive biosensors. Electroanalysis. Vol. 13, no. 3, pp. 173–180.

BERNABEI, M., CREMISINI, C., MASCINI, M. and PALLESCHI, G., 1991. Determination of organophosphorus and carbamic pesticides with a choline and acetylcholine electrochemical biosensor. Analytical Letters. Vol. 24, no. 8, pp. 1317–1331.

BERTHIER, J. and SILBERZAN, P., 2010. Microfluidics for biotechnology. Second. Boston: Artech House. ISBN 9781596934436.

BETTAZZI, F., LASCHI, S. and MASCINI, M., 2007. One-shot screen-printed thylakoid membrane-based biosensor for the detection of photosynthetic inhibitors in discrete samples. Analytica Chimica Acta. Vol. 589, no. 1, pp. 14–21.

BHALLA, V. and ZAZUBOVICH, V., 2011. Self-assembly and sensor response of photosynthetic reaction centers on screen-printed electrodes. Analytica Chimica Acta. 2011. Vol. 707, no. 1-2, pp. 184–190.

BITTON, G. and DUTKA, B. J., 1983. Bacterial and biochemical tests for assessing chemical toxicity in the aquatic environment: A review. C R C Critical Reviews in Environmental Control. Vol. 13, no. 1, pp. 51–67.

BONNET, C., 2003. Adsorption: an easy and efficient immobilisation of acetylcholinesterase on screen-printed electrodes. Analytica Chimica Acta. Vol. 481, no. 2, pp. 209–211.

BRAHIM, S., 2001. Amperometric determination of cholesterol in serum using a biosensor of cholesterol oxidase contained within a polypyrrole–hydrogel membrane. Analytica Chimica Acta. Vol. 448, no. 1-2, pp. 27–36.

BROOK, M. A., CHEN, Y., GUO, K., ZHANG, Z., JIN, W., DEISINGH, A., CRUZ-AGUADO, J. and BRENNAN, J. D., 2004. Proteins entrapped in silica monoliths prepared from glyceroxysilanes. Journal of Sol-Gel Science and Technology. Vol. 31, no. 1-3, pp. 343–348.

CAI, H., XU, Y., ZHU, N., HE, P. and FANG, Y., 2002. An electrochemical DNA hybridization detection assay based on a silver nanoparticle label. Analyst. Vol. 127, no. 6, pp. 803–808.

CAI, H., ZHU, N., JIANG, Y., HE, P. and FANG, Y., 2003. Cu@Au alloy nanoparticle as oligonucleotides labels for electrochemical stripping detection of DNA hybridization. Biosensors and Bioelectronics. Vol. 18, no. 11, pp. 1311–1319.

CAMPÀS, M., CARPENTIER, R. and ROUILLON, R., 2008. Plant tissue-and photosynthesis-based biosensors. Biotechnology Advances. Vol. 26, no. 4, pp. 370–378.

CASTILLO, M., 2001. Identification of cytotoxic compounds in European wastewaters during a field experiment. Analytica Chimica Acta. Vol. 426, no. 2, pp. 265–277.

CAYGILL, R. L., BLAIR, G. E. and MILLNER, P. A., 2010. A review on viral biosensors to detect human pathogens. Analytica Chimica Acta. Vol. 681, no. 1-2, pp. 8–15.

CENTI, S., LASCHI, S. and MASCINI, M., 2007. Improvement of analytical performances of a disposable electrochemical immunosensor by using magnetic beads. Talanta. Vol. 73, no. 2, pp. 394–399.

CLARK, L. C. and LYONS, Ch., 1962. Electrode systems for continuous monitoring in cardiovascular surgery. Annals of the New York Academy of Sciences. Vol. 102, no. 1, pp. 29–45.

COONS, A. H., 1956. Histochemistry with labeled antibody. International Review of Cytology. Vol. 5, pp. 1–23.

COOPER, M. A., 2003. Label-free screening of bio-molecular interactions. Analytical and Bioanalytical Chemistry. Vol. 377, no. 5, pp. 834–842.

CORBISIER, P., 1999. Whole cell- and protein-based biosensors for the detection of bioavailable heavy metals in environmental samples. Analytica Chimica Acta. Vol. 387, no. 3, pp. 235–244.

CROOKS, R. M., ZHAO, M., SUN, L., CHECHIK, V. and YEUNG, L. K., 2001. Dendrimer-encapsulated metal nanoparticles: Synthesis, characterization, and applications to catalysis. Accounts of Chemical Research. Vol. 34, no. 3, pp. 181–190.

CUI, H.-F., YE, J.-S., CHEN, Y., CHONG, S.-Ch. and SHEU, F.-S., 2006. Microelectrode array biochip: tool for in vitro drug screening based on the detection of a drug effect on dopamine release from PC12 cells. Analytical Chemistry. Vol. 78, no. 18, pp. 6347–6355.

CULLEN, D. C., SETHI, R. S. and LOWE, C. R., 1990. Multi-analyte miniature conductance biosensor. Analytica Chimica Acta. Vol. 231, pp. 33–40.

CUNNINGHAM, D., 2001. Fluidics and sample handling in clinical chemical analysis. Analytica Chimica Acta. Vol. 429, no. 1, pp. 1–18.

DEQUAIRE, M., DEGRAND, Ch. and LIMOGES, B., 2000. An electrochemical metalloimmunoassay based on a colloidal gold label. Analytical Chemistry. Vol. 72, no. 22, pp. 5521–5528.

DÍAZ-GONZÁLEZ, M., GONZÁLEZ-GARCÍA, M. B. and COSTA-GARCÍA, A., 2005. Recent advances in electrochemical enzyme immunoassays. Electroanalysis. Vol. 17, no. 21, pp. 1901–1918.

DUKE, S. O., 1990. Overview of herbicide mechanisms of action. Environmental Health Perspectives. Vol. 87, pp. 263–271.

EGUÍLAZ, M., MORENO-GUZMÁN, María, CAMPUZANO, S., GONZÁLEZ-CORTÉS, A., YÁÑEZ-SEDEÑO, P. and PINGARRÓN, J. M., 2010. An electrochemical immunosensor for testosterone using functionalized magnetic beads and screen-printed carbon electrodes. Biosensors and Bioelectronics. Vol. 26, no. 2, pp. 517–522.

EN ISO 8692, 2004. European Standard: freshwater algal growth inhibition test with unicellular green algae.

FRÁNEK, M. and HRUŠKA, K., 2005. Antibody based methods for environmental and food analysis: a review. Veterinary Medicine. Vol. 50, no. 1, pp. 1–10.

FULCRAND, R., JUGIEU, D., ESCRIBA, C., BANCAUD, A., BOURRIER, D., BOUKABACHE, A. and GUÉ, A. M., 2009. Development of a flexible microfluidic system integrating magnetic micro-actuators for trapping biological species. Journal of Micromechanics and Microengineering. Vol. 19, no. 10, pp. 105019.

GHICA, M. E. and BRETT, Ch. M. A., 2008. Glucose oxidase inhibition in poly(neutral red) mediated enzyme biosensors for heavy metal determination. Microchimica Acta. Vol. 163, no. 3-4, pp. 185–193.

GIARDI, M. T., KOBLÍŽEK, M. and MASOJÍDEK, J., 2001. Photosystem II-based biosensors for the detection of pollutants. Biosensors and Bioelectronics. Vol. 16, no. 9-12, pp. 1027–1033.

GIARDI, M. T. and PACE, E., 2005. Photosynthetic proteins for technological applications. Trends in Biotechnology. Vol. 23, no. 5, pp. 257–263.

GOSLING, J. P., 1990. A decade of development in immunoassay methodology. Clinical Chemistry. Vol. 36, no. 8, pp. 1408–1427.

GREGG, B. A. and HELLER, A., 1990. Cross-linked redox gels containing glucose oxidase for amperometric biosensor applications. Analytical Chemistry. Vol. 62, no. 3, pp. 258–263.

GRIESHABER, D., MACKENZIE, R., VÖRÖS, J. and REIMHULT, E., 2008. Electrochemical biosensors - sensor principles and architectures. Sensors. Vol. 8, no. 3, pp. 1400–1458.

GUESDON, J.-L. and AVRAMEAS, S., 1977. Magnetic solid phase enzyme-immunoassay. Immunochemistry. Vol. 14, no. 6, pp. 443–447.

GUNDERSEN, S. G., HAAGENSEN, I., JONASSEN, T. O., FIGENSCHAU, K. J., DE JONGE, N. and DEELDER, A. M., 1992. Magnetic bead antigen capture enzyme-linked immunoassay in microtitre trays for rapid detection of schistosomal circulating anodic antigen. Journal of Immunological Methods. Vol. 148, no. 1–2, pp. 1–8.

GWENIN, C. D., KALAJI, M., WILLIAMS, P. A. and JONES, R. M., 2007. The orientationally controlled assembly of genetically modified enzymes in an

amperometric biosensor. Biosensors and Bioelectronics. Vol. 22, no. 12, pp. 2869–2875.

HAEBERLE, S. and ZENGERLE, R., 2007. Microfluidic platforms for lab-on-a-chip applications. Lab on a Chip. Vol. 7, no. 9, pp. 1094.

HANEFELD, U., GARDOSSI, L. and MAGNER, E., 2009. Understanding enzyme immobilisation. Chemical Society Reviews. Vol. 38, no. 2, pp. 453.

HARRISON, D. J., MANZ, A., FAN, Z., LUEDI, H. and WIDMER, H. M., 1992. Capillary electrophoresis and sample injection systems integrated on a planar glass chip. Analytical Chemistry. Vol. 64, no. 17, pp. 1926–1932.

HEINEMAN, W. R., ANDERSON, C. W. and HALSALL, H. B., 1979. Immunoassay by differential pulse polarography. Science. Vol. 204, no. 4395, pp. 865–866.

HERNÁNDEZ-SANTOS, D., GONZÁLEZ-GARCÍA, M. B. and GARCÍA, A. C., 2002. Metal-nanoparticles based electroanalysis. Electroanalysis. Vol. 14, no. 18, pp. 1225–1235.

HOCK, B., SEIFERT, M. and KRAMER, K., 2002. Engineering receptors and antibodies for biosensors. Biosensors and Bioelectronics. Vol. 17, no. 3, pp. 239–249.

HULANICKI, A., GLAB, S. and INGMAN, F., 1991. Chemical sensors: definitions and classification. Pure and Applied Chemistry. Vol. 63, no. 9, pp. 1247–1250.

CHAKI, N. K. and VIJAYAMOHANAN, K., 2002. Self-assembled monolayers as a tunable platform for biosensor applications. Biosensors and Bioelectronics. Vol. 17, no. 1-2, pp. 1–12.

CHEN, Z.-P., PENG, Z.-F., LUO, Y., QU, B., JIANG, J.-H., ZHANG, X.-B., SHEN, G.-L. and YU, R.-Q., 2007. Successively amplified electrochemical immunoassay based on biocatalytic deposition of silver nanoparticles and silver enhancement. Biosensors and Bioelectronics. Vol. 23, no. 4, pp. 485–491.

CHOI, J. W., AHN, C. H., BHANSALI, S. and HENDERSON, H. T., 2000. A new magnetic bead-based, filterless bio-separator with planar electromagnet surfaces for integrated bio-detection systems. Sensors and Actuators B: Chemical. Vol. 68, no. 1-3, pp. 34–39.

CHOI, J.-W., OH, K. W., THOMAS, J. H., HEINEMAN, W. R., HALSALL, H. B., NEVIN, J. H., HELMICKI, A. J., HENDERSON, H. T. and AHN, Ch. H., 2002. An integrated microfluidic biochemical detection system for protein analysis with magnetic bead-based sampling capabilities. Lab on a Chip. Vol. 2, no. 1, pp. 27.

CHUNG, Y.-K., REBOUD, J., LEE, K. Ch., LIM, H. M., LIM, P. Y., WANG, K. Y., TANG, K. Ch., JI, H. M. and CHEN, Y., 2011. An electrical biosensor for the detection of circulating tumor cells. Biosensors and Bioelectronics. Vol. 26, no. 5, pp. 2520–2526.

KATZ, E., WILLNER, I. and WANG, J., 2004. Electroanalytical and bioelectroanalytical systems based on metal and semiconductor nanoparticles. Electroanalysis. Vol. 16, no. 12, pp. 19–44.

KOBLÍŽEK, M., MASOJÍDEK, J., KOMENDA, J., KUČERA, T., PILLOTON, R., MATTOO, A. K. and GIARDI, M. T., 1998. A sensitive photosystem II-based biosensor for detection of a class of herbicides. Biotechnology and Bioengineering. Vol. 60, no. 6, pp. 664–669.

KOBLÍŽEK, M., MALÝ, J., MASOJÍDEK, J., KOMENDA, J., KUČERA, T., GIARDI, M. T., MATTOO, A. K. and PILLOTON, R., 2002. A biosensor for the detection of triazine and phenylurea herbicides designed using Photosystem II coupled to a screen-printed electrode. Biotechnology and Bioengineering. Vol. 78, no. 1, pp. 110–116.

KOPNOV, F., COHEN-OFRI, I. and NOY, D., 2011. Electron transport between photosystem II and photosystem I encapsulated in sol-gel glasses. Angewandte Chemie International Edition. Vol. 50, no. 51, pp. 12347–12350.

KRAWCZYŃSKI VEL KRAWCZYK, T., MOSZCZYŃSKA, M. and TROJANOWICZ, M., 2000. Inhibitive determination of mercury and other metal ions by potentiometric urea biosensor. Biosensors and Bioelectronics. Vol. 15, no. 11-12, pp. 681–691.

KURAMITZ, H., 2009. Magnetic microbead-based electrochemical immunoassays. Analytical and Bioanalytical Chemistry. Vol. 394, no. 1, pp. 61–69.

LAKARD, B., HERLEM, G., LAKARD, S., ANTONIOU, A. and FAHYS, B., 2004. Urea potentiometric biosensor based on modified electrodes with urease immobilized on polyethylenimine films. Biosensors and Bioelectronics. Vol. 19, no. 12, pp. 1641–1647.

LALONDE, J., MARGOLIN, A., 2002. Immobilization of enzymes. In: Drauz, K., Waldmann, H., (eds) Enzyme Catalysis in Organic Synthesis: A Comprehensive Handbook, 2nd edn. Weinheim. Wiley-VCH. pp. 163–184. DOI: 10.1002/9783527618262.ch6

LAROM, S., SALAMA, F., SCHUSTER, G. and ADIR, N., 2010. Engineering of an alternative electron transfer path in photosystem II. Proceedings of the National Academy of Sciences. Vol. 107, no. 21, pp. 9650–9655.

LARSEN, L. H., KJÆR, T. and REVSBECH, N. P., 1997. A microscale NO 3- biosensor for environmental applications. Analytical Chemistry. Vol. 69, no. 17, pp. 3527–3531.

LAZCKA, O., CAMPO, F. J. D. and MUÑOZ, F. X., 2007. Pathogen detection: A perspective of traditional methods and biosensors. Biosensors and Bioelectronics. Vol. 22, no. 7, pp. 1205–1217.

LE FLOCH, F., HO, H. A. and LECLERC, M., 2006. Label-free electrochemical detection of protein based on a ferrocene-bearing cationic polythiophene and aptamer. Analytical Chemistry. Vol. 78, no. 13, pp. 4727–4731.

LEONARD, P., HEARTY, S., BRENNAN, J., DUNNE, L., QUINN, J., CHAKRABORTY, T. and O'KENNEDY, R., 2003. Advances in biosensors for detection of pathogens in food and water. Enzyme and Microbial Technology. Vol. 32, no. 1, pp. 3–13.

LIU, G. and LIN, Y., 2005. Electrochemical stripping analysis of organophosphate pesticides and nerve agents. Electrochemistry Communications. Vol. 7, no. 4, pp. 339–343.

LIU, G. and LIN, Y., 2007. Nanomaterial labels in electrochemical immunosensors and immunoassays. Talanta. Vol. 74, no. 3, pp. 308–317.

LIU, G., WANG, J., KIM, J., JAN, M. R., and COLLINS, G., E., 2004. Electrochemical Coding for Multiplexed Immunoassays of Proteins. Analytical Chemistry. Vol. 76, no. 23, pp. 7126–7130.

LOOSE, C. J., VON ELERT, E. and DAWIDOWITZ, P., 1993. Chemically-induced diel vertical migration in Daphnia: a new bioassay for kairomones exuded by fish. Archiv für Hydrobiologie. Vol. 126, no. 3, pp. 329–337.

LUO, X., MORRIN, A., KILLARD, A. J. and SMYTH, M. R., 2006. Application of nanoparticles in electrochemical sensors and biosensors. Electroanalysis. Vol. 18, no. 4, pp. 319–326.

LUPPA, P. B., SOKOLL, L. J. and CHAN, D. W., 2001. Immunosensors—principles and applications to clinical chemistry. Clinica Chimica Acta. Vol. 314, no. 1-2, pp. 1–26.

MALHOTRA, B. D. and CHAUBEY, A., 2003. Biosensors for clinical diagnostics industry. Sensors and Actuators B: Chemical. Vol. 91, no. 1-3, pp. 117–127.

MALÝ, J., LAMPOVÁ, H., SEMERÁDTOVÁ, A., ŠTOFIK, M. and KOVÁČIK, L., 2009. The synthesis and characterization of biotin-silver-dendrimer nanocomposites as novel bioselective labels. Nanotechnology. Vol. 20, no. 38, pp. 385101.

MALÝ, J., MASOJÍDEK, J., MASCI, A., ILIE, M., CIANCI, E., FOGLIETTI, V., VASTARELLA, W. and PILLOTON, R., 2005. Direct mediatorless electron transport between the monolayer of photosystem II and poly(mercapto-p-benzoquinone) modified gold electrode - new design of biosensor for herbicide detection. Biosensors and Bioelectronics. Vol. 21, no. 6, pp. 923–932.

MANI, V., CHIKKAVEERAIAH, B. V., PATEL, V., GUTKIND, J. S. and RUSLING, J. F., 2009. Ultrasensitive immunosensor for cancer iomarker proteins using gold nanoparticle film electrodes and multienzyme-particle amplification. ACS Nano. Vol. 3, no. 3, pp. 585–594.

MANZ, A., GRABER, N. and WIDMER, H. M., 1990. Miniaturized total chemical analysis systems: A novel concept for chemical sensing. Sensors and Actuators B: Chemical. Vol. 1, no. 1-6, pp. 244–248.

MARCO, M.-P. and BARCELÓ, D., 1996. Environmental applications of analytical biosensors. Measurement Science and Technology. Vol. 7, no. 11, pp. 1547–1562.

MARK, D., HAEBERLE, S., ROTH, G., VON STETTEN, F. and ZENGERLE, R., 2010. Microfluidic lab-on-a-chip platforms: requirements, characteristics and applications. Chemical Society Reviews. Vol. 39, no. 3, pp. 1153.

MARTINEK, K. and TORCHILIN, V. P., 1988. [55] Stabilization of enzymes by intramolecular cross-linking using bifunctional reagents. Methods in Enzymology Vol. 137, pp. 615–626.

MASOJÍDEK, J., SOUČEK, P., MÁCHOVÁ, J., FROLÍK, J., KLEM, K. and MALÝ, J., 2011. Detection of photosynthetic herbicides: Algal growth inhibition test vs. electrochemical photosystem II biosensor. Ecotoxicology and Environmental Safety. Vol. 74, no. 1, pp. 117–122.

MATTOO, A. K., GIARDI, M.-T., RASKIND, A. and EDELMAN, M., 1999. Dynamic metabolism of photosystem II reaction center proteins and pigments. Physiologia Plantarum. Vol. 107, no. 4, pp. 454–461.

MEHRVAR, M. and ABDI, M., 2004. Recent developments, characteristics, and potential applications of electrochemical biosensors. Analytical Sciences. Vol. 20, no. 8, pp. 1113–1126.

MELLO, L. D. and KUBOTA, L. T., 2002. Review of the use of biosensors as analytical tools in the food and drink industries. Food Chemistry. Vol. 77, no. 2, pp. 237–256.

MEUNIER, Ch. F., VAN CUTSEM, P., KWON, Y.-U. and SU, B.-L., 2009. Thylakoids entrapped within porous silica gel: towards living matter able to convert energy. Journal of Materials Chemistry. Vol. 19, no. 11, pp. 1535.

MICHAELI, L., GRECCO, R., BADEA, M., MOSCONE, D. and PALLESCHI, G., 2005. An electrochemical immunosensor for aflatoxin M1 determination in milk using screen-printed electrodes. Biosensors and Bioelectronics. Vol. 21, no. 4, pp. 588–596.

MIKKELSEN, S. R. and CORTÓN, E., 2004. Bioanalytical chemistry. Hoboken, N.J. John Wiley & Sons. ISBN 9780471544470.

MILLAN, K. M. and MIKKELSEN, S. R., 1993. Sequence-selective biosensor for DNA based on electroactive hybridization indicators. Analytical Chemistry. Vol. 65, no. 17, pp. 2317–2323.

MILLER, J. K. and LENZ, D. E., 2001. Development of an immunoassay for diagnosis of exposure to toxic organophosphorus compounds. Journal of Applied Toxicology. Vol. 21, no. S1, pp. S23–S26.

MORELAND, D. E., 1980. Mechanisms of action of herbicides. Annual Review of Plant Physiology. Vol. 31, no. 1, pp. 597–638.

MORENO-GUZMÁN, M., GONZÁLEZ-CORTÉS, A., YÁÑEZ-SEDEÑO, P. and PINGARRÓN, J. M., 2011. A disposable electrochemical immunosensor for prolactin involving affinity reaction on streptavidin-functionalized magnetic particles. Analytica Chimica Acta. Vol. 692, no. 1–2, pp. 125–130.

MULCHANDANI, P., MULCHANDANI, A., KANEVA, I. and CHEN, W., 1999. Biosensor for direct determination of organophosphate nerve agents. 1. Potentiometric enzyme electrode. Biosensors and Bioelectronics. Vol. 14, no. 1, pp. 77–85.

MYLAND, J. C. and OLDHAM, K. B., 2000. Uncompensated resistance. 1. The effect of cell geometry. Analytical Chemistry. Vol. 72, no. 17, pp. 3972–3980.

NAGEL, B., DELLWEG, H. and GIERASCH, L. M., 1992. Glossary for chemists of terms used in biotechnology (IUPAC Recommendations 1992). Pure and Applied Chemistry. Vol. 64, no. 1, pp. 143–168.

NAKANE, P. K. and PIERCE JR., G. B., 1966. Enzyme-labeled antibodies: preparation and application for the localization of antigens. Journal of Histochemistry and Cytochemistry. Vol. 14, no. 12, pp. 929–931.

NEWMAN, J. D. and TURNER, A. P. F., 2005. Home blood glucose biosensors: a commercial perspective. Biosensors and Bioelectronics. Vol. 20, no. 12, pp. 2435–2453.

NG, A. H. C., UDDAYASANKAR, U. and WHEELER, A. R., 2010. Immunoassays in microfluidic systems. Analytical and Bioanalytical Chemistry. Vol. 397, no. 3, pp. 991–1007.

NIEMEYER, Ch. M., 2001. Nanoparticles, proteins, and nucleic acids: biotechnology meets materials science. Angewandte Chemie International Edition. Vol. 40, no. 22, pp. 4128–4158.

NISHIZAWA, S., SAKAI, A., AMANO, Y. and MATSUZAWA, T., 1993. Cryopreservation of asparagus (Asparagus officinalis L.) embryogenic suspension cells and subsequent plant regeneration by vitrification. Plant Science. Vol. 91, no. 1, pp. 67–73.

NISTOR, C. and EMNEUS, J., 1999. Bioanalytical tools for monitoring polar pollutants. Waste Management. Vol. 19, no. 2, pp. 147–170.

NIU, Y. and CROOKS, R. M., 2003. Dendrimer-encapsulated metal nanoparticles and their applications to catalysis. Comptes Rendus Chimie. Vol. 6, no. 8-10, pp. 1049–1059.

NORTH, J. R., 1985. Immunosensors: Antibody-based biosensors. Trends in Biotechnology. Vol. 3, no. 7, pp. 180–186.

PADDLE, B. M., 1996. Biosensors for chemical and biological agents of defence interest. Biosensors and Bioelectronics. Vol. 11, no. 11, pp. 1079–1113.

PANAYOTOU, G., GISH, G., END, P., TRUONG, O., GOUT, I., DHAND, R., FRY, M. J., HILES, I., PAWSON, T. and WATERFIELD, M. D., 1993. Interactions between SH2 domains and tyrosine-phosphorylated platelet-derived growth factor beta-receptor sequences: analysis of kinetic parameters by a novel biosensor-based approach. Molecular and Cellular Biology. Vol. 13, no. 6, pp. 3567–3576.

PANCRAZIO, J. J., WHELAN, J. P., BORKHOLDER, D. A., MA, W. and STENGER, D. A., 1999. Development and application of cell-based biosensors. Annals of Biomedical Engineering. Vol. 27, no. 6, pp. 697–711.

PENN, S., 2003. Nanoparticles for bioanalysis. Current Opinion in Chemical Biology. Vol. 7, no. 5, pp. 609–615.

PIERRE, A. C., 2004. The sol-gel encapsulation of enzymes. Biocatalysis and Biotransformation. Vol. 22, no. 3, pp. 145–170.

PIUNNO, P. A. E. and KRULL, U. J., 2005. Trends in the development of nucleic acid biosensors for medical diagnostics. Analytical and Bioanalytical Chemistry. Vol. 381, no. 5, pp. 1004–1011.

PODOLA, B., NOWACK, E. C. M and MELKONIAN, M., 2004. The use of multiple-strain algal sensor chips for the detection and identification of volatile organic compounds. Biosensors and Bioelectronics. Vol. 19, no. 10, pp. 1253–1260.

POHANKA, M., SKLÁDAL, P. and KROČA, M., 2007. Biosensors for biological warfare agent detection. Defence Science Journal. Vol. 57, no. 3, pp. 185–193.

POLK, B. J., STELZENMULLER, A., MIJARES, G., MACCREHAN, W. and GAITAN, M., 2006. Ag/AgCl microelectrodes with improved stability for microfluidics. Sensors and Actuators B: Chemical. Vol. 114, no. 1, pp. 239–247.

PRIETO-SIMÓN, B., CAMPÀS, M., ANDREESCU, S. and MARTY, J.-L., 2006. Trends in flow-based biosensing systems for pesticide assessment. Sensors. Vol. 6, no. 10, pp. 1161–1186.

RAMADAN, Q., 2004. On-chip micro-electromagnets for magnetic-based bio-molecules separation. Journal of Magnetism and Magnetic Materials. Vol. 281, no. 2-3, pp. 150–172.

RAMADAN, Q., POENAR, D. P. and YU, Ch., 2008. Customized trapping of magnetic particles. Microfluidics and Nanofluidics. Vol. 6, no. 1, pp. 53–62.

RAMSAY, G., 1998. Commercial biosensors : applications to clinical, bioprocess, and environmental samples. New York. Wiley. ISBN 9780471585053.

RAO, S. V., ANDERSON, K. W. and BACHAS, L. G., 1998. Oriented immobilization of proteins. Mikrochimica Acta. Vol. 128, no. 3-4, pp. 127–143.

RICHARDSON, J., HAWKINS, P. and LUXTON, R., 2001. The use of coated paramagnetic particles as a physical label in a magneto-immunoassay. Biosensors and Bioelectronics. Vol. 16, no. 9–12, pp. 989–993.

ROBINSON, G. A., HILL, H., PHILO, R. D., GEAR, J. M., RATTLE, S. J. and FORREST, G. C., 1985. Bioelectrochemical enzyme-immunoassay of human chorio-gonadotropin with magnetic electrodes. Clinical Chemistry. Vol. 31, no. 9, pp. 1449–1452.

RODRIGUEZ-MOZAZ, S., LOPEZ DE ALDA, M. J. and BARCELÓ, D., 2006. Biosensors as useful tools for environmental analysis and monitoring. Analytical and Bioanalytical Chemistry. Vol. 386, no. 4, pp. 1025–1041.

ROGERS, K., 2006. Recent advances in biosensor techniques for environmental monitoring. Analytica Chimica Acta. Vol. 568, no. 1-2, pp. 222–231.

ROGERS, K. R., 2000. Principles of affinity-based biosensors. Molecular Biotechnology. Vol. 14, no. 2, pp. 109–130.

RUZGAS, T., 1995. The development of a peroxidase biosensor for monitoring phenol and related aromatic compounds. Analytica Chimica Acta. Vol. 311, no. 3, pp. 245–253.

SASSOLAS, A., BLUM, L. J. and LECA-BOUVIER, B. D., 2012. Immobilization strategies to develop enzymatic biosensors. Biotechnology Advances. Vol. 30, no. 3, pp. 489–511.

SHAH, J. and WILKINS, E., 2003. Electrochemical biosensors for detection of biological warfare agents. Electroanalysis. Vol. 15, no. 3, pp. 157–167.

SHELDON, R. A., 2007. Enzyme immobilization: The quest for optimum performance. Advanced Synthesis & Catalysis. Vol. 349, no. 8-9, pp. 1289–1307.

SHEPPARD, N. F., TUCKER, R. C. and WU, Ch., 1993. Electrical conductivity measurements using microfabricated interdigitated electrodes. Analytical Chemistry. Vol. 65, no. 9, pp. 1199–1202.

SHITANDA, I., TAKADA, K., SAKAI, Y. and TATSUMA, T., 2005. Compact amperometric algal biosensors for the evaluation of water toxicity. Analytica Chimica Acta. Vol. 530, no. 2, pp. 191–197.

SKLÁDAL, P., 1996. Biosensors based on cholinesterase for detection of pesticides. Food Technology and Biotechnology. Vol. 34, no. 1, pp. 43–49.

SKLÁDAL, P., NUNES, G. S., YAMANAKA, H. and RIBEIRO, M. L., 1997. Detection of carbamate pesticides in vegetable samples using cholinesterase-based biosensors. Electroanalysis. Vol. 9, no. 14, pp. 1083–1087.

SOARES, C. M. F., DOS SANTOS, O. A., DE CASTRO, H. F., DE MORAES, F. F. and ZANIN, G. M., 2006. Characterization of sol–gel encapsulated lipase using tetraethoxysilane as precursor. Journal of Molecular Catalysis B: Enzymatic. Vol. 39, no. 1-4, pp. 69–76.

SOLÉ, S., MERKOÇI, A. and ALEGRET, S., 2003a. Determination of toxic substances based on enzyme inhibition. Part I. Electrochemical biosensors for the determination of pesticides using batch procedures. Critical Reviews in Analytical Chemistry. Vol. 33, no. 2, pp. 89–126.

SOLÉ, S., MERKOÇI, A. and ALEGRET, S., 2003b. Determination of toxic substances based on enzyme inhibition. Part II. Electrochemical biosensors for the determination of pesticides using flow systems. Critical Reviews in Analytical Chemistry. Vol. 33, no. 2, pp. 127–143.

SOLÉ, S., ALEGRET, S., CÉSPEDES, F., FÀBREGAS, E. and DÍEZ-CABALLERO, T., 1998. Flow injection immunoanalysis based on a magnetoimmunosensor system. Analytical Chemistry. Vol. 70, no. 8, pp. 1462–1467.

SOLNA, R., SAPELNIKOVA, S., SKLADAL, P., WINTHERNIELSEN, M., CARLSSON, C., EMNEUS, J. and RUZGAS, T., 2005. Multienzyme electrochemical array sensor for determination of phenols and pesticides. Talanta. Vol. 65, no. 2, pp. 349–357.

SONG, S., XU, H. and FAN, Ch., 2006. Potential diagnostic applications of biosensors: current and future directions. International Journal of Nanomedicine. Vol. 1, no. 4, pp. 433–440.

SOUZA, E., NASCIMENTO, G., SANTANA, N., FERREIRA, D., LIMA, M., NATIVIDADE, E., MARTINS, D. and LIMA-FILHO, J., 2011. Label-free electrochemical detection of the specific oligonucleotide sequence of dengue virus type 1 on pencil graphite electrodes. Sensors. Vol. 11, no. 6, pp. 5616–5629.

SPRAGUE, J. B., 1969. Measurement of pollutant toxicity to fish I. Bioassay methods for acute toxicity. Water Research. Vol. 3, no. 11, pp. 793–821.

STOYTCHEVA, M., 2002. Electrochemical evaluation of the kinetic parameters of a heterogeneous enzyme reaction in presence of metal ions. Electroanalysis. Vol. 14, no. 13, pp. 923.

STOYTCHEVA, M., 2010. Enzyme vs. bacterial electrochemical sensors for organophosphorus pesticides quantification. In: SOMERSET, V. S. (ed.), InTech. pp. 217–230. ISBN 9789537619589. Available from: http://www.intechopen.com/books/intelligent-and-biosensors/enzyme-vs-bacterial-electrochemical-sensors-for-organophosphorus-pesticides-quantification

SUGIURA, M. and INOUE, Y., 1999. Highly purified thermo-stable oxygen-evolving photosystem II core complex from the thermophilic cyanobacterium Synechococcus elongatus having His-tagged CP43. Plant & Cell Physiology. Vol. 40, no. 12, pp. 1219–1231.

SZYMANSKI, M., PORTER, R., DEP, G. V., WANG, Y. and HAGGETT, B. G. D., 2011. Silver nanoparticles and magnetic beads with electrochemical measurement as a platform for immunosensing devices. Physical Chemistry Chemical Physics. Vol. 13, no. 12, pp. 5383.

SZYMANSKI, M., TURNER, A., P., F., and PORTER, R., 2010. Electrochemical dissolution of silver nanoparticles and its application in metalloimmunoassay. Electroanalysis. Vol. 22, no. 2, pp. 191–198.

ŠETLÍKOVÁ, E., SOFROVÁ, D., PRÁŠIL, O., BUDÁČ, P., KOBLÍŽEK, M. and ŠETLÍK, I., 1999. Integrity and activity of photosystem 2 complexes isolated from the thermophilic cyanobacterium Synechococcus elongatus using various detergents. Photosynthetica. Vol. 37, no. 2, pp. 183–200.

ŠTOFIK, M., STRÝHAL, Z. and MALÝ, J., 2009. Dendrimer-encapsulated silver nanoparticles as a novel electrochemical label for sensitive immunosensors. Biosensors and Bioelectronics. Vol. 24, no. 7, pp. 1918–1923.

TABELING, P., 2005. Introduction to microfluidics. Oxford. Oxford University Press. ISBN 9780198568643.

THÉVENOT, D. R., TOTH, K., DURST, R. A. and WILSON, G. S., 2001. Electrochemical biosensors: recommended definitions and classification. Biosensors & Bioelectronics. Vol. 16, no. 1-2, pp. 121–131.

TOMALIA, D. A., NAYLOR, A. M. and GODDARD, W. A., 1990. Starburst dendrimers: Molecular-level control of size, shape, surface chemistry, topology, and flexibility from atoms to macroscopic matter. Angewandte Chemie International Edition in English. Vol. 29, no. 2, pp. 138–175.

TOMBELLI, S., MINUNNI, M. and MASCINI, M., 2005. Analytical applications of aptamers. Biosensors and Bioelectronics. Vol. 20, no. 12, pp. 2424–2434.

TOULOUPAKIS, E., BOUTOPOULOS, Ch., BUONASERA, K., ZERGIOTI, I. and GIARDI, M. T., 2012. A photosynthetic biosensor with enhanced electron transfer generation realized by laser printing technology. Analytical and Bioanalytical Chemistry. Vol. 402, no. 10, pp. 3237–3244.

TOULOUPAKIS, E., GIANNOUDI, L., PILETSKY, S. A., GUZZELLA, L., POZZONI, F. and GIARDI, M. T., 2005. A multi-biosensor based on immobilized Photosystem II on screen-printed electrodes for the detection of herbicides in river water. Biosensors and Bioelectronics. Vol. 20, no. 10, pp. 1984–1992.

TROJANOWICZ, M. and HITCHMAN, M. L., 1996. Determination of pesticides using electrochemical biosensors. TrAC Trends in Analytical Chemistry. Vol. 15, no. 1, pp. 38–45.

TUDORACHE, M. and BALA, C., 2007. Biosensors based on screen-printing technology, and their applications in environmental and food analysis. Analytical and Bioanalytical Chemistry. Vol. 388, no. 3, pp. 565–578.

ULMAN, A., 1991. An introduction to ultrathin organic films : from Langmuir-Blodgett to self-assembly. Boston. Academic Press. ISBN 9780127082301.

VANDAVEER, W. R., PASAS-FARMER, S. A., FISCHER, D. J., FRANKENFELD, C. N. and LUNTE, S. M., 2004. Recent developments in electrochemical

detection for microchip capillary electrophoresis. Elecrtrophoresis. Vol. 25, no. 21-22, pp. 3528–3549.

VARLAN, A. R., SULS, J., JACOBS, P. and SANSEN, W., 1995. A new technique of enzyme entrapment for planar biosensors. Biosensors and Bioelectronics. Vol. 10, no. 8, pp. xv–xix.

VERMA, N. and SINGH, M., 2005. Biosensors for heavy metals. BioMetals. Vol. 18, no. 2, pp. 121–129

VO-DINH, T. and CULLUM, B., 2000. Biosensors and biochips: advances in biological and medical diagnostics. Fresenius' Journal of Analytical Chemistry. Vol. 366, no. 6-7, pp. 540–551.

WALT, D. R. and AGAYN, V. I., 1994. The chemistry of enzyme and protein immobilization with glutaraldehyde. TrAC Trends in Analytical Chemistry. Vol. 13, no. 10, pp. 425–430.

WANG, J., 1985. Stripping analysis: principles, instrumentation, and applications. Deerfield Beach, FL. VCH. ISBN 9783527261925.

WANG, J., 1999. New label-free DNA recognition based on doping nucleic-acid probes within conducting polymer films. Analytica Chimica Acta. Vol. 402, no. 1-2, pp. 7–12.

WANG, J., 2006a. Analytical electrochemistry. Hoboken NJ. J. Wiley. ISBN 9780471678793

WANG, J., 2006b. Electrochemical biosensors: Towards point-of-care cancer diagnostics. Biosensors and Bioelectronics. Vol. 21, no. 10, pp. 1887–1892.

WANG, J. and KATZ, E., 2010. Digital biosensors with built-in logic for biomedical applications—biosensors based on a biocomputing concept. Analytical and Bioanalytical Chemistry. Vol. 398, no. 4, pp. 1591–1603.

WANG, J., LIU, G. and MERKOÇI, A., 2003. Electrochemical coding technology for simultaneous detection of multiple DNA targets. Journal of the American Chemical Society. Vol. 125, no. 11, pp. 3214–3215.

WANG, X.-J., XIA, S.-Q., ZHAO, J.-F., ZHAO, H.-N. and RENAULT, N. J., 2009. Inhibitive determination of heavy metal Ions by conductometric nitrate reductase biosensor. Chemical Research in Chinese Universities. Vol. 25, no. 4, pp. 443–445.

WARSINKE, A., BENKERT, A. and SCHELLER, F. W., 2000. Electrochemical immunoassays. Fresenius' Journal of Analytical Chemistry. Vol. 366, no. 6-7, pp. 622–634.

WEETALL, H. H. and HOTALING, T., 1987. A simple, inexpensive, disposable electrochemical sensor for clinical and immuno-assay. Biosensors. Vol. 3, no. 1, pp. 57–63.

WEIBEL, D. and WHITESIDES, G., 2006. Applications of microfluidics in chemical biology. Current Opinion in Chemical Biology. Vol. 10, no. 6, pp. 584–591.

WOLLENBERGER, U., SCHUBERT, F. and SCHELLER, F. W., 1992. Biosensor for sensitive phosphate detection. Sensors and Actuators B: Chemical. Vol. 7, no. 1-3, pp. 412–415.

WONG, S. S. and WONG, L.-J. C., 1992. Chemical crosslinking and the stabilization of proteins and enzymes. Enzyme and Microbial Technology. Vol. 14, no. 11, pp. 866–874.

YAGER, P., EDWARDS, T., FU, E., HELTON, K., NELSON, K., TAM, M. R. and WEIGL, B. H., 2006. Microfluidic diagnostic technologies for global public health. Nature. Vol. 442, no. 7101, pp. 412–418.

YALOW, R. S. and BERSON, S. A., 1959. Assay of plasma insulin in human subjects by immunological methods. Nature. Vol. 184, no. 4699, pp. 1648–1649.

YIN, H.-S., ZHOU, Y.-L. and AI, S.-Y., 2009. Preparation and characteristic of cobalt phthalocyanine modified carbon paste electrode for bisphenol A detection. Journal of Electroanalytical Chemistry. Vol. 626, no. 1-2, pp. 80–88.

YU, D., BLANKERT, B., BODOKI, E., BOLLO, S., VIRÉ, J.-C., SANDULESCU, R., NOMURA, A. and KAUFFMANN, J.-M., 2006. Amperometric biosensor based on horseradish peroxidase-immobilised magnetic microparticles. Sensors and Actuators B: Chemical. Vol. 113, no. 2, pp. 749–754.

ZACCO, E., PIVIDORI, M. I., ALEGRET, S., GALVE, R. and MARCO, M.-P., 2006. Electrochemical magnetoimmunosensing strategy for the detection of pesticides residues. Analytical Chemistry. Vol. 78, no. 6, pp. 1780–1788.

ZHANG, F., 2004. Immobilization of uricase on ZnO nanorods for a reagentless uric acid biosensor. Analytica Chimica Acta. Vol. 519, no. 2, pp. 155–160.

7. Annexes

7.1. Paper I

Štofik, M., Šoltová, P., Formanová, M., Masojídek, J., and Malý, J., 2008. Development of novel immobilization strategies for a PSII biosensor based on sol-gel and thin layer methods. *Manuscript in preparation*.

Development of novel immobilization strategies for a PSII biosensor based on sol-gel and thin layer methods

Štofík, M., Šoltová, P., Formanová, M., Masojídek, J., and Malý, J.

Manuscript in preparation

Abstract

The recent emphasis on environmental pollution control and disadvantages of the expensive and time consuming standard analytical measurements have indicated the need for novel methods for environmental screening of herbicides. Development of biosensors as fast, highly sensitive, and low-cost detection devices has gained in importance in the past few decades.

Recently, a biosensor based on a photosystem II (PSII) complex isolated from the thermophilic cyanobacterium *Synechococcus ellongatus* f. *thermalis* and immobilized in bovine serum albumin and glutaraldehyde matrix (BSA-GA) has been developed. The main aim of the presented work was to improve the parameters of the PSII biosensor such as sensitivity and the strength and stability of the signal by development of an immobilization method of a PSII complex in a sol-gel matrix formed from a sol-gel precursor diglycerilsilane (DGS).

The immobilization protocols and the composition of the immobilization mixture of the sol-gel immobilization method were optimized and compared with the currently used immobilization of PSII within a BSA-GA matrix. Computer simulations of a PSII biosensor performed with a numerical model were employed with the aim to find out how the thickness of the biosensor immobilization membrane and the concentration of protein in the immobilization membrane can influence the biosensor parameters.

Concerning operational and long-term stability, the novel sol-gel immobilization method offered similar biosensor characteristics to the previously used BSA-GA immobilization matrix. Biosensors prepared by the new method showed higher responses to light stimulation. Detailed computer simulation studies performed with a numerical model of a PSII biosensor developed in our lab showed a great importance of the thickness of the gel membrane for the operational parameters of a PSII biosensor and resulted in new modified protocols of PSII immobilization and measurement. The results of the simulations were confirmed experimentally. The developed numerical model can be further used for a better understanding of the process mechanisms of the biosensor and of the potential influence of other parameters on the overall performance of a biosensor. By employment of the novel immobilization protocols, the limit of detection (LOD) for herbicide diuron has been determined as 4.0×10^{-10} M (sol-gel immobilization), 2.0×10^{-10} M (BSA-GA immobilization) and EC50 as 3.3×10^{-8} M (sol-gel immobilization) and 3.2×10^{-8} M (BSA-GA immobilization).

In conclusion, sol-gel immobilization can be used as an alternative to the currently used BSA-GA immobilization method. The newly-developed immobilization method

based on a thin membrane layer and the revised measurement protocols improved the biosensor sensitivity in a sense of more accurate measurements, lowered the LOD and enabled to shorten the whole biosensor assay significantly.

1. Introduction

Soil and water pollution by herbicides has become one of the major problems in developed but also in the third world countries. Although they have been used in agriculture for many decades, their presence in water is unwanted and can have a bad impact on crops and human health. In the U.S. and the EU, the presence of pollutants in drinking water is regulated by legislative bodies. The main drinking water regulation norms in the EU including the recommended analytical methods for pollutant determination are outlined in (Hecq et al. 2006). For herbicide determination, chromatography methods (HPLC-MS and GC-MS) according to several standards applicable to a selected herbicide are recommended. Although such techniques are selective and very sensitive, they are expensive, time consuming, and demanding on the qualification of the staff.

For rapid environmental screening, biosensors as new bioanalytical methods seem to be a good alternative. Some biosensor methods use phototrophic microorganisms such as micro-algae as a sensing element. Micro-algae are sensitive to water contamination and their responses to changes in water quality have been utilized in micro-algae cell biosensors for environmental pollutant monitoring (Brayner et al. 2011).

Herbicides are known to have several toxic mechanisms to act on phototrophic organisms (Duke 1990). One of the common mechanisms which inhibit the photosynthesis is blocking of the electron transport chain in the PSII complex (Draber et al. 1991). This mechanism is used by phenolureas, triazines and phenolic classes of herbicides (Fedtke 1982). An inhibitor (a herbicide) competes with a reversibly bound plastoquinone at the secondary quinon acceptor (the quinone-binding site, Q_B) in a D1 protein of a PSII complex. The fact that many commonly used herbicides inhibit light reactions of photosynthesis by targeting a PSII-dependent electron flow and that a stable isolated PSII reaction center has been available since the middle of 1980s (McTavish et al. 1989), a new opportunity for environmental screening of pollutants by the use of photosynthetic proteins as sensing elements arose. A number of published works dealing with the biosensors based on inhibition of the PSII function are reviewed in (Giardi et al. 2001; Giardi & Pace 2005).

A biosensor based on the principle of blocking the PSII function was developed by Koblizek et al. (2002). The biosensor consists of a PSII complex isolated from the thermophilic cyanobacterium *Synechococcus elongatus* (Koblížek et al. 1998; Šetlíková et al. 1999) immobilized on the surface of a screen printed electrode. The activity of the PSII complex is excited by light pulses from a red LED diode. The development of the biosensor started with optimization of the composition of a PSII immobilization matrix. A gelatin matrix containing manitol, an agarose entrapment matrix and a BSA-GA crosslinking matrix were employed. The BSA-GA crosslinking was evaluated as the best

suited immobilization matrix. The biosensor has been used for detection of herbicides such as diuron, atrazine, simazine, isoproturone (Malý et al. 2005; Masojídek et al. 2011) and since its first employment it has been developed further.

This study aims at an improvement of the above mentioned biosensor in a sense of more rapid, more accurate and more sensitive detection. It concentrates on adjustment of the immobilization technique of the PSII complex. It is known that a suitable immobilization method can preserve the functionality of an enzyme and enhance its stability (Klibanov 1979; Gianfreda & Scarfi 1991). Based on the natural complexity of an isolated PSII complex, an encapsulation of the PSII into an inorganic silicate matrix in a bulk membrane on the electrode surface was studied.

Immobilization of enzymes into silicate matrices by sol-gel process has been one of the progressing methods in the past two decades since the enzyme immobilization in a polymerizing tetramethoxysilane with retention of the enzyme activity was performed (Braun et al. 2007). A sol-gel process involves hydrolysis of precursor monomers either under acidic or basic conditions followed by polycondensation of the hydroxylated units. Metal alkoxides such as tetramethoxysilane (TMOS) or tetraethoxysilane (TEOS) are frequent reaction precursors. The entrapment of the enzyme into an immobilization matrix by a sol-gel process is based on the growing of siloxane polymer chains around the encapsulated biomolecules.

Advantages of the enzyme immobilization into silica-based sol-gel materials are the optical transparency and chemical inertia of the silica materials, their potential to be chemically modified by various polymer additives, redox modifiers, organically modified silanes and the possibility of tuning their pore size and pore distribution (Jin 2002), which allows them to be used in diverse biosensor applications (Gill 2001; Jin 2002; Avnir et al. 2006). Besides, it was the simplicity of the formation of the silica immobilization membrane and the mild temperatures of the sol-gel process that played an important role for the final choice of this method for the PSII complex immobilization.

A well-known problem during a sol-gel reaction is formation of alcohols during hydrolysis. The alcohols can negatively influence the activity of certain proteins present inside the immobilization matrices (Miller et al. 1996). To overcome this problem, the alcohol has to be evaporated or washed out of the membrane after gel is formed at the end of the sol-gel process. There have been attempts to develop a more biocompatible processing method. Such immobilization could be performed for example via an aqueous colloidal sol–gel process (Liu & Chen 1999). Other very promising attempts use precursors derived from glycerol (Gill & Ballesteros 1998). Glycerol is often used as a storage buffer and its presence in the silica membrane is thus favorable for preserving the enzyme activity.

Recently, a diglycerylsilane (DGS) precursor was synthetised (Besanger et al. 2003; Brook et al. 2004) and it was proven that the examined enzymes immobilized in silica membranes prepared with the glyceroxisilane precursor showed better activity,

better kinetic parameters and long-term stability compared with immobilization in a silica membrane prepared with a TEOS precursor. Since then, also other studies (Sui et al. 2005; Vila-Real et al. 2010) confirmed the suitability of this biocompatible precursor for protein immobilization. The DGS precursor has also been used successfully for biosensor immobilization (Dattelbaum et al. 2009).

The presented work provides a new approach to the immobilization of a PSII complex onto a screen printed electrode for a PSII biosensor (Koblížek et al. 2002) by a sol-gel process using a DGS precursor. The membrane composition is altered by variations of the concentration of bovine serum albumin (BSA) as a doping agent in the immobilization matrix. The properties of biosensor prepared with optimized silica immobilization are compared with biosensors prepared with crosslinking immobilization by GA. In this study newly designed immobilization and assay protocols based on results and knowledge gained from computer simulations of the PSII biosensor have been developed. They have been applied to biosensors prepared with both immobilization techniques. As a result, the operational and analytical performance of the biosensor has been improved.

2. Materials and methods

2.1. Chemicals and materials

Glutaraldehyde (GA), (3,4-dichlorophenyl)-1,1-dimethyl urea (DCMU, diuron), duroquinone (DQ) and bovine serum albumin (BSA) were purchased from SIGMA-ALDRICH spol. s r.o. Diglycerylsilane (DGS) was synthesized according to (Brook et al. 2004). The photosystem II complex (the content of chlorophyll in PSII suspension ~ 125 µg/mL) was isolated from the thermophilic cyanobacterium *Synechococcus ellongatus* f. *thermalis*, strain KROVOV 1972/8 in the laboratory of Dr. Jiří Masojídek in Třeboň (Czech Republic).

2.2. Protocols for PSII immobilization – the preparation of the enzyme electrodes

An isolated PSII complex was divided into aliquots and stored at -70 °C. For experiments, an aliquot was defrosted and used as follows. The surface of the amperometric sensors was cleaned with distilled water and dried out with a nitrogen flow before each immobilization. The sensors were put on a wetted filter paper into an opened Petri dish. The immobilization mixture was prepared and 0.4 µL of the mixture was pippeted (dropped) on the surface of the working electrode of every sensor immediately. The opened Petri dishes with the sensors were stored at 4 °C for 20 minutes and then closed. The sensors were stored at 4 °C (BSA-GA membrane) for at least 3 hours and at 4 °C (sol-gel membrane) for 6 hours before measurements were performed. In long-term stability experiments, after 3 hours of the storage at 4 °C, the sensors were put into -20 °C. The sensors were always stored in the dark. The BSA and GA solutions were prepared in distilled water. Any manipulation with the PSII was

performed in a dark room. When necessary, only a low intensity of green light was used in order to preserve the PSII activity.

2.2.1. BSA-DGS (sol-gel) mixture

First, DGS was sonicated in deionized water in an eppendorf tube for 15 minutes. The DGS to water ratio was 10 mg to 15 µL (Montereali et al. 2010) for all examined ratios of BSA-DGS-PSII. A PSII complex was defrosted and certain volumes of BSA and the PSII were mixed thoroughly in an eppendorf tube on a vortex. Immediately after the sonication, a certain volume of DGS was added to the prepared mixture and mixed thoroughly on a vortex again. The examined volumes of BSA, DGS, and PSII are listed in Tab. 1.

2.2.2. BSA-GA mixture

An aliquot of a PSII complex was defrosted. 5 µL of 10% (w/v) BSA and 5 µL of concentrated PSII were mixed thoroughly in an eppendorf tube on a vortex. Then, 2 µL of 5% (v/v) GA were added and the mixture was mixed again.

BSA concentration	Variant A			Variant B		
	volume ratios of membrane components [%]			volume ratios of membrane components [%]		
	DGS/25.00 PSII/56.25 BSA/18.75	DGS/33.30 PSII/50.00 BSA/16.70	DGS/50.00 PSII/37.50 BSA/12.50	DGS/25.00 PSII/37.50 BSA/37.50	DGS/33.33 PSII/33.33 BSA/33.33	DGS/50.00 PSII/25.00 BSA/25.00
20 mg/ml	11A	12A	13A	-	-	-
40 mg/ml	-	-	-	11B	12B	13B
50 mg/ml	21A	22A	23A	-	-	-
100 mg/ml	-	-	-	21B	22B	23B
80 mg/ml	31A	32A	33A	-	-	-
160 mg/ml	-	-	-	31B	32B	33B
110 mg/ml	41A	42A	43A	-	-	-
220 mg/ml	-	-	-	41B	42B	43B
130 mg/ml	51A	52A	53A	-	-	-
260 mg/ml	-	-	-	51B	52B	53B

Table 1. The concentrations and the volume ratios of the examined membrane components.

The marking of variants contains of two numbers and a letter. The first number corresponds to the concentrations of BSA in the column BSA concentration. The other number corresponds to the volume ratios of DGS, PSII and BSA. By increasing the number, the volume ratio of DGS increases and the volume ratio of the overall protein volume decreases (PSII and BSA proportionally). The letter corresponds to the columns Variant A and B. In the column Variant A, there is higher volume (concentration) of PSII in comparison with the column Variant B, but lower volume and lower concentration of BSA. Each variant was tested on four different sensors.

2.3. Amperometric measurements

Biosensor amperometric measurements were performed by using screen-printed 3-electrode sensors with a working, a reference, and an auxiliary electrode (type AC1.W1.R1), and a microflow cell system (MFS). Both were purchased from BVT Technologies, a. s. (Czech Republic). The MFS system consisted of a red light-emitting diode (LED), a glass-jacket vessel and a control box unit with appropriate software Bioanalyzer BEEP. The operation of the system including the illumination of the diode was controlled by the control box unit connected to the computer with the Bioanalyzer software. Such a compact device enabled semiautomated measurement with data processing.

Prepared sensors with an immobilized PSII complex were inserted into a microflow unit. The unit was placed into a glass-jacket vessel with buffered assay solution. The design of the unit enabled the solutions to bypass the sensor electrodes in a microcapillary channel and to illuminate the working electrode with red light. The start of the illumination pulses, the period of the light and the dark, the applied potential on working electrode (+620 mV vs. Ag/AgCl reference electrode) and the end of the measurement were controlled by a unit control box and by computer software Bioanalyzer BEEP. The assay solution consisted of 0.6 mL concentrated buffer (150 mM MES, 1 M NaCl, 50 mM $MgCl_2$ pH 6.5) mixed with 5.4 mL of distilled water. An artificial electron mediator duroquinone was always present in the concentration of 0.2 mM.

2.3.1. Sol-gel optimization bioassays

During optimization assays of the sol-gel immobilization method at the beginning of every measurement, the measured current of the sensors was let to stabilize. Then, a series of 5 or 10 light/dark periods (15/180 s) was initialized until the measurement was terminated.

2.3.2. A routine bioassay protocol for the detection of herbicides

A routine protocol for the detection of herbicides consists of three main steps, see Fig. 1. The first step is negative sample control, the measured current of the biosensor is let to stabilize and a series of four light pulses (light/dark) is initiated. The second step is sample analysis, the measured sample is added to the solution and another series of four light pulses (light/dark) is initiated. Finally, the reference standard of phytotoxicity (RSP) is added and the last 4 light pulses (light/dark) are initiated. The measurement finishes after a series of 12 pulses. The peaks present in the bioassay signal correspond to the light stimulation by light pulses. From the beginning of the bioassay, the height of peaks decreases in time. The natural decrease of the height of peaks is fitted to the power function. Data are evaluated in the way that first, they are normalized according to the highest peak. Then, the first four peaks are fitted to the power function and the 8th and the 12th peak are estimated. The extent of the inhibition of PSII by herbicide present in the measured sample correlates with the difference between the estimated and the

measured values of the 8th peak. The extent of the inhibition of PSII by RSP correlates with the difference between the estimated and the measured values of the 12th peak. Based on the obtained data, a dose-response curve could be plotted.

RSP represents the concentration of 1×10^{-7} M of diuron, see (Masojídek et al. 2011). This concentration results in a 50% reduction in the PSII biosensor activity.
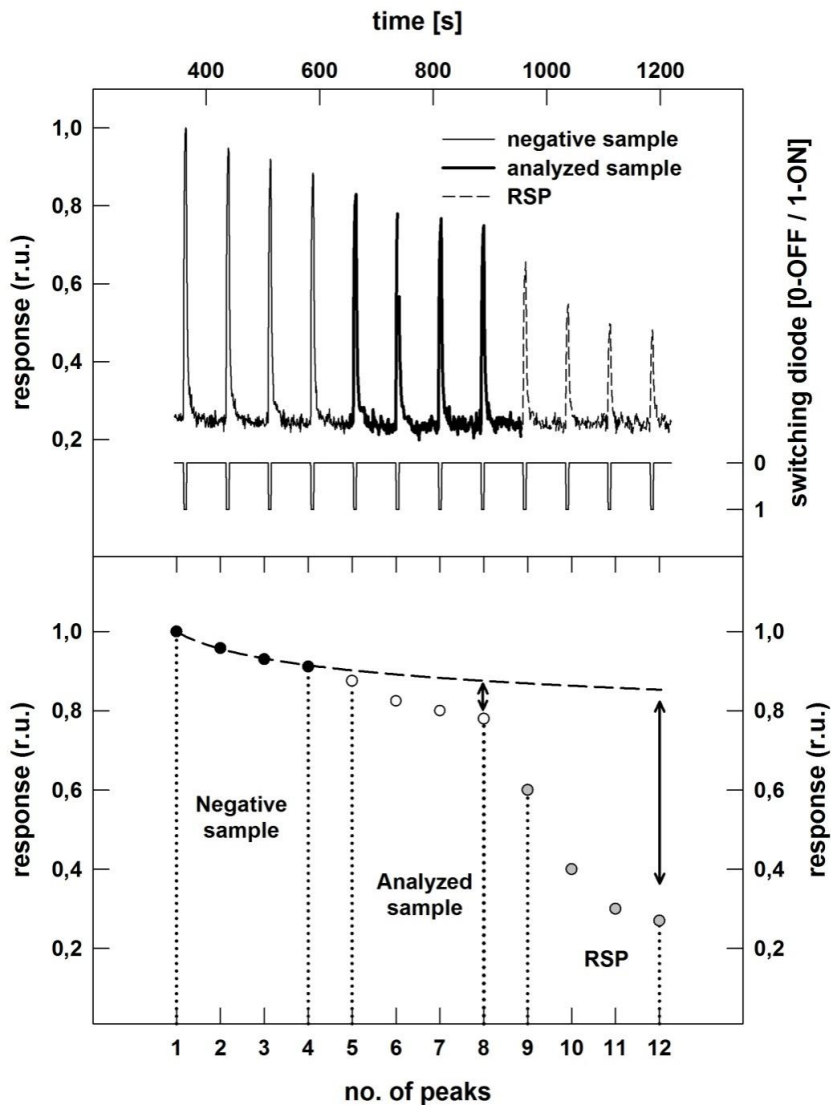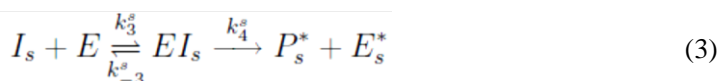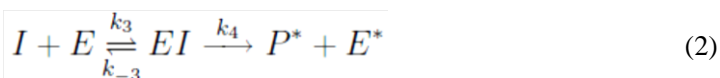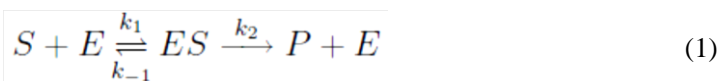

Figure 1. A measuring protocol of a PSII biosensor assay.

The assay starts with an equilibration period of 360 s. Then, 3 series of light/dark periods (5/70 s) are recorded and a negative sample (without herbicide), an analyzed sample (with herbicide) and the RSP are added to the examined solution subsequently. The upper panel shows the signal after normalization (the left y axis) and after 12 light/dark pulses (0-light is off, 1-light is on) during the assay. The bottom panel shows the normalized peak height for the calculation of the degree of the biosensor inhibition. The

bioassay signal decrease is evaluated by fitting to the power function, dashed line in the bottom panel.

2.4. Simulations performed by Biomodel software

Simulations of a PSII biosensor were performed by Biomodel software (Malý 2006). The simulations enabled to study amperometric responses of acetylcholinesterase and of PSII biosensors. The simulations of the PSII biosensor were based on three reactions as follows (Malý et al. 2006):

$$S + E \underset{k_{-1}}{\overset{k_1}{\rightleftharpoons}} ES \xrightarrow{k_2} P + E \tag{1}$$

$$I + E \underset{k_{-3}}{\overset{k_3}{\rightleftharpoons}} EI \xrightarrow{k_4} P^* + E^* \tag{2}$$

$$I_s + E \underset{k_{-3}^s}{\overset{k_3^s}{\rightleftharpoons}} EI_s \xrightarrow{k_4^s} P_s^* + E_s^* \tag{3}$$

where S is a substrate, E is enzyme, ES is a metastable complex enzyme-substrate, P is the product, I is an inhibitor (unknown), EI is a metastable complex enzyme-inhibitor, P^* is the product due to the decay of the EI, E^* is permanent modified enzyme formed by the decay of the EI, I_s is an inhibitor (standard), EI_s is a metastable complex enzyme-inhibitor standard, P_s^* formed by the decay of the EI_s, E_s^* is permanently modified enzyme formed by the decay of the EI_s and k_1, k_{-1}, k_2, k_3^i, k_{-3}^i, k_4^i, k_3^s, k_{-3}^s, k_4^s are the rate constants.

A numerical model was solved by an explicit network method where all equation parameters were controlled by the user. The model offered various modes of presentation of the results and was able to solve problems which were difficult to evaluate experimentally (Malý et al. 2006).

3. Results and discussion

3.1 The optimization of the composition of the sol-gel membrane

We had supposed that first, the amount of sol-gel precursor is important for creation of a suitable polymerizing network and second, the amount of loaded protein plays an important role in the distibution of the protein. These factors could influence the final gel properties for the retention of the PSII activity and suitable diffusion properties of the assay solutions inside the silica network. They could also influence the mechanical properties of the membrane. That is why various volume and weight combinations of proteins and sol-gel precursors were examined during the optimization of the sol-gel immobilization, as shown in Tab. 1. Two main parameters as the most important properties of the biosensor for further selection of the most suitable composition of the sol-gel membrane were followed: (i) the height of peaks of the amperometric signal after light stimulation and (ii) the profile of the signal decrease in time.

Although the mechanical properties of the immobilization matrix were not examined in detail, they became the limiting factor for the functioning of the biosensor from the beginning of the experiments. The poor mechanical attributes of the sol-gel matrices as a result of brittleness and low resistivity to mechanical stress are the main disadvantages of the sol-gel membranes (Gill 2001). The combination of membrane components marked as 11A, 12A, 13A, 21A, 22A, 23A, 11B, 12B, 13B, 21B, 22B, 23B, see Tab. 1, failed in adhesion to the electrode surface. After the sensors with an immobilized membrane were inserted into the MFS system and the measurement started, it was difficult to obtain a reasonable signal. In the majority of the examined sensors, the membranes dropped out from the sensor working electrode after the sensor was taken out from the cell. This led to the conclusion that membranes prepared with such combinations of the components are characterized by bad adhesion to the surface of the sensor working electrode. That is why no data related to this tested compositions are presented in Fig. 2. As can be seen in Tab. 1, the series of combination 11A, 12A, 13A, 21A, 22A, 23A, 11B, 12B, 13B, 21B, 22B, 23B have the lowest protein concentration loaded in the membrane. The membrane marked as 33A could not be measured either because of the same problems.

In the upper part of Fig. 2, responses of sensors prepared according to Tab.1 to light stimulation are plotted. The values present the means of 5 peaks (negative sample) of the 4 measured sensors. Only 1/3 of the 18 examined combinations had a signal higher than the overall mean. The highest signal was measured in combinations marked 31B, 31A and 32A, and the lowest signal in 53A, 52A, 42A. When the concentration of single components was studied carefully, it could be seen that the highest signal tended to appear in sensors with the highest content of the PSII. Such combinations had the middle label equal to 1 and they also had the lowest content of the sol-gel precursor. This was probably the result of high concentration of the PSII complex but also of a lower density of the silica network leading to better diffusion of the redox mediator inside of the membrane, and of a better encapsulation of the PSII complex not fixed in the membrane so firmly. The highest concentration of the PSII complex with relation to the overall protein presence in the immobilization membrane is in A type combinations. However, when comparing the signal of the combinations starting with number 5, we can see that B type combinations give higher measured signals despite lower concentration of the PSII complex. This is probably the result of more suitable protein distribution in the membrane and better accessibility of the PSII complex to the solution containing an artificial electron mediator. Based on these observations, we can see that the presence of an additional protein component in the immobilization membrane influences membrane properties and leads to improvement of the measured signal.

In the bottom part of Fig. 2, a standard deviation (SD) from the normalized signals of 5 peaks of 4 measured sensors is plotted. Due to the fact that a signal in a PSII biosensor has a tendency to decrease during a measurement, the best value of the standard deviation cannot be expected near to zero. As can be seen from the plotted data, the standard deviation fluctuates around the value of 0.1. Lower values indicate that the

signal does not decrease or increase in time, i.e. it is more or less stable. Higher values indicate that there are high differences in the measured signal and the signal drops or rises quickly.
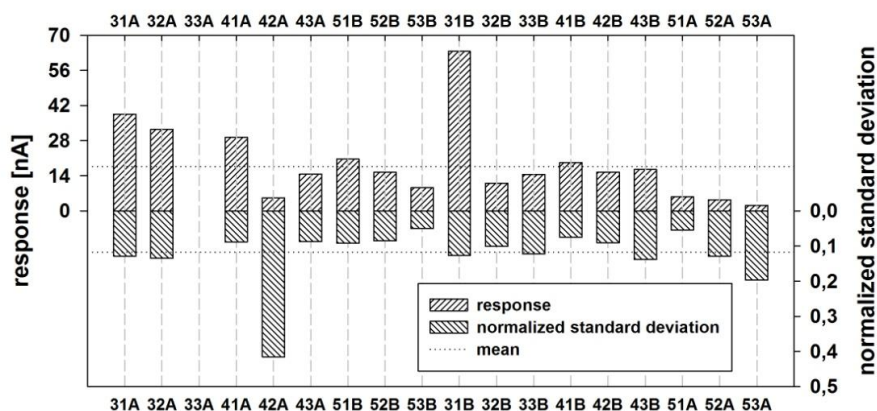

Figure 2. The responses of biosensor and their normalized standard deviation.

The top bars present the mean value of the heights of subsequent peaks (the response of the sensors to the diode light) of all tested sensors for a given combination of BSA, DGS and PSII particles. Sensors 31B, 31A and 32A have the highest measured signal. The bottom bars present the normalized standard deviation of the examined sensors. Sensors 53B, 41B and 52B have the lowest value of the SD. Sensors 42A and 53A have the highest value of the SD.

During biosensor assays, the first four peaks are important for the estimation of the height of the 8th and the 12th peak (the response is fitted to the power function). For investigation of a suitable profile of the biosensor signals, where first peak is the highest and subsequent peaks decrease in time, another graphical evaluation was performed (see Fig. 3). Four sensors were tested in each experimental variant and the first 5 peaks were recorded. The number of occurrences of their highest peaks in different positions (the first, the second, the third, the fourth, and the fifth) is demonstrated by a square symbol. The number of occurrences of the highest peaks expresses in how many different positions the highest peaks of the four tested sensors were counted. Since the biosensors were expected to have the same profile of the signal, the best value, with the highest peak always in the same position, was one and the worst value, where each highest peak was in a different position, was four (four sensors were tested). The best results were obtained from sensors 31A, 32A, 31B, 53B. A circle symbol demonstrates the position with the highest number of the occurrence of the highest peak. Because a decrease in signal is expected, the highest frequency of occurrences of the highest peak is expected in the first position (the first peak is the highest one) and therefore, the best value is one. In this case, more sensors obtained the best value. However, we can see that only sensors 31A, 32A and 31B have both, the highest peak always in the same position and the highest frequency of occurrences of the highest peak in the first position.
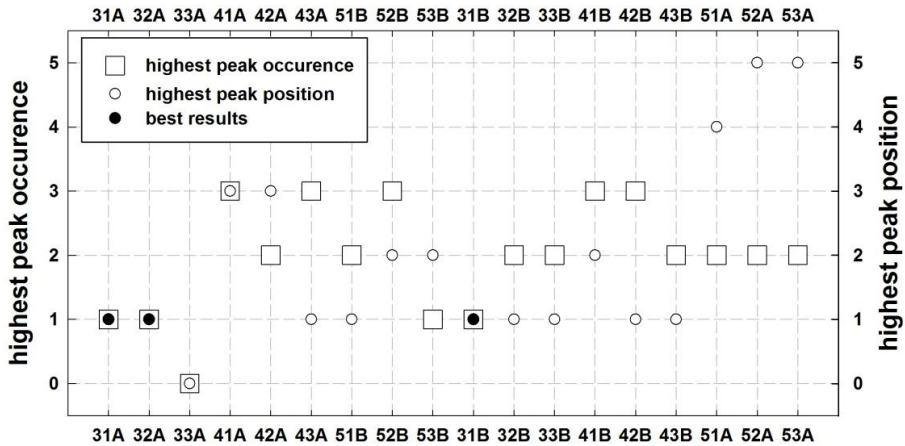
Figure 3. Investigation of a suitable profile of the biosensor signals.

The number of occurrences of the highest peaks at different positions is presented by a square. Four sensors were tested, so the possible values are 1, 2, 3 or 4. The position of the highest peaks with the highest frequency of occurrences is presented by a circle. The sensors were stimulated by a series of five subsequent illuminations, so the possible values are 1, 2, 3, 4 or 5. The best results are presented with a filled circle in a square.

As it had been described in Materials and methods, the bioassay signal decrease was evaluated by fitting to the power function. The obtained data were further fitted by this function and the mean values of the coefficient of determination (R^2) and its standard deviations were plotted. Fig. 4 shows that the measured signal of sensors marked as 43A, 31A and 51B had the best fitted values. Combinations with curves that could not be fitted (mostly when the highest peak was not in the first position) were not evaluated.
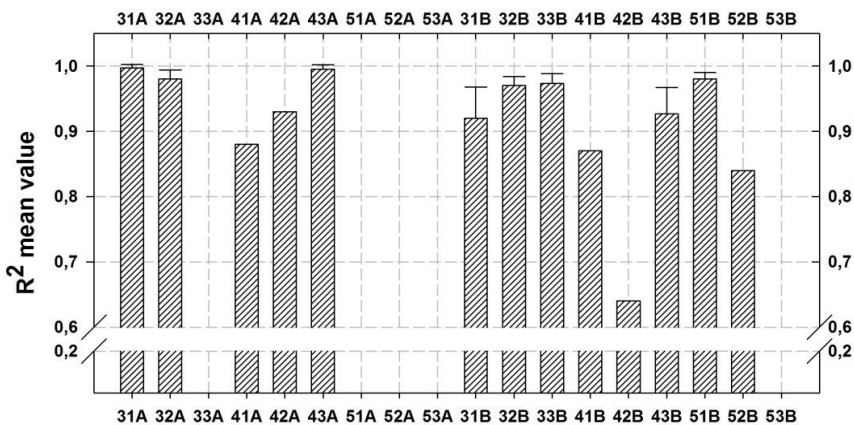
Figure 4. The R^2 of the power function fitted through the first five peaks of the sensor response.

The bars present the mean value of the R^2 of four sensors fitted to the power function. The values of the error bar caps present the SD.

Based on all three evaluation techniques, the 31A combination was selected for further studies. The composition of the membrane was the ratio 4:6:6 µL of DGS:PSII:BSA with BSA concentration of 80 mg/mL. The biosensor signal of the selected combination is presented in Fig. 5.
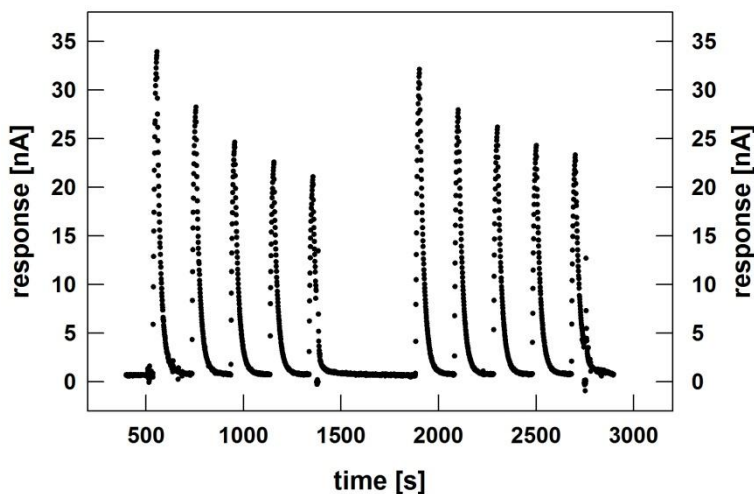
Figure 5. Responses of two different 31A sensors.

The 31A series was evaluated as the best one to fulfil all examined conditions and it was selected for further studies.

3.2. The stability of biosensors

The evaluation of the operational stability of biosensors prepared with a sol-gel membrane was performed and compared with the stability of sensors prepared with a BSA-GA membrane. For this purpose, a signal of 10 subsequent light stimulations (an assay consists of 8 light stimulations) was recorded. The operational stability of biosensors prepared with the sol-gel method was comparable with the stability of biosensors prepared by the BSA-GA membrane. Both biosensors were characterized by a stable signal.

Then, two groups of sensors were prepared in the quantity of 8 and 16 by a sol-gel encapsulation and a BSA-GA crosslinking method. The groups of 8 sensors consisted of one immobilization batch and the groups of 16 sensors consisted of two different batches. The intensity and the standard deviations of the signal are plotted in Fig. 6. The upper part of the plot presents the measured signal intensity with the standard deviation and the bottom part presents the standard deviation from the normalized signal. From the plotted data we can see that the sensors with a sol-gel membrane give a higher overall mean signal value (103.6 nA for 8 sensors) compared with the mean signal value (46.0 nA for 8 sensors) of the sensors with a membrane prepared by a BSA-GA method. In the group of 16 electrodes prepared with a sol-gel immobilization method, higher diversity of the measured signal (a higher normalized standard deviation) with lower mean signal value (80.3 nA) is present. The mean signal value (45.8 nA) of the sensors

prepared with a BSA-GA crosslinking method is similar to the previous evaluation and has a similar normalized standard deviation. This is assumed to be a result of worse adhesion of the sol-gel membrane to the working electrode, which causes high signal variations and lower overall signal strength. This assumption has been confirmed also by personal observations.
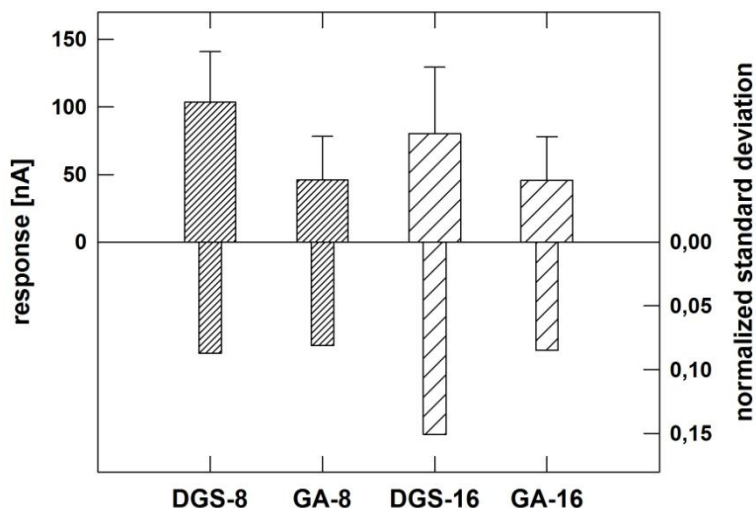

Figure 6. The signal intensity of biosensors with a BSA-DGS (DGS) and a BSA-GA (GA) immobilization matrix.

Responses of two different series of 8 and 16 sensors with a DGS and a GA immobilization matrix were examined and the mean value of the first ten peaks of all 8 and 16 sensors were calculated. The error caps of the top bars present the SD and the bottom bars express the normalized standard deviation.

The investigation of the long-term stability of a biosensor was performed in two parallel experiments. Two periods of time were set to 14 days and to 4 months. During the whole first period, the sensors were stored in MES buffer at 4 ºC. During the second interval, the prepared sensors with an immobilized membrane were frozen and stored at -20 ºC. Prior to the measurement, they were slowly defrosted at 4 ºC. Fig. 7A shows that the biosensor activity decreases most on the first and on the second day (40% BSA-DGS and 45% BSA-GA of the initial signal) when biosensors are stored at 4 ºC. The measured signals continue to decrease in biosensors prepared with a BSA-DGS method (3% of the initial activity on the 13th day). However, a decrease in the signal of biosensors prepared with BSA-GA stops and a plateau with approx. 25% of the initial activity can be observed in the last third of the storage time. For biosensors stored at -20 ºC, a decrease in the signal measured after 14 days of storage is 35% (BSA-DGS) and 50% (BSA-GA) of the initial activity and then, a plateau can be observed for both immobilization methods (Fig. 7B). At the end of the experiment, 4th month after the immobilization, 7% (BSA-DGS) and 6% (BSA-GA) of the initial activity was measured. Based on the exponential signal decay, half-life values of the biosensor activity was

evaluated as 2 (1.96) days for a BSA-DGS membrane and 4 (3.51) days for a BSA-GA membrane for sensors stored at 4 ºC. For sensors stored at - 20 ºC, the half-life value of the biosensor activity was 20 (20.48) days for a BSA-DGS membrane and 26 (26.47) days for BSA-GA membrane, respectively.
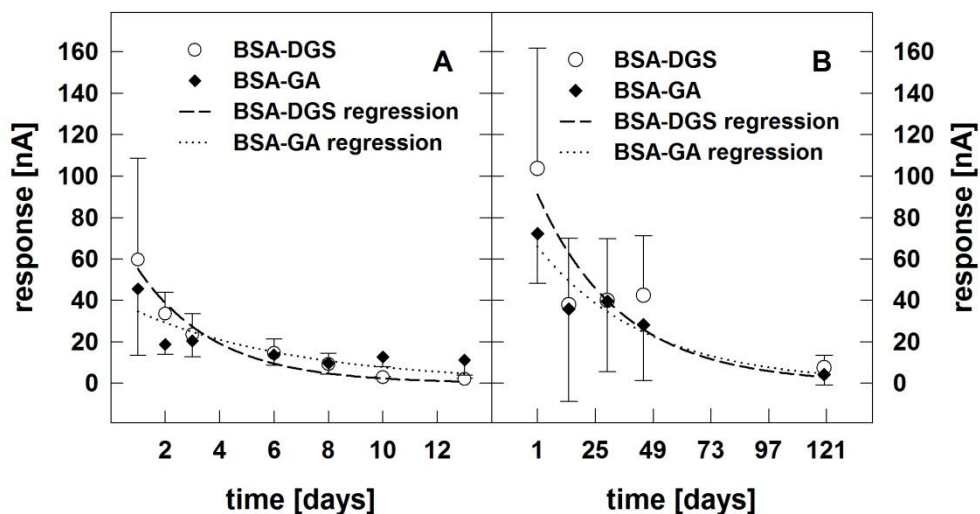

Figure 7. Long-term stability of sensors with a BSA and a DGS immobilization matrix.

The panels present the mean value of the responses (first ten peaks) of two different series of 5 sensors measured on a given day. The caps of the error bars present the SD. The experiments for the short-term and the long-term stability were performed by two different series of sensors. Panel A shows the short-term stability of the examined sensors. The sensors were stored at 4 ºC for two weeks. The long-term stability of the examined sensors is presented in panel B. The sensors were stored at -20 ºC for 4 month.

For both long-term evaluations of the half-life parameter of the biosensors activity, we can see that the biosensors prepared with sol-gel immobilization have significantly lower values compared with the biosensors prepared with BSA-GA crosslinking immobilization. It is apparent that a PSII complex crosslinked in an immobilization membrane with a BSA-GA preserves its activity better compared with a PSII complex encapsulated in a sol-gel. However, this is valid only for biosensors stored at 4 ºC. For biosensors stored at -20 ºC, BSA-DGS immobilization seems to be more suitable. Although we can see that the half-life parameter is significantly lower for the BSA-DGS immobilization, the signal values of the BSA-DGS measured in given time intervals are higher than the values of the BSA-GA signal. Significantly lower half-live parameters for sol-gel immobilization in this type of experiment were caused mainly by the fact that sol-gel biosensors had a significantly higher signal at the beginning of the immobilization. The values of the signal at the beginning of the immobilization were included in the half-life estimation.

Values for the apparent Michealis-Menten constant K_M^{app} were evaluated as 1.97×10^{-4} M for a sol-gel and 1.64×10^{-4} M for a BSA-GA crosslinking method. The values were calculated from the signal intensity dependence on the concentration of duroquinone (an artificial electron mediator) as the substrate (no graph is presented). Although the value of K_M^{app} for BSA-GA crosslinking is lower than the K_M^{app} for sol-gel encapsulation, both values differ only to a low degree. It means that different immobilization environment does not influence the kinetic parameters of the immobilized enzyme significantly.

3.3. Computer simulations of a PSII biosensor

In this study, a series of numerical simulations were performed with fixed basic biosensor parameters (the initial concentration of the substrate and the enzyme, diffusion coefficient for the substrate, for the product and for the inhibitor, and kinetic constants). The altered parameters were membrane thickness and enzyme concentration. The signal of the biosensor was studied in relation with the responses of the biosensor to low $(5 \times 10^{-9}$ M$)$ and high $(1 \times 10^{-7}$ M$)$ inhibitor concentrations. A detailed description of the model is not included in this work as it is discussed thoroughly in the software manual (Malý et al. 2006). The absolute values of the biosensor signal obtained in simulations depended on the definition of the initial parameters and could not be directly compared to values from real measurements. However, the changes of the biosensor responses caused by adjustments of the initial parameters can predict changes in the behavior of the signal of a real biosensor.

First, membrane thickness was altered as can be seen in Fig. 8. The overall biosensor signal rises with an increase in the membrane thickness (the plots from the left to the right) from 0.5, 1.1, 2 µm. This set of simulations shows a quick response of the biosensor to low (the upper plots) and high (the bottom plots) inhibitor concentrations and quick stabilization of the signal when a thin membrane is present.
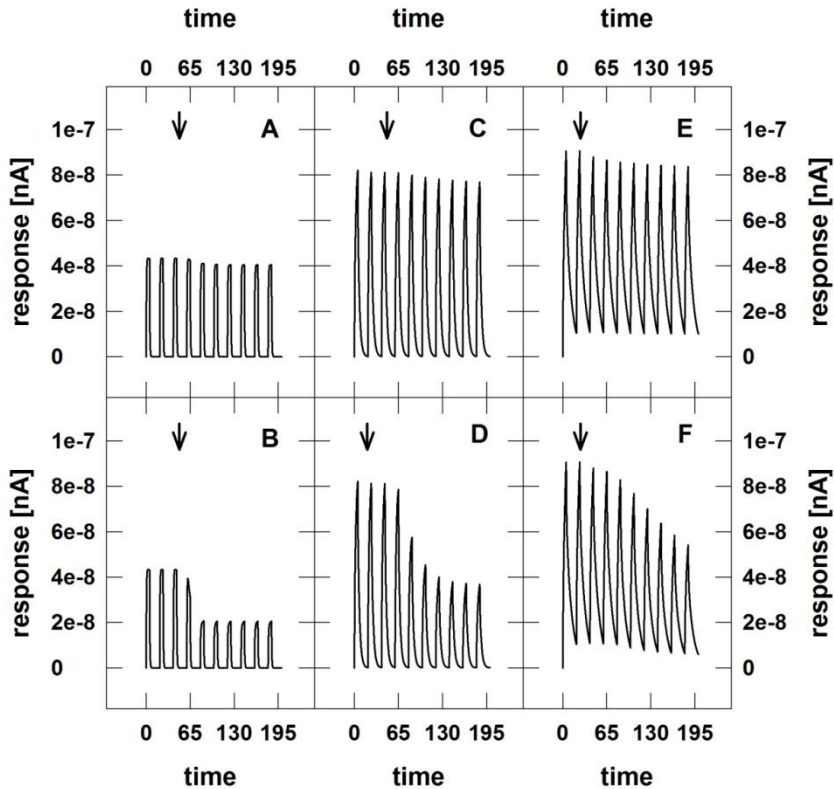
Figure 8. Simulations of the signal of a biosensor.

Three different values of membrane thickness are presented in separate columns. They are set to 5×10^{-4} m (panels A, B), 1.1×10^{-3} m (panels C, D), 2×10^{-3} m (panels E, F), respectively. The top panels (A, C, E) show the signal responses to the addition of 5×10^{-9} M concentration of an inhibitor. The bottom panels (B, D, F) show the signal responses to the addition of 1×10^{-7} M concentration of an inhibitor.

Based on the results, another set of simulations was performed (see Fig. 9). The whole biosensor assays (as will be explained further) were simulated with two additions of an inhibitor (concentrations of 4×10^{-8} and 1×10^{-7} M) and three different membrane thickness values were set like in the previous simulations (5×10^{-4}, 1.1×10^{-3}, and 2×10^{-3} m). From the course of the simulated responses, we can see that the biosensor responses have a comparable behavior with the responses in the previous simulations. The signal intensity of the biosensor falls with a thinner membrane and rises slightly with an increased membrane thickness (from the top to the bottom panels, Fig. 9). A response of the biosensor to the presence of an inhibitor is also observable. Moreover, the response is fast and the signal stabilizes rapidly not only after light stimulations but also after inhibitor addition in biosensors with a thin membrane (Fig. 9A). The responses are quick and highly distinguishable. In a biosensor with a thick membrane, the changes as reactions to additions of an inhibitor are more difficult to observe and the stabilization of the signal is very slow (Fig. 9C).
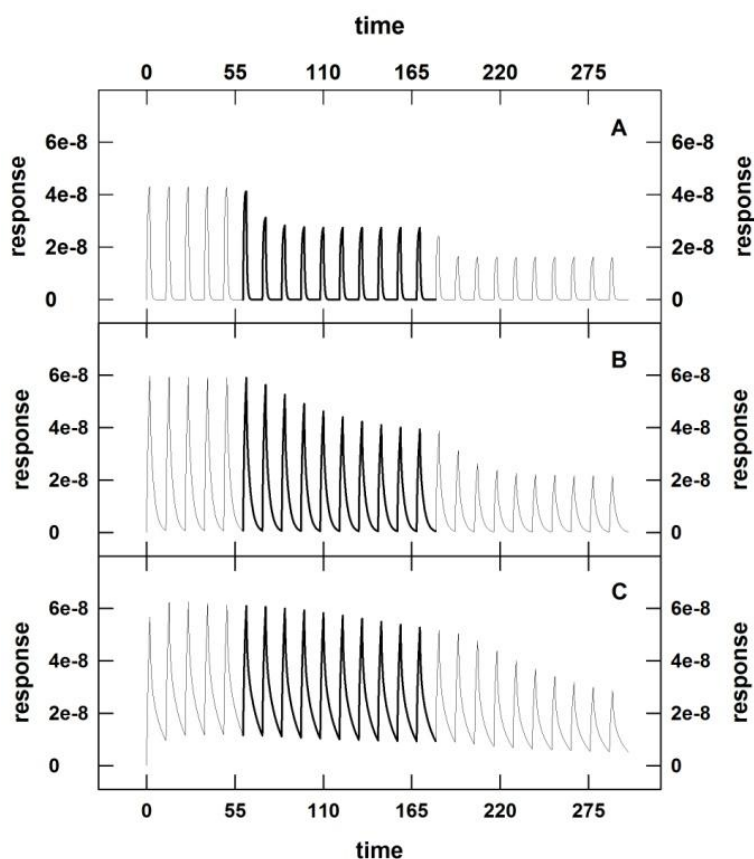
Figure 9. Three simulations of the overall biosensor assays.

The assay proceeds as a negative control (peaks 1-5), as an analyzed sample (peaks 6-15), as an RSP (peaks16-25). Membrane thickness is set to 5×10^{-4} m (panel A), 1.1×10^{-3} m (panel B), and 2×10^{-3} m (panel C) and the inhibitor concentrations to 4×10^{-8} M (the analyzed sample) and 1×10^{-7} M (the RSP).

Simulated behavior of biosensors with a thick and a thin membrane is important for setting the experimental conditions of a biosensor. Moreover, it is difficult to evaluate correct values of dose-response curves from the signal of biosensors with a thick membrane, which can be seen in the following simulations. Depending on the speed of the signal stabilization, it is evident that the stabilization of the signal of a biosensor with a thick membrane is longer in comparison with the stabilization of the signal of a biosensor with a thin membrane. Generally, the assays can be shortened by shortening the time of the light/dark period pulses.

Simulations of the biosensor signal where the dose-response curves were evaluated as biosensor responses to the inhibitor concentration are presented in Fig. 10 at the bottom. Thickness of the membrane was set to 1.1×10^{-3} m (a sample simulation is shown in Fig. 10, on the top) and the responses of the biosensor to different inhibitor concentrations (1×10^{-9}, 1×10^{-8}, 5×10^{-7}, 1×10^{-7}, 5×10^{-6}, 1×10^{-6}, 1×10^{-5} M) were recorded and analyzed.
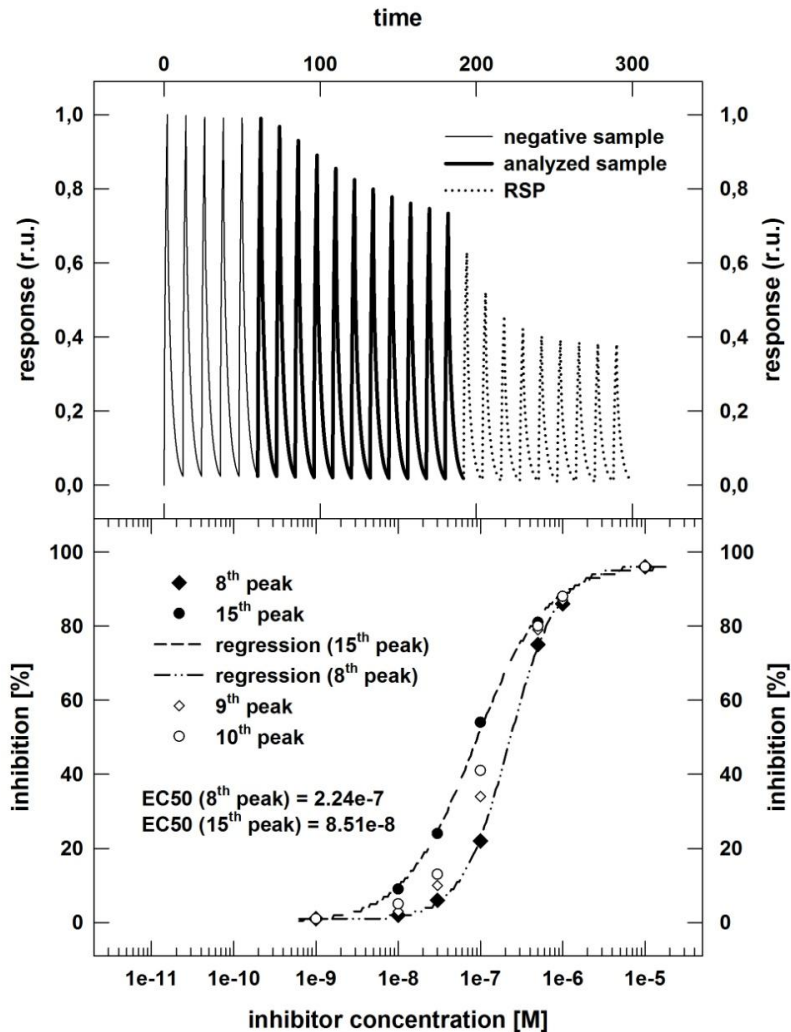
Figure 10. Dose-response curves of the simulated data.

The top panel shows a simulated biosensor assay. An addition of 1×10^{-8} M (after the 5th peak) and 1×10^{-7} M (after the 16th peak) concentration of an inhibitor was simulated. The bottom panel shows the plotted dose-response curves evaluated by the determination of the inhibition from the 8th, 9th, 10th and the 15th peak. The fitted curves for the 8th and the 15th peak are demonstrated.

The 8th, 9th, 10th and 15th peak were evaluated for the determination of the signal decrease in the presence of an inhibitor. Parameters C, D, b and EC50 were calculated according to Eq. 1. They are presented in Tab. 2. The shapes of the dose-response curves show that the results differ depending on the evaluated peak. The differences are confirmed by listing the calculated parameters. The evaluated data after better signal stabilization (evaluations from the 8th to the 15th peak) have a broader range of detectable concentration of the inhibitor and lower EC50 values. Even lower inhibitor concentrations can be detected, which leads to lower limits of detection of the biosensor.

Evaluated peaks	C	D	b	EC50
8th	0.01	0.960	1.50	2.24×10^{-7}
9th	0.01	0.960	1.31	1.63×10^{-7}
10th	2.41×10^{-3}	0.960	1.20	1.30×10^{-7}
15th	3.02×10^{-3}	0.960	1.00	8.51×10^{-8}

Table 2. The calculated parameters of the evaluated data from simulated biosensor assays as presented in Fig. 10.

Beside the simulations of biosensor performance with different values of membrane thickness, also variations of enzyme concentration in a thin (5×10^{-4} m) and a thick (2×10^{-3} m) membrane were simulated. The results can be seen in Fig. 11 and 12, respectively. Here, a similar effect as in the simulation of the membrane thickness can be observed. With an increase in the enzyme concentration (5×10^{-7}, 1×10^{-6}, 5×10^{-6} M) in the thin membrane (Fig. 11), a slight increase in the signal is present. However, slower responses to an inhibitor and slower signal stabilization after addition of an inhibitor are observed.
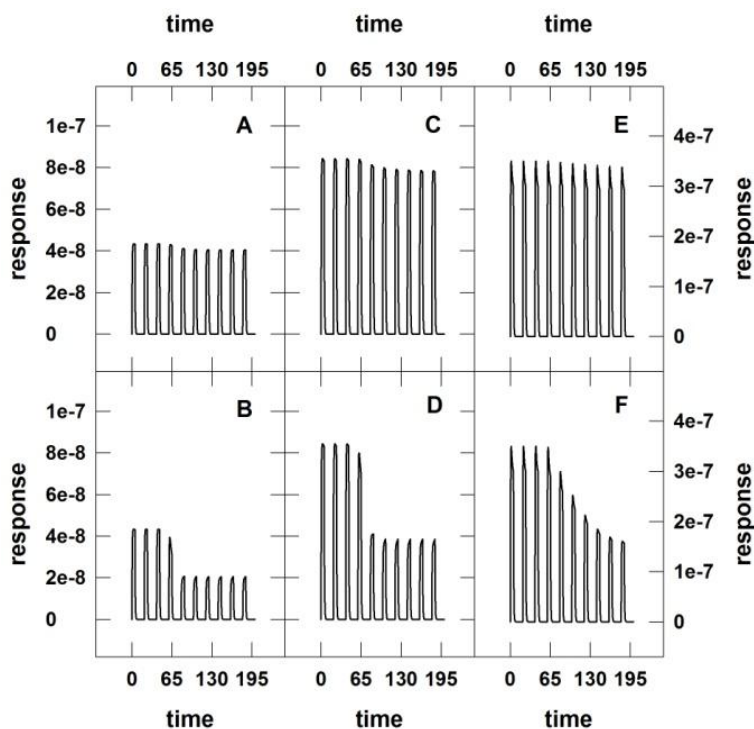
Figure 11. The signal of a biosensor depending on enzyme concentration in a thin immobilization membrane (5×10^{-4} m).

The top panels (A, C, E) show the behavior of a biosensor after addition of low (5×10^{-9} M) inhibitor concentration and the bottom panels (B, D, F) after addition of high (1×10^{-7} M) inhibitor concentration. The enzyme concentration in the membrane increases from the left to the right (5×10^{-7} M – panels A, B, 1×10^{-6} M – panels C, D, 5×10^{-6} M – panels E, F).

Fig. 12 shows the same simulations with a thick membrane. The responses of the biosensor to the inhibitor are less distinguishable in comparison with the thin membrane. In case of high enzyme concentrations in a thick membrane, it can be impossible to evaluate the signal in certain circumstances (the middle and the right panels in Fig. 12).
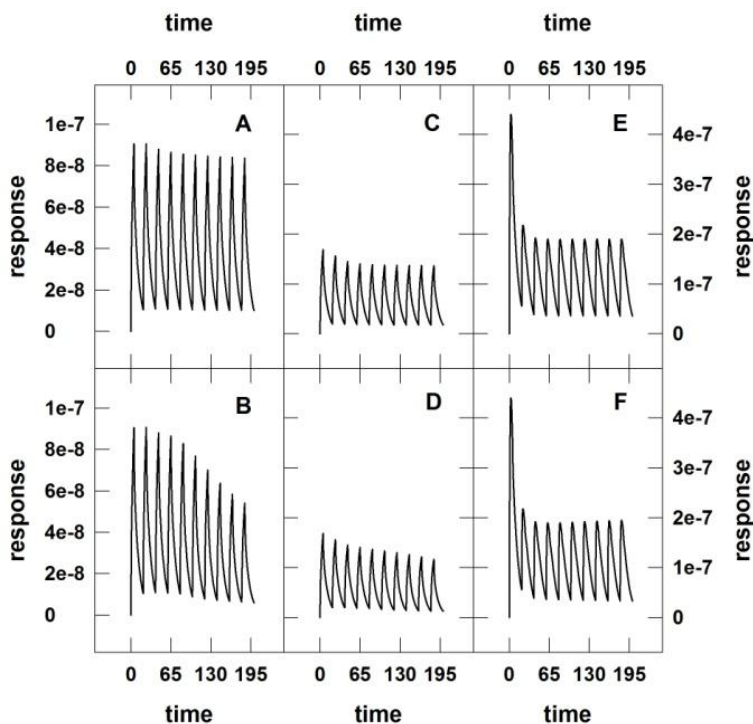
Figure 12. The signal of a biosensor depending on enzyme concentration in a thick immobilization membrane (2×10^{-3} m).

The top panels (A, C, E) show the behavior of a biosensor after addition of low (5×10^{-9} M) inhibitor concentration and the bottom panels (B, D, F) after addition of high (1×10^{-7} M) inhibitor concentration. The enzyme concentration in the membrane increases from the left to the right (5×10^{-7} M – panels A, B, 1×10^{-6} M – panels C, D, 5×10^{-6} M – panels E, F).

In Fig. 13 (bottom panels), selected experimentally recorded signals of a biosensor are presented (the top plots present a normalized signal, the bottom plots present non-normalized biosensor signals). It can be observed that the registered signal of the experimental data resembles the simulated conditions. The left bottom part of Fig. 13 resembles Fig. 12E and 12F. The right bottom part of Fig. 13 resembles Fig. 12B.

It was found out that the signal of a biosensor can be adjusted by appropriate setting of the length of the light and the dark period depending on the membrane thickness of the biosensor. Longer time for signal stabilization in thicker membranes described above is demonstrated by experimental data on the top of Fig. 13 where different light/dark periods were set (5/70 s, 5/50 s, 5/25 s from the left to the right). The signal was recorded on one biosensor (membrane thickness was not changed). This experiment demonstrates that the experimental signal behavior resembles the simulated

signal behavior, at the bottom panel of Fig. 9 (the first 5 peaks at the beginning of the assay).
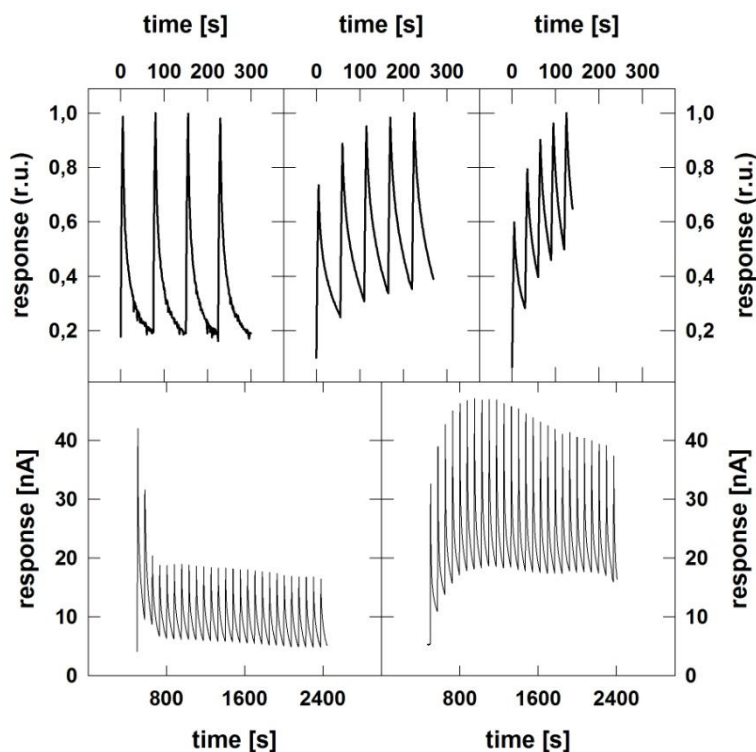
Figure 13. Unexpected biosensor responses. Experimental data.

The bottom panels show different types of biosensor responses (no inhibitor was added). The top panels show changes of the biosensor signal behavior depending on variation of light/dark periods.

Before the presented simulations were performed, there had not been any satisfactory explanation for strange behavior of the biosensor in some cases (the bottom part of Fig. 13). Since the PSII biosensor is a complicated type of a biosensor, it is not only the simulated parameters (membrane thickness and enzyme concentration) that are important but also the experimental conditions (the length of the light and the dark periods). They can have a strong impact on the signal behavior of the biosensor. Some of the conditions are presented in this study, however, there is a number of other possible transition cases observed in the experimental conditions which are not presented here. Such deviations of the signal behavior of the biosensor have to be considered when data are evaluated. The results obtained from the numerical model show the importance of proper adjustment of the membrane thickness. It is evident that by increasing the membrane thickness, low concentrations of an inhibitor are detected with difficulty and the data can be evaluated inaccurately. Also the signal stabilization is slow. This behavior results from a slower penetration of the inhibitor and the artificial electron mediator through the immobilization membrane. A similar effect can be observed when the concentration of enzyme in the membrane increases. This behavior probably relates

to quicker binding of the inhibitor in the surface layers of the immobilization membrane and to a shift of the substrate and of the product concentration gradient into deeper layers of the membrane. Because surface layers have a weaker impact on the overall signal and the amount of binding sites of the inhibitor is sufficient to bind low inhibitor concentrations on the surface of the membrane, low concentrations of the inhibitor are more difficult to detect and to evaluate. Both simulated membrane properties (the thickness of the membrane and the amount of enzyme in the membrane) are important for employment of experimental methods.

Although it is always the same volume of the immobilization mixture which is transferred on the working electrode, it can be spilled on the surface in a different manner which results in a different membrane thickness. Concerning the enzyme concentration, it is difficult to evaluate how many active binding sites of the isolated PSII complex relate to the mediated electron transport and preserve their property of binding the inhibitor. Experimental conditions (the light and the dark periods) also have a strong impact on the overall behavior of the biosensor and they have to be set properly.

3.4. The novel immobilization method and the novel measurement protocol employment

The biosensor simulations showed that membrane thickness and concentration of immobilized enzyme can have an important impact on the improvement of the biosensor. Based on this knowledge, we concentrated on searching an effective solution for adjustment of the thickness of the biosensor membrane with the aim to improve the biosensor performance.

One of the widely studied methods of forming a very thin layer of a protein (enzyme) and using it in biosensor applications is to create a self-assembled monolayer (SAM) of a protein (Chaki & Vijayamohanan 2002). Covalently immobilized monolayers of a photosynthetic reaction center can be found in the literature (Katz 1994). An attempt to hybridize PSII for a direct linkage of site-selective His-tag on the PSII and a Ni-NTA-terminated SAM on a gold electrode has also been presented (Terasaki et al. 2008). The hypothesis that SAM formation techniques may lead to improvements of the biosensor performance was confirmed when immobilization of a PSII complex by adsorption on a SAM of poly-mercapto-p-benzoquinone (polySBQ) was performed (Malý et al. 2005).

Our study concentrated on reducing the thickness of the bulk immobilization matrix by limiting the quantity of the prepared immobilization matrix on the surface of the working electrode. It was not an easy task due to fact that the common laboratory pipettes do not offer lower dosing volumes than 0.5 µL (0.1 µL) and a uniform coverage of the working electrode was needed. After several successful attempts it was found out that immobilization of PSII complex mixture could be performed by only drop imprints on the electrode surface. 0.5 µL of the PSII mixture was dropped on the surface of the working electrode and the whole volume was sucked back into the pipette immediately.

Such immobilization procedure seemed to be optimal with no loss of the measured biosensor signal. The pictures of the immobilized membrane can be seen in Fig. 14.
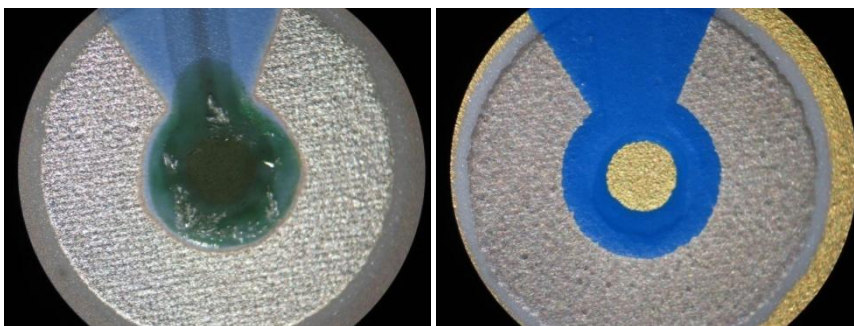

Figure 14. Sensors with a thick (on the left) and a thin (on the right) immobilization membrane.

This newly developed simple immobilization procedure had a significant impact on the overall biosensor performance. An experimental protocol and an assay optimized for such a thin membrane is presented in Fig. 15. By several adjustments of the length of the light and the dark period, it was set to 3 s and 9 s, respectively. In comparison with the conventional method, where the light/dark period was 5/70 s, the overall time for one period shortened more than 6 times, from 70 s to 12 s, which enabled to insert more light/dark periods into the measurement protocol and shorten the time for stabilization of the sensor. The final protocol (Fig. 15) started with a period of 180 s for biosensor stabilization followed by 60 light/dark periods. The total time for one assay was adjusted to 900 s (15 min). These changes improved the accuracy of the assay evaluation significantly. The number of the evaluated peaks increased from 4 to 20, which resulted in better identification of any changes of the biosensor response to light stimulation or to addition of an inhibitor. The total time of an assay was shortened from 21 min to 15 min.

Apart from that, the new protocol led to new evaluation of the decrease of the biosensor signal. In the traditional protocol, a power function was preferred for fitting data of the first four peaks. In the new protocol, it was found out that for signal evaluation, a linear function is more suitable for fitting the last ten peaks from the first series of 20 peaks (a negative sample). When data were fitted by both the linear and the power function, the mean values of R^2 were 0.971 (SD = 0.0276) and 0.966 (SD = 0.0264), respectively. The linear function was selected to fit the measured data as evaluation of the signal decrease (see the bottom part of Fig. 16).
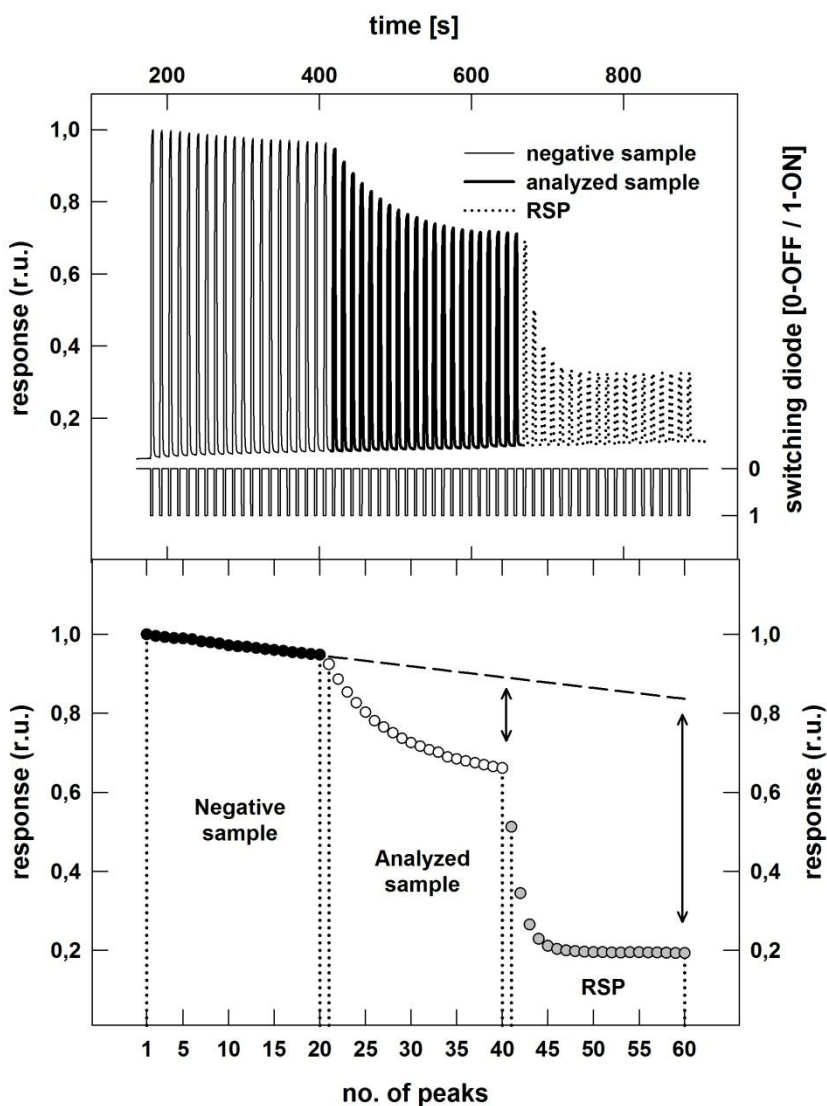
Figure 15. A newly designed measuring protocol of a PSII biosensor assay.

The assay starts with an equilibration period of 180 s. Then, 3 series of light/dark periods (3/9 s) are registered and a negative sample (without herbicide), an analyzed sample (with herbicide) and a reference standard of phytotoxicity (RSP) are added to the examined solution subsequently. The upper panel shows the signal with 60 light/dark pulses (0-light is off, 1-light is on) after normalization. The bottom panel shows the normalized peak height for the calculation of the degree of the biosensor inhibition.

During evaluation of the data of biosensors prepared by a thin membrane it was found out that the signal of the first 10 peaks did not always decrease regularly. Based on the results of the numerical model and on further analysis, it can be concluded that such behavior is a result of formation of the membrane with different thickness on the surface of the working electrode of the sensor. An analysis of two similar assays of biosensors with addition of 10^{-9} M (the analyzed sample) and 10^{-7} M (RSP)

concentration of an inhibitor is presented in Fig. 16. The top panels of Fig. 16 present the biosensor signals, the middle panel presents the normalized signals, the left bottom panel the evaluated signals, and the right bottom panel the stabilization of the signal after light stimulation. Comparing these two biosensors, we can see that the left signal is higher than the right signal, see the top panel of Fig. 16. The biosensor model assumed that by decreasing the membrane thickness, the biosensor signal decreases as well. Even after the signal is normalized, a very slight increase in the signal of the left biosensor is still present, see the middle panel of Fig. 16. The hypothesis that a biosensor with a higher signal has a thicker membrane can also be confirmed by a detailed analysis of a single biosensor peak, see the right bottom part of Fig. 16. The stabilization of the signal of a biosensor with a thinner membrane is faster. There is no observable decrease in the signal, 6 s after the stimulation started. The signal of the biosensor with a thicker membrane is slightly decreasing even 11 s after the stimulation started (the end of a light/dark period cycle). Such slow stabilization of the current during the dark period is observable in the simulation of biosensors with a thick membrane, see the bottom part of Fig. 9 and Fig. 12. Similar observations concerning slower stabilization of the signal of a thicker membrane in comparison with a thiner membrane can be found in several published articles. Malý et al. (2005) compares the signal stabilization in an immobilized PSII complex by adsorption onto a polySBQ layer of a gold electrode with the signal of a PSII complex immobilized in a bulk BSA-GA membrane. Bhala et Zazubovich (2011) compares the signal of PSII cores covalently bonded to a SAM of mercaptopropionic acid (MPA) with the signal of PSII cores immobilized in a BSA-GA matrix. In both publications, the stabilization of the biosensor signal is several times quicker in comparison with the bulk immobilization matrix. In addition, an improvement in biosensor sensitivity was achieved in both cases.

There will always be a difference in the thickness of the membrane in the biosensors because an immobilization membrane prepared by drop imprinting is very thin and the immobilization is performed manually, which leads to a nonuniformity of the biosensors prepared by this method. The degree of uniformity of the prepared biosensors depends on manual dexterity of the operator during the immobilization process. In spite of that, there are several other options how to enhance the control of the thickness of the membranedepending on the equipmentof a laboratory such as spincoating, nanoliter dropcasting, or dipcoating. These were not evaluated in this work.

The importance of a suitable method for evaluation of the data and selection of a suitable biosensor signal for the evaluation is presented in the left bottom part of Fig. 16. Here, based on the new protocols, the signals are evaluated by a linear approximation and the signal difference of the 40th approximated and the measured peak including R^2 is compared. R^2 for the biosensor signal fitted by the linear approximation (the signal from the 10th to the 20th peak) was calculated as 0.876 for the thicker and 0.996 for the thinner membrane. The difference of the signal between the approximated and the measured values was calculated as 0.041 for the thick and 0.021 for the thin membrane biosensor. This leads to a conclusion that the data obtained from biosensors with thin membranes

are more accurate and that the selection of a suitable biosensor signal for bioassays can be evaluated simply by controlling the biosensor signal behavior at the beginning of the measurement.
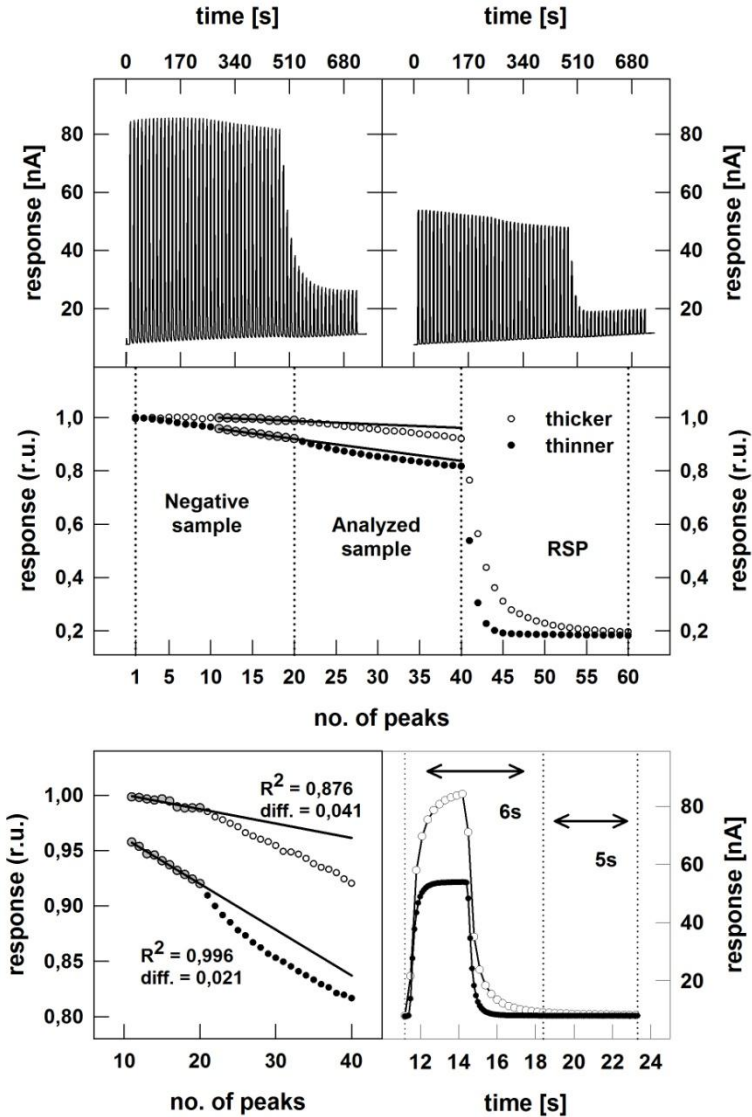

Figure 16. Comparison of two biosensors prepared with a thin immobilization membrane.

The analyzed sample contains 1×10^{-9} M of herbicide diuron, the RSP contains 1×10^{-7} M of diuron. The top panel shows the measured signal of the biosensors. Based on the results of the biosensor simulation, we can identify the left biosensor as the biosensor with a thicker membrane. The middle panel shows the normalized signal of both biosensors. The left bottom panel shows the analyzed inhibition of the biosensors to 1×10^{-9} M. The signal decrease in 11-20 peaks is fitted by a linear function and the extent of the inhibition is deducted at the 40th peak signal. The right bottom panel shows the difference in the stabilization of the signal after the biosensor was activated by a light pulse of 3 s.

Based on the new assay protocol, dose-response curves of a biosensor with a BSA-DGS and a BSA-GA immobilization membrane were plotted, see Fig. 17. The curves were analyzed by fitting the experimental data to the logistic dose-response curve, where mathematical expression of the response (the biosensor signal) is y and the dose (herbicide concentration) is x, expressed as (Streibig 1988)

$$y = C + \frac{D - C}{1 + exp\{b(\log(x) - \log(EC50))\}} \tag{1}$$

where C and D are the lower and the upper asymptote, respectively, and EC50 is the concentration causing 50% inhibition of the measured signal.

LOD of a bioassay is equal to (Seiden et al. 1998)

$$Y_{min} = Y_0 - \varepsilon \tag{2}$$

where Y_0 is the response obtained from a zero dose and t is the error of this response estimate. It can be calculated from the equation (Rodbard 1978)

$$Y_{min} = Y_0 - ts\sqrt{\frac{1}{n_0} + \frac{1}{n_1}} \tag{3}$$

where Y_0 is the mean of the control, t is the percentage from Students t-distribution at the chosen fractal and the appropriate number of degrees of freedom (n_1-2), s is the standard deviation of the control, and n_0 and n_1 are the number of replicates for Y_0 and the unknown sample, respectively.
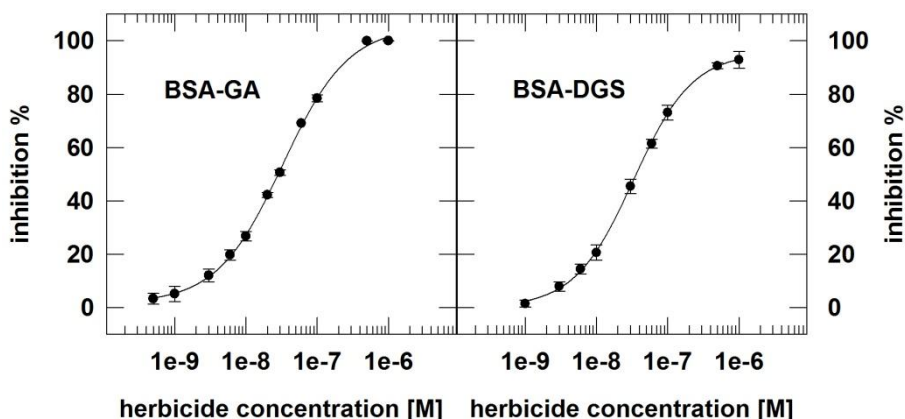
Figure 17. Dose-response curves of a biosensor with a thin immobilization membrane.

The curves correspond with the biosensor inhibition by the herbicide diuron. The biosensor immobilization membranes were prepared with a BSA-GA crosslinking method (left) and a BSA-DGS sol-gel method (right).

Based on this approach, the EC50 values were determined as 3.27×10^{-8} M (the slope b was evaluated as 0.94) for the BSA-GA and 3.31×10^{-8} M (slope b was evaluated as 1.05) for the BSA-DGS immobilization method. The LOD values were

determined as 2.0×10^{-10} M for the BSA-GA and 4.0×10^{-10} M for the BSA-DGS immobilization method. There are only slight differences between the two compared types of the biosensor in EC50. However, the LOD of the BSA-GA method is two times lower than the LOD of biosensor prepared by the BSA-DGS method.

Biosensors prepared by a BSA-GA immobilization method seem to be more sensitive and the range of detectable concentration of the herbicide diuron is slightly broader than in biosensors prepared by the sol-gel method. Moreover, no adhesion problems are present, slightly better affinity of the artificial electron mediator as the substrate to the PSII complex was evaluated, and slightly better or similar long-term stability was observed when using the crosslinking method in comparison with the sol-gel immobilization. These advantages make the immobilization of a PSII complex by covalent crosslinking a more suitable method than the sol-gel encapsulation method. On the other hand, in spite of a lower percentage of the enzyme (the isolated PSII complex) present in the sol gel immobilization membrane, 37.5 % of PSII in the sol-gel membrane and 41.7 % of PSII in the membrane crosslinked by GA, there was always a higher signal by the encapsulation of the PSII complex. This behavior is difficult to explain without further studies of both systems.

One of the possible reasons can be concluded from the fact that the encapsulation method is better suited for preserving the activity of a PSII complex, which as a result has more active sites and can give a higher measured signal. However, covalent crosslinking of PSII into a membrane seems to be preferable as it reduces the number of active sites of a PSII complex resulting in a lower signal. When the number of active sites in a membrane is reduced, a biosensor is more sensitive to lower concentrations of herbicides. This suggestion was also confirmed by the presented simulation where lowering of the concentration of enzyme led to better sensitivity of the biosensor to low herbicide concentrations, see Fig. 10. The fact that high activity of a PSII complex can lead to lower sensitivity to herbicides was also discussed in (Krejčí et al. 2006).

Another reason can be worse adhesion of the sol-gel membrane to the surface of the working electrode, caused probably by the brittleness and shrinkage of the silicate membrane. The problem with adhesion appeared several times during this study and caused difficulties in evaluation of biosensors with several combinations of the components in immobilization membranes. Although lower shrinkage is observed in membranes prepared by a DGS in comparison with a widely used TEOS precursor (Brook et al. 2004), their adhesion to a gold electrode was not sufficient in our study. A possible solution to an improvement of the sol-gel membrane adhesion to gold surface is to apply a SAM formation by using organosilanes such as mercaptopropyl-trimethoxisilane (Shen et al. 2005; Walcarius & Sibottier 2005). An increase in the adhesion properties of the silicate matrix to the gold working electrode will probably result in better diffusion of the artificial electron mediator to the electrode surface and thus to more accurate detection of the processes occurring in a PSII complex including the changes resulting from the presence of an inhibitor.

Also binding interactions of the BSA with the artificial electron mediator of quinone-type or with the herbicide can be considered, since the concentration of the BSA in the sol-gel membranes is 7 times higher than the concentration in the membranes prepared by the crosslinking method. If sol-gel immobilization is better suited for preserving the native state of BSA, the effect of interaction of the BSA with the herbicide or the mediator can be increased more than 7 times in comparison with the cross-linked BSA in the immobilization membrane. Interactions of commercial herbicides (including phenol types of herbicides) to bovine and human serum albumin have been studied and confirmed in (Purcell et al. 2001; Cserháti & Forgács 1995; Cserháti et al. 2003; Han et al. 2009). It is possible that the marked differences between the compared immobilization methods in the LOD and EC50 are caused by lower accessibility of lower concentrations of the inhibitor to the PSII active sites that might already be bound by high concentration of BSA in the immobilization membrane. Interactions between albumin proteins and quinone derivatives have also been published (Ito 2003; Bittner 2006; Skupińska et al. 2006). It was found out that the presence of $MgCl_2$ (50 mM $MgCl_2$ is present in the buffer solution of the PSII biosensor assays) can improve binding of certain types of quinone derivatives to BSA (Alegria et al. 2008). BSA binding capacity of duroquinone and durohydroquinone has been discussed in (Audi et al. 2003). It can be concluded that the amount of reduced and oxidized quinon molecules diffusing through the immobilization membrane can be influenced in negative way by the interaction of the mediator with the BSA although the presence of the BSA protein can improve the overall mass transport through the immobilization matrix (Malý et al. 2005).

When comparing the results obtained from biosensors prepared with the newly designed protocols with the already published performances of biosensors based on a PSII complex (Koblížek et al. 2002; Bhalla et al. 2011; Masojídek et al. 2011; Touloupakis et al. 2012), a significant improvement of the time of an assay and of the sensitivity was achieved by a simple adjustment of the immobilization technique.

Conclusions

Herbicides are the most frequently detected pesticides in ground and surface waters (Carter 2000). As analytical devices for their detection, Photosynthetic biosensors based on an immobilized PSII complex have been developed. They can detect the presence of herbicides which inhibit the photosynthesis by blocking the electron transport chain in a PSII complex.

In the presented study, sol-gel immobilization of a PSII complex on a screen printed electrode was performed and studied as an alternative to a crosslinking immobilization method in a BSA and a GA matrix with the aim to improve the performance of an amperometric biosensor for detection of herbicides. A sol-gel process using a DGS precursor seems to be suitable for preserving the activity of the PSII complex. The optimal composition of the sol-gel immobilization matrix was set. The measured signal obtained from biosensors prepared by a sol-gel method was improved

and it was always approximately two times higher than the signal from biosensors prepared with crosslinking by GA. The main disadvantage of the sol-gel matrix was poor adhesion to the surface of a gold working electrode. Apart from that, the biosensor prepared by the sol-gel method showed similar or slightly worse performance in given parameters such as in the long-term stability of the biosensor, in K_M^{app}, EC50 and in the LOD. Several suggestions for improvement of the performance of the biosensor have been introduced and we suppose that by a deeper study of the introduced issues, the properties of the biosensors prepared with the sol-gel immobilization method can overcome the properties of the biosensors prepared by crosslinking immobilization by GA.

For determination of dose-response curves of biosensors, newly designed immobilization and measurement protocols were employed. The creation of newly designed protocols was motivated by the results obtained from computer simulations. The simulated responses of biosensors under several different conditions showed a good correlation with the experimental results. It was found out that thickness of the immobilization membrane has a significant impact on the overall biosensor performance and that the amount of immobilized enzyme also plays an important role in sensitivity of the biosensor. With employment of a drop imprint immobilization method and by adjustment of the biosensor assay, accuracy and sensitivity of the biosensor was increased. Also the biosensor assay time was reduced by a quarter in comparison with the published protocol (Masojídek et al. 2011).

In conclusion, although BSA-DGS immobilization did not show significant improvements on a PSII biosensor, the experimental work indicates a high potential of silica derivatives as immobilization supports in biosensors. A sol-gel matrix prepared from a DGS precursor for immobilization of a PSII complex is a promising alternative to crosslinking immobilization by GA. The employment of a thin immobilization membrane leads to an overall improvement of the biosensor.

Acknowledgement

References

ALEGRIA, A. E., SANCHEZ-CRUZ, P., KUMAR, A., GARCIA, C., GONZALEZ, F. A., ORELLANO, A., ZAYAS, B. and GORDALIZA, M., 2008. Thiols oxidation and covalent binding of BSA by cyclolignanic quinones are enhanced by the magnesium cation. Free Radical Research. Vol. 42, no. 1, pp. 70–81.

AUDI, S. H., BONGARD, R. D., DAWSON, Ch. A., SIEGEL, D., ROERIG, D. L. and MERKER, M. P., 2003. Duroquinone reduction during passage through the

pulmonary circulation. American Journal of Physiology. Lung Cellular and Molecular Physiology. Vol. 285, no. 5, pp. L1116–1131.

AVNIR, D., CORADIN, T., LEV, O. and LIVAGE, J., 2006. Recent bio-applications of sol–gel materials. Journal of Materials Chemistry. Vol. 16, no. 11, pp. 1013–1030.

BESANGER, T. R., CHEN, Y., DEISINGH, A. K., HODGSON, R., JIN, W., MAYER, S., BROOK, M. A. and BRENNAN, J. D., 2003. Screening of inhibitors using enzymes entrapped in sol−gel-derived materials. Analytical Chemistry. Vol. 75, no. 10, pp. 2382–2391.

BHALLA, V. and ZAZUBOVICH, V., 2011. Self-assembly and sensor response of photosynthetic reaction centers on screen-printed electrodes. Analytica Chimica Acta. Vol. 707, no. 1-2, pp. 184–190.

BHALLA, V., ZHAO, X. and ZAZUBOVICH, V., 2011. Detection of explosive compounds using Photosystem II-based biosensor. Journal of Electroanalytical Chemistry. Vol. 657, no. 1-2, pp. 84–90.

BITTNER, S., 2006. When quinones meet amino acids: chemical, physical and biological consequences. Amino Acids. Vol. 30, no. 3, pp. 205–224.

BRAUN, S., RAPPOPORT, S., ZUSMAN, R., AVNIR, D. and OTTOLENGHI, M., 2007. Biochemically active sol-gel glasses: The trapping of enzymes. Materials Letters. Vol. 61, no. 14-15, pp. 2843–2846.

BRAYNER, R., COUTÉ, A., LIVAGE, J., PERRETTE, C. and SICARD, C., 2011. Micro-algal biosensors. Analytical and Bioanalytical Chemistry. Vol. 401, no. 2, pp. 581–597.

BROOK, M. A., CHEN, Y., GUO, K., ZHANG, Z., JIN, W., DEISINGH, A., CRUZ-AGUADO, J. and BRENNAN, J. D., 2004. Proteins entrapped in silica monoliths prepared from glyceroxysilanes. Journal of Sol-Gel Science and Technology. Vol. 31, no. 1-3, pp. 343–348.

CARTER, A. D., 2000. Herbicide movement in soils: principles, pathways and processes. Weed Research. Vol. 40, no. 1, pp. 113–122.

CSERHÁTI, T. and FORGÁCS, E., 1995. Charge transfer chromatographic study of the binding of commercial pesticides to various albumins. Journal of Chromatography A. Vol. 699, no. 1-2, pp. 285–290.

CSERHÁTI, T., FORGÁCS, E., DEYL, Z., MIKSIK, I. and ECHARDT, A., 2003. Binding of low molecular mass compounds to proteins studied by liquid chromatographic techniques. Biomedical Chromatography. Vol. 17, no. 6, pp. 353–360.

DATTELBAUM, A. M., BAKER, G. A., FOX, J. M., IYER, S. and DATTELBAUM, J. D., 2009. PEGylation of a maltose biosensor promotes enhanced signal response when immobilized in a silica sol-gel. Bioconjugate Chemistry. Vol. 20, no. 12, pp. 2381–2384.

DRABER, W., TIETJEN, K., KLUTH, J. F. and TREBST, A., 1991. Herbicides in photosynthesis research. Angewandte Chemie International Edition in English. Vol. 30, no. 12, pp. 1621–1633.

DUKE, S. O., 1990. Overview of herbicide mechanisms of action. Environmental Health Perspectives. Vol. 87, pp. 263–271.

FEDTKE, C., 1982. Biochemistry and physiology of herbicide action. Berlin. Springer-Verlag. ISBN 9780387112312.

GIANFREDA, L. and SCARFI, M.R., 1991. Enzyme stabilization: state of the art. Molecular and Cellular Biochemistry. Vol. 100, no. 2, pp. 97–128.

GIARDI, M. T., KOBLÍŽEK, M. and MASOJÍDEK, J., 2001. Photosystem II-based biosensors for the detection of pollutants. Biosensors and Bioelectronics. Vol. 16, no. 9-12, pp. 1027–1033.

GIARDI, M. T. and PACE, E., 2005. Photosynthetic proteins for technological applications. Trends in Biotechnology. 2005. Vol. 23, no. 5, pp. 257–263.

GILL, I., 2001. Bio-doped nanocomposite polymers: sol−gel bioencapsulates. Chemistry of Materials. Vol. 13, no. 10, pp. 3404–3421.

GILL, I. and BALLESTEROS, A., 1998. Encapsulation of biologicals within silicate, siloxane, and hybrid sol−gel polymers: an efficient and generic approach. Journal of the American Chemical Society. Vol. 120, no. 34, pp. 8587–8598.

HAN, X.-L., MEI, P., LIU, Y., XIAO, Q., JIANG, F.-L. and LI, R., 2009. Binding interaction of quinclorac with bovine serum albumin: a biophysical study. Spectrochimica Acta Part A: Molecular and Biomolecular Spectroscopy. Vol. 74, no. 3, pp. 781–787.

HECQ, P., HULSMANN, A., HAUCHMAN, F. S., MCLAIN, J. L. and SCHMITZ, F., 2006. Drinking water regulations. In: QUEVAUVILLER, P. and THOMPSON, K. C. (eds.), Analytical Methods for Drinking Water: Advances in Sampling and Analysis. Chichester. John Wiley & Sons pp. 1–37. ISBN 9780470094938

CHAKI, N. K. and VIJAYAMOHANAN, K., 2002. Self-assembled monolayers as a tunable platform for biosensor applications. Biosensors and Bioelectronics. Vol. 17, no. 1-2, pp. 1–12.

ITO, S., 2003. The IFPCS presidential lecture: a chemist's view of melanogenesis. Pigment Cell Research. Vol. 16, no. 3, pp. 230–236.

JIN, W., 2002. Properties and applications of proteins encapsulated within sol−gel derived materials. Analytica Chimica Acta. Vol. 461, no. 1, pp. 1–36.

KATZ, E., 1994. Application of bifunctional reagents for immobilization of proteins on a carbon electrode surface: Oriented immobilization of photosynthetic reaction centers. Journal of Electroanalytical Chemistry. Vol. 365, no. 1-2, pp. 157–164.

KLIBANOV, A., 1979. Enzyme stabilization by immobilization. Analytical Biochemistry. Vol. 93, pp. 1–25.

KOBLÍŽEK, M., MASOJÍDEK, J., KOMENDA, J., KUČERA, T., PILLOTON, R., MATTOO, A. K. and GIARDI, M. T., 1998. A sensitive photosystem II-based biosensor for detection of a class of herbicides. Biotechnology and Bioengineering. Vol. 60, no. 6, pp. 664–669.

KOBLÍŽEK, M., MALÝ, J., MASOJÍDEK, J., KOMENDA, J., KUČERA, T., GIARDI, M. T., MATTOO, A. K. and PILLOTON, R., 2002. A biosensor for the detection of triazine and phenylurea herbicides designed using Photosystem II coupled to a screen-printed electrode. Biotechnology and Bioengineering. Vol. 78, no. 1, pp. 110–116.

KREJČÍ, J., VRBA, R., MALÝ, J., KREJČOVÁ, D., KOPECKÝ, J., 2006. Inteligentní biosenzorický systém pro detekci pesticidů a herbicidů v životním prostředí. Dílčí správa projektu MPO ev. č. FT-TA/089 za rok 2006. Brno.

LIU, D.-M. and CHEN, I.-W., 1999. Encapsulation of protein molecules in transparent porous silica matrices via an aqueous colloidal sol–gel process. Acta Materialia. Vol. 47, no. 18, pp. 4535–4544.

MALÝ, J., KLEM, K., LUKAVSKÁ, A. and MASOJÍDEK, J., 2005. Degradation and movement in soil of the herbicide isoproturon analyzed by a Photosystem II-based biosensor. Journal of Environmental Quality. Vol. 34, no. 5, pp. 1780–1788.

MALÝ, J., KREJČÍ, J., ILIE, M., JAKUBKA, L., MASOJÍDEK, J., PILLOTON, R., SAMEH, K., STEFFAN, P., STRÝHAL, Z. and SUGIURA, M., 2005. Monolayers of photosystem II on gold electrodes with enhanced sensor response—effect of porosity and protein layer arrangement. Analytical and Bioanalytical Chemistry. Vol. 381, no. 8, pp. 1558–1567.

MALÝ, J., MASOJÍDEK, J., MASCI, A., ILIE, M., CIANCI, E., FOGLIETTI, V., VASTARELLA, W. and PILLOTON, R., 2005. Direct mediatorless electron transport between the monolayer of photosystem II and poly(mercapto-p-benzoquinone) modified gold electrode—new design of biosensor for herbicide detection. Biosensors and Bioelectronics. Vol. 21, no. 6, pp. 923–932.

MALÝ, M., 2006. Biomodel software. Personal communication, 2006.

MALÝ, M., MALÝ, J. and KREJČÍ, J., 2006. Manuál pro simulační biosenzorický software. Personal communication, 2006.

MASOJÍDEK, J., SOUČEK, P., MÁCHOVÁ, J., FROLÍK, J., KLEM, K. and MALÝ, J., 2011. Detection of photosynthetic herbicides: Algal growth inhibition test vs. electrochemical photosystem II biosensor. Ecotoxicology and Environmental Safety. Vol. 74, no. 1, pp. 117–122.

MCTAVISH, H., PICOREL, R. and SEIBERT, M., 1989. Stabilization of isolated photosystem II reaction center complex in the dark and in the light using polyethylene glycol and an oxygen-scrubbing system. Plant Physiology. Vol. 89, no. 2, pp. 452–456.

MILLER, J. M., DUNN, B., VALENTINE, J. S. and ZINK, J. I., 1996. Synthesis conditions for encapsulating cytochrome c and catalase in SiO2 sol-gel materials. Journal of Non-Crystalline Solids. Vol. 202, no. 3, pp. 279–289.

MONTEREALI, M. R., SETA, L. D., VASTARELLA, W. and PILLOTON, R., 2010. A disposable Laccase–Tyrosinase based biosensor for amperometric detection of phenolic compounds in must and wine. Journal of Molecular Catalysis B: Enzymatic. Vol. 64, no. 3-4, pp. 189–194.

PURCELL, M., NEAULT, J. F., MALONGA, H., ARAKAWA, H., CARPENTIER, R. and TAJMIR-RIAHI, H. A., 2001. Interactions of atrazine and 2,4-D with human serum albumin studied by gel and capillary electrophoresis, and FTIR spectroscopy. Biochimica et Biophysica Acta. Vol. 1548, no. 1, pp. 129–138.

RODBARD, D., 1978. Statistical estimation of the minimal detectable concentration ("sensitivity") for radioligand assays. Analytical Biochemistry. Vol. 90, no. 1, pp. 1–12.

SEIDEN, P., KAPPEL, D. and STREIBIG, J. C., 1998. Response of Brassica napus in tissue culture to metsulfuron-methyl and chlorsulfuron. Weed Research. Vol. 38, no. 3, pp. 221–228.

SHEN, Y., WU, T., ZHANG, Y. and LI, J., 2005. Comparison of two-typed (3-mercaptopropyl)trimethoxysilane-based networks on Au substrates. Talanta. Vol. 65, no. 2, pp. 481–488.

SKUPIŃSKA, K., ZYLM, M., MISIEWICZ, I. and KASPRZYCKA-GUTTMAN, T., 2006. Interaction of anthracene and its oxidative derivatives with human serum albumin. Acta Biochimica Polonica. Vol. 53, no. 1, pp. 101–112.

STREIBIG, J. C., 1988. Herbicide bioassay. Weed Research. Vol. 28, no. 6, pp. 479–484.

SUI, X., CRUZ-AGUADO, J. A., CHEN, Y., ZHANG, Z., BROOK, M. A. and BRENNAN, J. D., 2005. Properties of human serum albumin Entrapped in sol−gel-derived silica bearing covalently tethered sugars. Chemistry of Materials. Vol. 17, no. 5, pp. 1174–1182.

ŠETLÍKOVÁ, E., SOFROVÁ, D., PRÁŠIL, O., BUDÁČ, P., KOBLÍŽEK, M. and ŠETLÍK, I., 1999. Integrity and activity of photosystem 2 complexes isolated from the thermophilic cyanobacterium Synechococcus elongatus using various detergents. Photosynthetica. Vol. 37, no. 2, pp. 183–200.

TERASAKI, N., IWAI, M., YAMAMOTO, N., HIRAGA, T., YAMADA, S. and INOUE, Y., 2008. Photocurrent generation properties of Histag-photosystem II immobilized on nanostructured gold electrode. Thin Solid Films. Vol. 516, no. 9, pp. 2553–2557.

TOULOUPAKIS, E., BOUTOPOULOS, Ch., BUONASERA, K., ZERGIOTI, I. and GIARDI, M. T., 2012. A photosynthetic biosensor with enhanced electron

transfer generation realized by laser printing technology. Analytical and Bioanalytical Chemistry. Vol. 402, no. 10, pp. 3237–3244.

VILA-REAL, H., ALFAIA, A. J., ROSA, M. E., CALADO, A. R. and RIBEIRO, M. H.L., 2010. An innovative sol–gel naringinase bioencapsulation process for glycosides hydrolysis. Process Biochemistry. Vol. 45, no. 6, pp. 841–850.

WALCARIUS, A. and SIBOTTIER, E., 2005. Electrochemically-induced deposition of amine-functionalized silica films on gold electrodes and application to Cu(II) detection in (hydro)alcoholic medium. Electroanalysis. Vol. 17, no. 19, pp. 1716–1726.

7.2.   Paper II

Dendrimer-encapsulated silver nanoparticles as a novel electrochemical label for sensitive immunosensors

Štofik, M., Strýhal, Z., and Malý, J.

Marcel Štofik was partially responsible for management of experiments, measurements and preparation the manuscript.

Abstract

This paper reports on the synthesis and characterization of a novel electrochemical label for sensitive electrochemical stripping metalloimmunoassays based on silver dendrimer-encapsulated nanoparticles (NPs). Silver dendrimer nanocomposites (Ag-DNCs) were synthesized from a generation 5-7 (G5-7) hydroxyl-terminated ethylenediamine-core-type (2-carbon core) PAMAM dendrimer. Several fixed ratios of Ag^+/dendrimer were prepared with the aim to obtain stable nanocomposites with maximal silver loading in the interior of a polymeric shell. Synthesized Ag-DNCs were characterized by UV-vis spectrophotometry, atomic force microscopy (AFM), transmission electron microscopy (TEM) and X-ray photoelectron spectroscopy (XPS). The G7 Ag-DNC synthesized in 2000 molar excess of silver (1/4 ratio of tertiary amine/Ag^+) turned out a more suitable candidate for the label development. By combination of the differential pulse voltammetry (DPV) and the anodic stripping analysis (ASV) on a carbon electrode, down to $1.35 \times 10^{+10}$ of individual Ag-DNCs (LOD = 0.9 pM, 25 ml volume) was detected after the dissolution of silver nanoparticles in a diluted nitric acid. The potential advantages of proposed electrochemical label are discussed.

Abstract [in Czech]

Článek popisuje syntézu a charakterizaci nových kovových elektrochemických značek pro citlivou elektrochemickou stripping imunoanalýzu. Charakterizované elektrochemické značky jsou stříbrné nanočástice (NPS) syntetizované v dendrimerním polymeru. Stříbrné dendrimerní nanokompozity (Ag-DNCs) byly syntetizovány z generace 5-7 (G5-7) PAMAM dendrimeru s jádrem z ethylendiaminu a s hydroxylovými funkčními skupinami. Pro syntézu stabilních nanokompozitů s co největším obsahem stříbra vevnitř dendrimeru bylo připraveno několik roztoků s pevně daným poměrem stříbra a dendrimeru. Syntetizované Ag-DNCs byly charakterizovány UV-vis spektrofotometrií, mikroskopií atomárních sil (AFM), transmisní elektronovou mikroskopií (TEM) a rentgenovou fotoelektronovou spektroskopií (XPS). Syntetizovaný G7 Ag-DNC s 2000 molárním přebytkem stříbra (1/4 podíl terciárního aminu/Ag^+) se ukázal jako nejhodnější kandidát pro přípravu elektrochemické značky. Po rozpuštění nanočástic stříbra ve zředěné kyselině dusičné bylo na uhlíkové elektrodě pomocí diferenční pulsní voltametrie (DPV) a anodické rozpouštěcí analýzy (ASV) detekováno

$1{,}35 \times 10^{+10}$ jednotlivých Ag-DNCs (LOD = 0,9 pM, v objemu 25 ml). V článku je také diskutováno možné využití připravených elektrochemických značek.

7.3.   Paper III

Malý, J., Lampová, H., Semerádtová, A., **Štofik, M.** and Kováčik, L., 2009. The synthesis and characterization of biotin-silver-dendrimer nanocomposites as novel bioselective labels. Nanotechnology. Vol. 20, no. 38, pp. 385101. DOI: 10.1088/0957-4484/20/38/385101

The synthesis and characterization of biotin-silver-dendrimer nanocomposites as novel bioselective labels

Malý, J., Lampová, H., Semerádtová, A., Štofik, M. and Kováčik, L.

Marcel Štofik collaborated on experiments, measurements and revision of the manuscript.

Abstract

This paper presents a synthesis of a novel nanoparticle label with selective biorecognition properties based on a biotinylated silver-dendrimer nanocomposite (AgDNC). Two types of labels, a biotin-AgDNC (bio-AgDNC) and a biotinylated AgDNC with a poly(ethylene)glycol spacer (bio-PEG-AgDNC), were synthesized from a generation 7 (G7) hydroxyl-terminated ethylenediamine-core-type (2-carbon core) PAMAM dendrimer (DDM) by an N,N'-dicyclohexylcarbodiimide (DDC) biotin coupling and a NaBH$_4$ silver reduction method. Synthesized conjugates were characterized by several analytical methods, such as UV-vis, FTIR, AFM, TEM, ELISA, HABA assay and SPR. The results show that stable biotinylated nanocomposites can be formed either with internalized silver nanoparticles (AgNPs) in a DMM polymer backbone ('type I') or as externally protected ('type E'), depending on the molar ratio of the silver/DMM conjugate and type of conjugate. Furthermore, the selective biorecognition function of the biotin is not affected by the AgNPs' synthesis step, which allows a potential application of silver nanocomposite conjugates as biospecific labels in various bioanalytical assays, or potentially as fluorescence cell biomarkers. An exploitation of the presented label in the development of electrochemical immunosensors is anticipated.

Abstract [in Czech]

Článek popisuje syntézu nových elektrochemických značek z nanočástic, které mají selektivní biorekogniční vlastnosti. Elektrochemické značky byly připraveny biotinylací stříbrných dendrimerních nanokompozitů (AgDNC). Byly syntetizovány dva druhy značek, biotinylované AgDNC (bio-AgDNC) a biotinylované AgDNC se spacerem z polyethylenglykolu (bio-PEG-AgDNC). Pro syntézu značek byl použit PAMAM dendrimer (DDM) sedmé generace s jádrem z ethylendiaminu a s hydroxylovými funkčními skupinami. Jako redukční činidlo bylo použito NaBH$_4$. Biotinylace byla provedena pomocí N, N'-dicyklohexylkarbodiimidu (DDC). Syntetizované konjugáty byly charakterizovány několika analytickými metodami jako je UV-vis, FTIR, AFM, TEM, ELISA, HABA test a SPR. Výsledky ukázaly, že v závislosti na molárním poměru stříbra a DMM konjugátu (důležitý byl typ konjugátu) mohou být stabilní biotinylované nanokompozity tvořeny buď nanočásticemi stříbra (AgNPs) syntetizovanými v DMM vnitřní struktuře ("typ I") nebo v DDM povrchové oblasti ("typ E"). Kromě toho bylo

ukázáno, že syntéza AgNPs neovlivňuje selektivní biorekogniční funkce biotinu. To umožňuje potenciální použití biotinylovaných stříbrných nanokompozitů jako biospecifických značek v různých bioanalytických testech. Biotinylované stříbrné nanokompozity by mohly být využity i jako fluorescenční buněčné biomarkery. Syntetizované značky budou dále využity při vývoji elektrochemických imunosenzorů.

7.4. Paper IV

Štofik, M., Malý, J., and Frolík, J., 2010. An electrochemical microfluidic detector for ASV detection of metallic labels in immunoanalytical assays. *Manuscript prepared for submission*.

An electrochemical microfluidic detector for ASV detection of metallic labels in immunoanalytical assays

Štofik, M., Malý, J., and Frolík, J.

Abstract

We present a microfluidic electrochemical sensor-based flow-injection analysis (FIA) of silver-dendrimer nanocomposite (Ag-DNC) nanoparticle labels with differential pulse anodic stripping voltammetry (DPASV) detection. This concept of anodic stripping analysis (ASV) of metallic nanoparticle labels is applicable in development of electrochemical metalloimmunoassays.

The microfluidic device was fabricated by combination of photolithography and micromolding techniques. The microchannel with an integrated working (carbon microfiber), counter (gold), and reference (silver) electrodes was prepared from SU-8 negative photoresist. The channel was enclosed with a polydimethoxysilane (PDMS) cover providing connection with the FIA set-up. The basic system performance was characterized by amperometry (H_2O_2) and cyclic voltammetry (FeCy) measurements.

DPASV analysis of silver (I) in the FIA mode was optimized with regard to the deposition potential and the velocity of flow. Further on, an optimization of Ag-DNCs dissolution in nitric acid was performed. The microfluidic based DPASV analysis of the released silver (I) showed that up to $\sim 9.71 \times 10^7$ of individual Ag-DNC (LOD $= 6.45 \times 10^{-12}$ M in a 25 μL detection volume) was possible to detect. A short detection time (min), a low volume analysis (several μL), a full automatization, and an environment-friendly process (no mercury) make this microfluidic system fully competitive. It can be easily adapted for most types of metal nanoparticle labels or target analytes in metalloimmunoassays.

1. Introduction

Recent progress in microfabrication technologies has brought new perspectives in the development of analytical devices for chemical (Suga et al. 2005), biological (Huang & Lee 2007) and biochemical (Rodriguez et al. 2003) applications. An enzyme-linked immunosorbent assay (ELISA) is a well-known standard immunoanalytical method. Recently, a biosensor-based immunoassay has attempted to be its adequate alternative (Lee et al. 2008; Labib et al. 2009). What is more, a miniaturization of a biosensing device by application of microfabrication techniques can significantly decrease the sample volume, shorten the analysis time and costs, and even increase the sensitivity (Bhattacharyya & Klapperich 2006; Herr et al. 2007). Fluorescent (Kartalov et al. 2008), chemiluminiscent (Bhattacharyya & Klapperich 2006), or electrochemical (Redha et al. 2009) detection methods are commonly applied in these systems. Metalic nanoparticles (Lin et al. 2005; Chen et al. 2007; Mao et al. 2007) and super-paramagnetic beads

(Huang et al. 2009) were tested as alternative immunolabels with the aim to replace the classical enzyme label-based optical or electrochemical detection.

One of the new progressive approaches recently in focus is a metalloimmunoassay based on electrochemical stripping voltammetric (ESV) detection of metal ions released from metal or semiconductor nanoparticle labels after their oxidative dissolution. Silver (Chen et al. 2007), gold (Mao et al. 2007), and cadmium-sulfide (Liu et al. 2004) nanoparticles are the most frequently used. Due to a high sensitivity of ESV techniques and to a high metal/binding event ratio, a significant enhancement effect is present, which results in picomolar LODs (Javanbakht et al. 2009). Despite the high sensitivity, the ESV detection step, mostly performed in classical electrochemical cells, is characterized by high volumes (several mL), long analysis times (tens of minutes/sample), and low throughput with manual replacement of samples. A possible solution to overcoming these drawbacks could be to perform the ESV analysis in the microfluidic flow cells (Economou & Voulgaropoulos 2007; Siriangkhawut et al. 2009). Despite the promising concept, there has not been so much work done in this field yet, mainly due to the practical tasks connected with the fabrication of a suitable microfluidic electrochemical cell.

The fabrication of a microfluidic electrochemical immunosensing detector requires specific conditions and equipment. However, one of the advantages of the micromachining process is the variety of microfluidic detector designs which can be applied. Generally, an electrochemical detector requires a build-in working, a reference, and auxiliary electrodes. One of the possibilities of introducing electrodes into the microfluidic system is through drilled holes (Xia et al. 2005) while high accuracy is necessary. Another possibility is to use screen-printing techniques (Wang et al. 2002), electroplating (Subramani & Selvaganapathy 2009), or metal sputtering with an electron-beam evaporation process. Frequently used electrode materials are gold, platinum, or silver. Because of their low fouling and excellent electrochemical properties, carbon materials are often used for ASV working electrodes. They can be prepared from a carbon conductive paste (Shiddiky et al. 2006) or ink (Walker et al. 2008). The use of carbon microfibers (Cheng et al. 2007), glassy carbon, and carbon screen-printed electrodes modified with carbon nanotubes (Crevillén et al. 2008), or carbon nanotube nanoelectrode arrays (Miserendino et al. 2006) has also been published.

Recently, we have reported synthesis and characterization of a novel electrochemical label for electrochemical immunosensors based on silver-dendrimer nanocomposites (Ag-DNCs) and their sensitive detection (LOD = 9 x 10^{-12} M in 25 mL) by differential-pulse anodic stripping voltammetry (DPASV) after silver dissolution step (Štofik et al. 2009). Biotinylated Ag-DNCs (bio-AgDNCs) conjugates were also synthesized and successfully used in model immunoassays (Malý et al. 2009). However, the practical application of the presented technique was restricted by the need of high detection volumes, long time of analysis and low throughput without the possibility of automatization. Therefore, this paper presents a DPASV strategy for Ag-DNCs detection, which employs an electrochemical microfluidic cell assembly built by

photolithography and micromolding techniques. Thanks to the microdetector design, the precisely controlled analyte flow maintained by a flow injection system and a commercial microsampler, the automatic system is able to determine 6.45×10^{-12} M of Ag-DNCs in 25 µL within 5 minutes. Because of the multicomponent assembly, the constructed device is very compact and the sensing parts can be exchanged rapidly. Currently, our lab is working on a development of a miniaturized sensing unit for immunochemical detection of human interferon gamma based on the principle described above.

2. Materials and methods

2.1. Chemicals

Hydroxyl-terminated G7 PAMAM ethylenediamine core type dendrimers in methanol solution (5 wt.%), silver nitrate ($AgNO_3$), nitric acid (HNO_3), sodium borohydrid ($NaBH_4$), kalium chloride (KCl), hydrogen peroxide (H_2O_2), ferricyanide $K_3[Fe(CN)_6]$ were purchased from Sigma Aldrich, Inc. All aqueous solutions were prepared in ultrapure water with conductivity below 1 µScm^{-1} (Goro Pharmapur system, Czech Republic).

2.2. FIA electrochemical microfluidic system

The electrochemical microfluidic FIA detection system consisted of several parts: (i) a syringe pump, an injection valve, and a microautosampler (FIAlab, USA); (ii) an electrochemical microfluidic cell (fabrication details see below); (iii) a potenciostat with fA preamplifier (PGSTAT 12, EcoChemie, Netherlands), and (iv) a computer with appropriate software for pump and valve timing and electrochemical data processing.

2.3. Electrochemical microfluidic cell preparation

2.3.1. Integration of carbon fibre electrode with an SU-8 photoresist layer

The electrochemical microfluidic cell (Fig. 1) was prepared by combination of photolithography, PDMS molding and metal sputtering methods in several steps (Fig. 2). Two layers of photoresist were created on the silicon wafer substrates. Silicon wafer (100 mm diameter, ON Semiconductor Czech Republic, s.r.o.) was cut into 6 pieces (25 x 35 mm each) and treated in acetone for 10 min. The substrates were washed in deionized water, dried under a stream of nitrogen and let to dehydrate completely on a hotplate for 5 minutes at 250 °C. After cooling, 1 mL of negative photoresist SU-8 (NANO^{TM} SU-8 25, MicroChem Corp., USA) was spincoated on the substrates in a two step process: (i) 500 rpm for 10 s and (ii) 1000 rpm for 30 s. The substrates were further softbaked for 20 min (12 min ramp to 90 °C and baking for 8 min). Then, two methods of carbon microfiber working electrode (CM WE) integration were tested. In the first method, the substrates were taken from a hotplate immediately after the softbaking for approximately 30-60 s to allow the top level of the photoresist to harden. Then, a single carbon microfibre (diameter 10 µm), separated from a multi-filament tow (purchased

from Goodfellow Cambridge Ltd, UK), was put on the photoresist surface and the substrates were transferred again to the hotplate. During several seconds, the photoresist melted and allowed the bottom side of the carbon microfibre to stick firmly on its surface. After the microfibre deposition, the substrates were taken from the hotplate and let to cool to the room temperature (1-1.5 h). In the second method, the carbon microfibre was put on the second layer of the photoresist (this layer is patterned with a microfluidic channel) just before it was softbaked.

The first softbaked layer of the photoresist was exposed to UV light (40 s). Rays from a 100 W mercury arc lamp were collimated using a collimation lense (Oriel Aspherab, USA) and reflected by a dichroic mirror with 350-450 nm reflectance range. The substrates were treated with a post-exposure bake for 20 min (5 min ramp to 65 °C were followed by a 15 min baking) and let to relax overnight.

2.3.2. Deposition of metals and photolitography of the microfludic channel

Gold and silver layers, Au counter electrode (Au CE) and Ag reference electrode (Ag RE), were deposited onto the prepared photoresist layer through a mask by sputtering. The deposition was performed by a sputter-coating (Agar, Agar Scientific Ltd, UK) for 220 s under 0.3 mbar vacuum. Then, the second photoresist layer was spun on substrates and softbaked under the same conditions as above. This layer was exposed to UV light (25 s) through a mask with microchannel patterns (printed on transparency with a laser photoplotter, Pragoboard, s.r.o., Czech Rep.). The post-exposure bake substrates were let to relax overnight again. The microchannels were finally developed in a developer solution (4-hydroxy-4-methyl-2-pentanone, purchased from Sigma Aldrich, Inc., Germany) by immersion into two consequent shaking developer baths for 5 min., rinsed with isopropanol and dried with nitrogen. The exposed parts of the carbon fiber and deposited metals outside of the channel were connected to an electric wire through a carbon conducting tape.

2.3.3. Fabrication of PDMS ceiling and outlet connections

The ceiling part of the microfluidic channel was prepared from PDMS (Sylgard® 184 Silicone Elastomer kit, purchased from Dow Corning, USA). First, a mold was milled from acrylic glass and holes were drilled for tubings. Than PDMS polymer was mixed with a curing agent in a volume ratio 10:1. Bubbles were eliminated with a vacuum pump and the mixture was poured into the prepared mold. Crosslinking took place in an oven at 45 °C overnight. Two fixing panels were cut from acrylic glass. They served as a squeezing support for the microfluidic cell. Further on, holes were drilled into the top acrylic panel to introduce the tubings (Upchurch Scientific, USA). The top panel and a PDMS ceiling were connected through tubings and glued precisely with a PDMS polymer. Finally, the top (cealing) part of the microfluidic system was pressed against the electrochemical microchannel and fixed to the bottom acrylic glass panel by using four screws.

2.4. Electrochemical analysis

The electrochemical microfluidic cell was characterized by amperometric measurements and cyclic voltammetry. All measurements were performed on Autolab PGSTAT 12 potentiostat (EcoChemie, Netherlands) and the data were processed with General Purpose Electrochemical system (GPES) Autolab software. Ag (I) and Ag-DNCs were analyzed by DPASV. The limit of detection (LOD) was calculated as LOD = (b + kSb)/m, where b is the intercept of the linear approximation of the calibration curve, k=3, Sb is the standard deviation of the blank and m is the slope of the calibration curve. Basic amperometry measurements were performed with 0.1 M H_2O_2 (25 μL of sample was injected) in PBS pH 7 containing 0.1 M KCl as the running buffer. Cyclic voltammetry was performed with 0.01 M ferricyanide (FeCy) solution in PBS buffer.

Based on the results of the initial amperometric analysis, the FIAlab system timing and macro algorithms for several consequent DPASV measurements (in automatic mode) were set. Stripping voltammograms were collected with 0.1 M HNO_3 as the running buffer with the following constant settings: equilibration time 15 s, modulation time 0.05 s, interval time 0.1 s, step potential 0.00495 V, modulation amplitude 0.12 V.

The sample analysis working cycle consisted from several steps. First, a 25 μL of the sample was aspirated into the system from a microsampler. The working electrode was conditioned at 0.8 V vs. Ag RE for 90 s (to remove contamination). Silver deposition followed for 240 s (at deposition potential and flowrate). Then, DPV strips from -0.45 V to 0.45 V vs. Ag RE at 0.0495 $V.s^{-1}$ scanrate were applied. After the voltammetric strip, the electrochemical cell was treated with a continuous running buffer flow for another 240 s. One measurement cycle including the washing procedure thus took approx. 10 min.

2.5. Synthesis and characterization of Ag-DNC

The synthesis and characterization of Ag-DNCs have already been published (Štofik et al. 2009). For the purpose of this study, we synthesized dendrimer nanocomposites by: (i) mixing the generation 7 (G7) PAMAM-OH dendrimer (10 mL, 4 x 10^{-7} M) and silver nitrate water solution (10 mL, 8 x 10^{-4} M) (molar ratio 1:2000 dendrimer/Ag (I)) and (ii) subsequent reduction of silver with sodium borohydride water solution (1:1 volume ratio to dendrimer/Ag (I) mixture). The synthesized Ag-DNCs were further desalted in a dialysis column (3 kDa MWCO, regenerated cellulose) overnight and stored in water at 4 °C. The stability of the prepared Ag-DNCs was periodically controlled by monitoring of UV-VIS spectra (Unicam UV 500, Thermo Spectronics, USA).

The dissolution step of Ag-DNCs by nitric acid was optimized by monitoring the plasmonic peak stability of silver nanoparticles in a micro-titer plate. Ag-DNCs show a sharp plasmonic peak at 410 nm. Using an ELISA reader (Tecan Sunrise Remote, Tecan Group Ltd., Switzerland), the change of an absorbance at 410 nm with a 650 nm reference wavelength was investigated as the function of time and nitric acid

concentration. The absorbance data were being collected during an hour of a continuous shaking.

3. Results and discussion

3.1. Microfluidic electrochemical system fabrication

Conventional stripping voltammetry methods which employ a mercury either in form of mercury film electrodes (MFE) or hanging mercury drop electrodes (HDME) are not suitable to combine with lithographic methods although mercury can be plated (Ivaska & Kubiak 1997) or deposited (Tay et al. 1989) on a metalic working electrode. As was already shown by others, the ESV of several metals, including silver, can alternatively be performed on various types of carbon electrodes as are carbon fibre microelectrode (Cai et al. 2002), glassy carbon electrode (Chu et al. 2005), carbon paste (Labar & Lamberts 1997) or carbon paste modified electrode (Javanbakht et al. 2009), or thick-film carbon screen-printed electrodes (Reeder & Heineman 1998). Contrary to metal electrodes, patterning of carbon electrodes in microfluidic assembly is not so common although several approaches were proposed (Stanishevsky 1999; Wang et al. 2002; Walton et al. 2007; Walker et al. 2008). Therefore, the use of carbon fibre microelectrodes with defined diameters and properties integrated in a microfluidic device is still a challenge. We present a simple and reliable method of carbon fibre integration in the microchannels formed from negative photoresist.

Motivated by the need of microcell simplicity and a fast replacement of the functional units, we separated our system into two main parts: (i) a replaceable SU-8 negative photoresist based microchannel with integrated electrodes and (ii) a PDMS ceiling with integrated inlets and outlets (Fig. 1). In this way, the time needed to assemble both parts (and to replace a used or a mal-functioned channel) into a functional unit was minimized.
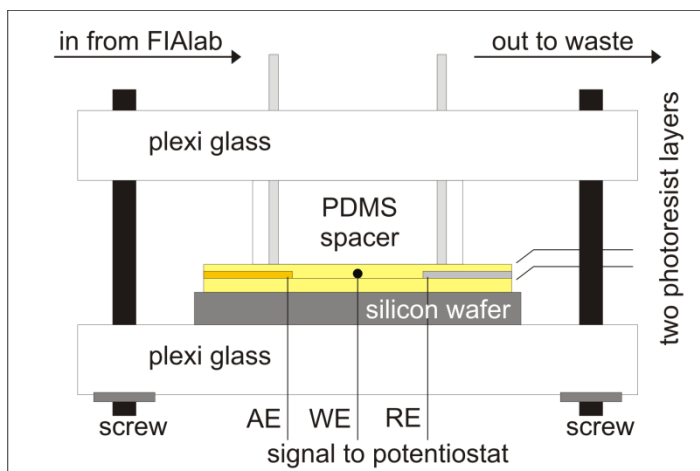
Figure 1. A general scheme of a complete electrochemical microfluidic cell assembly.

The replaceable microchannel part with integrated CM WE, Au CE and Ag RE electrodes was prepared in several steps by using photolithography techniques (Fig. 2, see chapter Material and methods). The first layer of the SU-8 photoresist served as adhesion layer (typically ~ 45 µm thick) promoting the attachment of carbon fibre and adherence of gold and silver electrodes. The second layer of the photoresist served for the microchannel definition (400 µm wide, 40 µm thick and 2 cm long, ~ 0.016 mm^2 in the crossection of the microfluidic channel area).
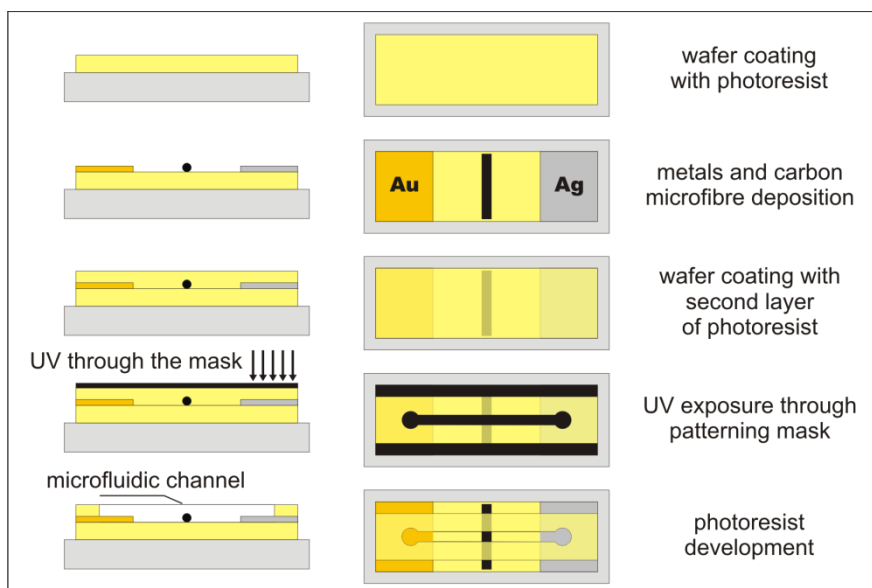
Figure 2. A photolithography process – a microfluidic electrochemical cell fabrication.

Usually, the SU-8 process has to be optimized for any application (Zhang et al. 2001; Keller et al. 2008). The most important factors are the softbake and post-exposure temperatures, their timing and exposure time able to influence polymerization kinetics of SU-8 monomers. We optimized the SU-8 process only for mild conditions (Anhoj et al. 2006). The softbake temperature was set to 90 °C and the postbake temperature 65 °C (for details, see chapter Materials and methods). The exposure time was the most important factor to influence the microfluidic channel resolution and carbon fibre WE integration in the microchannel. The effect of the exposure time on the channel formation (100 µm width) is shown in Fig. 3a. We found out that higher exposure times (>30 s) caused irregular photoresist polymerization close to the borders of the channels. The longer the exposure time, the stronger the effect is.
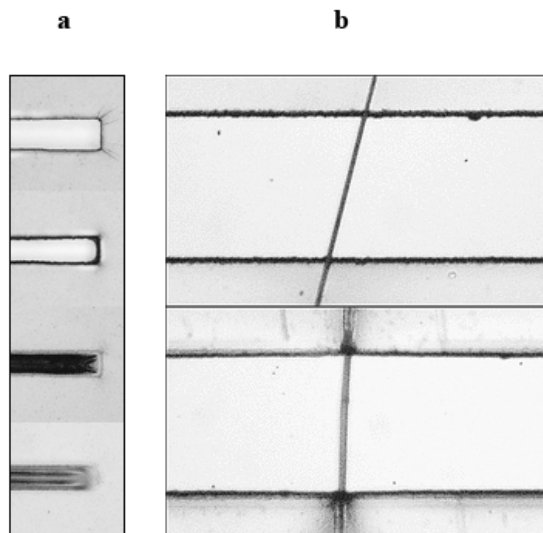
Figure 3. Pictures of a carbon fibre WE integrated into the SU-8 microchannel.
Pictures were taken with an optical microscope. Pictures on panel (a) show photoresist exposed through the mask with microchannel patterns (channels width is 100 μm). We can see how the exposure time influences the polymerization of SU-8 under the mask patterns (time exposure from the top to the bottom: 10 s, 60 s, 90 s, 120 s). Pictures on the panel (b) show two investigated approaches for the carbon microfibre WE deposition (channels width is 400 μm). The deposition onto the first (top picture) and into the second (bottom picture) photoresist layer.

Fig. 3b shows the carbon microfibre integrated in the microchannel for both investigated approaches with the working electrode deposited (i) on the first or (ii) into the second photoresist layer. The polymerization of the thin layer of the photoresist under the carbon fibre was investigated depending on the exposure time in the first approach. We found out that an overexposure for 40 s is enough to initiate the photoresist polymerization in the microfibre proximity and allows a firm WE attachment on the photoresist surface. Such overexposure did not cause other defects, such as photoresist surface crumpling. For the second layer, a shorter exposure time (25 s) was sufficient for a fine microchannel fabrication and a good sealing of the carbon fibre without subsequent problems with a leakage of the measuring solutions (Fig.3b, top).

In the second approach, the carbon microfibre put onto the substrates coated with the second layer of the photoresist settled down to the substrate bottom during the softbaking. Since the integration of the microfiber and the microchannel development was performed in a single step, the overexposure was inconvenient as it created microchannel defects. Therefore, due to the lower exposure time (25 s), the photoresist close to the microfibre was not completely polymerized and cavities near to the

microfluidic channel were observed (Fig.3b, bottom). Due to the worse results with the microfiber sealing, the first approach was used for a further fabrication of the microcell.

3.2. General electrochemical analysis

The fluid control in the assembled electrochemical cell was performed with FIAlab system (FIAlab Instruments, Inc., USA). With a 250 µL syringe, it was possible to set the flow speed down to 0.21 µL.s^{-1}. The samples were aspirated from an autosampler and dispensed into the measurement cell. By this way, the volumes of several few microliters could be introduced in the system and measured reliably. The FIAlab and GPES software provided an automatization of measurements by programming macros. Several samples could be thus measured through a long period of time without manual assistance.

Every prepared cell was first inspected in PBS buffer pH 7 with 0.1 M KCl at 25 µL.min^{-1} flow velocity. When positive potential from 0.6 to 0.8 V vs. silver RE was applied to the working electrode, an amperometric baseline current approximated to the value of 30-80 pA with an average noise lower than 5-9 pA. Similar values were obtained also in 0.1 M HNO$_3$, which was used as the running solution for all DPASV measurements. Amperometric detection of hydrogen peroxide was a simple and valuable method for software macros time-adjustment and basic electrochemical tests. The Fig. 4 (inset) shows an amperometric detection of 0.1 M H$_2$O$_2$ (25 µL) under different flow conditions (0.25-0.58 µL.s^{-1}). By decreasing the flowrate, the current response is lower, but a significantly broader peak is observed. The high sensitivity and excellent reproducibility of the cell response is documented by the sequential injections of hydrogen peroxide performed for a series of potential values (0.5 to 0.9 V vs. Ag RE) (Fig. 4). Due to very low noise and high sensitivity, the LOD for H$_2$O$_2$ (6.19 x 10^{-6} M) was competitive with many specialized hydrogen peroxide sensors already published (Li et al. 2007; Ekanayake et al. 2008). Therefore, we may conclude that the presented microfluidic cell is also suitable for sensitive amperometric detection of various electrochemically active substances.
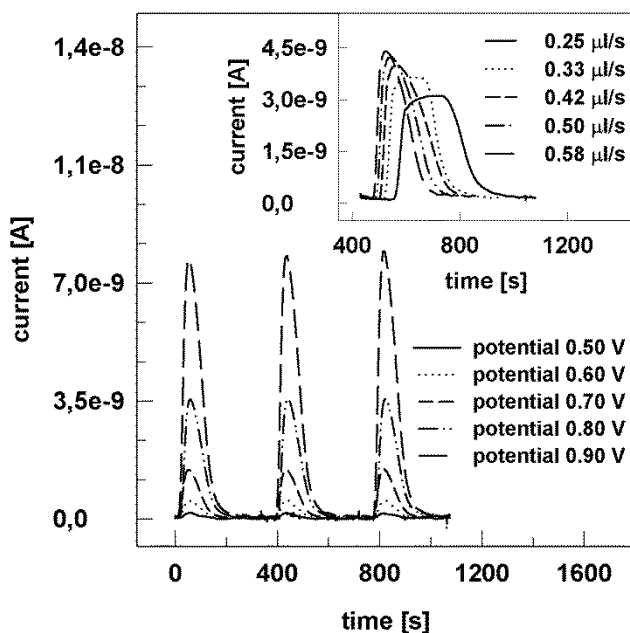
Figure 4. Amperometric responses to 0.1 M H$_2$O$_2$ measured in three consequent measurements with potential variations.
The inset figure shows the dependence of the responses to the H$_2$O$_2$ on a flowrate. The potentials are given vs. Ag RE.

The cyclic voltammetry experiments were performed with 0.01 M FeCy under different scanrates (0.025; 0.050; 0.070; 0.100; 0.150 V.s^{-1}). The observed separation of anodic (E$_{pa}$ = 83 mV) and cathodic peak maximum (E$_{pc}$ = 186 mV) is ΔE$_p$ = 103 mV at the minimal scan rate (υ = 0.025 V.s^{-1}), which does not fully meet the reversibility criteria for a fast one-electron process (ΔE$_p$ = 59 mV). With an increasing scan rate, the peak separation increases slightly. It indicates a certain uncompensated resistance between CM WE and Ag RE electrode. The formal redox potential of redox couple is E$^{0'}$ = 133 mV.

3.3. Differential pulse anodic stripping analysis of silver

Generally, the DPASV of metal ions is known to depend on many different parameters. It is important to optimize some of them such as the deposition potential, the incubation time, the presence of supporting electrolytes etc. In an electrochemical environment where the saturated calomel electrode serves as a reference and the pyrolytic graphite (Wantz et al. 2005) or glassy carbon (Štofik et al. 2009) as a working electrode, the optimal silver deposition potential varies around ~ -500 mV. Due to the pseudo-reference silver electrode used in our microflow cell, we expected a shift of optimal deposition potentials and we investigated how the deposition potential can influence the device sensitivity in a set of measurements. For an optimization process we investigated the potential from the lowest (-0.9 V) to the highest value (-0.5 V) vs. Ag RE. In a

typical anodic stripping voltammogram obtained after a deposition of 10^{-7} M solution of silver (I) in 0.1 M HNO$_3$ (25 µL injection, 0.25 µL.s^{-1}, - 900 mV vs. RE), a relatively sharp wave was observed at E = -0.018 V vs. Ag RE corresponding to the oxidation of accumulated Ag (0). Fig. 5 presents a set of the stripping curves optimization in the form of a 3D graph. The curves (Fig. 5, top right) were plotted as a function of WE deposition potential applied (10^{-7} M Ag (I), 25 µL injection, 0.25 µL.s^{-1}). Compared to blank experiments (Fig. 5, top left), a significant increase of the stripping voltammetric peak is evident up to -0.9 V vs. Ag RE. Occasionally, when the flow was stopped or at very low flowrates, a negligible contamination of WE from silver RE (located down-flow of WE) was also observed at the blank experiments when -0.9 V deposition potential was applied. To avoid this, a -0.8 V deposition potential was used as optimal for further experiments.
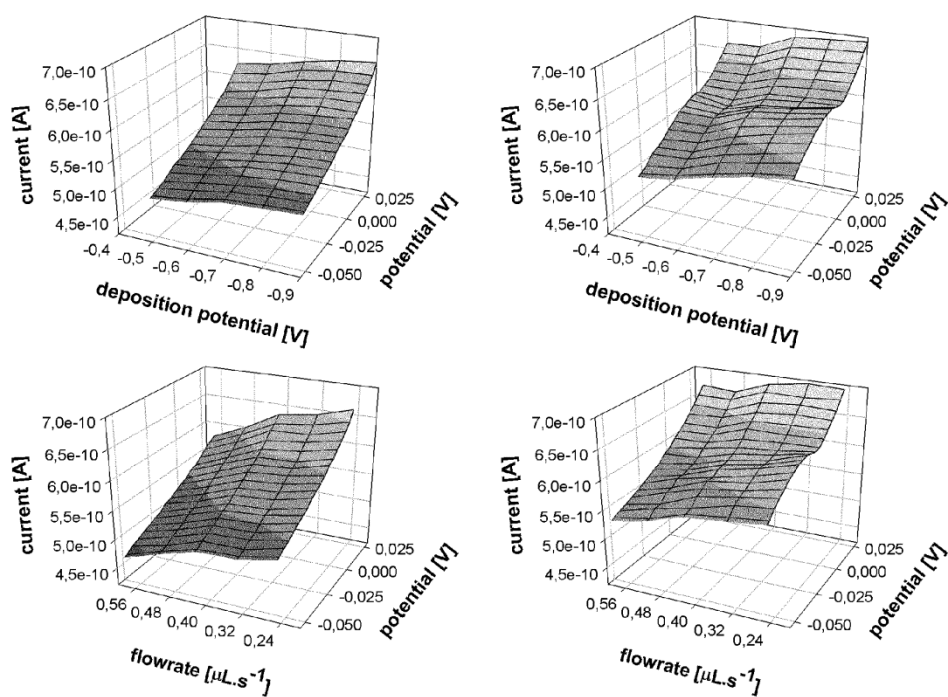
Figure 5. Dependence of the ADSV detection on the deposition potential and the flowrate.

The voltametric responses of the silver stripping peaks are plotted for different deposition potentials (top panels) and flowrates (bottom panels). Left panels represent blank measurents and right panels represent measurements with 10^{-7} M concentration of Ag (I) (injection of 25 µL). On the right panels we can see how the stripping peaks arise when the deposition potential lowers (top) and the flowrate slows down (bottom).

Experiments with a variation of flowrate at 0.25, 0.33, 0.42, 0.50 and 0.58 µL.s^{-1} (Fig. 5, bottom pannels) demonstrate how significantly this parameter effects the stripping responses of the detection cell (10^{-7} M Ag (I), 25 µL injection, deposition potential -0.9 V vs. Ag RE). The stripping peak of silver increases with decreasing

flowrates and reaches its maximum in the lowest achievable flowrates. Therefore, we believe that there is a potential for a further improvement of sensitivity if the flowrates were lower or the distance which silver ions have to migrate to WE was shorter. This could be achieved by a slower pumping or by a change of the channel geometry. On the other hand, the lower flowrates increase the time of analysis. This could be compromised by decreasing the detection volumes (to units of µL) and profit from the preservation of comparable detection limits.

Based on optimized settings, the calibration curve for silver ions detection was obtained. Investigated silver concentrations (10^{-9} to 10^{-6} M, 25 µL injection, deposition potential -0.8 V vs. Ag RE, 0.25 µL.s^{-1}) showed a linear dependence for both a peak current maximum and a peak area plotted against the silver concentration ($y = 8.96 \times 10^{-6} x + 6.57 \times 10^{-13}$, $R^2 = 0.974$). The calculated limit of detection based on area analysis was LOD = 1.40×10^{-7} M. The LOD obtained on carbon microfibre electrode is within the meaning of silver concentrations comparable or little higher compared to the others reported in the literature (Labar & Lamberts 1997; Saterlay et al. 2000; Chu et al. 2005; Wantz et al. 2005; Chen et al. 2007). Nevertheless, these methods tend to be optimized for concentration analysis and the volume of the analyzed samples is not usually considered, it is not a limiting factor. Our sensor is aimed at an analysis of the absolute silver content in the sample where low volume is crucial for the application. Therefore, the LOD obtained in 25 µL (3.51 pmol Ag (I)) is comparable or even lower than other systems reported above and in (Javanbakht et al. 2009).

3.4. Ag-DNC dissolution and stripping analysis

For a successful ASV detection of Ag-DNCs, silver ions, Ag (I), have to be accessible to the detection device. It happens only if colloidal silver is fully dissolved by e.g. nitric acid. We have run experiments where the effect of the concentration of nitric acid on the dissolution of Ag-DNCs was inspected. The inset of Fig. 6 shows the time-dependence of 410 nm absorbance changes (silver nanoparticles plasmon peak) in the presence of various HNO_3 concentrations. Concentrations lower than 1.5 M did not allow the nanoparticles to be completely dissolved even after 1 hour. Therefore, if the Ag-DNCs were used as electrochemical labels in a metalloimmunoassay, the final step, Ag-DNCs dissolution, would be crucial for the consequent sensitive label detection. Depending on the added volume of acid to the sample with Ag-DNCs labels, the concentration of Ag (I) decreases rapidly. For that reason, it is necessary to consider the silver nanoparticles dissolution conditions carefully before a metalloimmunoassay is performed.
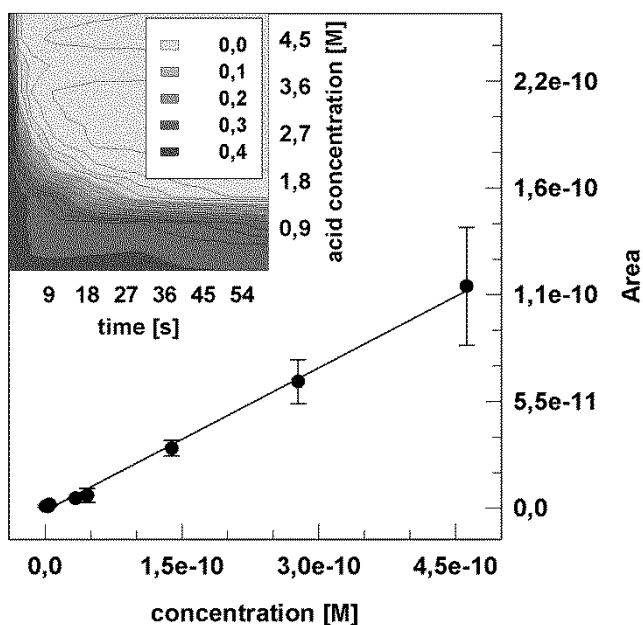
Figure 6. ADSV calibration curve for Ag-DNCs conjugates.
Calibration responses are plotted as a voltammetric peak area vs. the concentration of the Ag-DNCs conjugates. The inset figure shows how the dissolution of the Ag-DNCs depends on the nitric acid concentration and on time. The vertical range in the contour plot represents the absorbance of the Ag-DNCs plasmonic peak which is characteristic for silver nanoparticles at 410 nm. The data were collected at 410 nm against 650 nm reference wavelength.

Fig. 6 presents calibration curve of Ag-DNCs obtained with a microfluidic cell. Ag-DNCs were first dissolved in a concentrated nitric acid (3 M HNO_3, for 30 min.), diluted to final 0.1 M HNO_3 and directly measured (25 µL injection, deposition potential -0.8 V vs. Ag RE, 0.25 µL.s^{-1}). A linear dependence for both a peak current maximum and a peak area plotted against the Ag-DNCs concentration was obtained (y = 0.25 x - 1.39×10^{-12}, R^2 = 0.957). The calculated limit of detection based on area analysis was LOD = 6.45×10^{-12} M. Assuming a 25 µL detection volume, it represents 1.61×10^{-16} mol of Ag-DNCs particles ($\sim 9.71 \times 10^{7}$). This value is up to two orders of magnitude lower compared to our previous work (Štofik et al. 2009) where ASV analysis was performed in 25 mL commercial electrochemical cell.

Conclusions

Developments in area of electrochemical metalloimmunoassays show highly sensitive detection strategies based on anodic stripping voltammetry of metal nanoparticle labels. Here we show a microfluidic-based DPASV detection of Ag (I) released from silver-dendrimer nanocomposite labels, which brings a potential for a rapid automatic sensitive analysis of many samples in µL detection volumes.

We prepared an electrochemical microfluidic measurement ensemble consisting from two parts: (i) an SU-8 negative photoresist based microchannel with integrated CM WE, Au CE and Ag RE electrodes and (ii) a PDMS cover serving as a channel enclosure and a connection with the outer tubings. The process of carbon microfiber integration into the microchannel was optimized. A microfluidic device was connected with a programmable FIA system enabling a rapid automatic analysis of several µL of sample. The system performance was characterized by (i) amperometric detection of hydrogen peroxide; (ii) cyclic voltammetry of FeCy. Both methods have shown a reliable, sensitive and reproducible electrochemical analysis in a microflow device.

Anodic stripping voltammetry of silver in FIA injection mode was optimized regarding to the deposition potential, the velocity of flow and the DPASV settings. The calibration curve shows a sensitive Ag (I) detection with LOD = 1.40×10^{-7} M. The conditions of Ag-DNCs dissolution in nitric acid were optimized showing a need for relatively high concentrations of HNO_3 (>1.5 M) and a longer time for a complete dissolution. By DPASV analysis in the microfluidic system, up to $\sim 9.71 \times 10^{7}$ of individual Ag-DNCs (LOD = 6.45×10^{-12} M in a 25 µL detection volume) was possible to detect. The presented microfluidic device has the advantage of low analysis volumes (several µL), a short detection time (min), and a fully automatic process. What is more, it is environment-friendly (no mercury) and can be further developed and tested in immunoassays with alternative metalic labels.

Acknowledgements

References

ANHOJ, T. A., JORGENSEN, A. M., ZAUNER, D. A. and HÜBNER, J., 2006. The effect of soft bake temperature on the polymerization of SU-8 photoresist. Journal of Micromechanics and Microengineering. Vol. 16, no. 9, pp. 1819–1824.

BHATTACHARYYA, A. and KLAPPERICH, C. M., 2006. Design and testing of a disposable microfluidic chemiluminescent immunoassay for disease biomarkers in human serum samples. Biomedical Microdevices. Vol. 9, no. 2, pp. 245–251.

CAI, H., XU, Y., ZHU, N., HE, P. and FANG, Y., 2002. An electrochemical DNA hybridization detection assay based on a silver nanoparticle label. Analyst. Vol. 127, no. 6, pp. 803–808.

CREVILLÉN, A. G., PUMERA, M., GONZÁLEZ, M. C. and ESCARPA, A., 2008. Carbon nanotube disposable detectors in microchip capillary electrophoresis for water-soluble vitamin determination: analytical possibilities in pharmaceutical quality control. Electrophoresis. Vol. 29, no. 14, pp. 2997–3004.

ECONOMOU, A. and VOULGAROPOULOS, A., 2007. On-line stripping voltammetry of trace metals at a flow-through bismuth-film electrode by means of a hybrid flow-injection/sequential-injection system. Talanta. Vol. 71, no. 2, pp. 758–765.

EKANAYAKE, E.M.I. M., PREETHICHANDRA, D.M.G. and KANETO, K., 2008. Bi-functional amperometric biosensor for low concentration hydrogen peroxide measurements using polypyrrole immobilizing matrix. Sensors and Actuators B: Chemical. Vol. 132, no. 1, pp. 166–171.

HERR, A. E., HATCH, A. V., THROCKMORTON, D. J., TRAN, H. M., BRENNAN, J. S., GIANNOBILE, W. V. and SINGH, A. K., 2007. Microfluidic immunoassays as rapid saliva-based clinical diagnostics. Proceedings of the National Academy of Sciences. Vol. 104, no. 13, pp. 5268–5273.

HUANG, H., ZHENG, X. L., ZHENG, J. S., PAN, J. and PU, X. Y., 2009. Rapid analysis of alpha-fetoprotein by chemiluminescence microfluidic immunoassay system based on super-paramagnetic microbeads. Biomedical Microdevices. Vol. 11, no. 1, pp. 213–216.

HUANG, Ch.-W. and LEE, G.-B., 2007. A microfluidic system for automatic cell culture. Journal of Micromechanics and Microengineering. Vol. 17, no. 7, pp. 1266–1274.

CHEN, Z.-P., PENG, Z.-F., LUO, Y., QU, B., JIANG, J.-H., ZHANG, X.-B., SHEN, G.-L. and YU, R.-Q., 2007. Successively amplified electrochemical immunoassay based on biocatalytic deposition of silver nanoparticles and silver enhancement. Biosensors and Bioelectronics. Vol. 23, no. 4, pp. 485–491.

CHENG, H., HUANG, W.-H., CHEN, R.-S., WANG, Z.-L. and CHENG, J.-K., 2007. Carbon fiber nanoelectrodes applied to microchip electrophoresis amperometric detection of neurotransmitter dopamine in rat pheochromocytoma (PC12) cells. Electrophoresis. Vol. 28, no. 10, pp. 1579–1586.

CHU, X., FU, X., CHEN, K., SHEN, G.-L. and YU, R.-Q., 2005. An electrochemical stripping metalloimmunoassay based on silver-enhanced gold nanoparticle label. Biosensors and Bioelectronics. Vol. 20, no. 9, pp. 1805–1812.

IVASKA, A. and KUBIAK, W. W., 1997. Application of sequential injection analysis to anodic stripping voltammetry. Talanta. Vol. 44, no. 4, pp. 713–723.

JAVANBAKHT, M., DIVSAR, F., BADIEI, A., FATOLLAHI, F., KHANIANI, Y., GANJALI, M. R., NOROUZI, P., CHALOOSI, M. and ZIARANI, G. M., 2009. Determination of picomolar silver concentrations by differential pulse anodic stripping voltammetry at a carbon paste electrode modified with phenylthiourea-functionalized high ordered nanoporous silica gel. Electrochimica Acta. Vol. 54, no. 23, pp. 5381–5386.

KARTALOV, E. P., LIN, D. H., LEE, D. T., ANDERSON, W. F., TAYLOR, C. R. and SCHERER, A., 2008. Internally calibrated quantification of protein analytes in

human serum by fluorescence immunoassays in disposable elastomeric microfluidic devices. Electrophoresis. Vol. 29, no. 24, pp. 5010–5016.

KELLER, S., BLAGOI, G., LILLEMOSE, M., HAEFLIGER, D. and BOISEN, A., 2008. Processing of thin SU-8 films. Journal of Micromechanics and Microengineering. Vol. 18, no. 12, pp. 125020.

LABAR, C. and LAMBERTS, L., 1997. Anodic stripping voltammetry with carbon paste electrodes for rapid Ag(I) and Cu(II) determinations. Talanta. Vol. 44, no. 5, pp. 733–742.

LABIB, M., HEDSTRÖM, M., AMIN, M. and MATTIASSON, B., 2009. A capacitive immunosensor for detection of cholera toxin. Analytica Chimica Acta. Vol. 634, no. 2, pp. 255–261.

LEE, J. H., YANG, S. S., KIM, B. W., SIM, S. J., CHAE, H. and YOON, H. C., 2008. Electrochemical immunosensor signaling by employing enzyme-tagged antibody for the determination of antigen or antibody under single competition reaction format. Colloids and Surfaces A: Physicochemical and Engineering Aspects. Vol. 313-314, pp. 509–514.

LI, Z., CUI, X., ZHENG, J., WANG, Q. and LIN, Y., 2007. Effects of microstructure of carbon nanofibers for amperometric detection of hydrogen peroxide. Analytica Chimica Acta. Vol. 597, no. 2, pp. 238–244.

LIN, F. Y. H., SABRI, M., ALIREZAIE, J., LI, D. and SHERMAN, P. M., 2005. Development of a nanoparticle-labeled microfluidic immunoassay for detection of pathogenic microorganisms. Clinical and Vaccine Immunology. Vol. 12, no. 3, pp. 418–425.

LIU, G., WANG, J., KIM, J., JAN, M. R. and COLLINS, G. E., 2004. Electrochemical Coding for Multiplexed Immunoassays of Proteins. Analytical Chemistry. Vol. 76, no. 23, pp. 7126–7130.

MALÝ, J., LAMPOVÁ, H., SEMERÁDTOVÁ, A., ŠTOFIK, M. and KOVÁČIK, L., 2009. The synthesis and characterization of biotin-silver-dendrimer nanocomposites as novel bioselective labels. Nanotechnology. Vol. 20, no. 38, pp. 385101.

MAO, X., JIANG, J., HUANG, Y., SHEN, G. and YU, R., 2007. Gold nanoparticle accumulation using magnetic particles: A new strategy for electrochemical immunoassay based on the reversible reaction between dethiobiotin and avidin. Sensors and Actuators B: Chemical. Vol. 123, no. 1, pp. 198–203.

MISERENDINO, S., YOO, J., CASSELL, A. and TAI, Y.-Ch., 2006. Electrochemical characterization of parylene-embedded carbon nanotube nanoelectrode arrays. Nanotechnology. Vol. 17, no. 4, pp. S23–S28.

REDHA, Z. M., BALDOCK, S.. J., FIELDEN, P. R., GODDARD, N. J., BROWN, B. J. T., HAGGETT, B. G. D., ANDRES, R. and BIRCH, B. J., 2009. Hybrid microfluidic sensors fabricated by screen printing and injection molding for

electrochemical and electrochemiluminescence detection. Electroanalysis. Vol. 21, no. 3-5, pp. 422–430.

REEDER, G. S. and HEINEMAN, W. R., 1998. Electrochemical characterization of a microfabricated thick-film carbon sensor for trace determination of lead. Sensors and Actuators B: Chemical. Vol. 52, no. 1-2, pp. 58–64.

RODRIGUEZ, I., LESAICHERRE, M., TIE, Y., ZOU, Q., YU, Ch., SINGH, J., MENG, L. T., UPPILI, S., LI, S. F. Y., GOPALAKRISHNAKONE, P. and SELVANAYAGAM, Z. E., 2003. Practical integration of polymerase chain reaction amplification and electrophoretic analysis in microfluidic devices for genetic analysis. Electrophoresis. Vol. 24, no. 12, pp. 172–178.

SATERLAY, A., MARKEN, F., FOORD, J. S. and COMPTON, R. G., 2000. Sonoelectrochemical investigation of silver analysis at a highly boron-doped diamond electrode. Talanta. 2000. Vol. 53, no. 2, pp. 403–415.

SHIDDIKY, M. J. A., WON, M.-S. and SHIM, Y.-B., 2006. Simultaneous analysis of nitrate and nitrite in a microfluidic device with a Cu-complex-modified electrode. Electrophoresis. Vol. 27, no. 22, pp. 4545–4554.

SIRIANGKHAWUT, W., PENCHAREE, S., GRUDPAN, K. and JAKMUNEE, J., 2009. Sequential injection monosegmented flow voltammetric determination of cadmium and lead using a bismuth film working electrode. Talanta. Vol. 79, no. 4, pp. 1118–1124.

STANISHEVSKY, A., 1999. Focused ion beam patterning of diamondlike carbon films. Diamond and Related Materials. Vol. 8, no. 7, pp. 1246–1250.

SUBRAMANI, B. G. and SELVAGANAPATHY, P. R., 2009. Surface micromachined PDMS microfluidic devices fabricated using a sacrificial photoresist. Journal of Micromechanics and Microengineering. Vol. 19, no. 1, pp. 015013.

SUGA, S., OKAJIMA, M., FUJIWARA, K. and YOSHIDA, J., 2005. Electrochemical combinatorial organic syntheses using microflow systems. ChemInform. Vol. 36, no. 49.

ŠTOFIK, M., STRÝHAL, Z. and MALÝ, J., 2009. Dendrimer-encapsulated silver nanoparticles as a novel electrochemical label for sensitive immunosensors. Biosensors and Bioelectronics. Vol. 24, no. 7, pp. 1918–1923.

TAY, E. B.-T., KHOO, S.-B. and LOH, S.-W., 1989. Characterisation of mercury deposition on a platinum thin-ring ultramicroelectrode and its application to flow injection anodic stripping voltammetry. Analyst. Vol. 114, no. 9, pp. 1039.

WALKER, C. E., XIA, Z., FOSTER, Z. S., LUTZ, B. J. and FAN, Z. H., 2008. Investigation of airbrushing for fabricating microelectrodes in microfluidic devices. Electroanalysis. Vol. 20, no. 6, pp. 663–670.

WALTON, M. D., KIM, Y. S., JAN, C. J., MCCONNEL, E. P., EVERETT, W. N. and GRUNLAN, J. C., 2007. Deposition and patterning of conductive carbon black thin films. Synthetic Metals. Vol. 157, no. 16-17, pp. 632–639.

WANG, J., PUMERA, M., PRAKASH CHATRATHI, M., RODRIGUEZ, A., SPILLMAN, S., MARTIN, R. S. and LUNTE, S. M., 2002. Thick-film electrochemical detectors for poly(dimethylsiloxane)-based microchip capillary electrophoresis. Electroanalysis. Vol. 14, no. 18, pp. 1251–1255.

WANTZ, F., BANKS, C. E. and COMPTON, R. G., 2005. Edge plane pyrolytic graphite electrodes for stripping voltammetry: a comparison with other carbon based electrodes. Electroanalysis. Vol. 17, no. 8, pp. 655–661.

XIA, F., JIN, W., YIN, X. and FANG, Z., 2005. Single-cell analysis by electrochemical detection with a microfluidic device. Journal of Chromatography A. Vol. 1063, no. 1-2, pp. 227–233.

ZHANG, J., TAN, K. L., HONG, G. D., YANG, L. J. and GONG, H. Q., 2001. Polymerization optimization of SU-8 photoresist and its applications in microfluidic systems and MEMS. Journal of Micromechanics and Microengineering. Vol. 11, no. 1, pp. 20–26.

7.5. Paper V

Štofik, M., and Malý, J., 2011. Držák pro mikrofluidní čip z polymeru polydimethylsiloxanu, Utility model application, PUV 2011-25393, registered on 27-12-2011 at the Industrial Property Office, Czech Republic.

<u>Název technického řešení</u>

Držák pro mikrofluidní čip z polymeru polydimethylsiloxanu

<u>Oblast techniky</u>

Miniaturizace dnes není hlavní doménou jen technických oborů, ale prosazuje se i v oborech přírodovědných v oblasti chemických, biochemických nebo biologických analytických metod. Výrobní postupy z oblasti mikro a nanoelektroniky umožňují výrobu mikroelektromechanických zařízení (MEMS), jejichž součástí jsou objekty o velikosti v řádu desítek mikrometrů až nanometrů. Tyto objekty mohou sloužit například jako senzory nebo aktuátory a mohou být navzájem integrovány na prostoru o velikosti několika stovek mikrometrů až desítek milimetrů (MENZ, Wolfgang; MOHR, Jürgen; PAUL, Oliver. Microsystem technology. Weinheim : Wiley-VCH, 2001. 500 s. ISBN 9783527296347). Dostupnost těchto technologií pro oblast analytiky umožňuje vyrábět zařízení, která mohou plnit různé funkce laboratorních přístrojů a jsou navzájem integrována na velmi malém prostoru. Pro tato zařízení se zavedla zkratka µTAS (micro Total Analysis Systems) (MANZ, Andreas; GRABER, N.; WIDMER, Michael H. Miniaturized total chemical analysis systems : A novel concept for chemical sensing. Sensors and Actuators B: Chemical. 1990, 1, 1-6, s. 244-248. ISSN 0925-4005; HARRISON, Jed D., et al. Capillary electrophoresis and sample injection systems integrated on a planar glass chip. Analytical chemistry. 1992, 64, 19, s. 1926–1932. ISSN 0003-2700) nebo také Lab-On-Chip. Jsou to mikrofluidní zařízení, ve kterých dochází k manipulaci s roztoky. Mezi hlavní výhody mikrofluidních zařízení patří nízká spotřeba analytů, vysoká citlivost měření, krátký čas a nízká cena analýzy vzhledem k ceně jednoho testu. Využití těchto zařízení je téměř neomezené (MARK, Daniel, et al. Microfluidic lab-on-a-chip platforms: requirements, characteristics and applications. Chemical Society Reviews. 2010, 39, 3, s. 1153-1182. ISSN 0306-0012; HAEBERLE, Stefan; ZENGERLE, Roland. Microfluidic platforms for lab-on-a-chip applications. Lab on a Chip. 2007, 7, 9, s. 1094–1110. ISSN 1473-0189). Jako příklad lze uvést extrakci nebo separaci biomolekul (CHEN, Hong; FAN, Z. Hugh. Two-dimensional protein separation in microfluidic devices. ELECTROPHORESIS. 2009, 30, 5, s. 758-765. ISSN 0173-0835), buněčných struktur nebo celých buněk (LENSHOF, Andreas; LAURELL, Thomas. Continuous separation of cells and particles in microfluidic systems. CHEMICAL SOCIETY REVIEWS. 2010, 39, 3, s. 1203-1217. ISSN 0306-0012). Mohou sloužit jako sekvenátory nukleových kyselin nebo zařízení pro různé typy enzymatických stanovení (GRAYSON, ACR, et al. A BioMEMS review : MEMS technology for physiologically integrated devices. PROCEEDINGS OF THE IEEE. 2004, 92, 1, s. 6-21. ISSN 0018-9219). Možná je analýza celých buněk nebo buněčných procesů (YI, Changqing, et al. Microfluidics technology for manipulation and analysis of biological cells. Analytica Chimica Acta. 2006, 560, 1-2, s. 1-23. ISSN 00032670). Mohou sloužit jako systémy pro kontrolovanou syntézu polymerů, různých nanomateriálů (SONG, Yujun; HORMES, Josef; KUMAR, Challa S. S. R. Microfluidic Synthesis of Nanomaterials. Small. 2008, 4, 6, s. 698-711. ISSN 16136810) nebo jako

systémy pro manipulaci s mikro nebo nanočásticemi (PAMME, Nicole. Magnetism and microfluidics. Lab on a Chip. 2006, 6, 1, s. 24-38. ISSN 1473-0189) apod. Proto se v posledním desetiletí rapidně zvýšil zájem o vývoj mikrofluidních zařízení. To dokládá i rychlým tempem se zvyšující počet vydaných vědeckých publikací na téma mikrofluidika, v současné době nalezeno více než 18 000 publikací v citační databázi Scopus.

Dosavadní stav techniky

Pro přípravu mikrofluidních zařízení, čipů, se využívají již dlouhodobě zavedené postupy pro výrobu mikrosystémů. Patří mezi ně například elektronová litografie, fotolitografie, soft litografie, depozice tenkých vrstev materiálů fyzikálními nebo chemickými metodami, suché nebo mokré leptání, odlévání, mikroobrábění atd. (JAEGER, Richard C. Introduction to microelectronic fabrication. 2nd ed. Upper Saddle River, N.J. : Prentice Hall, 2002. 316 s. ISBN 9780201444940). Velmi důležitou etapou výroby, která při přípravě těchto zařízení prozatím nemá žádné zavedené standardy, je vytvoření mikrofluidního rozhraní. Rozhraní mikrofluidního zařízení zabezpečuje spolehlivé propojení a komunikaci čipu s okolím. Toto propojení je potřeba zabezpečit z důvodu nutnosti přítoku a odtoku analyzovaných roztoků a možnosti připojení čipu k analyzátoru, který využívá vhodnou měřící (detekční) metodu. Spolehlivé propojení čipu s okolím ovlivňuje funkčnost navrženého řešení jako celku. Mezi hlavní požadavky, které se kladou na mikrofluidní rozhraní, patří spolehlivost, mechanická odolnost a snížení počtu míst, skrz které může docházet k prosakování roztoků, a také jednoduchá montáž, snadné připojení a odpojení konektorů a možnost udržet co nejnižší mrtvý objem analytů (FREDRICKSON, Carl K.; FAN, Z. Hugh. Macro-to-micro interfaces for microfluidic devices. Lab on a Chip. 2004, 4, 6, s. 526-533. ISSN 1473-0189). Existuje mnoho různých přístupů, jak zabezpečit kontakt čipu s okolím. Obecně je můžeme rozdělit na dvě skupiny: (i) skupinu, která využívá přímé připojení konektorů na čip, (ii) skupinu, která využívá vhodný adaptér nebo držák.

V zahraničí existuje několik firem, které se věnují komerční výrobě mikrofluidních čipů. Některé z nich se věnují také problematice výroby mikrofluidního rozhraní. Jsou také dostupná komerční řešení držáků čipů. Kompatibilita různých typů čipů je zde omezená na konkrétního výrobce. Návrhy úprav čipů ze strany zákazníka jsou zpravidla řešeny v úzké spolupráci s výrobcem. Některé firmy nabízejí zakoupení mikrofluidního rozhraní a výroba čipu zůstává v kompetenci zákazníka. Zde je ovšem nutné pracovat s velkou přesností dle přesně definovaného zadání výrobce, což klade vysoké nároky na technické vybavení zákazníka. Ve většině případů jsou tato řešení navíc určená výhradně pro křemíkové, skleněné nebo plastové čipy bez polymerních částí.

Jedním z nejrozšířenějších materiálů využívaných pro konstrukci mikrofluidních čipů je pružný polymer polydimethylsiloxan (PDMS) (NG, Jessamine M. K., et al. Components for integrated poly(dimethylsiloxane) microfluidic systems. ELECTROPHORESIS. 2002, 23, 20, s. 3461-3473. ISSN 1522-2683). V případě jeho užití je možné pro vytvoření mikrofluidního rozhraní použít oba výše uvedené přístupy.

Při použití držáku je jednou z nejdůležitějších podmínek pro správnou funkčnost adaptéru dodržení vysoké rovinnosti vrchní a spodní části držáku a dosažení vhodného a rovnoměrného tlaku v oblastech kontaktu polymeru se substrátem a polymeru s držákem. Častým řešením je příprava držáku například z polykarbonátu (plexiskla). Výhodou je dobrá manipulace a opracovatelnost a nízká finanční nákladnost. Nevýhodou takového řešení jsou problémy související s mechanickými vlastnostmi plexiskla, zejména s jeho pružností a v některých aplikacích i nízkou chemickou odolností (např. vůči organickým rozpouštědlům).

<u>Podstata technického řešení</u>

Předkládané technické řešení je kovový držák určený pro mikrofluidní čipy sestavené z kombinace dvou nebo více samostatných, ale vzájemně se doplňujících součástí, a to z polymeru polydimethylsiloxanu (PDMS) a z křemíkového nebo skleněného substrátu. Vrchní část čipu by měla být tvořená PDMS a měla by obsahovat otvory v definovaných místech pro přístup roztoků k/z čipu. Křemíkový nebo skleněný substrát může a nemusí obsahovat mikrofluidní kanály a další součásti čipu jako například elektrochemický detektor sestavený z kovových elektrod nebo elektrické konektory. PDMS stejně jako křemíkový nebo skleněný substrát může a nemusí obsahovat výše uvedené součásti čipu. Samozřejmostí je možnost využití čipu sestaveného jen z PDMS.

Držák mikrofluidního čipu tvoří propojovací rozhraní mezi čipem a systémem přívodu a odvodu analyzovaných roztoků a umožňuje pohodlné a spolehlivé sestavení měřícího zařízení. Vyznačuje se sendvičovým způsobem sestavení horního a dolního víka držáku, bez pantů. Do držáku je možno vkládat čipy o přesně dané velikosti. Výhodou předkládaného řešení je robustnost a pevná kovová konstrukce, u které nedochází k deformaci nebo kroucení materiálu. Hmotnost kovové konstrukce horního víka umožňuje vytvářet dostatečný přítlak na povrch čipu, čímž dochází k velmi dobré adhezi mezi PDMS a substrátem a zároveň nedochází k deformaci kanálků ovlivňujících funkci čipu. Velikost přítlaku je možné dále zvýšit pomocí dvou zámků (upínacích svorek nebo matek), které se upínají do čepu zámku v rozích držáku.

Držák umožňuje dodržení vysoké rovinnosti horního a dolního víka při vytváření přítlaku na PDMS a substrát bez nutnosti dotahování zámků. To je důležité pro celkovou správnou funkčnost mikrofluidního čipu obecně. Vysoká rovinnost je dosažena pomocí dvou centrovacích trnů umístěných v dolním víku držáku.

Držák je určený pro uchycení mikrofluidního čipu, na kterém probíhá mikrofluidní analýza. Přesné usazení čipu do držáku umožňují otvory v definované oblasti v dolním a horním víku. Tyto otvory vymezují polohu vrchní a spodní části čipu tak, aby byl umožněn přístup roztoků k čipu skrz konektory s hadičkami. Otvor v horním víku je určen pro polymerní (PDMS) část čipu. Součástí horního víka je neměnné, ale dostatečné množství otvorů pro přívod a odvod roztoků. Připojení hadiček k otvorům je možné pomocí konektorů s typizovanou velikostí závitů.

Dále držák umožňuje připojení vloženého čipu k měřicímu přístroji pomocí elektrických kontaktů, které musí být integrovány ve vymezené oblasti na mikrofluidním čipu. Propojovací kontakty jsou vyvedeny definovaným otvorem v horním víku držáku. Samostatné rozhraní pro připojení přístroje k elektrickým kontaktům držák neobsahuje. Je však možné ho dodatečně do držáku implementovat v předem vymezené oblasti otvoru v horním víku držáku. Držák je opatřen průhlednou zónou v centrální oblasti horního a dolního víka držáku a umožňuje tak provádět vizuální kontrolu čipu a analýzu vzorků prostřednictvím zvolené optické metody (např. UV-VIS spektrofotometrické popř. fluorescenční metody detekce).

Přehled obrázků na výkresech

Obrázek č. 1 znázorňuje kompletní držák s vloženým mikrofluidním čipem, včetně zámků pro zvýšení přítlaku na čip.

Obrázek č. 2 znázorňuje dolní víko držáku s centrovacími trny a mikrofluidním čipem.

Obrázek č. 3 znázorňuje horní víko držáku – pohled shora

Obrázek č. 4 znázorňuje dolní víko držáku (otočeno o 180° oproti obrázku č. 3) – pohled zdola.

Obrázek č. 5 znázorňuje čep zámku držáku.

Obrázek č. 6 znázorňuje centrovací trn.

Obrázek č. 7 zobrazuje pohled na horní víko – pohled shora.

Obrázek č. 8 zobrazuje pohled na držák (řez v rovině AA na obrázku č. 7)

Obrázek č. 9 zobrazuje pohled na horní víko – pohled zdola.

Obrázek č. 10 zobrazuje pohled na horní víko (řez v rovině BB na obrázku č. 9)

Obrázek č. 11 zobrazuje pohled na horní víko (řez v rovině CC na obrázku č. 9)

Obrázek č. 12 zobrazuje pohled na oblast určenou pro konektor s hadičkami (oblast D z obrázku č. 9)

Obrázek č. 13 nahoře zobrazuje pohled na dolní víko – pohled shora.

Obrázek č. 13 dole zobrazuje pohled na dolní víko – pohled ze strany.

Obrázek č. 14 zobrazuje pohled na dolní víko (řez v rovině EE na obrázku č. 13)

Obrázek č. 15 zobrazuje pohled na dolní víko (řez v rovině FF na obrázku č. 13)

Popis vztahových značek na obrázcích: 1 – horní víko, 2 – dolní víko, 3 – protiskluzová gumová nožička, 4 – rohy držáku upravené pro uchycení zámků, 5 – centrovací trn, 6 – tělo centrovacího trnu, 7 – závit centrovacího trnu, 8 – otvor pro centrovací trn, 9 – otvor se závitem pro našroubování centrovacího trnu, 10 – zámek držáku, 11 - čep zámku držáku, 12 – tělo čepu zámku držáku, 13 – závit čepu zámku držáku, 14 – otvor pro umístění čepu zámku držáku, 15 – mikrofluidní čip, 16 – PDMS část mikrofluidního čipu, 17 – skleněný substrát mikrofluidního čipu, 18 – kontakty mikrofluidního čipu, 19 – otvor pro umístění horní části mikrofluidního čipu, 20 – otvor pro umístění dolní části mikrofluidního čipu, 21 – otvor pro polykarbonátovou destičku, 22 – polykarbonátová

destička, 23 – průhledná zóna držáku, 24 – otvor pro přívod a odvod roztoků, 25 – otvor pro přívod a odvod roztoků (část se závitem pro našroubování konektorů s hadičkami), 26 – otvor pro přívod a odvod roztoků (část přímého přístupu roztoků k čipu), 27 – otvor pro připojení kontaktů umístěných na mikrofluidním čipu.

Příklad technického řešení

Horní 1 a dolní 2 víko držáku mikrofluidního čipu 15 je vyrobeno z nerezové oceli, AISI 304. Pro pohodlnou manipulaci a pevné umístění držáku na podložku jsou k dolnímu víku 2 v spodní části připevněny čtyři protiskluzové gumové nožičky 3. Dolní víko 2 obsahuje po stranách horní části dva otvory 8 pro umístění centrovacích trnů 5 z bronzu. Součástí těchto otvorů jsou otvory s typizovaným závitem M6 9, do kterých se centrovací trny 5 našroubují. Horní víko 1 obsahuje také dva otvory 8 pro centrovací trny. Centrovací trny 5 umožňují přesné uložení horního víka 1 nad dolní 2 a kontrolují rovinnost tohoto uložení. V centrální části horního 1 a dolního 2 víka jsou dva velké otvory obdélníkového tvaru 19, 20. Mají malou hloubku a umožňují přesné uložení horní a spodní části čipu 15 do držáku. Součástí těchto otvorů jsou otvory menší 21. Umožňují vložení průhledné polykarbonátové destičky 22 do horního 1 a dolního 2 víka držáku. Polykarbonátové destičky 22 a průhledná zóna 23 držáku jsou určeny k vizuální kontrole centrální části čipu. Výška polykarbonátové destičky 18 je přesně definovaná tak, aby byla dodržena rovinnost přítlakové plochy na vrchní a spodní část čipu 15. Horní víko 1 držáku obsahuje šest otvorů 24 pro přívod a odvod roztoků. Otvory 24 mají ve vrchní části 25 typizovaný závit M6, do kterého se našroubují konektory s hadičkami. Spodní část otvorů 24 je úzká 26 a umožňuje přímý vstup/výstup roztoku do/z polymerní části čipu 16. Otvory 24 leží mimo průhlednou zónu 23 a mimo otvory 21 pro polykarbonátové destičky 22. Jsou však součástí velkého otvoru 19 spodní části horního víka 1 tak, aby umožňovaly přímý kontakt s PDMS části mikrofluidního čipu 16. Dva proti sobě ležící rohy 4 horního a dolního víka jsou upraveny pro uchycení zámků držáku 10. Do otvorů 14 v rozích dolního víka 2 se umístí čepy zámků 11. Ty mají vnitřní závity 13, do kterých se našroubují zámky. Zámky 10 jsou určeny k vytváření dodatečného tlaku na vrchní část čipu 16.

Průmyslová využitelnost

Předložené řešení je možné průmyslově využít v oblastech, kde se používají mikrofluidní čipy z PDMS. To je jeho velkou výhodou, protože technologické postupy při přípravě mikrofluidních čipů z PDMS patří mezi nejlevnější technologické varianty v oblasti mikrofluidiky. Příkladem konkrétního využití může být chemická, biochemická, biologická nebo fyzikální analýza vzorků. Protože držák není měřicí přístroj, předpokládá se jeho využití hlavně výzkumnými pracovišti, která mají zkušenosti s přípravou mikrofluidních čipů a hledají spolehlivé mikrofluidní rozhraní.

Nároky na ochranu

1. Držák pro mikrofluidní čip z polymeru polydimethylsiloxanu určený pro mikrofluidní čipy tvořené částečně nebo celé z PDMS se vyznačuje sendvičovým řešením uzavírání horního (1) a dolního (2) víka, bez pantů, vysokým stupněm rovinnosti uložení obou vík a pevnou konstrukcí. Přesnost uložení a vysoká rovinnost vík držáku je dána velkými centrovacími trny (5) umístěnými v otvorech (8, 9) dolního víka (2) držáku. Pevnost konstrukce je dána materiálem a jeho váhou, nerezová ocel AISI 304.

2. Držák podle nároku 1 se vyznačuje možností nastavení dodatečného přítlaku na čip (15) pomocí dvou zámků (10) držáku, které se našroubují do čepů (11) zámků. Zámky (10) jsou umístěny v protilehlých rozích držáku.

3. Držák podle nároku 1 se vyznačuje velkou přesností uložení horní a dolní části mikrofluidního čipu (15). Přesnost uložení čipu (15) je dána definovanými otvory (19, 20) ve spodní části horního (1) a horní části dolního (2) víka držáku. Přesnost uložení mikrofluidního čipu (15) je důležitá pro přesný překryv otvorů (26) pro přívod a odvod roztoků k čipu (15) a otvorů, které jsou umístěné v PDMS části čipu (16).

4. Držák podle nároku 1 se vyznačuje možností vizuální kontroly centrální části čipu nebo možností využití optické metody pro analýzu vzorků v mikrofluidním čipu, což je dáno umístěním průhledných zón (23) v horním (1) a dolním (2) víku držáku.

5. Držák podle nároku 1 se vyznačuje možností připojit čip k měřicímu přístroji skrz otvor pro připojení kontaktů umístěných na mikrofluidním čipu (23).

Výkresy
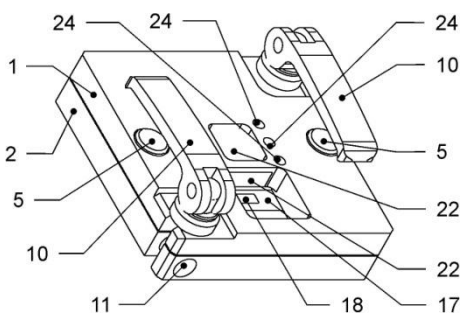
Obrázek č. 1
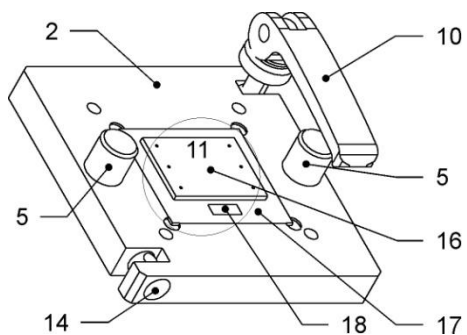
Obrázek č. 2
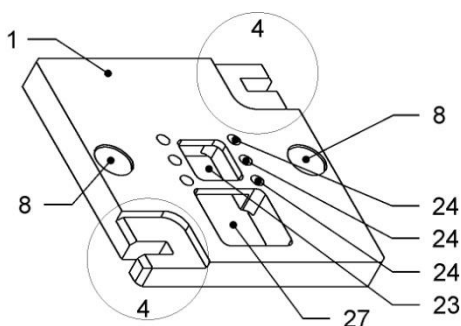
Obrázek č. 3
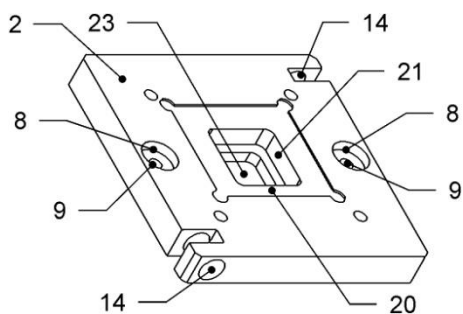
Obrázek č. 4
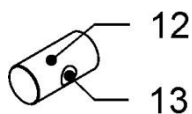
Obrázek č. 5
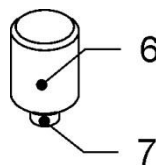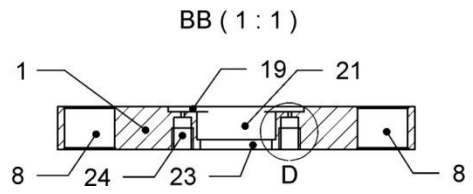
Obrázek č. 6
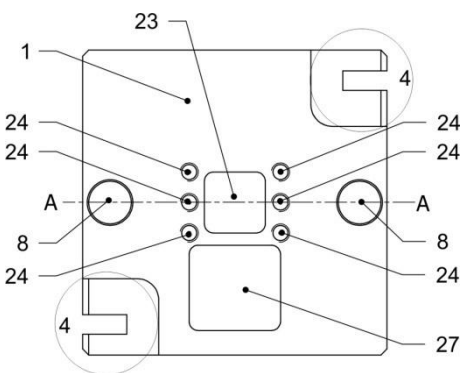
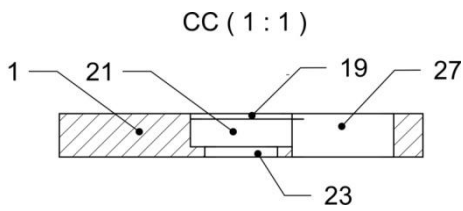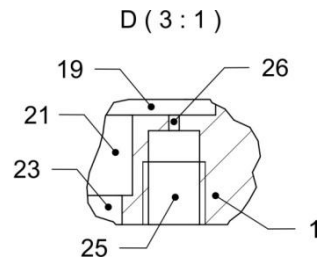AA (1 : 1)
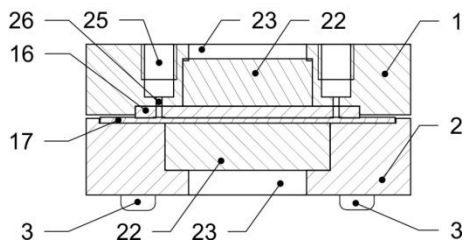
Obrázek č. 7
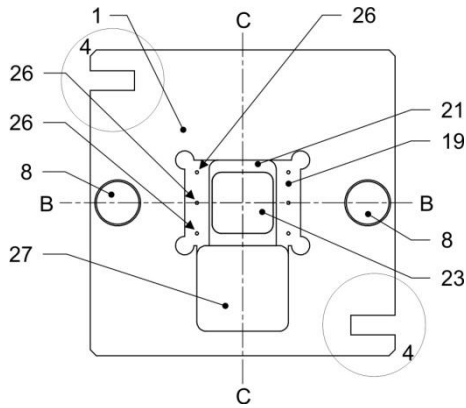
Obrázek č. 8

Obrázek č. 9

Obrázek č. 10

Obrázek č. 11

Obrázek č. 12

7.6.   Paper VI

Štofik, M., and Malý, J., 2012. Magnetic beads trapping in a microfluidic system - computer simulations of magnetic field and fabrication of a magnetic separator. *Manuscript in preparation*.

Magnetic beads trapping in a microfluidic system - computer simulations of magnetic field and fabrication of a magnetic separator

Štofik, M., and Malý, J.

Manuscript in preparation.

Abstract

In biosensors, magnetic particles can be used as detection labels as well as immobilization support. In this study, a microfluidic separator of magnetic beads (MBs) was designed and tested successfully. A single metallization layer was employed during the microfabrication process.

A multiwire planar meander microcoil was designed and its effectiveness in generation of magnetic field was compared to the effectiveness of a simple planar meander microcoil by computer simulations. The results showed that when the multiwire microcoil was used, magnetic field and magnetic energy gradient did not drop as rapidly in larger distances from the microcoil as when a simple planar microcoil was used. Thus, multiwire microcoils are more effective in the generation of magnetic forces acting on MBs in microfluidic channels in comparison with simple microcoils. The newly designed planar electromagnetic microcoil was fabricated as a microstructure embedded into a microfluidic chip. The microfabricated separator proved to be effective in MBs trapping in combination with small external permanent magnets. The separator of MBs will be further developed and implemented into an electrochemical immunosensor based on bio-functionalized MBs. In the presented study, manufacturing procedures including mask preparation by electron beam lithography (EBL), UV and soft lithography and copper electroplating were optimized.

1. Introduction

Recent advances in magnetic particle synthesis facilitated the fabrication of nanoparticles with different magnetic properties and with different size distributions and shapes (Huber 2005; Lu et al. 2007). They started to be utilized in many biotechnological applications (Whitesides et al. 1983; Dunlop et al. 1984). Over the past two decades, also magnetic separation (Gerber & Birss 1983; Parker 1990) in a fluid flow on the microscale (Zborowski et al. 1999; Zborowski et al. 2002) has been studied and interpreted widely with the aim to handle and manipulate magnetic particles in microfluidic systems (Gijs 2004; Pamme 2006; Gijs et al. 2010; Nguyen 2011). For practical applications in a fluid flow, bead shapes of nanoparticles are essential (Horák et al. 2007). Such magnetic particles are often referred to as magnetic beads.

From the fabrication complexity point of view, the simplest MBs manipulation in microfluidic systems can be achieved by permanent magnets (Pamme & Manz 2004; Pamme et al. 2006; Abonnenc et al. 2009). A big advantage of permanent magnets is their ability to generate high magnetic fields and gradients of magnetic field. However, it

is difficult to generate localized forces in microscale dimensions when using such magnets. Localized forces can be generated by microfabricated conductors. The need for micromachined inductive structures as magnetic micropower components in microsystems and the progress in microfabrication techniques resulted in fabrication and study of microfabricated microconductors on silicon substrates (Ahn & Allen 1998; Burghartz 1998). Multistep multimask processes enabled to microfabricate microcoils not only as simple planar spiral coils (Nguyen & Meyer 1990; Sadler et al. 1997) but also as more complex multilevel-spiral coils (Burghartz et al. 1996) and as coils with implemented magnetic cores (Ahn & Allen 1994).

Successful manufacturing of magnetic microstructures enabled their integration within micro total analysis systems (µTAS) directly on a microfluidic chip together with other microfabricated components. Such structures were fabricated not only on silicon but also on glass substrates (Choi et al. 2000; Choi et al. 2001). An advantage of microfabricated electromagnetic structures over permanent magnets is the possibility to switch the structures on and off and to adjust the strength of magnetic field or gradient of magnetic field in several orders of magnitude depending on their design. Because microfabrication of such structures requires expensive equipment, there have been attempts to simplify their fabrication, for example by a simple copper plate etching (Derec et al. 2009) or by an injection of molten solder into polydimethylsiloxane (PDMS) microchannels (Siegel et al. 2006). Such methods have been applied only to MBs displacements applications. They are not suitable for trapping of MBs in the flow of microfluidic systems because they generate weak magnetic forces. Also microfabricated planar electromagnetic structures with simple design (Ramadan et al. 2008) generate weaker magnetic forces. For effective trapping of MBs, they can be combined with small external permanent magnets. They help to magnetize the MBs (Nguyen 2011) and attract MBs close to the microcoil in a microchannel, where localized magnetic forces induced by the microcoil can effectively trap MBs at a desired place.

Despite the recent progress in development of novel microfabrication systems and processes, prototyping of microsystems remains both challenging and time consuming. Therefore, a number of researchers try to design and characterize their structures by the use of computer simulations prior to their fabrication. Up to now, different shapes and designs of microstructures have been investigated analytically and by using computer simulations (Rostaing et al. 2007; Ramadan et al. 2008; Fulcrand et al. 2009). For computer simulations and predictions of magnetic field properties, computer software with a finite element analysis (FEA) method such as Opera-3d (formerly TOSCA) (Ramadan 2004) or COMSOL Multiphysics (formerly FEMLAB) (Smistrup et al. 2005; Lin et al. 2007; Gooneratne et al. 2011), ANSYS Maxwell (Fulcrand et al. 2009) can be used. The predicted models can also be implemented into Matlab (Beyzavi & Nguyen 2008).

1.1. A brief introduction to the theory of magnetic separation in microfluidics

The theory of magnetic separation in microfluidic systems is often denoted as magnetophoresis. The term magnetophoresis refers either to migration analysis techniques of magnetically susceptible particles or to the motion of dispersed magnetic particles relative to a fluid under magnetic field.

Magnetic field can be generated by magnets or electromagnets. Magnetic field lines can reach a certain density within material. Magnetic flux density B describes the number of field lines per unit area. The highest value of magnetic flux density is near the magnet and it decreases quickly when moving further from the magnet. In homogeneous magnetic field, the magnetic flux density is constant over a given distance. In nonhomogenous magnetic field, the magnetic flux density is not constant and a gradient in the flux density ∇B can be observed. If $\nabla B = 0$, there are no net magnetic forces acting on magnetic particles. If $\nabla B \neq 0$, magnetic forces acting on magnetic particles appear.

Magnetic force F_{mag} acting on magnetically susceptible particles can be expressed as (Zborowski et al. 1999; Pamme 2006)

$$\boldsymbol{F}_{mag} = (\boldsymbol{m} \cdot \nabla)\boldsymbol{B} = V_p \Delta\chi(\boldsymbol{H} \cdot \nabla)\boldsymbol{B} = \frac{V_p\Delta\chi}{\mu_0}(\boldsymbol{B} \cdot \nabla)\boldsymbol{B} = \frac{V_p\Delta\chi}{2\mu_0}\nabla B^2 \qquad (1)$$

where m is magnetic dipole moment, B is magnetic flux density, V_p is the volume of a magnetic particle, $\Delta\chi$ is effective magnetic susceptibility ($\Delta\chi=\chi_p-\chi_m$, χ_p is magnetic susceptibility of a particle immersed in a fluid medium of the susceptibility χ_m), H is the magnetic field strength, and the term ∇B^2 is expressed as $\nabla B^2=2(B\cdot\nabla)B$.

The strength of the magnetic force is tunable through magnetic flux density B, where the term ∇B^2, also denoted as magnetic energy gradient (Chalmers et al. 1999), is important. The term $V_p\Delta\chi/2\mu_0$ is the proportionality factor between the force acting on a particle and the strength of the magnetic energy gradient. The sign of magnetic force depends on this factor through the sign of the effective magnetic susceptibility. In magnetic field, magnetic particles are repealed if the proportionality factor is negative and attracted if it is positive.

For magnetic separation in microchannels, hydrodynamic drag forces are important and have to be considered. When viscous forces dominate inertial forces, the microfluidic flow is laminar (Berthier & Silberzan 2006). The ratio of inertia (convective forces) and viscous forces in fluid flows is expressed by Reynold's number Re

$$Re = \frac{UD}{\vartheta} \qquad (2)$$

where U stands for the average velocity of the fluid, D is the characteristic dimension of the channel and ϑ is kinematic viscosity. If Re is high, the flow is

turbulent. At low levels of Re, in microsystems Re does not exceed the value of 0.1 (Zhang et al. 2005), the flow is known as laminar. Therefore, Stokes law can be applied to express the hydrodynamic drag force in microchannels as

$$\boldsymbol{F}_{drag} = -6\pi\eta R(v_p - v_m) = -6\pi\eta R\Delta v \tag{3}$$

where η stands for dynamic viscosity of the medium, R is the radius of the particle, and $\Delta v = v_p - v_m$ is the difference in velocities of the particle and the medium.

There are also other forces acting on MBs in microchannels such as gravitational force expressed as

$$\boldsymbol{F}_g = mg = V_p\varrho_p g = \frac{3}{4}\pi R^3\varrho_p g \tag{4}$$

and buoyant force expressed as

$$\boldsymbol{F}_b = V_p\varrho_m g = \frac{3}{4}\pi R^3\varrho_m g \tag{5}$$

where V_m is the volume of the particle, R is the particle radius, ϱ_m is the medium density and g is the gravitational constant. Both forces are included in sedimentation force expressed by

$$\boldsymbol{F}_s = \boldsymbol{F}_g - \boldsymbol{F}_b = \frac{3}{4}\pi R^3(\varrho_p - \varrho_m) \tag{6}$$

Sedimentation force is strongly dependent on the particle size and density. For example, by setting the density of MBs to 1.5 g/mL and its diameter to 2 µm according to the data in Tab. 1, we can calculate the sedimentation force as 1.2×10^{-14} N. When compared to 1.88×10^{-12} N of the hydrodynamic drag force calculated from Stokes law equation, where $\eta = 10^{-3}$ Ns/m^2, and $\Delta v = 10^{-4}$ ms, the sedimentation forces are smaller of two orders of magnitude and can be neglected. However, with a rising diameter of the MBs or by a significant reduction of the fluid velocity, they become important in the overall consideration.

Particle type	Diameter [µm]	Density [g/mL]	Susceptibility SI	Reference
Dynabeads® M-280	2.83	1.4	0.728	(Fonnum et al. 2005)
Dynabeads® M-450	4.4	1.6	1.632	(Fonnum et al. 2005)
Dynabeads® MyOne™	1.05	1.7	1.377	(Fonnum et al. 2005)
Dynabeads® M-270	2.8	1.6	0.165	(Fulcrand et al. 2009)
Estapor	1		0.245	(Ramadan et al. 2008)

Table 1. Properties of MBs reported in the literature.

Besides the above mentioned magnetic, hydrodynamic, and sedimentation forces, there are other forces in microchannels which can act on MBs dissolved in a fluid

medium (Brownian motion, particle and microchannel surface interactions characterized by van der Waal's force, electrostatic and lubrication force, different types of particle and fluid interactions, Saffman and Magnuss forces, interparticle effects such as magnetic dipole-dipole interaction or Basset force) (Zhang et al. 2005; Zhu et al. 2011). However, their strength cannot compete with magnetic or drag forces.

Therefore, when a magnetic particle is suspended in an aqueous solution, the particle motion can be described as,

$$\boldsymbol{F}_{mag} = \boldsymbol{F}_{mag} \tag{7}$$

$$6\pi\eta R = V_p \Delta\chi \frac{\nabla B^2}{2\mu_0} \tag{8}$$

For the magnetophoretic velocity v_m we can derive

$$v_m = \frac{V_p \Delta\chi}{6\pi\eta R}\frac{\nabla B^2}{2\mu_0} = \frac{2\Delta\chi R^2}{9\eta}\frac{\nabla B^2}{2\mu_0} \tag{9}$$

In the magnetophoretic methodology, the term

$$\frac{2\Delta\chi R^2}{9\eta} \tag{10}$$

is denoted as magnetophoretic mobility.

From the equations above, we can see that for manipulation with particles in a microfluidic flow, there are three important parameters (i) the particles properties (their radius and magnetic susceptibility) (ii) the fluid velocity Δv (depending on possible settings of external actuators and on the microchannel geometry, which do not usually influence the velocity difference by more than one order of magnitude), and (iii) the properties of magnetic field such as the magnetic flux density and its gradient. Commercially available MBs reported in the literature (see also the Tab. 1) have several micrometers and their magnetic susceptibility cannot be tuned. Therefore, the only factors having an impact on the trapping efficiency of the MBs are the fluid medium velocity and the gradient in the magnetic flux density or the magnetic energy gradient.

This study concentrated on optimization of the design of a planar meander microcoil by computer simulations suitable for MBs trapping in microfluidic channels. The main aim was to fabricate an effective magnetic separator with the most suitable microcoil design embedded into a microfluidic chip and to prove its ability to trap MBs experimentally. As it will be discussed further, a multiwire planar meander microcoil was selected for fabrication. In combination with small external permanent magnets, it was able to trap MBs effectively. The fabricated separator will be further developed and implemented into a magnetic electrochemical immunosensor using functionalized MBs. This concept had already been proposed by (Choi et al. 2000).

2. Chemicals, materials and protocols

Isopropylalcohol p.a., acetone p.a. were purchased from PENTA (Czech Republic). Copper sulfate (pentahydrate) ($CuSO_4.5H_2O$), sulphuric acid (H_2SO_4), natrium chloride (NaCl), silver chloride (AgCl), sodium thiosulphate ($Na_2S_2O_3$), sodium bisulphite ($NaHSO_3$), dimethyl sulfoxide (DMSO), carboxylated magnetic beads were purchased from SIGMA-ALDRICH spol. s r.o. (Czech Republic). All water solutions were prepared in deionized water with conductivity below 1 μS cm^{-2} prepared by Goro Pharmapur system (Czech Republic).

PDMS elastomer was prepared from Sylgard® 184 Silicone Elastomer kit, purchased from Dow Corning (USA). Photoresists SU-8, NANOTM SU-8 25 and NANOTM SU-8 2150 were purchased from MicroChem Corp. (USA). Negative UV resist nLOF 2070, an AZ 826 MIF developer, positive UV resists AZ 6224, AZ 9260, AZ 400K developer, an AZ 100 Remover were purchased from MicroChemicals GmbH (Germany). A mr-DEV 600 developer was purchased from Micro Resist Technology GmbH (Germany). Positive e-beam resist AR-P 669.04, negative e-beam resist AR-N 7025.18, negative e-beam and UV resist SX AR-N 7700/37, an AR 600-55 developer, an AR 300-47 developer, an AR 300-475 developer, an AR 600-60 stopper, an AR 300-70 and AR 600-70 remover were purchased from Allresist GmbH. A chromium etcher was purchased from SIGMA-ALDRICH spol. s r.o. (Czech Republic).

Microscope slides (smooth and ground edges) 26x76mm from Fisher Scientific, spol. s r.o. (Czech Republic) and borosilicate glass windows (double side polished, dimension: 45mm (±0.0/-0.4mm) x 50mm (±0.0/-0.4mm), thickness 1.1mm (±0.1), (CNC precision-cut, unbeveled) from Praezisions Glas & Optik GmbH (Germany) were used for chips and PDMS master fabrication. Silicon wafers with 100 mm diameter from ON SEMICONDUCTOR CZECH REPUBLIC, s.r.o. (Czech Republic) were tested.

The main components and tubings for microfluidic chips packing were manufactured by Upchurch Scientific (USA) and purchased from SIPOCH, spol. s r.o. (Czech Republic). Punching needles were supplied by Fisnar Inc. (USA). Small permanent magnets were purchased from Webcraft GmbH (Germany).

A laboratory power supply HC-D3030DPD for electrochemical deposition was purchased from GM electronic, spol. s r.o. (Czech Republic). The sputtering was performed on a Q150T Turbo-Pumped Sputter Coater/Carbon Coater fabricated by Quorum Technologies Ltd (UK). Sputter gold (Au), silver (Ag), copper (Cu) and chromium (Cr) targets were supplied by EDLIN, s.r.o. (Quorum Technologies Ltd, UK).

The microfluidic fluids sampling was performed by syringe pumps, injection valves, and a microautosampler from FIAlab Instruments Inc. (USA) with appropriate software for pump and valve timing.

The metallic parts of the PDMS mold were fabricated by VAKUUM PRAHA, spol. s r.o. (Czech Republic).

Electron beam lithography (ELB) was performed by using a DrawBeam software module of an electron microscope TESCAN VEGAII purchased from TESCAN, a.s. (Czech Republic).

2.1. Optimized microfabrication protocols

2.1.1. Substrate cleaning

There were two types of substrates used during the study, silicon wafers and glass substrates. Silicon wafers were carefully taken out of the boxes and sonicated for 15 min in a Piranha solution (conc. H_2SO_4 and conc. H_2O_2, 3:1). They were washed properly and rinsed five times in deionized water. Then, they were sonicated again in isopropylalcohol for 10 min, dried out with a nitrogen flow and dehydrated on a hotplate for 5 minutes at 250 °C. After cooling down, they were ready for resist coatings. Microscope slides were halved by a conventional glass pen scriber and washed in deionized water with detergent. The cut slides were rinsed thoroughly, put into a Hellendahl staining jar with isopropylalcohol, and sonicated for 30 min. Finally, the slides were dried out by a nitrogen flow and dehydrated on a hotplate for 5 minutes at 250 °C. After cooling down, they were ready for resist coatings. Borosilicate glass was treated by the same protocol.

2.1.2. Masks designing

A mask for UV lithography was designed in a vector editor CorelDRAW X5. After patterns were designed in the editor, they were exported to bitmaps in TIFF format, and sliced into smaller images by a bitmap editor GIMP or Adobe Photoshop and saved as TIFFs in a grayscale 8 bits mode. The mask designing work flow has been established as: (i) mask designing in CorelDRAW (picture slicing is planned during the design and coordinates for stage movements are noted), (ii) picture saving in the CorelDRAW native format and subsequent exporting to TIFF or PSD bitmap files, (iii) picture slicing based on the notes from the slicing planning and (iv) saving the sliced pictures into TIFF files in a grayscale 8 bits color depth mode.

2.1.3. Masks fabrication

The fabrication of masks required negative and positive patterns, thus negative and positive resists were employed. First, glass substrates were cleaned as described above and a chromium (Cr) opaque layer was deposited by sputtering. Then, the resist deposited on glass substrates was processed by electron beam lithography (EBL). Designed masks patterns were deposited by an electron beam in several steps. Such multistep deposition required movement of the microscope stage and simultaneous exchange of the deposited sliced pattern in each deposition step. Finally, the resist was developed and the Cr layer was etched.

An optimized protocol for positive e-beam resist AR-P 669.04. 100 mL of the resist was deposited by a pipette onto the substrates and spincoated at 3000 rpm for 30 s, ramp 500 rpm. The substrates were further baked for 120 s on a hotplate at 170 °C and left to

cool down and relax for 2 hours. Then, the resist was exposed to an electron beam at 20 kV with a dose of 100 μC/cm^2. The substrates were developed for 120 s in an AR 600-55 developer and transferred immediately to a stopper AR 600-60 for 30 s. Finally, they were rinsed with deionized water and dried out with a nitrogen flow. Then, the resist was baked again on a hotplate at 120 °C for 120 s. The substrates were left to relax for another 2 hours and etched in a chromium etcher. The resist residues were cleaned with an AR 300-70/AR 600-70 remover, rinsed with isopropylalcohol, and dried out with a nitrogen flow.

An optimized protocol for negative e-beam resist AR-N 7025.18. 100 mL of the resist was deposited by a pipette onto the substrates and spincoated at 4000 rpm for 60 s, ramp 500 rpm. The substrates were further baked for 60s on a hotplate at 85 °C and left to cool down and relax for 2 hours. Subsequently, they were exposed to an electron beam at 20 kV with a dose of 25 μC/cm^2. Then, the substrates were baked on a hotplate at 85 °C for 120s and left to relax for 2 hours. The resist was further developed in an AR 300-47 developer mixed with deionized water in 4:1 ratio for 120 s. The substrates were baked again at 130 °C for 60 s and left to relax for 2 hours. Then, they were etched in a chromium etcher and the resist residues were cleaned with an AR 300-70/AR 600-70 remover. Finally, the substrates were rinsed with isopropylalcohol and dried out with a nitrogen flow.

An optimized protocol for negative e-beam and UV resist SX AR-N 7700/37. 100 mL of the resist was deposited by a pipette onto the substrates and spincoated at 4000 rpm for 60 s, ramp 500 rpm. The substrates were further baked for 60 s on a hotplate at 85 °C and left to cool down and relax for 2 hours. Then, they were exposed to an electron beam at 20 kV with a dose of 3 μC/cm^2 or with UV for 20 s. The substrates were baked on a hotplate at 100 °C for 120 s. The resist was further developed in a concentrated AR 300-475 developer for 60 s. The substrates were rinsed with deionized water, dried out in a nitrogen flow and hard-baked at 130 °C for 120 s and left to relax for 2 hours. The etching was performed in a chromium etcher and the hard-baked resist residues were stripped with an AR 300-70 remover. Finally, the substrates were rinsed with deionized water and dried out in a nitrogen flow.

2.1.4. Fabrication of an SU-8 resist mold

For the purpose of PDMS casting, silicon wafers and borosilicate glass substrates were tested for the fabrication of a PDMS mold. Wafers and glass substrates were cleaned and cured according to the protocol described above. SU-8 2150 resist was deposited by a pipette onto the center of the substrate (5 mL) and spincoated in a two-step process (i) 500 rpm for 15 s, ramping 500 rpm and (ii) 3000 rpm for 30 s, ramping 300 rpm. According to the conditions, the resist height can vary slightly around 200 μm. The height of the fabricated structures was not measured. The substrates were further softbaked on a hotplate in a three-step process: (i) baking for 5 min at 60 °C, (ii) 2 min ramp to 80 °C, and (iii) baking for 30 min. Then, they were left to relax for 2 hours. Subsequently, they were exposed to UV light for 4 minutes and left to relax for another

2 hours. A three-step post-exposure process followed (i) baking for 5 min at 60 °C, (ii) ramping to 80 °C for 2 min., and (iii) baking for 15 min at 70 °C. Again, the substrates were left to relax, this time for 5 hours. SU-8 resist patterns were developed in a mr-DEV 600 developer. Finally, the substrate was rinsed by isopropanol and dried out by a nitrogen flow.

2.1.5. PDMS casting

The casting of PDMS can be performed in several ways. Based on personal experience gained during this study, the following protocol was adopted in the end. A special metal mold was manufactured and employed. PDMS polymer was thoroughly mixed with a curing agent in a plastic Petri dish in a volume ratio 10:1. The Petri dish was then put into vacuum and cured until all bubbles disappeared plus extra 15 minutes. While the PDMS mixture was cured in the vacuum, a metal mold for casting (Fig. 1) was prepared. The whole mold consisted of a silicon wafer or glass substrate (master mold) with SU-8 resist containing patterns of a microfluidic channel, a metal mold with openings for insertion of the substrate, a glass board and a metal desk for loading of the mold top. The most important part of the mold was the silicon wafer or the glass substrate with SU-8 resist containing microfluidic channel patterns. The glass board was cleaned according to the protocol described above. The glass board and the substrates were rinsed with isopropanol and dried out with a nitrogen flow. The substrate was inserted into the opening of the metal mold. The height of the side walls of the opening limited the height of the final PDMS cast. The height was adjusted by inserting more glass substrates into the opening under the master mold. The cured PDMS was carefully poured into the mold in such a way that it overflowed the edges of the metal opening slightly. Then, the glass board was carefully installed on the metal mold in order to prevent bubble formation. Finally, a metal desk was installed on the top of the metal mold. The complete mold was transferred onto a hotplate with 90 °C immediately. The PDMS was cured on a hotplate in the following process: (i) 4 min ramp from 90 °C to 120 °C, (ii) baking for 15 min at 120 °C, (iii) the mold with the PDMS was left to cool down and finally, it was put for 15 min into 4 °C, which facilitated the peeling of the PDMS from the glass board and the substrates. The cured mold was dismantled into pieces. First, the upper glass part was gently removed by a spin motion. Then, the substrate with PDMS was pressed up from the metal mold opening and finally, the PDMS was gently peeled off from the substrate. The PDMS cast was cut as needed and holes for fluid were punched in it with a suitable needle.
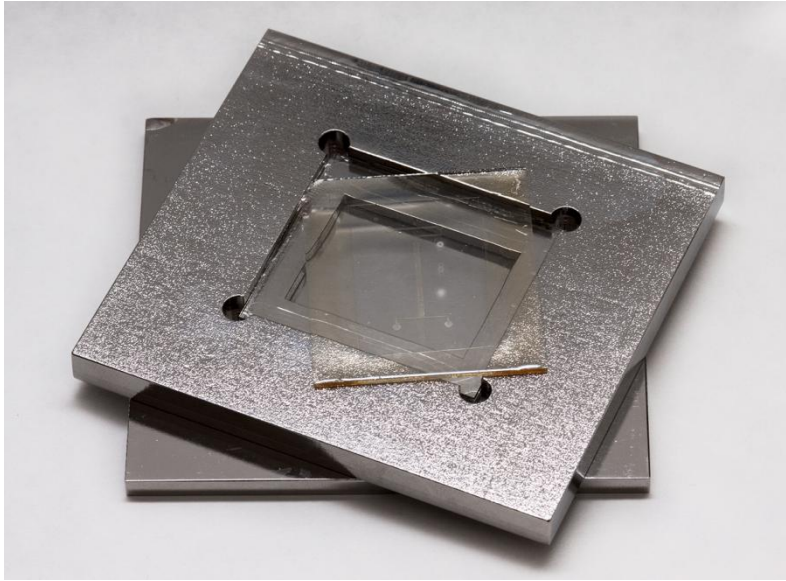
Figure 1. Metal mold for PDMS casting.

2.1.6. Metal sputtering

Metal sputtering is one of the physical techniques for metal deposition on substrates used in microfabrication technologies. Depending on the purpose of the final application, different types of metal can be sputtered. The conditions for copper (Cu) and chromium (Cr) sputtering were optimized according to the application need and the final settings were set as follows. Cu was used as a seed layer for electrochemical deposition of copper in the protocol for the fabrication of an electromagnetic microcoil and was sputtered for 200 s (sputter current 60 mA, tooling factor 2.3). Cr was used as an opaque layer for masks fabrication and was sputtered for 300 s (sputter current 120 mA, tooling factor 2.3) on cleaned substrates.

2.1.7. Fabrication of copper microcoils

First, Cu was sputtered on the top of the Cr adhesion layer (Cr was sputtered for 10 s, sputter current 120 mA, tooling factor 2.3) on cleaned substrates as described above. Then 500 mL of positive resist AZ 9260 was deposited by a pipette onto the center of the substrate and spincoated at 2400 rpm for 60 s, ramp 300 rpm. In these conditions, the resist thickness of 8.5-9.5 µm was achieved. The substrate was softbaked on a hotplate at 110 °C for 165 s and left to relax and cool down for 1 hour. Exposure for 60 s and relaxation for another hour followed. The substrates were developed for 30 s in an AZ 400K developer, mixed with deionized water in 1:1 ratio and then transferred immediately and developed in an AZ 400K developer mixed with deionized water in 1:3 ratio for another 30 s. The substrates were then rinsed thoroughly with deionized water and dried out with a nitrogen flow. Then, copper electroplating was performed in an electroplating solution. The electroplating solution consisted of 100 g $CuSO_4$. $5H_2O$, 13 mL of concentrated H_2SO_4, and 100 mg NaCl dissolved in 500 mL of deionized water.

The scheme of the electroplating arrangement is further discussed. The optimized process was run at 150 mA for 4 min. After the electroplating was successfully performed, the resist residues were stripped using an AZ 400T stripper and the Cu seed layer was etched in a chromium etcher. The fabricated microcoils were then isolated by SU-8 25 resist encapsulation as follows. The SU-8 25 resist was deposited by a pipette onto the center of the substrate (700 μL) and spincoated in a two-step process (i) 500 rpm for 15 s, ramp 300 rpm, (ii) 2000 rpm for 30 s, ramp 300 rpm. The resist was then softbaked in a three-step process (i) 5 min at 55 °C, (ii) ramp for 2 min to 70 °C and (iii) baking on a hotplate at 70 °C for 30 min. Then, the substrates were left to cool down and relax for 2 hours. Exposure for 90 s with 2 hours of relaxation followed. Post-exposure baking followed in a three-step process (i) baking for 5 min at 55 °C, (ii) ramp to 70 °C for 2 min and (iii) baking for 15 min at 70 °C. The substrates were then left to relax for 5 hours. The patterns were developed in a mr-DEV 600 developer. Finally, the substrates were rinsed by isopropanol and dried out in a nitrogen flow.

2.2. Microcoils design and computer simulations

The design of microcoils and computer simulations of their magnetic field properties were performed in COMSOL Multiphysic software by a static physical model on a standard computer. The simulations were performed by solving partial differential equations with a finite element method (FEM). A GMRES solver was used. First, the model evaluated current density in microcoil wires and second, calculated magnetic field, magnetic field gradient and magnetic energy gradient.

3. Results and discussion

3.1. Simulations of magnetic field

Recently, it has been shown that planar microcoils can be effective in magnetic beads trapping in microfluidic channels and that the geometry of microcoils has a strong impact on the trapping profile of magnetic beads and magnetic forces exerting on them (Ramadan et al. 2008). Planar microcoils can differ by several orders of magnitudes in the means of magnetic forces and they can be divided into two main groups according to the fabrication process. Microcoils fabricated by employment of one metallization layer and microcoils fabricated by employment of more than one metallization layer. One metallization layer microcoils can be fabricated in a number of shapes such as meander, mesh-shaped meander, rosette-shaped meander, different loop arrays or double spirals. Their fabrication process is simpler but they generate weaker magnetic forces. The microcoils fabricated by more than one metallization layer include mainly circular or square spirals which can be manufactured with inner magnetic cores. Their fabrication process is more complex and they generate very strong magnetic forces. Comparative studies of such structures can be found in (Ramadan 2004; Ramadan et al. 2008; Fulcrand et al. 2009).

Because fabrication of a microcoil by employment of one metalization layer is less technically demanding and more suitable for rapid prototyping, we concentrated on this

fabrication process. Therefore, a planar meander microcoil design with three adjacent wires with a parallel current direction and three adjacent wires with the opposite current direction has been suggested as a more powerful microcoil in comparison with a simple meander microcoil. Magnetic properties of a simple planar meander microcoil and of a multiwire planar meander microcoil were studied by computer simulations. For this purpose, Cu wires were designed with the width of 10 µm and height of 10 µm. Current density was set to 1×10^9 A/m^2.

First, magnetic fields of a single wire, then of two adjacent wires, and finally of three adjacent wires with a parallel current direction were simulated. The scheme of the electric potential of the designed wires is presented in Fig. 2.
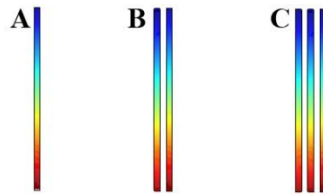
Figure 2. Plotted electric potential of the designed wires.

The plotted electric potential demonstrates the electric current directions in the designed wires. The electric current is directed from a red to a blue color. In panels A, B, and C, the electric potential of one wire, two and three adjacent wires is presented, respectively.

As can be seen in Fig. 3, the magnitudes of the generated magnetic fields do not differ much in the immediate vicinity of the wires (1 µm). Only different profiles are observed. At a distance of 20 µm above the wires, the magnetic fields have magnitudes of 0.78 mT, 1.4 mT and 1.8 mT comparing one wire, two wires, and three wires, respectively. The magnetic field of one wire is more than two times lower than the magnetic field generated by the current of three adjacent wires. The difference increases slightly with an increase in the distance from the surface of the wires. At a distance of 50 µm above the wires, the magnetic field generated by the electric current of one wire (0.49 mT) is more than two and a half times lower than the magnetic field of the current generated by the electric current of three adjacent wires (1.3 mT).
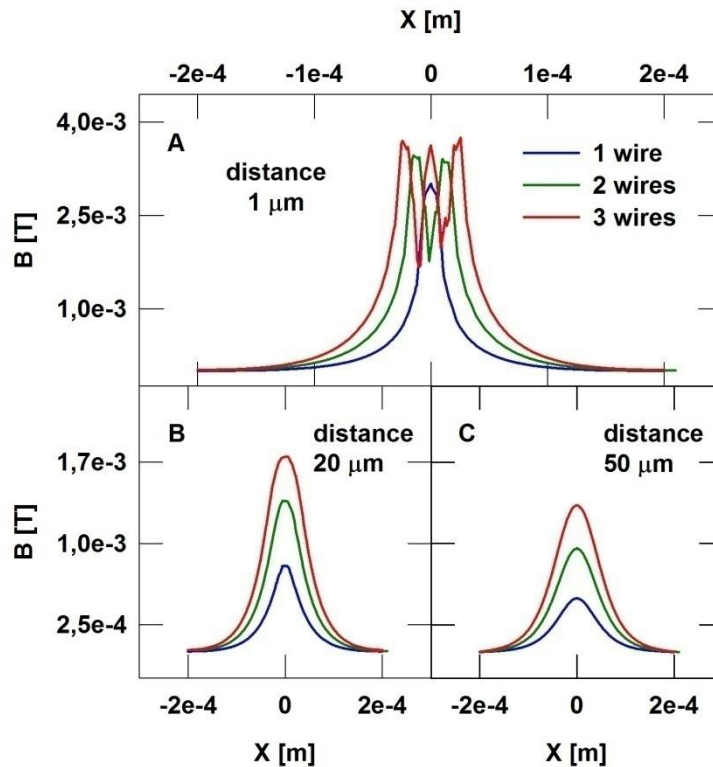
Figure 3. Simulated magnetic fields of a single, two (spacing 10 μm) and three (spacing 10 μm) coupled wires with a parallel current direction.

The profile of the wires is 10 μm x 10 μm. Panels A, B, and C show the simulated magnetic fields at a distance of 1, 20 and 50 μm above the designed wires, respectively.

This difference observed in the profiles of magnetic fields (Fig. 3A) is caused by mutual interaction of the magnetic fields of adjacent wires (Ramadan 2004). Generated magnetic field of adjacent wires can be cancelled or reinforced by the opposite or the same direction of magnetic field lines of the neighboring wires. This property of a planar meander microcoil causes the generated magnetic field to decrease rapidly further from the surface of the microcoils and to become more uniform at distances higher than two times the thickness of the meander microcoil. Therefore, a simple meander coil is less powerful than other coil designs, mainly in comparison with coils with spiral design.

Further, a simulation of magnetic field and the magnetic field gradient of two, four, and six adjacent wires spaced by the same distance as in the previous simulations was performed. The electric current has the opposite direction in two neighboring (one by one design), four neighboring coupled by two (two by two design) and three neighboring coupled by three (three by three design) wires as can be seen in Fig. 4.
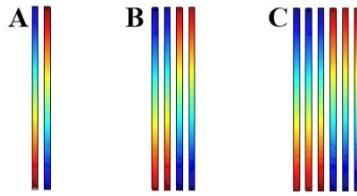
Figure 4. Plotted electric potential of the designed wires.

The plotted electric potential demonstrates the electric current directions in the designed wires. The electric current is directed from a red to a blue color. In panels A, B, and C, the electric potential of one by one, two by two and three by three designs is presented, respectively.

In Fig. 5, it can be seen that neighboring wires combined in two by two design and three by three design generate higher magnetic fields in the center of their magnetic profile directly above them (1 µm) in comparison with one by one design. Various profiles of magnetic field are observed depending on the number of the employed wires. At a distance of 20 µm above the wires, the magnetic field (0.5 mT) of one by one design is three times lower in comparison with the magnetic field (1.5 mT) of three by three design and at a distance of 50 µm above the wires, a difference of four and a half times can be observed between one by one (0.19 mT) and three by three design (0.88 mT). When comparing the magnetic field gradient, only slight differences can be observed directly above (1 µm) the wires. However, the difference in magnetic field gradients rises at a distance of 20 µm. Moreover, at a distance of 50 µm above the wires, there is a difference of more than one order of magnitude comparing one by one design (0.99 mT/m) and three by three designs (28.0 mT/m).
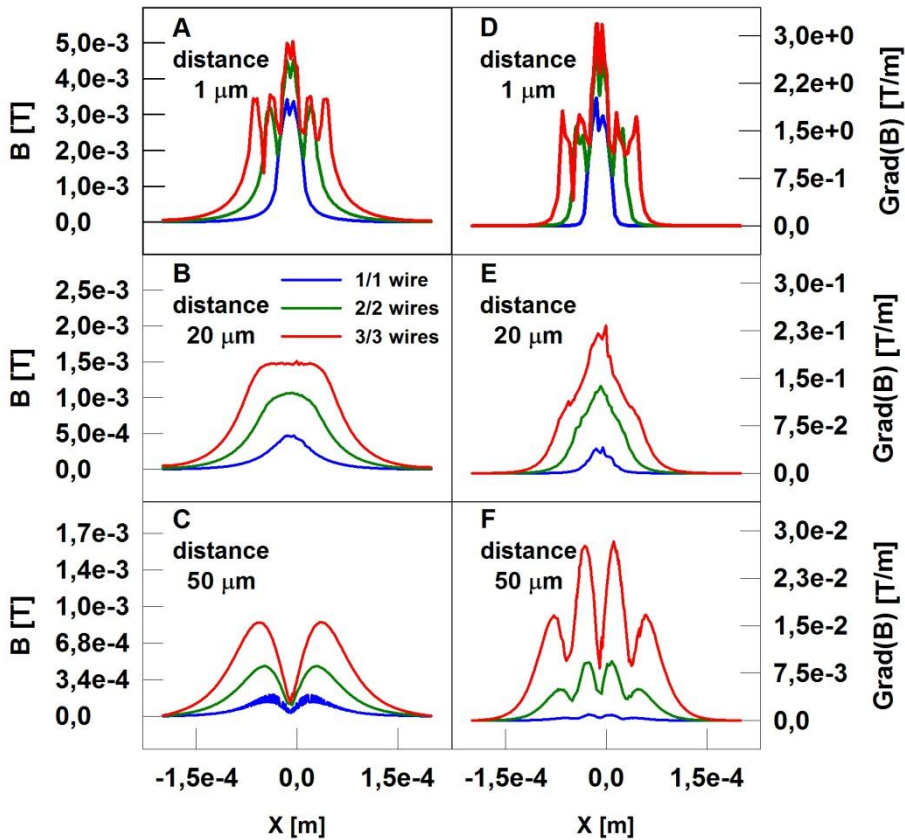
Figure 5. Simulated magnetic fields and magnetic field gradients of one by one, two by two and three by three designs are presented.

The left panels (A, B, C) present simulated magnetic fields at distances 1, 20 and 50 μm above the wires. The right panels (E, F, G) present simulated magnetic field gradients at distances 1, 20 and 50 μm above the wires.

The results prove that coupled magnetic field of four and six adjacent wires where half of them have the same current direction and half of them have the opposite current direction can generate more efficient magnetic forces at higher distances above the wires and by this configuration of wires, the spatial distribution of the generated forces is better. Such knowledge is important when trapping of MBs at distances of several tens or hundreds microns is needed. By fabrication of multiwire planar meander microcoils with the presented current distribution, the magnetic forces will drop slowly by increasing the distance from microcoils and the trapping of MBs will be more efficient.

To validate this statement, magnetic properties of 24 adjacent wires with one by one, two by two and three by three designs were simulated. The directions of the currents in the wires are presented in Fig. 6.
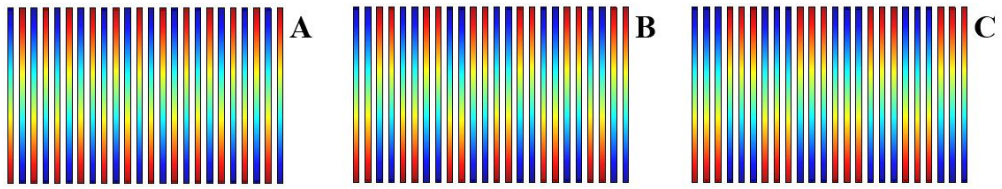
Figure 6. Plotted electric potential of the designed wires.

The plotted electric potential demonstrates the electric current directions in the designed wires. The electric current is directed from a red to a blue color. In panels A, B, and C, the electric potential of one by one, two by two and three by three designs is presented, respectively.

In Fig. 7, we can see the profiles of the x and the y component of the magnetic field gradient of all simulated designs at distances of 1, 50 and 100 µm above the wires. The z component of the magnetic field gradient has the highest magnitude and thus has the strongest contribution to the overall magnetic field gradient. It can be seen that the profiles of the magnetic field gradient of one by one and two by two designs form one potential well above the microcoil at distances of 20 and 50 µm, respectively. This profile is also observable in three by three designs when increasing the distance from the wires. However, the middle part is not as flat as in the other two designs. The shape of the x component of the magnetic field gradient resembles a wave which flatters in the middle part when increasing the distance from the surface of the wires in all presented profiles. This wave is nearly unobservable in one by one design, however, it can be observed clearly at a distance of 50 um in two by two and three by three designs. At a distance of 100 um, it is present only in three by three design and it is still evident on both (x and z) components of the magnetic field gradient. This observation makes three by three design the most suitable design for MBs trapping. It generates the strongest and localized magnetic forces at higher distances above the wires with a given spatial arrangement. Because three by three design is from the family of planar meander microcoils, also its profile flatters at further distances from the wires as can be seen in Fig. 7H, I. This typical behavior of meander type microcoils was also observed in (Ramadan 2004).
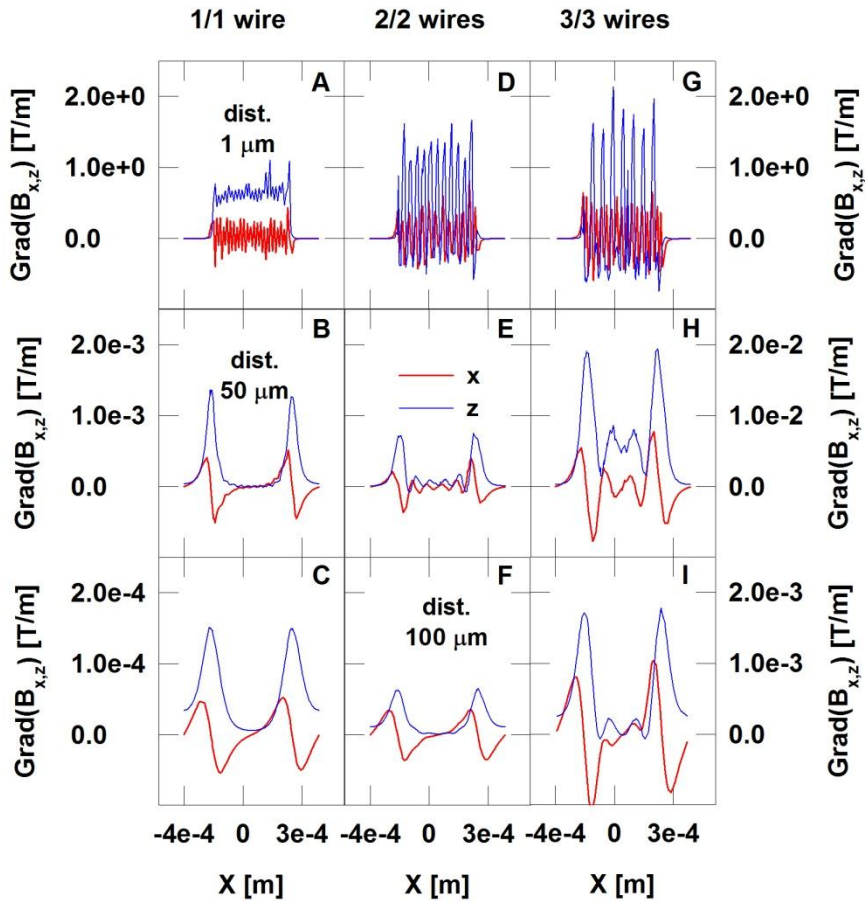
Figure 7. Simulated x (red) and z (blue) components of the magnetic field gradient of one by one, two by two and three by three designs are presented.

The left panels (A, B, C) present one by one design, the middle panels (D, E, F) present two by two designs and the right panels (G, H, I) present three by three design. Graphs plotted in the first, second and third row are simulated at a distance of 1 μm, 50 μm and 100 μm above the wires.

The effects discussed above were observed in the middle of unconnected neighboring wires. When the wires are connected on both ends by a conductor, a real meander microcoil is formed. In Fig. 8, we can see how such changes in design influence the distribution of magnetic field gradient. It can be seen in the simulations that connected wires have an important and a strong contribution to the overall generated magnetic field profile and to the distribution of magnetic forces in the compared systems. A simulated profile of three by three design, Fig. 8C, shows that at a distance of 50 μm, the magnetic field gradient is periodically but differently distributed above the upper and the bottom part of the microcoil. The upper moiety is characterized by higher magnitudes of the magnetic field gradient and the upper and the bottom maxima are mutually shifted according to the curvatures of the microcoil. A microcoil with one by

one design generates, at a distance of 50 µm, only a slightly observable potential hole in the middle of the microcoil.
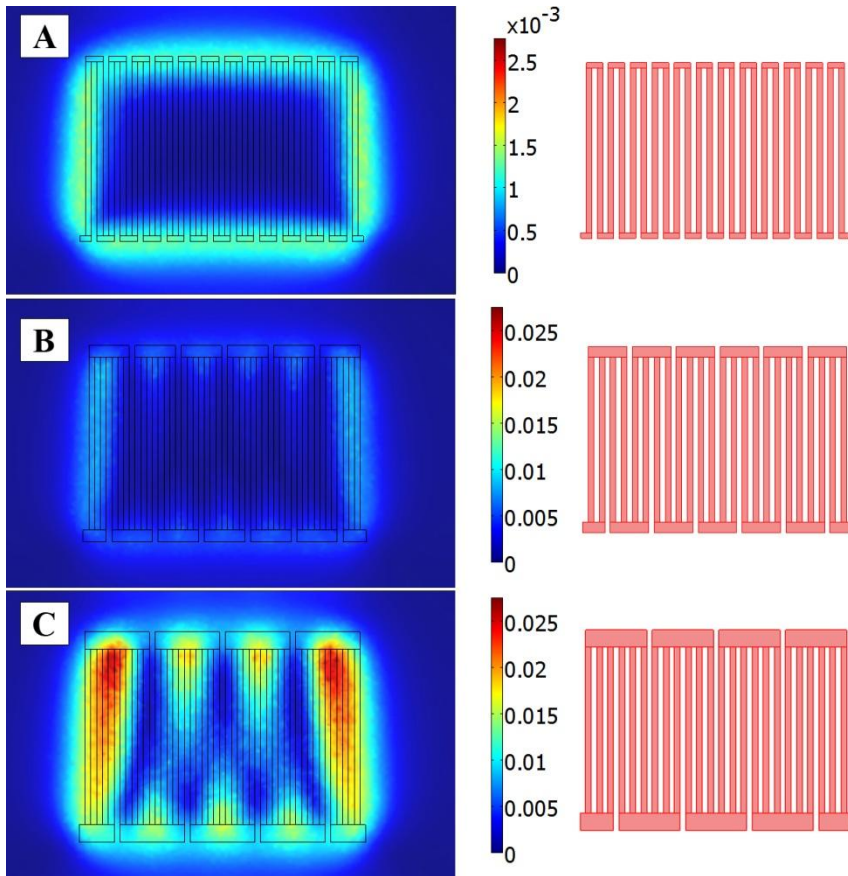

Figure 8. The magnetic field gradients (T/m) at a distance of 50 µm above the microcoils are presented in the left panels (A, B, C) and the corresponding designs in the right panels.

Spatial distribution of the x and the z component of the magnetic energy gradient are presented in Fig. 9. It was confirmed again that the regularity of spatial distribution is dependent on the microcoil design. A more regular design (Fig. 9B, C) generates more regular profiles in comparison with only a slightly modified design (Fig. 9A). It was also simulated (data are not presented) that by introducing more coupled wires into the middle of the microcoil with three by three design, the distribution of magnetic energy gradient in the upper and bottom part is more regular in the center of the microcoil and more irregular when approaching the edges.
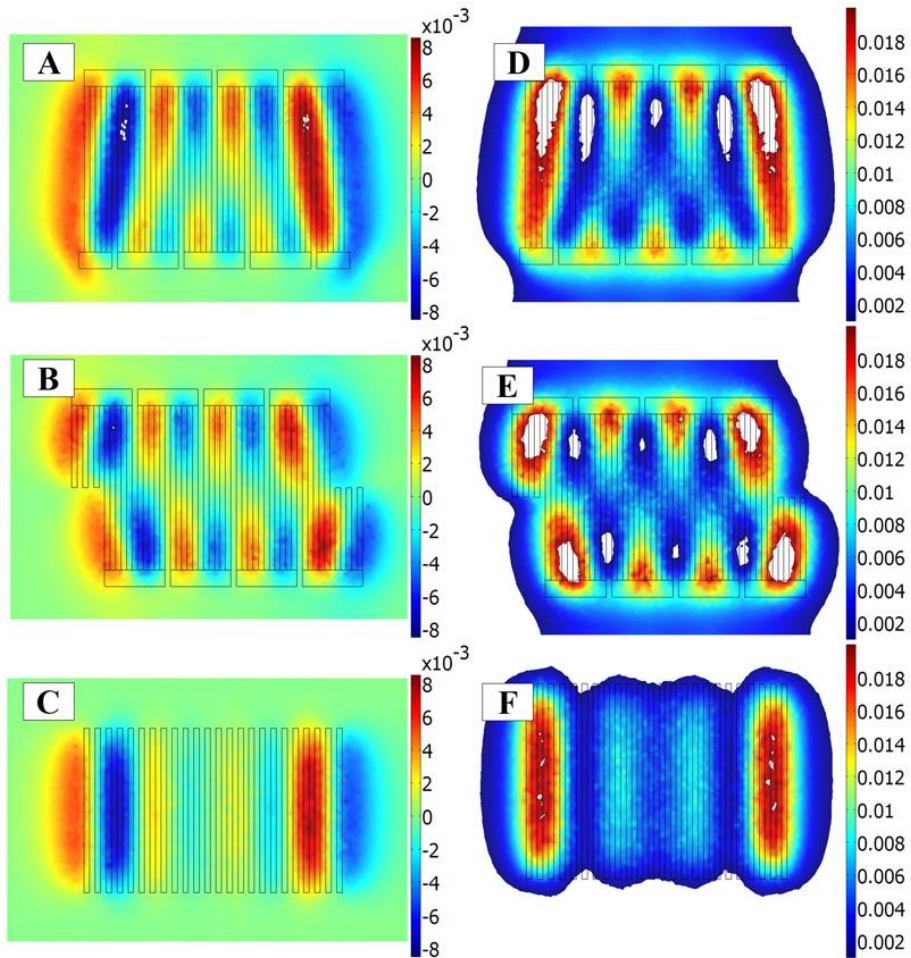
Figure 9. Simulated x and z components of the magnetic energy gradient (T^2/m) of microcoils (by column) corresponding to their design (by row) at a distance of 50 μm are presented.

In panels A, B, and C, the changes in profiles of the magnetic energy gradient are compared. In panels A, B and D, E it can be observed how the contribution of magnetic field of connected wires can change the overall profile of the magnetic energy gradient. Regular design in panels B, E creates a more regular profile compared to panel A, D. Connected wires in panel A and B have a positive effect of reinforcement of the magnetic energy gradient and its more regular distribution in the upper and bottom part of the microcoil.

A simulation of the magnetic energy gradient of larger spacing between every three coupled wires of a microcoil with three by three design has also been performed and it is presented in Fig. 10. It can be observed that the profile curves of the x and the z component of the magnetic energy gradient flatter when the spacing is increased although the magnitude of the z component increases. This behavior can be explained by mutual interaction of magnetic fields of adjacent wires discussed above.
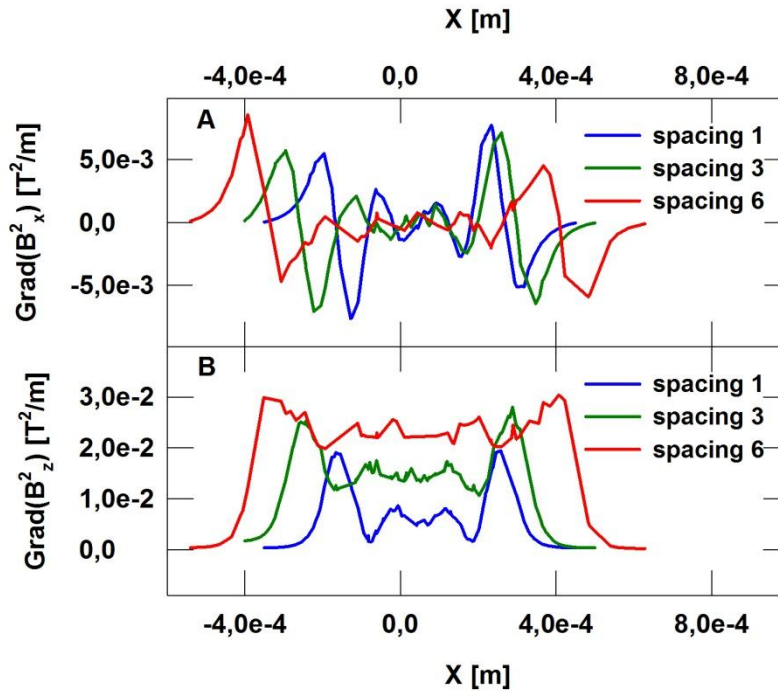
Figure 10. Simulated x (panel A) and z (panel B) components of the magnetic energy gradient of microcoils are presented.

Both panels show how the profiles of the x and the z components of the magnetic energy gradient change by increasing the spacing between coupled wires. Spacing 1 means that the distance between the coupled wires equals to 20 μm, spacing 3 equals to 60 μm and spacing 6 equals to 120 μm.

The effect of the thickness of the wire on generation of magnetic field was not simulated. It is well known from the Biot-Sawart law that an increase in the thickness of the wire enables the injection of more electrical intensities to the conductor and thus higher magnetic fields can be generated. For practical purposes, the current maximum is limited by the heat generated by the wires. However, practical utilization of this effect is dependent on microfabrication facilities and their limits. A simulation of magnetic field of two adjacent wires with different heights with the same cross-section spaced by the same distance as their width can be found in (Ramadan 2004).

3.2. Microcoils microfabrication

While manufacturing a microfluidic system for trapping MBs, several microfabrication techniques such as EBL, magnetron metal sputtering, soft and UV lithography, and electroplating, and testing of different packing methods were performed.

3.2.1. Electron beam lithography (EBL) – masks fabrication

The masks for microfabrication were produced by EBL on an electron microscope Tescan Vega II. An EBL module DrawBeam was used. The DrawBeam enabled to create simple shapes and to pattern them onto e-beam resist. Patterning modes were extended by the use of bitmap images as designed patterns. Any graphic editor could be

used for the bitmap design, however, there was a restriction on the color depth mode of the images. The only possible mode was a grayscale 8 bits color depth mode. Because of the need for high quality of the pattern with microscale resolution (a small field of view of the microscope had to be applied) and the need for patterns sized several millimeters (a large field of view of the microscope had to be applied), the pattern could not be deposited at once. When a large microscope field of view was used, image distortions occurred at the edges of the image, see Fig. 11A, and the patterned image was of poor quality. Therefore, the use of centered patterns in the microscope image using small fields of view was important. For this purpose, the patterned image was sliced into smaller pieces according the smaller fields of view of the microscope. Such multistep deposition required movement of the microscope stage and simultaneous exchange of the deposited pattern in each deposition step. The movement of the microscope stage caused another problem such as pattern misalignment, see Fig. 11B. This problem was fixed by precise and well calibrated movement of the microscope stage. Although it is a common problem in electron microscopy, it has to be taken into account in the process of mask fabrication.
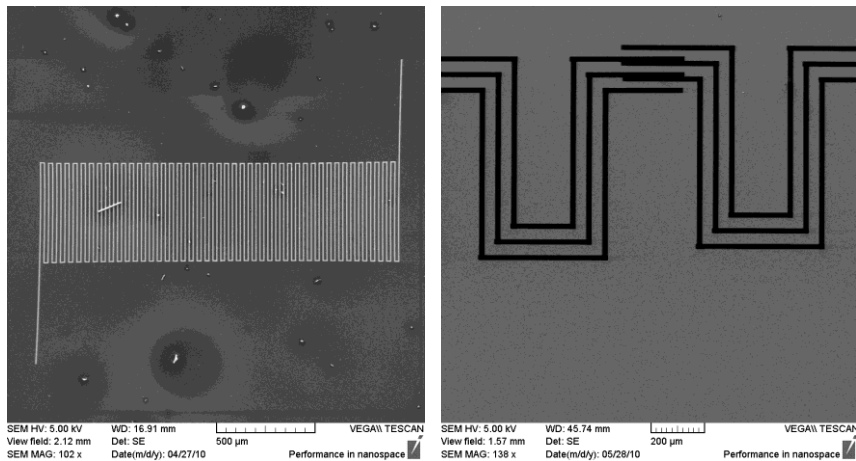

**Figure 11. Electron microscopy pictures of deposited patterns in EBL resist.**

In the left panel, deformation of the patterned structure in the corners of the picture due to the image distortion can be observed. In the right panel, misalignment of the patterned structure is present as a result of improper microscope stage calibration before the EBL process was performed.

The EBL process was optimized for three types of resists. Positive e-beam resist AR-P 669.04 and negative e-beam resist AR-N 7025.18 were the first e-beam resists tested. Both resists could be used for negative or positive masks production. The protocols were optimized after several optimization steps according to the manufacturer recommendations. Due to low sensitivity of AR-P 669.04 and AR-N 7025.18 resists, the whole EBL process was time-consuming and other alternatives were needed. Finally, a very sensitive negative e-beam SX AR-N 7700/37 resist was selected and successfully employed. It was designated as the resist for the mask manufacturing and its main

advantage is its sensitivity not only to an electron beam, but also to light in a UV range from 248 to 436 nm. Therefore, it is suitable for mix&match processes. After optimization of both processes (EBL and UV lithography) for the SX AR-N 7700/37 resist, no other types of resists were needed for the mask production.

3.2.2. Copper electroplating – microcoils fabrication

Electrochemical deposition of metals is one of the most widely used methods for fabrication of microcomponents (Watanabe et al. 1996; Park et al. 2011) and microelectronic circuits (Andricacos et al. 1998). An electroplating process requires an electric circuit to be completed through an electroplating bath. Electrons flow from an anode to a cathode and return through a conductive electrolyte containing metal ions. The process is driven by a direct current (DC). The anode serves as a metal source and the metal is deposited on the cathode. Generally, a copper electroplating process is performed in an electroplating solution of $CuSO_4$ with additives increasing the number of nucleation sites and keeping their size small for a smooth growth. The process can be expressed as

$$at\ the\ cathode: \quad Cu^{2+} + 2e^- \rightarrow Cu(s)$$

$$at\ the\ anode: \quad Cu(s) \rightarrow Cu^{2+} + 2e^-$$
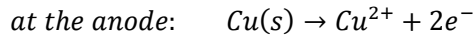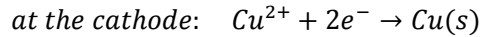
and the thickness of the deposited metal can be calculated according to the Faraday's law,

$$mass = \alpha \frac{ItM}{nF} \tag{11}$$

where mass is the thickness, α is the deposited efficiency, I is the current, t is the time, M is the molar mass, n is the ion valence and F is the Farradays constant (Franssila 2010).
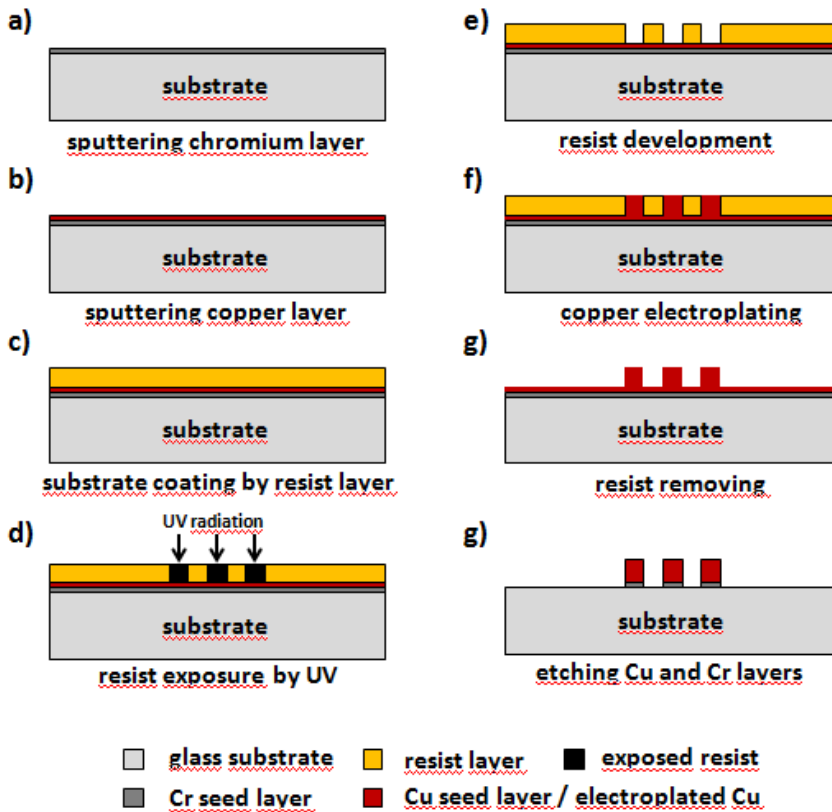
Figure 12. A scheme of the fabrication process of a Cu microstructure.

Cr adhesion (a) and Cu seed (b) layer is sputtered onto a substrate. The substrate is covered by resist (c). The resist is exposed to UV radiation through the mask with the desired pattern (d). The resist is developed (e) and the Cu is electroplated. Finally, the resist is removed (g) and the Cu and the Cr layer is etched.

A scheme of the microcoil fabrication can be seen in Fig. 12. First, the seed layer of copper was sputtered on the top of the chromium adhesion layer. Then, the substrates were coated with resist and microstructures were patterned. SU-8 resist can be used for making electroplating molds (Seidemann & Buettgenbach 2001). However, this type of resist is difficult to dissolve or strip off from the substrate after it was fully cross-linked (Ho & Hsu 2004). For successful stripping of SU-8 resist, a special sacrificial layer has to be applied by additional chemicals such as Omnicoat[TM]. This step facilitates the SU-8 stripping when larger structures of 100 μm are prepared. Nevertheless, there is still a problem with smaller structures of several 10 μm (Wang et al. 2009). For such structures (Guodong et al. 2003), plasma etching is more suitable. Both approaches increase the price of the process and require other technical equipment. Although we had experience with SU-8 resist, due to the problems reported in the literature, we concentrated on the resist suitable especially for electroplating. We tested positive resists AZ 6624, AZ 9260 supplied by MicroChemicals GmbH. The resists can be deposited in a thickness of 2-4 μm, 4-20 μm, respectively. By processing the resists according to the basic manufacturer

guides, only the UV-exposure had to be adjusted to obtain high quality patterns. Higher thickness of AZ 9260 (24 µm) can be achieved by a two-step coating process with an intermediate softbake step. When we performed this step, we encountered a difficulty with uneven substrate coating and despite a high number of experiments with many diverse modifications we were not able to achieve uniform resist coating in our conditions. This was a crucial problem for a further process of the resist because with variation of UV-exposures, the uneven coating caused improper development of the resist at areas with a higher thickness. As a result, the protocols for the thickest layer of the AZ 6624 and AZ 9260 (a one-step coating process) resist were optimized for a height of 3.5 and 8.5-9.5 µm, respectively.
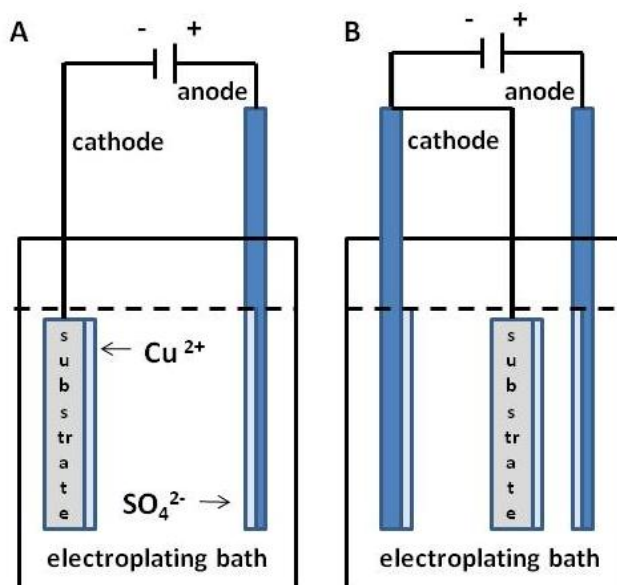

Figure 13. Two arrangements of electrodes in a DC circuit during electroplating in a CuSO4 bath.

Panel A shows a simple arrangement of the anode and the substrate when copper patterns were not successfully electroplated on the copper seed layer.
Panel B shows the final successful arrangement for the electroplating.

An electroplating process can be performed after a successful preparation of the molds on the seed layer. Although the optimization of electroplating seemed to be a simple task accomplishable in several adjustments, it was not as straightforward as it had been expected. First, a simple scheme, see Fig. 13A, was adopted. The electroplating was performed in a Hellendahl jar with cut microscopy slides as substrates. It was found out that by altering the current and the distances between the anode and the substrate, no copper was electrodeposited. Moreover, seed layers exposed to the electroplating solution were stripped from the substrates. It was considered that it was caused by high current density. After several alternations of the arrangement of the cathode, the anode and the substrate in the electroplating jar, the best current distribution for effective electroplating was set, see Fig. 13B. A drawback of this arrangement was that it was only centers of the substrates that were electroplated effectively. The closer to the edges

of the substrates, the less effective the electroplating was, or in the majority of cases, the seed layers were stripped from the substrates. We dealt with the problem by using wider electrodes and the whole process was performed in a wider baker. The time for effective plating of patterned molds was adjusted experimentally and finally, the distance of the substrate from the anode and the electroplating time were the most important factors during the process.

Samples of the fabricated structures can be seen in electron microscope pictures in Fig. 14. The difficulty with non-uniform current density described above has always been an issue in the semiconductor industry. During Cu electroplating of interconnects on a semiconductor wafer, the structure has to be plated with an extreme thickness uniformity. Because there is a number of important parameters which can influence the whole process such as configuration of the electroplating cell, seed thickness, various electrolyte properties and flow conditions, and current densities, computer simulation methods can be helpful in the optimization process (Masuku et al. 2002; Malyshev et al. 2003).
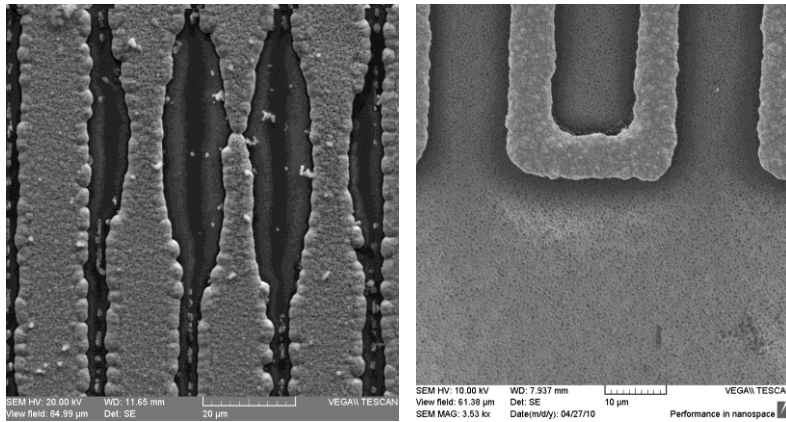

Figure 14. Electron microscopy images of fabricated Cu microstructures.

The left panel shows overplated microstructures after the resist was stripped and the Cu seed layer was etched. Deformities in the wire continuity can be observed as a result of improper resist development before the electroplating. Overplated edges are distinct in this picture. The right panel shows a properly electroplated Cu microstructure.

Changes in the parameters of electroplating process can lead to different properties of electric resistance of plated copper films, their smoothness and the uniformity of their surface area (Teh et al. 2001; Lin & Lin 2004). This phenomenon was not studied. The fabricated microcoils were stable for the injected currents (up to 600 mA for several minutes) and the gradient of magnetic field was successfully generated as discussed further. It can be concluded that the fabrication protocols were successfully optimized.

The prepared microcoils on glass substrates were isolated with a layer of SU-8 25 resist. By using an appropriate mask during the SU-8 25 process, the edges on the substrate were opened for further connection of the microfabricated Cu wires to a power supply with a conductive epoxy adhesive.

3.2.3. Microchannels fabrication and packing of a microfluidic chip

Packing of the fabricated microchip with a microfluidic channel into a compact ensemble was another task. A sandwich type of the device consisting of the following main parts was selected: (i) a microchip, (ii) a PDMS spacer containing microchannels and holes for an inlet and an outlet of the fluid, (iii) a polymethyl methacrylate (PMMA) holder or a glass cover.

The whole process of soft lithography including master fabrication by UV-lithography and microchannels casting was performed, see Fig. 15. Although this process is straightforward and many recommendations can be found in specialized internet forums or in the literature, it was found out that a significant amount of personal invention and practice was necessary for fabrication of a high quality PDMS product. The requirements for packing of the microfluidic chip and the need for simplification of the fabrication resulted in several restrictions to be considered. It was essential for the bottom and top parts to be extremely flat and to have parallel surfaces. At the same time, the PDMS required to be cured at temperatures over 100 °C to accelerate the time of polymerizing. Several casting approaches were investigated.
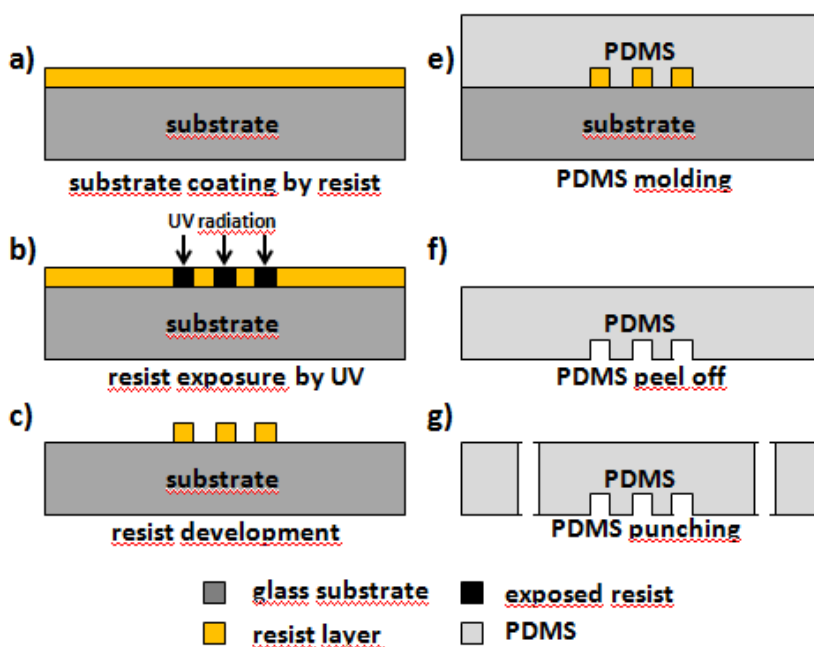

Figure 15. A scheme of a PDMS master mold and of PDMS replica fabrication.

(a) A substrate is coated by a resist layer; (b) the resist is exposed to UV radiation through a mask with the desired pattern; (c) the resist development follows. PDMS is casted (e) and after a curing process, it is peeled off the master mold (f). Finally, fluid holes are punched into the PDMS (g) and the PDMS can be cut depending on the intended use.

First, a master mold was fabricated on a silicon wafer using SU-8 2150 resist. PMMA was used as the casting mold. A plate of PMMA with a cutout opening was put

on the top of the prepared silicon wafer to prevent the PDMS from overflowing. The height of the PDMS spacer was adjusted by the height of the PMMA. The PDMS was poured onto the wafer in such a way that it overflowed the opening slightly. Another plate from PMMA was placed on the top gently and the PDMS was left to polymerize at 45 °C. A problem occurred when the PMMA pieces were not compressed tightly. The PDMS passed the junctions and it was nearly impossible to take the casting form into pieces. Other reasons why the whole ensemble did not seem suitable was the bending property of PMMA and the fact that it could not be cured under higher temperatures.

Another tested procedure was casting in a Petri dish. In this case, the height of the PDMS spacer was difficult to adjust and it was found out that dishes do not have a planar base. Because the upper and the bottom parts of the PDMS spacer were required to be flat and their surfaces to be parallel, this approach was evaluated as unsuitable.

Another difficulty during our investigations arose from the properties of silicon wafers. Silicon wafers are brittle and can be bent and broken easily while the PDMS is peeled off from the master mold. This can destroy the master mold with the patterned channels. It was also found out that the PDMS has to be degassed perfectly when treated under higher temperatures. Otherwise, bubbles occur during polymerization. When the PDMS polymer was not mixed properly with the polymerization initiator, the cured PDMS spacer was too sticky or it was too difficult to peel it off from the master. The investigation of several different tools for punching the holes was an issue as well and in the end, a stainless steel straight cannula (Fisnar Inc., USA) was selected as the punching needle.

Soft lithography protocols were established after a metal casting mold was designed, fabricated and tested, see Fig. 1 (introduced in Chemicals, materials and protocols). Glass substrates with a thickness of 1.1 mm were cut precisely so that they fitted into the metal mold opening. The height of the PDMS spacer could be adjusted by introducing several glass substrates under the fabricated master. An advantage of a master mold fabricated from glass substrates was that it was not as brittle as silicon wafers and was able to endure more pressure. Using this ensemble, the PDMS was cured on a hotplate under high temperatures and after the mold was dismantled into pieces, the spacer surfaces were parallel, extremely flat, and showed high adhesion forces to glass and the SU-8 resist as it had been expected.
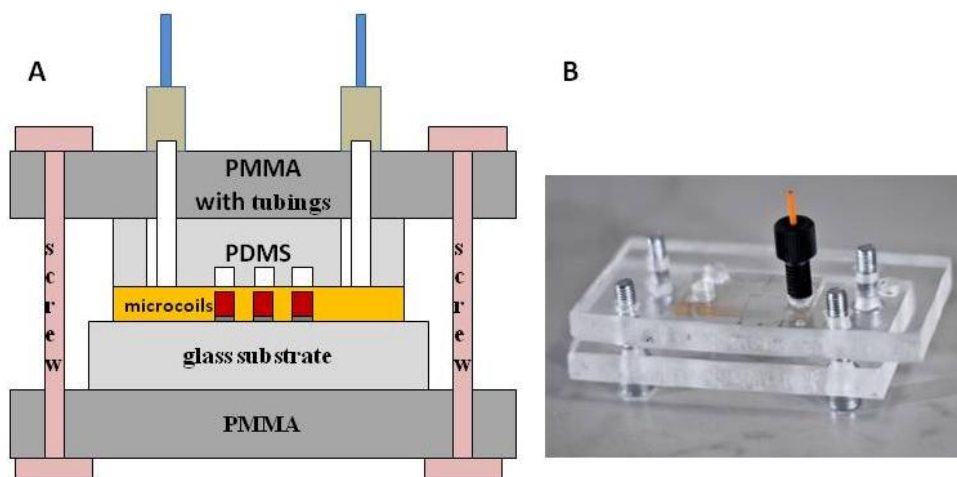
Figure 16. A packing ensemble of a microfluidic device using a PDMS spacer and a microchip in a PMMA holder.

The left panel (A) shows a scheme of the ensemble. The right panel (B) shows a picture of the ensemble.

Two approaches were investigated for the packing. The first approach can be seen in Fig. 16. A microfluidic chip holder was fabricated from PMMA with precisely drilled inlets and outlets for a fluid access to the chip. Precisely fabricated M6 threads enabled to connect all tubings to the holder. The pressure of the upper and the bottom part of the holder on the chip with the PDMS spacer was adjusted with four screws. After several employments of this holder, it was found out that using screws causes a problem with adhesion of the PDMS to the upper part of the holder and to the fabricated chip, which led to fluid permeation outside from the microchannels. Based on personal experience, it was caused mainly by the fact that the upper and the bottom parts were not tightened properly in a parallel manner and by weak bond of the PDMS to the PMMA.
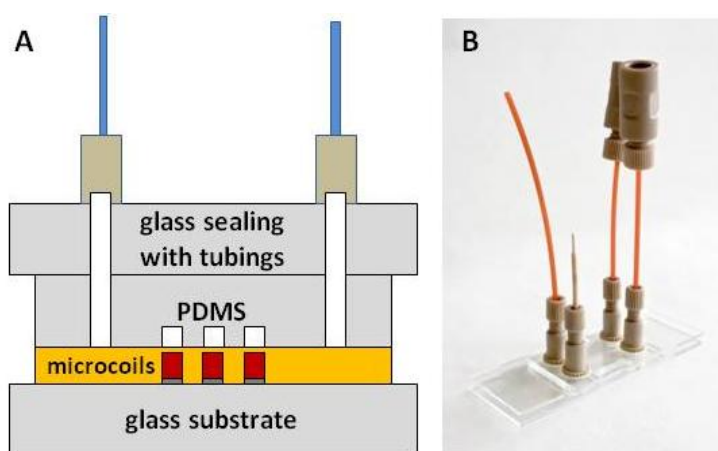

Figure 17. A packing ensemble of a microfluidic device using a PDMS spacer and a glass cover.

The left panel (A) shows a scheme of the ensemble. The right panel (B) shows a picture of the ensemble including two fluid inlets and two outlets.

Another packing approach is demonstrated in Fig. 17. The manufactured device was upgraded by a glass housing and a precisely fabricated PDMS spacer in a metal casting mold. In the literature, the bonding properties of PDMS to different materials have been studied widely as they play an important role in analytical microfluidic devices (Mata et al. 2005; Kuncova-Kallio & Kallio 2006). PDMS can bond to glass and other solids reversibly by van der Waals forces. These forces are sufficient for applications where the flow in microchannels is driven by low pressure. In high pressure applications, there have been successful attempts to use oxygen plasma treatment of PDMS or additional adhesives and adhesion promoters (Bhattacharya et al. 2005; Samel et al. 2007; Eddings et al. 2008; Cai & Neyer 2010). Although PDMS can be bonded to PMMA reversibly as tested in the previous approach, the bond is too weak (Duffy et al. 1998) and insufficient for proper microfluidic functioning.

In the second type of the packing arrangement, neither screws nor tightening tools were employed in the whole ensemble. The upper part of the microfluidic ensemble was fabricated from microslide glass with precisely drilled openings for fluid inlets and outlets with a glued connector for tubings. This arrangement was found optimal for the microfluidic system. Adhesive forces of PDMS to glass and SU-8 resist were sufficient and further studies were performed without any sealing holder. There was no fluid passing through the PDMS-glass and the PDMS-SU-8 surface after several chip replacements and the microfluidic device was able to work for hours under the employed conditions.

3.3. Experimental setup

The results from the magnetic field simulations indicated that by coupling three adjacent wires with the same current direction, a multiwire planar meander magnetic microcoil can generate higher magnetic field gradients and magnetic forces exerted on MBs than a simple planar meander microcoil. Therefore, a multiwire planar meander magnetic microcoil with three coupled wires was selected for further fabrication and testing. Also from the technological point of view, a microchip with a multiwire microcoil is preferable. A microcoil with one wire design could be destroyed if the wire was interrupted or deformed. In a multiwire microcoil design, in case of an interruption of one wire at any place in the microcoil, the neighboring wires can lead the current and in spite of higher electric density in the wires, which can deform the profile of the magnetic field, the microcoil keeps its function.

Finally, microcoils with a wires width of 20 µm and with a spacing of 20 µm between the adjacent wires were designed. The width of the joint wire was set to three times the width of the wire, as it was performed in the simulations. The spacing between the coupled wires was set to 40 µm (two times the width of the wire). The length of the microcoil wires was set to 1200 µm. The fabricated microcoils on glass substrates are presented in Fig. 18.
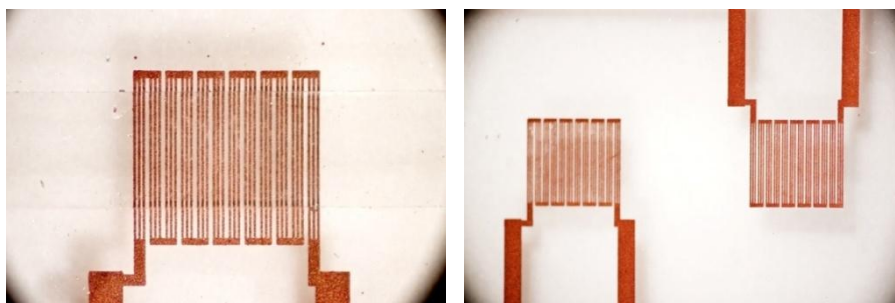
Figure 18. The final design of experimentally tested Cu microcoils.

The left panel presents microfabricated structures isolated in an SU-8 resist and covered by a PDMS spacer with a microchannel situated directly above the microcoil. The right panel shows two, side by side fabricated microcoils on one glass substrate.

As can be seen in Fig. 19, various designs were fabricated during the optimization of the fabrication protocol. The presented microchips include a microchannel fabricated from SU-8 25 resist above the microcoil insulation layer, which also leads to a functional device, however, an additional fabrication step is required and the fabrication is more challenging. These chips were not effective for MBs trapping but local magnetic forces was generated during testing.
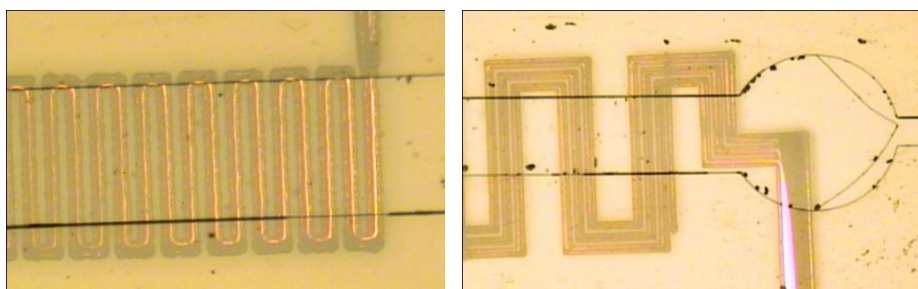

Figure 19. The fabricated Cu microstructures using AZ 6224 resist.

The left panel presents a simple meander microcoil. The right panel presents a variation of a multiwire microcoil design. In both panels, the microfabricated Cu structures are isolated in the layer of SU-8 resist. Above this layer, another layer of SU-8 resist is fabricated including a microfluidic channel.

MBs trapping experiments were performed with carboxylated magnetic beads (diameter 1 µm). Stock solution of MBs was dissolved in a phosphate buffered saline (PBS) running buffer, pH 7.6 with 1% Tween, in a ratio of 1:10000. Actuation of a micropump was performed through programmable software with a repetitive injection of 100 µL of MBs into the microfluidic flow. Based on several flow rate optimizations, the final flowrate of 0.4 µL/s was evaluated as optimal for MBs trapping with injected current of 400 mA, as can be seen in Fig. 20. For experimental purposes, the flow of MBs was set in such a way that the MBs flowed only in the left part of the fluid flow above the top part of the fabricated microcoil, see Fig. 18A and 20.

In initial experiments, no magnetic trapping was observed although very high current intensities (600-800 mA) were inserted into the wires. Using high currents was

undesirable due to increased heating of the fluid above the microcoils, which led to formation of bubbles in the fluid. These observations confirmed the statement that planar meander microcoils embedded into a microfluidic chip generate weak magnetic forces which cannot compete effectively with the drag force of the fluid in the microchannels. Therefore, a combination of microcoils with permanent magnet is needed (Nguyen 2011). External permanent magnets magnetize MBs in the solution and can attract MBs close to the microcoil where localized generated magnetic forces can trap MBs effectively at a desired place. The profile of magnetic field generated by microcoils can be influenced by the profile of magnetic field of permanent magnets. This problem was not studied.

In our further experiments, the advantage of the combination of permanent magnets and embedded microcoils was confirmed. Four neodymium-iron-boron (NdFeB) nickel-plated cube magnets (1x1x1 mm) were placed at an adjusted distance under the fabricated magnetic microfluidic chip. The distance between the magnets and the fabricated chip was adjusted in such a way that the MBs were magnetized and attracted as close as possible above the microcoil, and that the movement of MBs in the fluid flow at the bottom of the microchannel was preserved. By this modification, successful trapping of MBs was performed by magnetic forces generated by the fabricated multiwire microcoil.

A micrograph sequence in Fig. 20 shows how MBs trapping in a fluid flow develops under time with a subsequent switching the current on and off. The trapping is performed in the microfluidic device. Most MBs are trapped at the beginning of the microcoil (above the left part of the first coupled wires). This behavior can be explained by two facts. First, most MBs pass through the first coupled wires and second, in a magnetic field simulation it was found out that the highest gradient of magnetic field and the magnetic energy gradient are generated at the beginning and at the end of the microcoil (Fig. 7-10). By switching the current off, the MBs dissolve in the fluid flow and are driven in the direction of the flow (from the left to the right). After the current is switched on again, the MBs become more concentrated also above the following coupled wires. With the next switching off, the MBs are again transferred further in the direction of the fluid flow. With the final switching on, the MBs are observable also above the last couple of wires. The spatial distribution of trapping cages induced by magnetic forces correlates mainly with the spatial distribution of the x component of the simulated magnetic energy gradient above the microcoil, see Fig. 9. This can lead to a conclusion that the x component of generated magnetic forces is the most important component if the trapping is performed in a fluid driven environment because only this component can act in the opposite direction of the acting drag force.
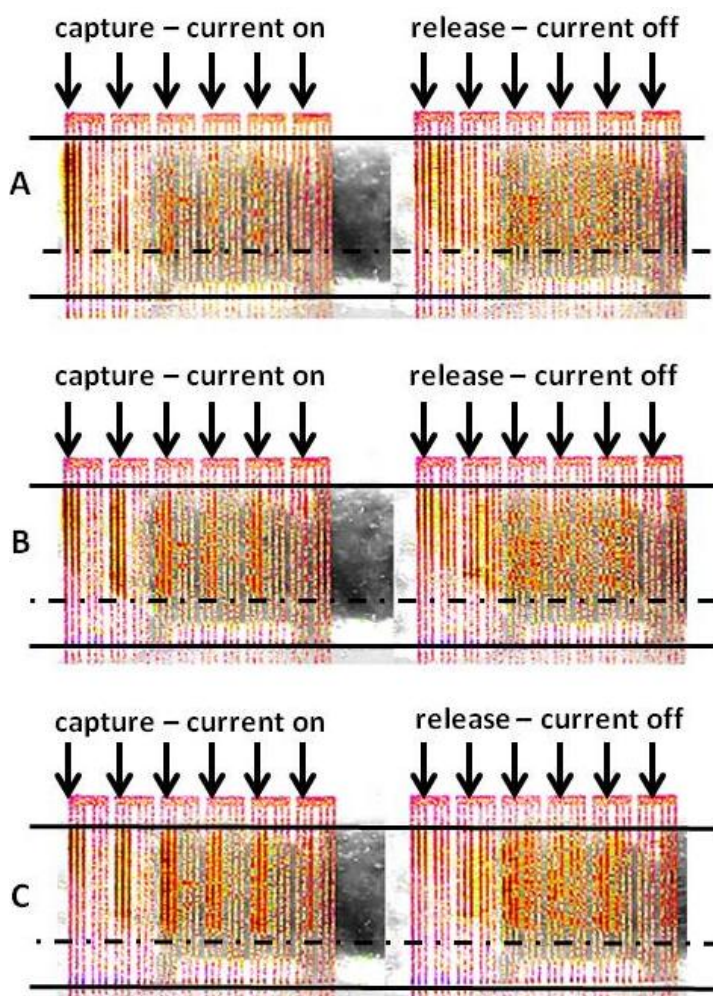
Figure 20. Trapping of MBs is presented in a micrograph sequence.

The microchannel is marked out by a solid line. The flow is represented by a continuous flow of a buffer medium with a velocity of 0.2 μL/s (below the dot dash line) and a medium containing MBs with a velocity of 0.4 μL/s (above the dot dash line) from the left to the right. Both of the flows were mixed by a T-mixer located in front of the microcoils (a laminar separation of the flow was observed). The trapping was recorded with a digital camera video option and the sequence was edited into micrographs. Without current injected into the microcoil, no trapping was observed. Sequence A represents the first current injection for 8s and release for 1s, sequence B represents an immediate second current injection for 4 s and release for 1 s and C represents an immediate third current injection for 4 s.

It was demonstrated that MBs can be trapped at given places according to generated magnetic forces dependent on the microcoil design. By switching the current on and off, the MBs separated from the fluid flow could be shifted sequentially in the direction of the flow. It is possible to separate or drift particles by using magnetic field generated by microcoils embedded within a microfluidic system. The combination of

magnetic forces generated by embedded microcoils and external permanent magnets is important for systems employing microcoils generating weaker magnetic forces.

Conclusions

MBs can serve as solid supports in immunosensing assays. Immunoassays based on MBs and performed in a microfluidic system require trapping of MBs in microchannels. For this purpose, external permanent magnets or electromagnetic microstructures embedded directly into the microfluidic chip can be employed. This study focused on optimization of the design of a meander microcoil by computer simulations. Then, fabrication protocols of a newly designed magnetic separator embedded in a microfluicic chip were optimized. And finally, trapping of micron-sized MBs was tested in the fabricated microfluidic system.

The optimization of the design of a meander microcoil was performed by computer simulations with COMSOL Multiphysics software. A multiwire meander microcoil was suggested as a more powerful microcoil in comparison with a simple meander microcoil. Higher performance of the newly proposed multiwire meander microcoil in comparison with a simple meander microcoil was confirmed. The generated magnetic field and the magnetic energy gradient of the multiwire microcoil did not drop as rapidly in larger distances from the microcoil as in case of a simple planar microcoil with one wire. Thus, the multiwire microcoils will be more effective for MBs trapping. The simulated profile of the magnetic field of the meander microcoil correlated with the results reported in the literature (Ramadan 2004).

A multiwire microcoil with three coupled wires was fabricated on glass substrates by employment of several optimized microfabrication techniques such as EBL, UV lithography, and copper electroplating. The workflow of the mask design for the use in EBL was established and three types of EBL resists were investigated. SX AR-N 7700/3 e-beam and UV resist was found out to be the most suitable resist for fabrication of negative and positive masks. AZ 9260 resist was selected for fabrication of microcoil patterns on glass substrates. Optimal conditions for electroplating were achieved by a suitable spatial arrangement of the electroplating electrodes. The electroplated microcoil was isolated in SU-8 resist and a microfluidic sandwich type device with a PDMS spacer with microchannels was manufactured. For the packing of the microfluidic device, a glass enclosure with fittings for tubings proved to be a more suitable solution than a home-made PMMA holder.

The fabricated microfluidic chip with an embedded magnetic separator was tested for MBs trapping. It was found out that magnetic forces generated by the multiwire microcoil are not sufficient for MBs trapping. Small external permanent magnets had to be employed. By an adjustment of the fluid flow and of the distance of the permanent magnets from the bottom of the microfluidic chip, effective trapping of MBs was achieved and the profile of the trapped MBs corresponded to the x component of the magnetic energy gradient simulated by computer.

The magnetic separator together with an electrochemical detector will be integrated into a microfluidic chip and an electrochemical immunosensor based on MBs will be further developed.

Acknowledgement

References

ABONNENC, M., GASSNER, A.-L., MORANDINI, J., JOSSERAND, J. and GIRAULT, H. H., 2009. Magnetic track array for efficient bead capture in microchannels. Analytical and Bioanalytical Chemistry. Vol. 395, no. 3, pp. 747–757.

AHN, C. H. and ALLEN, M. G., 1994. A new toroidal-meander type integrated inductor with a multilevel meander magnetic core. IEEE Transactions on Magnetics. Vol. 30, no. 1, pp. 73–79.

AHN, C. H. and ALLEN, M. G., 1998. Micromachined planar inductors on silicon wafers for MEMS applications. IEEE Transactions on Industrial Electronics. Vol. 45, no. 6, pp. 866–876.

ANDRICACOS, P. C., UZOH, C., DUKOVIC, J. O., HORKANS, J. and DELIGIANNI, H., 1998. Damascene copper electroplating for chip interconnections. IBM Journal of Research and Development. Vol. 42, no. 5, pp. 567–574.

BERTHIER, J. and SILBERZAN, P., 2006. Microfluidics for biotechnology. Boston. Artech House. ISBN 9781580539616.

BEYZAVI, A. and NGUYEN, N.-T., 2008. Modeling and optimization of planar microcoils. Journal of Micromechanics and Microengineering. Vol. 18, no. 9, pp. 095018.

BHATTACHARYA, S., DATTA, A., BERG, J. M. and GANGOPADHYAY, S., 2005. Studies on surface wettability of poly(dimethyl) siloxane (PDMS) and glass under oxygen-plasma treatment and correlation with bond strength. Journal of Microelectromechanical Systems. Vol. 14, no. 3, pp. 590–597.

BURGHARTZ, J. N., 1998. Spiral inductors on silicon-status and trends (invited article). International Journal of RF and Microwave Computer-Aided Engineering. Vol. 8, no. 6, pp. 422–432.

BURGHARTZ, J. N., JENKINS, K. A. and SOYUER, M., 1996. Multilevel-spiral inductors using VLSI interconnect technology. IEEE Electron Device Letters. Vol. 17, no. 9, pp. 428–430.

CAI, D. and NEYER, A., 2010. Cost-effective and reliable sealing method for PDMS (polydimethylsiloxane)-based microfluidic devices with various substrates. Microfluidics and Nanofluidics. Vol. 9, no. 4-5, pp. 855–864.

DEREC, C., WILHELM, C., SERVAIS, J. and BACRI, J.-C., 2009. Local control of magnetic objects in microfluidic channels. Microfluidics and Nanofluidics. Vol. 8, no. 1, pp. 123–130.

DUFFY, D. C., MCDONALD, J. C., SCHUELLER, O. J. A. and WHITESIDES, G. M., 1998. Rapid prototyping of microfluidic systems in poly(dimethylsiloxane). Analytical Chemistry. Vol. 70, no. 23, pp. 4974–4984.

DUNLOP, E. H., FEILER, W. A. and MATTIONE, M. J., 1984. Magnetic separation in biotechnology. Biotechnology Advances. 1984. Vol. 2, no. 1, pp. 63–74.

EDDINGS, M. A., JOHNSON, M. A. and GALE, B. K., 2008. Determining the optimal PDMS–PDMS bonding technique for microfluidic devices. Journal of Micromechanics and Microengineering. Vol. 18, no. 6, pp. 067001.

FONNUM, G., JOHANSSON, C., MOLTEBERG, A., MORUP, S. and AKSNES, E., 2005. Characterisation of Dynabeads by magnetization measurements and Mössbauer spectroscopy. Journal of Magnetism and Magnetic Materials. Vol. 293, no. 1, pp. 41–47.

FRANSSILA, S., 2010. Introduction to microfabrication. Chichester, West Sussex . John Wiley & Sons. ISBN 9780470749838.

FULCRAND, R., JUGIEU, D., ESCRIBA, C., BANCAUD, A., BOURRIER, D., BOUKABACHE, A. and GUÉ, A. M., 2009. Development of a flexible microfluidic system integrating magnetic micro-actuators for trapping biological species. Journal of Micromechanics and Microengineering. Vol. 19, no. 10, pp. 105019.

GERBER, R. and BIRSS, R. R., 1983. High gradient magnetic separation. New York. Research Studies Press. ISBN 9780471901624.

GIJS, M. A. M., 2004. Magnetic bead handling on-chip: new opportunities for analytical applications. Microfluidics and Nanofluidics. Vol. 1, no. 1, pp. 22–40.

GIJS, M. A. M., LACHARME, F. and LEHMANN, U., 2010. Microfluidic applications of magnetic particles for biological analysis and catalysis. Chemical Reviews. Vol. 110, no. 3, pp. 1518–1563.

GOONERATNE, Ch. P., LIANG, C. and KOSEL, J., 2011. A planar conducting microstructure to guide and confine magnetic beads to a sensing zone. Microelectronic Engineering. Vol. 88, no. 8, pp. 1757–1760.

GUODONG, H., HOLMES, A. S. and HEATON, M. E., 2003. SU8 resist plasma etching and its optimisation. In: IEEE Conference Publications [online]. S.l.: IEEE. 2003. pp. 268–271. Available from: http://ieeexplore.ieee.org/lpdocs/epic03/wrapper.htm?arnumber=1287050.

HO, Ch.-H. and HSU, W., 2004. Experimental investigation of an embedded root method for stripping SU-8 photoresist in the UV-LIGA process. Journal of Micromechanics and Microengineering. Vol. 14, no. 3, pp. 356–364.

HORÁK, D., BABIČ, M., MACKOVÁ, H. and BENEŠ, M. J., 2007. Preparation and properties of magnetic nano- and microsized particles for biological and environmental separations. Journal of Separation Science. 2007. Vol. 30, no. 11, pp. 1751–1772.

HUBER, D. L., 2005. Synthesis, properties, and applications of iron nanoparticles. Small. Vol. 1, no. 5, pp. 482–501.

CHALMERS, J. J., ZHAO, Y., NAKAMURA, M., MELNIK, K., LASKY, L., MOORE, L. and ZBOROWSKI, M., 1999. An instrument to determine the magnetophoretic mobility of labeled, biological cells and paramagnetic particles. Journal of Magnetism and Magnetic Materials. Vol. 194, no. 1-3, pp. 231–241.

CHOI, J. W., AHN, C. H., BHANSALI, S. and HENDERSON, H. T., 2000. A new magnetic bead-based, filterless bio-separator with planar electromagnet surfaces for integrated bio-detection systems. Sensors and Actuators B: Chemical. Vol. 68, no. 1-3, pp. 34–39.

CHOI, J.-W., LIAKOPOULOS, T. M. and AHN, C. H., 2001. An on-chip magnetic bead separator using spiral electromagnets with semi-encapsulated permalloy. Biosensors and Bioelectronics. Vol. 16, no. 6, pp. 409–416.

KUNCOVA-KALLIO, J. and KALLIO, P. J., 2006. PDMS and its suitability for analytical microfluidic devices. In: IEEE Conference Publications [online]. New York, NY, USA: IEEE. 2006. pp. 2486–2489. Available from: http://ieeexplore.ieee.org/lpdocs/epic03/wrapper.htm?arnumber=4462299.

Engineering in Medicine and Biology Society, 2006. EMBS '06. 28th Annual International Conference of the IEEE

LIN, Ch.-T. and LIN, K.-L., 2004. Effects of current density and deposition time on electrical resistivity of electroplated Cu layers. Journal of Materials Science: Materials in Electronics. Vol. 15, no. 11, pp. 757–762.

LIN, Y. "A.," WONG, T.-S., BHARDWAJ, U., CHEN, J.-M., MCCABE, E. and HO, Ch.-M., 2007. Formation of high electromagnetic gradients through a particle-based microfluidic approach. Journal of Micromechanics and Microengineering. Vol. 17, no. 7, pp. 1299–1306.

LU, A.-H., SALABAS, E. L. and SCHÜTH, F., 2007. Magnetic nanoparticles: synthesis, protection, functionalization, and application. Angewandte Chemie International Edition. Vol. 46, no. 8, pp. 1222–1244.

MALYSHEV, E., LANDAU, U. and CHIVILIKHIN, S., 2003. Modeling the deposit thickness distribution in copper electroplating of semicondutor wafer interconnects. In: Proceedings of the AIChE Annual Meeting [on line]. San-

Francisco, CA, Nov 16-21, 2003. Available from: http://www.l-chem.com/Papers/Deposit_Thickness_Distribution.pdf.

MASUKU, E. S., MILEHAM, A. R., HARDISTY, H., BRAMLEY, A. N., JOHAL, C. and DETASSIS, P., 2002. A finite element simulation of the electroplating process. CIRP Annals - Manufacturing Technology. Vol. 51, no. 1, pp. 169–172.

MATA, A., FLEISCHMAN, A. J. and ROY, S., 2005. Characterization of polydimethylsiloxane (PDMS) properties for biomedical micro/nanosystems. Biomedical Microdevices. Vol. 7, no. 4, pp. 281–293.

NGUYEN, N. M. and MEYER, R. G., 1990. Si IC-compatible inductors and LC passive filters. IEEE Journal of Solid-State Circuits. Vol. 25, no. 4, pp. 1028–1031.

NGUYEN, N.-T., 2011. Micro-magnetofluidics: interactions between magnetism and fluid flow on the microscale. Microfluidics and Nanofluidics. Vol. 12, no. 1-4, pp. 1–16.

PAMME, N., 2006. Magnetism and microfluidics. Lab on a Chip. Vol. 6, no. 1, pp. 24.

PAMME, N., EIJKEL, J. and MANZ, A., 2006. On-chip free-flow magnetophoresis: Separation and detection of mixtures of magnetic particles in continuous flow. Journal of Magnetism and Magnetic Materials. Vol. 307, no. 2, pp. 237–244.

PAMME, N. and MANZ, A., 2004. On-chip free-flow magnetophoresis: Continuous flow separation of magnetic particles and agglomerates. Analytical Chemistry. Vol. 76, no. 24, pp. 7250–7256.

PARK, J., FUJITA, H. and KIM, B., 2011. Fabrication of metallic microstructure on curved substrate by optical soft lithography and copper electroplating. Sensors and Actuators A: Physical. Vol. 168, no. 1, pp. 105–111.

PARKER, R. J, 1990. Advances in permanent magnetism. New York: Wiley-Interscience. ISBN 9780471822936.

RAMADAN, Q., 2004. On-chip micro-electromagnets for magnetic-based bio-molecules separation. Journal of Magnetism and Magnetic Materials. Vol. 281, no. 2-3, pp. 150–172.

RAMADAN, Q., POENAR, D. P. and YU, Ch., 2008. Customized trapping of magnetic particles. Microfluidics and Nanofluidics. Vol. 6, no. 1, pp. 53–62.

ROSTAING, H., CHETOUANI, H., GHEORGHE, M. and GALVIN, P., 2007. A micromagnetic actuator for biomolecule manipulation. Sensors and Actuators A: Physical. Vol. 135, no. 2, pp. 776–781.

SADLER, D. J., WENJIN, Z., CHONG, H. A., HI, J. K. and SUK, H. H., 1997. Micromachined semi-encapsulated spiral inductors for microelectromechanical systems (MEMS) applications. IEEE Transactions on Magnetics. Vol. 33, no. 5, pp. 3319–3321.

SAMEL, B., CHOWDHURY, M. K. and STEMME, G., 2007. The fabrication of microfluidic structures by means of full-wafer adhesive bonding using a

poly(dimethylsiloxane) catalyst. Journal of Micromechanics and Microengineering. Vol. 17, no. 8, pp. 1710–1714.

SEIDEMANN, V. and BUETTGENBACH, S., 2001. Novel fabrication process for 3D meander-shaped microcoils in SU-8 dielectric and their application to linear micromotors. Proc. SPIE. Vol. 4407, pp. 304–309

SIEGEL, A. C., SHEVKOPLYAS, S. S., WEIBEL, D. B., BRUZEWICZ, D. A., MARTINEZ, A. W. and WHITESIDES, G. M., 2006. Cofabrication of electromagnets and microfluidic systems in poly(dimethylsiloxane). Angewandte Chemie. Vol. 118, no. 41, pp. 7031–7036.

SMISTRUP, K., HANSEN, O., BRUUS, H. and HANSEN, M., 2005. Magnetic separation in microfluidic systems using microfabricated electromagnets—experiments and simulations. Journal of Magnetism and Magnetic Materials. Vol. 293, no. 1, pp. 597–604.

TEH, W. H., KOH, L. T., CHEN, S. M., XIE, J., LI, C. Y. and FOO, P. D., 2001. Study of microstructure and resistivity evolution for electroplated copper films at near-room temperature. Microelectronics Journal. Vol. 32, no. 7, pp. 579–585.

WANG, P., TANAKA, K., SUGIYAMA, S., DAI, X. and ZHAO, X., 2009. Wet releasing and stripping SU-8 structures with a nanoscale sacrificial layer. Microelectronic Engineering. Vol. 86, no. 11, pp. 2232–2235.

WATANABE, Y., EDO, M., NAKAZAWA, H. and YONEZAWA, E., 1996. A new fabrication process of a planar coil using photosensitive polyimide and electroplating. Sensors and Actuators A: Physical. Vol. 54, no. 1–3, pp. 733–738.

WHITESIDES, G. M., KAZLAUSKAS, R. J. and JOSEPHSON, L., 1983. Magnetic separations in biotechnology. Trends in Biotechnology. Vol. 1, no. 5, pp. 144–148.

ZBOROWSKI, M., MOORE, L., WILLIAMS, P. and CHALMERS, J., 2002. Separations based on magnetophoretic mobility. Separation Science and Technology. Vol. 37, no. 16, pp. 3611–3633.

ZBOROWSKI, M., SUN, L., MOORE, L. R., STEPHEN WILLIAMS, P. and CHALMERS, J. J., 1999. Continuous cell separation using novel magnetic quadrupole flow sorter. Journal of Magnetism and Magnetic Materials. Vol. 194, no. 1-3, pp. 224–230.

ZHANG, Y., BARBER, R. W. and EMERSON, D. R., 2005. Particle separation in microfluidic devices - SPLITT fractionation and microfluidics. Current Analytical Chemistry. Vol. 1, no. 3, pp. 345–354.

ZHU, T., CHENG, R. and MAO, L., 2011. Focusing microparticles in a microfluidic channel with ferrofluids. Microfluidics and Nanofluidics. Vol. 11, no. 6, pp. 695–701.

8. A list of the published author's papers

Štofik, M., Strýhal, Z., and Malý, J., 2009. Dendrimer-encapsulated silver nanoparticles as a novel electrochemical label for sensitive immunosensors. Biosensors and Bioelectronics. Vol. 24, no. 7, pp. 1918-1923 (IF = 5.361).

Malý, J., Lampová, H., Semerádtová, A., **Štofik, M.**, and Kováčik, L., 2009. The synthesis and characterization of biotin-silver-dendrimer nanocomposites as novel bioselective labels. Nanotechnology. Vol. 20, no. 38, pp. 385101 (IF = 3.652).

Krejčí, J., Ondruch, V., Malý, J., **Štofik, M.**, Krejčová, D., and Vránová, H., 2011. High sensitivity biosensor measurement based on synchronous detection. Journal of Photochemistry and Photobiology B: Biology. Vol. 102, no. 3, pp. 192–199 (IF = 2.116).

Cited without self-citations: 11

H-index: 2

9. Author's participations at international conferences

The Ninth World Congress on Biosensors

Canada, Toronto, May 2006, poster presentation

Štofik, M., Malý, J., Šoltová, P., Montereali, M., R., Nardi, L., Vastarella, W., Pilloton, R., Krejčí, J., Masojídek, J., 2006. Sol-gel immobilization procedure for amperometric biosensor based on active photosystem II particles.

Third Workshop on Biosensors for Food Safety and Environmental Monitoring

Moroko, Fes, October 2007, poster presentation

Štofik, M., Malý, J., Malý, M., Krejčí, J., 2007. A numerical model of photosystem II biosensor for herbicide detection.

9th Workshop "Nanoscience & Nanotechnology"

Bulgaria, Sofia, November 2007, oral presentation

Štofik, M., Malý, J., 2007. Dendrimer encapsulated metal nanoparticles as amplifiers in electrochemical biosensing.

Nanotech Northern Europe 2008

Denmark, Copenhagen, September 2008, poster presentation

Štofik, M., Malý, J., 2008. An electrochemical biosensor based on dendrimer encapsulated silver nanoparticles.

2nd International Symposium on Biological Applications of Dendrimers

France, Porquerolles, Jun 2010, poster presentation

Frolík, J., Malý, J., **Štofik, M.**, 2010. Synthesis and characterization of oligonucleotides conjugated silver-dendrimer nanocomposites – development of a novel label for aptasensors.

Lab-on-a-Chip European Congress

Germany, Hamburg, Jun 1011, poster presentation

Štofik, M., Malý, J., Frolík, J., Semerádtová, A., 2011. A microfluidic electrochemical detector for sensing of metallic labels in immunoanalytical assays.

10.   Author's curriculum vitae

Name: Mgr. Marcel Štofik

Date of birth: 22 December 1974

Nationality: Slovak

E-mail: marcel.stofik@ujep.cz

Education

Since 2005   Doctoral study at the Faculty of Science, University of South Bohemia, České Budějovice, Czech Republic, study programme: biophysics

1993-1998   Master's degree at the Faculty of Humanities and Natural Sciences, University of Prešov in Prešov, Prešov, Slovakia, programme: teacher of biology and physical education

1989-1993   High school, Snina, Slovakia

Professional experience

Since 2008   lecturer and research assistant, Department of Biology, Faculty of Science, University of J.E.Purkyně in Ústí nad Labem

2005-2008   research assistant, Department of Biology, Institute of Natural Sciences, University of J.E.Purkyně in Ústí nad Labem

Practical internship

2009   A two-month internship in a biotechnology company VIDIA, spol. s r.o. with participation in the development of lateral flow immunoassay (LFIA) tests.

Specialization

Electrochemical biosensors and microfluidic devices; use of dendrimers, dendrimer-based metal nanocomposites and magnetic particles for detection of bioactive molecules in biosensors.